AD-A053 691 MASSACHUSETTS INST OF TECH CAMBRIDGE AEROPHYSICS LAB F/G 20/4
A STUDY OF THE LIFT-TO-DRAG RATIO CAPABILITY OF CARET WING WAVE--ETC(U)
MAR 78 M D SOLOMON F44620-76-C-0049
UNCLASSIFIED TR-200 AFOSR-TR-78-0758 NL

1 OF 3
AD
A053691

AFOSR-TR- 78-0758

(2)

AD A053691

DDC FILE COPY

A STUDY OF THE LIFT-TO-DRAG RATIO
CAPABILITY OF CARET WING WAVERIDERS

MASSACHUSETTS INSTITUTE OF TECHNOLOGY
AEROPHYSICS LABORATORY

by

Marshall D. Solomon

Interim Scientific Report

March 1978

TR 200

DDC
RECEIVED
MAY 9 1978
B

AFOSR Contract F44620-76-C-0049

Distribution Unlimited

DISTRIBUTION STATEMENT A
Approved for public release;
Distribution Unlimited

AIR FORCE OFFICE OF SCIENTIFIC RESEARCH (AFSC)
NOTICE OF TRANSMITTAL TO DDC
This technical report has been reviewed and is approved for public release IAW AFR 190-12 (7b).
Distribution is unlimited.
A. D. BLOSE
Technical Information Officer

2

A STUDY OF THE LIFT-TO-DRAG RATIO CAPABILITY OF CARET WING WAVERIDERS

by

Marshall D. Solomon

Interim Scientific Report.

March 1978

217 P.

TR-200

F44620-76-C-0049

2307

A1

AFOSR

TR-78-0758

DDC
RECEIVED
MAY 9 1978
B

AFOSR Contract F44620-76-C-0049

Distribution Unlimited

DISTRIBUTION STATEMENT A
Approved for public release;
Distribution Unlimited

009 300 308

PRECEDING PAGE BLANK

FOREWORD

This research was sponsored jointly by the Massachusetts Institute of Technology's Lincoln Laboratory under P.O. No. CC-164 and the United States Air Force, Office of Scientific Research under Contract F44620-76-C-0049.

This material was submitted by Marshall D. Solomon as a thesis for the Degree of Master of Science in Aeronautics and Astronautics in May of 1977.

ACCESSION for
NTIS White Section
DDC Buff Section
UNANNOUNCED
JUSTIFICATION
BY
DISTRIBUTION/AVAILABILITY CODES
Dist. AVAIL. and/or SPECIAL
A

PRECEDING PAGE BLANK

TABLE OF CONTENTS

Chapter Number		Page Number
I	INTRODUCTION	14
II	A MODEL OF THE CARET WING FLOW FIELD	19
	2.1 Analysis of the Caret Wing Flow Field at Design Conditions	19
	2.2 Extension of the Swept Wedge Analysis to Off-Design Conditions	24
	2.3 The Upper Surface Flow Field	28
	2.4 Estimate of Skin Friction	29
	2.5 Estimate of Base Pressure	30
III	CALCULATION OF THE LIFT COEFFICIENT, DRAG COEFFICIENT AND LIFT-TO-DRAG RATIO	32
	3.1 Introduction	32
	3.2 Mach Number and Wedge Angle Normal to the Leading Edge	33
	3.3 Pressure Ratio Across Lower Surface Shock	40
	3.4 Pressure Ratio Across Upper Surface Expansion	41
	3.5 Average Skin Friction Coefficient	43
	3.6 Base Pressure Ratio	49
	3.7 Lift Coefficient, Drag Coefficient and Lift-to-Drag Ratio	51
	3.8 Computer Program	56
IV	RESULTS	58
	4.1 Test Matrix	58
	4.2 Variable Geometry Test	60
	4.3 Fixed Geometry Test	73
V	CONCLUSIONS and RECOMMENDATIONS	76
Appendix I - Computer Program Listing		83
Tables		123
Figures		125
References		215

LIST OF TABLES

Table Number		Page Number
1	Laminar base pressure data	123
2	Test matrix	124

LIST OF FIGURES

Figure Number		Page Number
1	Construction of caret wing from known flow field	125
2	Classification of caret wings	126
3	Caret wing geometry	127
4	Family of caret wings derived from a single wedge flow	128
5	Γ_{max}, $\Gamma_{\perp}$ and $\Gamma_{max}-\Gamma_{\perp}$ vs. Φ - $\delta=5^{o}$, $\Theta=34^{o}$	129
6	Φ_{trans} vs. Θ	130
7	Pressure ratio across leading edge shock vs. Φ - $\delta=5^{o}$, $\Theta=34^{o}$	131
8	Caret wing shock patterns	132
9	Base pressure data	133
10	Caret wing wetted surfaces	134
11	Computer program flow chart	135
12-23	Lift coefficient vs. delta	136-147
24-35	Drag coefficient vs. delta	148-159
36-47	Lift-to-drag ratio vs. delta	160-171
48-53	Lift coefficient vs. theta	172-177
54-59	Drag coefficient vs. theta	178-183
60-65	Lift-to-drag ratio vs. theta	184-189
66-71	Lift coefficient vs. phi	190-195
72-77	Drag coefficient vs. phi	196-201
78-83	Lift-to-drag ratio vs. phi	202-207
84-85	Lift coefficient vs. Mach Number	208-209
86-87	Drag coefficient vs. Mach Number	210-211
88-89	Lift/drag ratio vs. Mach Number	212-213
90	Comparison of caret wing and delta wing L/D	214

LIST OF SYMBOLS

A	Caret wing apex
A_ℓ	Wetted area of lower surface
A_u	Wetted area of upper surface
$\overline{ABC}_\perp$	Unit vector normal to lower surface
$\overline{ABC'}_\perp$	Unit vector normal to upper surface
a	Speed of sound
B	Left-hand wing tip of caret wing; base area
b_2, b_3	y and z coordinates of Point B
C	Intersection of internal rib with base
C'	Intersection of upper surface rib with base
c_2, c_2'	y coordinates of Points C and C'
C_L	Lift coefficient
C_D	Drag coefficient
C_f	Skin friction coefficient
$C_{f\ell\ell}$	Average skin friction coefficient - laminar boundary layer, lower surface
$C_{ft\ell}$	Average skin friction coefficient - turbulent boundary layer, lower surface
$C_{f\ell u}$	Average skin friction coefficient - laminar boundary layer, upper surface
C_{ftu}	Average skin friction coefficient - turbulent boundary layer, upper surface

LIST OF SYMBOLS (continued)

$C_{f\ell}(x)$	Local laminar skin friction coefficient
$C_{ft}(\ell)$	Average turbulent skin friction coefficient on flat plate of length ℓ
c	Constant in equation of a plane
$\bar{c}$	Two-thirds of the root chord
E_ℓ	Area of projection of lower surface onto plane $\perp$ to free stream
E_u	Area of projection of upper surface onto plane $\perp$ to free stream
h	Semi-span in plane of wing panel
$\hat{i}$	Unit vector in x-direction
L/D	Lift-to-drag ratio
ℓ_1	Caret wing length measured from apex to base plane
ℓ_2	Length of internal rib
ℓ_3	Length of upper surface rib
$\ell(z)$	Distance from leading-to-trailing edge measured parallel to internal or upper surface rib
ℓ,m,n	Direction cosines
M	Mach number
p_b	Base pressure
p_ℓ	Lower surface pressure
p_u	Upper surface pressure

LIST OF SYMBOLS (continued)

q_∞	Free stream dynamic pressure
Re	Reynolds number
S	Plan area
T	Static temperature
V	Velocity
x,y,z	Coordinates in free stream, vertical and horizontal directions
x,z	Coordinates parallel and $\perp$ to internal or upper surface ribs in skin friction calculations
β	Angle between $M_\perp$ and $\overline{ABC}_\perp$
β'	Angle between $M_\perp$ and $\overline{ABC'}_\perp$
$\Gamma_\perp$	Wedge angle normal to leading edge (lower surface)
$\Gamma_\perp'$	Expansion angle normal to leading edge (upper surface)
Γ_{max}	Maximum stream deflection angle
δ	Angle between internal rib and free stream direction
δ'	Angle between upper surface rib and free stream direction
η_ℓ	Correlation parameter for laminar base pressure data
η_t	Correlation parameter for turbulent base pressure data
Θ	Angle between plane spanning leading edges and free stream direction
μ	Viscosity

LIST OF SYMBOLS (continued)

ν	Prandtl-Meyer angle
ξ_{ℓ}	Pressure ratio across lower surface shock
ξ_{u}	Pressure ratio across upper surface expansion
$\xi_{b\ell}$	Base pressure ratio, laminar boundary layer
ξ_{bt}	Base pressure ratio, turbulent boundary layer
ρ	Density
τ	Thickness ratio
τ_{ℓ}	Shear stress, lower surface
τ_{u}	Shear stress, upper surface
Φ	Angle between projection of leading edges onto plane $\perp$ to free stream
Φ_{trans}	Value of Φ at which design point shock is both weak and strong with respect to flow normal to the leading edge
ω	Shock angle
$\omega\|_{\Gamma_{max}}$	Shock angle corresponding to maximum stream deflection angle

LIST OF SYMBOLS (continued)

Subscripts

$( )_b$	Base
$( )_{\bar{c}}$	Two-thirds of the root chord
$( )_{cf}$	Component parallel to leading edge (cross flow)
$( )_{des}$	Design point
$( )_i$	Incompressible
$( )_\ell$	Lower surface; laminar boundary layer; length
$( )_r$	Reference condition
$( )_t$	Turbulent boundary layer
$( )_u$	Upper surface
$( )_x$	Distance from leading edge
$( )_\infty$	Free stream condition
$( )_\perp$	Normal to leading edge
$( )'$	Upper surface

CHAPTER I

INTRODUCTION

Aircraft designed for flight at low supersonic Mach numbers have, for a long time, employed the swept wing with subsonic leading edge to prevent the appearance of shock waves in the flow field (at least ahead of the trailing edge) and thereby avoid the losses associated with them. At higher Mach numbers, say above 3, such a wing would be so highly swept that its low speed performance is unacceptable. One must therefore go to either a variable geometry wing or a wing with a supersonic leading edge. In the latter case, it is desirable from the standpoint of lifting efficiency to have the shock waves attached to the leading edge and confined to the flow over the lower surface. Wings supporting a flow of this type are known collectively as waveriders (1).

The general problem of calculating the flow field about an arbitrary three-dimensional body in a supersonic stream is unmanageable. Thus another approach is usually taken with waveriders, the inverse method, wherein one starts with a simple known flow field and constructs a body to fit it by replacing stream surfaces with the solid walls of the body. The flows which have been used in this context are two-dimensional wedge flow, two-dimensional Prandtl-Meyer expansion and axi-symmetric cone flow.

The first published report of a body of this type is by G. I. Maikapar (2) of the U.S.S.R. in which a pyramid whose base is a polygon with concave (reentrant) sides is surrounded by n regions of wedge flow with the plane oblique shocks spanning the n corners of the polygon. A lifting body derived from wedge flow was first reported by T. Nonweiler (3,4) and is actually $1/n^{th}$ of the Maikapar body. This body, the caret wing, has an inverted V cross section from which it received its name (Figure 1). J. W. Flower (5) has described upper expansion surfaces derived from a Prandtl-Meyer expansion and the combination of these with caret wing lower surfaces. A survey of much of the work done in Great Britain using the inverse method has been presented by J. Seddon (1) and A. Spence.

All bodies derived from a known flow field necessarily have a "design point", the free stream Mach number of the deriving flow and the angle of incidence of the body to that flow. At other flight conditions the simple two-dimensional or axi-symmetric flow will not be maintained and some approximate method must be used to describe the off-design behavior. J. Venn (6) and J. W. Flower have given a qualitative description of the shock patterns for off-design caret wings and have shown that exact solutions other than at the design point exist for certain of these wings. The flow field of a body similar to the reentrant pyramid but with blunt rather

than sharp corners and a shock attached only at the apex has been solved numerically by B. Ziph (7) using a finite difference approximation to the equations governing conical flow. The approximate method used in this study will be described in Chapter II.

This study is concerned only with the caret wing wave-rider. The lower surface of the caret wing can be described by the three parameters δ, Θ and Φ (Figure 1). Delta is the angle between the internal rib and the free stream direction. Theta is the angle between the plane spanning the leading edges and the free stream direction. Phi is the angle between the two free stream surfaces containing the leading edges; i.e., the angle between the projection of the leading edges onto a plane perpendicular to the free stream. The volume in δ, Θ, Φ space of all possible caret wing lower surfaces is shown in Figure 2 as the cylinder with triangular ends ABC and DEF. The ranges of the parameters are $0^\circ \leq \Phi \leq 180^\circ$, $0^\circ \leq \Theta \leq 90^\circ$ and $0^\circ \leq \delta \leq \Theta$. Note that in the limit $\Phi \to 180^\circ$ the caret wing becomes a two-dimensional wedge.

Caret wings for which a design Mach number, M_{des}, exists form a more restricted class. At the design point a plane oblique shock spans the leading edges and δ and Θ are the stream deflection angle and shock angle, respectively, of the corresponding wedge flow. For any given Θ there is a maximum δ, occurring at infinite Mach number, above which wedge flow

does not have an attached shock solution. Thus M_{des} will exist only for those values of δ less than or equal this maximum. In Figure 2, the volume of all caret wings that have a design point is the cylinder with end surfaces AGB and DHE.

This volume can itself be divided into two parts, depending on whether the wedge flow corresponding to any δ, Θ pair is a weak or strong shock solution. For wedge flow, the strong shock is not observed in practice and it is therefore not expected to occur in the caret wing flow field either. Only caret wings derivable from wedge flow of the weak type will be considered in the remainder of this paper. In Figure 2, the volume in δ, Θ, Φ space of these caret wings is the cylinder with end surfaces AGIB and DHJE. The terms "weak" and "strong" are used above in the conventional sense and should not be confused with their use later on in discussions about the component of the free stream velocity normal to the leading edge.

The caret wing body studied here will be completed with an upper expansion surface defined in a manner analogous to the lower surface and a base surface normal to the free stream direction (Figure 3). Just as the lower surface is defined by the parameters δ, Θ and Φ, the upper surface will be defined by δ', Θ and Φ where δ' is the angle between the upper surface rib and the free stream direction and Θ and Φ are the

same as for the lower surface. The common values of Θ and Φ guarantee that the leading edges of the lower and upper surfaces coincide. To reduce the number of independent variables, δ' will always be taken equal to 3^{o} less than δ. As a result, the thickness ratio will be about 0.05.

The main concern of this study is the estimation of the lift coefficient, drag coefficient and lift-to-drag ratio of caret wings and the identification of their dependence on body geometry, Mach number and Reynolds number. Mach numbers and Reynolds numbers considered range from 1.5 to 5.0 and from 10^{5} to 10^{8} respectively. The aerodynamic coefficients are calculated by combining estimates of the upper, lower and base surface pressures and estimates of the skin friction on the upper and lower surfaces. Calculations of the pressures on the upper and lower surfaces are based on supersonic, inviscid, perfect fluid gas dynamics and calculations of base pressures rely on published experimental data. The skin friction calculations are for flat plates with zero pressure gradient.

A comparison of the performance of caret wings to delta wings will also be made.

CHAPTER II

A MODEL OF THE CARET WING FLOW FIELD

2.1 Analysis of the Caret Wing Flow Field at Design Conditions

It is well known that the velocity component parallel to an oblique shock wave passes through unchanged and that the shock acts as a normal shock to the normal velocity component. Except for relations involving ratios of static-to-total conditions, the changes in properties across an oblique shock are the same as for the normal velocity components and a normal shock. On this basis the use of normal shock tables is extended to oblique shock waves (8). More generally, one can take any oblique shock flow, add or subtract a velocity component of any magnitude which is tangent to the shock and calculate - based on the new velocities, shock angle and stream deflection angle - the change in properties across the shock in the original flow.

An interesting phenomenon associated with this calculation procedure is that, while the changes in properties across the shocks are the same for both flows, the shock type ("weak" or "strong") may change. In a simple case, for example, to find the pressure ratio across a weak oblique shock in two-dimensional wedge flow one might calculate the Mach number of the velocity component normal to the shock and look up the

pressure ratio in a normal shock table. However, the normal shock is of the strong type (the weak solution corresponding to the normal shock is a Mach wave) and thus the question arises, whether to use the weak or strong solution. Clearly, the spatial location of the shock cannot change. In the example under discussion, the Mach number component used in the table look up is normal to the shock and the solution which preserves this orientation, the strong solution, is the desired one.

A slightly different application of the concept of subtracting velocity components tangent to a shock wave is found in the analysis of the swept wedge of infinite span. The component of the free stream velocity which is parallel to the leading edge of the wedge will also be tangent to any shock attached to the leading edge. Therefore, this velocity component can be subtracted from the flow field by a Galilean transformation of coordinates leaving an upstream velocity which is normal to the leading edge and which is deflected by the wedge through the angle the wedge makes as measured in a plane perpendicular to the leading edge. This is just two-dimensional wedge flow. If the normal velocity component is supersonic and the wedge angle normal to the leading edge is small enough, weak and strong attached shock solutions are mathematically possible. In practice the weak shock is always observed in two-dimensional wedge flow and the

existence of crossflow in the swept wedge problem will not alter this, even though the strong shock with respect to the normal velocity component is, in some cases, weak with respect to the free stream. If the normal velocity component is subsonic or the wedge angle is too large, no attached shock solution exists.

These ideas will now be applied to the caret wing flow field. The caret wing's lower surface is formed from sections of two swept wedges which are joined at the vertical symmetry plane of the wing. At the design point, a plane shock spans the leading edges and deflects the free stream through the angle δ, the angle between the free stream and the internal rib. In the same manner as the swept wedge of infinite span, the component of the free stream velocity parallel to either of the caret wing's leading edges, $\bar{V}_{cf}$, must be tangent to the design point shock and, therefore, can be subtracted from the free stream, $\bar{V}_\infty$. The shock can then be analyzed using the component of the free stream velocity normal to the leading edge, $\bar{V}_\perp$, and the wedge angle normal to the leading edge, $\Gamma_\perp$, just as well as from the point of view of $\bar{V}_\infty$ and δ.

Consider a family of caret wings, all derivable from the same two-dimensional wedge flow. They will have the angles δ and Θ in common while Φ varies from zero to 180 degrees

(Figure 4). A single design Mach number determined by δ and Θ will also be common to the members of this family.

In the limit $\Phi = 180^{\circ}$ the caret wing is a two-dimensional wedge. The velocity component normal to the leading edge is equal to the free stream velocity and the wedge angle normal to the leading edge is equal to δ. As mentioned in the introduction, only caret wings whose design point shocks are weak with respect to the free stream are being considered. So when $\Phi = 180^{\circ}$ the design point shock is also weak with respect to $\overline{V}_{\perp}$.

In the limit $\Phi = 0^{\circ}$ the velocity component normal to the leading edge is also perpendicular to the design point shock. Thus the shock must be strong with respect to $\overline{V}_{\perp}$. As explained earlier, this shock is never found on the swept wedge of infinite span and therefore doubt is cast on the existence of the caret wing's design point flow as Φ approaches zero. However, the fact that the strong shock is never observed on an isolated swept wedge is not sufficient grounds for dismissing the possibility of its occurrence here, since each leading edge of the caret wing lies within the Mach cone of influence of the opposite wing panel. More will be said about the tenability of these strong shock solutions in the next section.

Evidently, at some value of Φ between zero and 180 degrees the design point shock's type with respect to $\bar{V}_\perp$ undergoes a transition from weak to strong. The value of Φ at which this occurs, Φ_{trans}, must be characterized by a smooth transition between types because physically the shock is the same regardless of Φ, only the velocity component being analyzed changes with Φ. For any given Mach number there is a maximum angle, Γ_{max}, through which a streamline can be deflected by a single oblique shock wave and at which the weak and strong shocks coincide (the governing cubic equation has a double root). Thus Φ_{trans} is that value of Φ where Γ_{max} equals $\Gamma_\perp$. This is illustrated in Figure 5 for the particular caret wing family $\delta = 5.0^\circ$ and $\Theta = 34.0^\circ$, where Γ_{max}, $\Gamma_\perp$ and $\Gamma_{max} - \Gamma_\perp$ are plotted as functions of Φ. $\Gamma_{max} - \Gamma_\perp$ goes to zero at $\Phi = \Phi_{trans} = 42.29^\circ$.

Caret wings whose design point shocks are weak with respect to $\bar{V}_\infty$ can now be further classified according to whether the shock is weak or strong with respect to $\bar{V}_\perp$. Wings with Φ greater than Φ_{trans} have the weak solution and those with Φ less than Φ_{trans} the strong one. Φ_{trans} is plotted as a function of Θ with δ as a parameter in Figure 6. Using the curve corresponding to the value of δ one is interested in, caret wings lying to the left of the curve have design point shocks that are weak with respect to $\bar{V}_\perp$ and those lying to the right,

strong shocks. The range of Θ for a given δ varies from a minimum when $M_{des} = \infty$ to a maximum when $\Gamma_{max}\ (M_{des}) = \delta$.

It is interesting to plot, for the flow normal to the leading edge of a family of caret wings, the pressure ratio of both the weak and strong shocks as a function of Φ. This is done for the family $\delta = 5.0^{o}$ and $\Theta = 34.0^{o}$ at $M = M_{des} = 2.02$ in Figure 7. Starting at $\Phi = 180^{o}$ and down to $\Phi = \Phi_{trans} = 42.29^{o}$ the weak shock gives the design point pressure ratio which is a constant independent of Φ. At $\Phi = \Phi_{trans}$ the strong shock picks up where the weak shock leaves off and continues the design point pressure ratio down to $\Phi = 0^{o}$. The weak and strong solutions, patched together at $\Phi = \Phi_{trans}$, give the flow field the family of caret wings was derived from.

2.2 Extension of the Swept Wedge Analysis to Off-Design Conditions

Schlieren photographs taken in wind tunnel studies of Maikapar bodies at Mach numbers below M_{des} indicate that a convex curved shock attached to the leading edges replaces the plane shock found at the design point (9). For $M_{\infty} < M_{des}$ and $\Phi > \Phi_{trans}$, Venn (6) and Flower suggest a convex shock composed of a curved central section joined to plane shocks emanating from the leading edges (Figure 8). The shock is plane outside the Mach cone from the caret wing's apex and is the weak shock calculated using $\bar{V}_{\perp}$ and $\Gamma_{\perp}$.

For $M_\infty > M_{des}$, Venn (6) and Flower suggest either a bifurcated shock pattern or a pattern where plane shocks from the leading edges intersect at the vertical symmetry plane and are followed by a complex system of shocks further inside the wing (Figure 8). In either case the leading edge shocks are plane outside the Mach cone from the wing's apex, are inclined inside the plane spanning the leading edges and are the weak shock calculated using $\bar{V}_\perp$ and $\Gamma_\perp$.

These complicated shock patterns will be approximated here by two plane shocks, one from each leading edge, that intersect at the wing's vertical symmetry plane (Figure 8). It was shown in the previous section that the on-design caret wing can be treated as a swept wedge. The model of the caret wing's off-design behavior adopted here will be to extend the use of the swept wedge calculations to all conditions, except for $\Phi < \Phi_{trans}$. Within this approximation, the pressure on the caret wing's lower surface is a constant determined by the pressure ratio across the leading edge shocks.

The model just described for the caret wing's lower surface flow field gives the exact solution under the assumptions of steady, supersonic, inviscid, perfect fluid aerodynamics when the free stream Mach number, M_∞, is equal to the design Mach number. It also gives the exact solution in the limits $\Phi = 180^\circ$ or $\delta = 0^\circ$.

Under the same assumptions, the model gives a shock tangent to the actual shock at the leading edges regardless of the influence of the opposite wing panel. This is because the Mach number and stream deflection angle at the leading edges are known and are sufficient to determine the shock. Furthermore, the shocks given by the model will also be correct outside of the Mach cone from the apex of the caret wing. It should be noted that this model of the flow field violates the boundary condition that there be no flow across the vertical symmetry plane.

The average pressure on the lower surface of a caret wing is approximated by the pressure downstream of the model's leading edge shocks. Useful bounds on the magnitude of the error in this approximation are not known. However, something can be said about the sign of the error. A method of determining the magnitude of the error will be suggested in Chapter V.

For cases where $M_\infty < M_{des}$, the model's shocks are inclined outside of the plane spanning the leading edges. Therefore, they direct the flow away from the vertical symmetry plane and expansions will be present in the actual flow which curve the shock toward the internal rib so that it is perpendicular to the symmetry plane at their intersection (6). Thus the model gives too high a pressure in this case.

For cases where $M_\infty > M_{des}$, the model's shocks are inclined inside the plane spanning the leading edges. Therefore they direct the flow toward the symmetry plane and further compression will be present in the actual flow (6). In this case the model gives a pressure below the correct value.

More can now be said about the strong shock solutions for $\Phi < \Phi_{trans}$. At the design Mach number it was possible to make a smooth transition from the weak to strong cases. This transition occurred at Φ_{trans}, where Γ_{max} is equal to $\Gamma_\perp$ and the weak and strong solutions coincide. $\Gamma_\perp$ is a geometric property of the caret wing and does not change with M_∞. However, Γ_{max} is a monotonically increasing function of M_∞. If M_∞ is raised above M_{des}, then there will no longer be any value of Φ for which Γ_{max} is equal to $\Gamma_\perp$ and no smooth transition from the weak to the strong cases is possible. In Figure 5 the entire curve for Γ_{max} vs. Φ is shifted upwards when $M_\infty > M_{des}$ and $\Gamma_{max} - \Gamma_\perp$ never goes to zero. It is not likely that a discontinuous change in shock pattern or lower surface pressure will occur with an infinitesimal change in body geometry or flight conditions and for this reason the strong shock solutions must be considered untenable. Other possibilities include a weak shock at the leading edge followed by a complicated system of shocks further inside the wing, unsteady behavior or detachment. Venn (6) and Flower suggest the first of these on the

grounds that weak shocks are always observed on two-dimensional wedges. Because of the uncertainty here, caret wings with design point shocks that are strong with respect to $\bar{V}_\perp$ will not be considered in calculations of lift, drag and lift-to-drag ratio.

One additional generalization about the caret wing's off-design behavior will be made. When M_∞ is reduced below M_{des}, the entire curve for Γ_{max} vs. Φ in Figure 5 is shifted downward. This leaves a neighborhood about Φ_{trans} in which Γ_{max} is less than $\Gamma_\perp$ and consequently, the shock is detached.

2.3 The Upper Surface Flow Field

The model for the upper surface flow field is analogous to the model for the lower surface. Corresponding to the shock on the lower surface is a Prandtl-Meyer expansion of the flow normal to the leading edge for the upper surface. The component of the free stream velocity normal to the leading edge, $\bar{V}_\perp$, is the same as before and the expansion angle is calculated in the same way as $\Gamma_\perp$ except that δ' is used instead of δ. The average pressure on the upper surface of a caret wing is approximated by the pressure downstream of the Prandtl-Meyer expansion at the leading edge. Since the expansion at the leading edge directs the flow toward the vertical symmetry plane, additional compression will take place in the actual flow and the model's estimate of the upper

surface pressure must be too low. This model also violates the boundary condition of no flow across the symmetry plane.

2.4 Estimate of Skin Friction

An approximation of the skin friction drag consistent with the constant pressure surfaces of the upper and lower surface flow field models is employed here. The calculation is for a two-dimensional flat plate with zero pressure gradient. The Mach numbers and Reynolds numbers downstream of the lower surface shock and upper surface expansion are used as the free stream conditions in the calculation of the skin friction on the lower and upper surfaces respectively. A power law for the variation of viscosity with temperature valid in the range $300^{\circ}R$ to $900^{\circ}R$ is used to calculate the Reynolds numbers downstream of the shock and expansion (8). Skin friction estimates for both laminar and turbulent boundary layers are made.

The local value of the skin friction coefficient for laminar, incompressible flow based on distance from the leading edge in the direction of the external flow (parallel to the internal rib for the lower surface and parallel to the upper surface rib for the upper surface) is integrated over the lower and upper wetted surfaces to obtain the average skin friction coefficients on the lower and upper surfaces.

These are multiplied by the ratio of compressible to incompressible skin friction coefficients based on an adiabatic wall, Prandtl number equal to one and exponent in the viscosity law equal to 0.765 given by Schlichting (10) for the Mach number range zero to ten.

Schlichting (10) found an empirical equation which, in the range $5 \times 10^5 < Re_\ell < 10^9$, fits the exact formula for the turbulent, incompressible skin friction coefficient based on a logarithmic velocity profile. This is integrated over the lower and upper wetted surfaces to give the average skin friction coefficients on the lower and upper surfaces. These are then multiplied by the ratio of compressible to incompressible skin friction coefficients from the theory of R. E. Wilson as reported by Schlichting (10). This ratio is valid for the Mach number range zero to ten.

2.5 Estimate of Base Pressure

The calculations of caret wing base pressure rely on published experimental data. The main source of this data is Chapman (11), Wimbrow and Kester's wind tunnel study of blunt trailing edge wings at Mach numbers 1.5, 2.0 and 3.1 for both laminar and turbulent boundary layers. Base pressure data taken on the vertical fin of the X-15 at Mach 5 has been used to extend the Mach number range of the turbulent boundary layer data (12). The work of Rom (13), Gadd (14) and Korst (15) have been compared to Chapman's data. Base pressure data

taken on Maikapar bodies at the Aerophysics Laboratory (16,17) have also been compared to the other data. Chapman's graphs of base pressure ratio vs. ratio of boundary layer thickness to trailing edge thickness appear in Figure 9 with the other authors' data added for comparison. The Maikapar body base pressures tend to be higher than the other data. This is apparently due to the lower aspect ratio.

Chapman (11) found that base pressure data at a given free stream Mach number is correlated to the ratio of boundary layer thickness at the trailing edge to trailing edge thickness. This variable depends on the thickness ratio and Reynolds number based on wing chord. The thickness ratio of a caret wing is constant at all spanwise locations. The free stream Reynolds number based on half the length is used as an average value over the span.

Straight lines have been fit to Chapman's (11) turbulent boundary layer base pressure curves and a line through the X-15 data point and parallel to Chapman's $M_\infty = 3.1$ line has been used for $M_\infty = 5.0$. Curves have been fitted to Chapman's laminar boundary layer base pressure curves. At intermediate Mach numbers linear interpolation between the curves is used.

CHAPTER III

CALCULATION OF THE LIFT COEFFICIENT, DRAG COEFFICIENT AND LIFT-TO-DRAG RATIO

3.1 Introduction

There are six independent variables in this problem. Four of them, δ, δ', Θ and Φ, define the caret wing's geometry and incidence to the free stream. The other two, the free stream Mach number, M_∞, and the free stream Reynolds number, Re_∞, specify the flight conditions. For convenience, the free stream Reynolds number has been based on the square root of the plan area, S, so that by holding Re_∞ constant wings of the same plan area rather than length can be compared. A simple trigonometric formula which relates the Reynolds numbers based on $\sqrt{S}$ and length is presented in Section 3.6.

The lift coefficient, C_L, drag coefficient, C_D, and lift-to-drag ratio, L/D, are to be calculated as functions of the six independent variables. Five cases are considered: 1, no skin friction or base drag; 2, with laminar skin friction but no base drag; 3, with turbulent skin friction but no base drag; 4, with laminar skin friction and base drag; 5, with turbulent skin friction and base drag.

Given a set of values for the independent variables, a preliminary procedure must be undertaken to make sure the caret wing belongs to the group being considered in this study. To be a member of this group M_{des} must exist, the design point shock must be weak with respect to the free stream and Φ must be greater than or equal to Φ_{trans}.

If the above conditions are satisfied, the calculation of C_L, C_D and L/D can proceed. The equations for inviscid, compressible flow are taken from NACA Report 1135 (8). The ratio of specific heats, c_p/c_v, is assumed equal to 1.4.

3.2 Mach Number and Wedge Angle Normal to the Leading Edge

Formulas for $\bar{M}_\perp$ and $\Gamma_\perp$ will be needed in three phases of the calculation of C_L, C_D and L/D. They are necessary in the determination of Φ_{trans}, the pressure ratio across the lower surface shock and the pressure ratio across the upper surface expansion. In the derivation which follows, the Mach number will be treated as a vector.

Let the x-axis of a cartesian coordinate system be aligned with the free stream direction and the y and z-axes be vertical and horizontal respectively. Also, let the origin of coordinates be located at the apex of a caret wing of unit length (Figure 3). Point A is the caret wing apex, point B is the left-hand wing tip and point C is the

intersection of the internal rib with the base. Vector $\bar{B}$ is a vector pointing from the origin to point B.

The (x,y,z) coordinates of points A, B and C are

$$A = (0,0,0) \tag{3.2.1}$$

$$B = (1,b_2,b_3) \tag{3.2.2}$$

$$C = (1,c_2,0) \tag{3.2.3}$$

where

$$b_2 = - \tan \Theta \tag{3.2.4}$$

$$b_3 = \tan \Theta \tan \frac{\Phi}{2} \tag{3.2.5}$$

$$c_2 = - \tan \delta. \tag{3.2.6}$$

The component of $\bar{M}_\infty$ parallel to the left-hand leading edge, $\bar{M}_{cf}$, will be calculated by forming the dot product of $\bar{M}_\infty$ and a unit vector parallel to the leading edge. The free stream Mach number in vector form is

$$\bar{M}_\infty = M_\infty \hat{i} = (M_\infty,0,0). \tag{3.2.7}$$

A unit vector parallel to the leading edge is

$$\frac{\bar{B}}{|\bar{B}|} = \frac{(1,b_2,b_3)}{\sqrt{1+b_2^2+b_3^2}}. \tag{3.2.8}$$

The Mach number parallel to the leading edge is

$$\bar{M}_{cf} = \left[\bar{M}_\infty \cdot \frac{\bar{B}}{|\bar{B}|}\right] \frac{\bar{B}}{|\bar{B}|}$$

$$= \frac{M_\infty}{1+b_2^2+b_3^2} \quad (1, b_2, b_3) \qquad (3.2.9)$$

and its magnitude is given by

$$M_{cf} = |\bar{M}_{cf}| = \frac{M_\infty}{\sqrt{1+b_2^2+b_3^2}} \qquad (3.2.10)$$

Calculation of the Mach number normal to the left-hand leading edge is now simply a matter of subtracting $\bar{M}_{cf}$ from $\bar{M}_\infty$.

$$\bar{M}_\perp = \bar{M}_\infty - \bar{M}_{cf} = \frac{M_\infty}{1+b_2^2+b_3^2} \quad (b_2^2+b_3^2, -b_2, -b_3) \qquad (3.2.11)$$

$$M_\perp = |\bar{M}_\perp| = \frac{M_\infty \sqrt{b_2^4+2b_2^2b_3^2 + b_3^4+b_2^2+b_3^2}}{1 + b_2^2 + b_3^2} \qquad (3.2.12)$$

The wedge angle normal to the left-hand leading edge, $\Gamma_\perp$, is the angle between $\bar{M}_\perp$ and the plane containing the left-hand lower surface of the caret wing (Figure 3). It will be found using the dot product of $\bar{M}_\perp$ and a unit vector normal to the lower surface, $\overline{ABC}_\perp$.

The equation of a plane with normal vector (ℓ,m,n) is

$$\ell x + my + nz = c. \tag{3.2.13}$$

Equation (3.2.13) can be solved for ℓ, m, n and c subject to the condition that the plane contain the points A, B and C and that vector (ℓ,m,n) be of unit length. The solution is

$$\ell = -c_2 m \tag{3.2.14}$$

$$m = \pm \left[c_2^2 + 1 + \left(\frac{c_2-b_2}{b_3}\right)^2 \right]^{-1/2} \tag{3.2.15}$$

$$n = \left(\frac{c_2-b_2}{b_3}\right) m \tag{3.2.16}$$

$$c = 0. \tag{3.2.17}$$

Thus a unit vector normal to the caret wing's left-hand lower surface is

$$\overline{ABC}_{\perp} = \left[c_2^2 + 1 + \left(\frac{c_2 - b_2}{b_3}\right)^2 \right]^{-1/2} \left(-c_2, 1, \frac{c_2 - b_2}{b_3}\right). \quad (3.2.18)$$

$\overline{ABC}_{\perp}$ is the inward normal due to the selection of the positive sign in Equation (3.2.15).

The angle between $\bar{M}_{\perp}$ and $\overline{ABC}_{\perp}$, β, satisfies the relation

$$\bar{M}_{\perp} \cdot \overline{ABC}_{\perp} = M_{\perp} \cos \beta \quad (3.2.19)$$

and is equal to $90^{\circ}-\Gamma_{\perp}$ (Figure 3). Solving Equation (3.2.19) for $\Gamma_{\perp}$

$$\sin \Gamma_{\perp} = \frac{\bar{M}_{\perp} \cdot \overline{ABC}_{\perp}}{M_{\perp}} \quad (3.2.20)$$

$$\Gamma_{\perp} = \sin^{-1} \frac{-c_2(1 + b_2^2 + b_3^2)}{\sqrt{c_2^2+1+\left(\frac{c_2-b_2}{b_3}\right)^2}\ \sqrt{b_2^4+2b_2^2b_3^2+b_3^4+b_2^2+b_3^2}} \quad (3.2.21)$$

The preliminary procedure mentioned in Section 3.1 can now be carried out. Calculation of M_{des} is the first step. At the design point, δ and Θ are the stream deflection angle and shock angle with respect to the free stream of the flow

through an oblique shock. Thus the formula for the Mach number upstream of an oblique shock can be used to find M_{des}. If M_{des} does not exist, Equation (3.2.22) will give a number less than 1.

$$M_{des}^2 = \frac{10(\cot \Theta + \tan \delta)}{5 \sin 2\Theta - \tan \delta(7 + 5 \cos 2\Theta)} \qquad (3.2.22)$$

The second step is to determine whether or not the design point shock is weak with respect to the free stream. For a given Mach number the shock angle can range from the Mach angle, $\sin^{-1} \frac{1}{M}$, to 90°, depending on the stream deflection angle. At the maximum stream deflection angle the shock angle has some intermediate value. Below this are the weak shocks, above it the strong ones and exactly at this value the shock is both weak and strong. Thus the design point shock is weak with respect to the free stream if Θ is less than or equal to the shock angle which would give the largest possible deflection of a streamline at M_{des}. This condition is expressed in Equation (3.2.23).

$$\Theta \leq \sin^{-1} \sqrt{\frac{3 M_{des}^2 - 5 + \sqrt{3(3M_{des}^4 + 4 M_{des}^2 + 20)}}{7 M_{des}^2}} \qquad (3.2.23)$$

The third step is to determine whether or not $\Phi \geq \Phi_{trans}$ which means Φ_{trans} must be found. Given M_{des}, δ and Θ, Φ_{trans} is the value of Φ for which $\Gamma_{max} - \Gamma_{\perp}$ goes to zero. $\Gamma_{\perp}(\delta,\Theta,\Phi)$ is given by Equations (3.2.21) and (3.2.4-6). Γ_{max} is a function of $M_{\perp}(M_{des},\Theta,\Phi)$, which is given by Equations (3.2.12), (3.2.22), (3.2.4) and (3.2.5). The relation between Γ_{max} and $M_{\perp}$ is

$$\Gamma_{max} = \cot^{-1}\left[\tan(\omega|_{\Gamma_{max}})\left[\frac{6\ M_{\perp}^2}{5(M_{\perp}^2\sin^2(\omega|_{\Gamma_{max}})-1)}\right]\right] \quad (3.3.24)$$

where $\omega|_{\Gamma_{max}}$ is the shock angle that would occur if a streamline were deflected through the angle Γ_{max} and is given by

$$\sin^2(\omega|_{\Gamma_{max}}) = \frac{3\ M_{\perp}^2 - 5 + \sqrt{3(3M_{\perp}^4 + 4\ M_{\perp}^2 + 20)}}{7\ M_{\perp}^2} \quad (3.2.25)$$

The equations are too cumbersome to set $\Gamma_{max} - \Gamma_{\perp}$ equal to zero and solve for Φ_{trans}. It is simpler, especially on the computer, to search for the value of Φ at which $\Gamma_{max} - \Gamma_{\perp}$ goes to zero. Once Φ_{trans} is found, it can be

compared to Φ. If $\Phi \geq \Phi_{trans}$, the design point shock is weak with respect to $M_\perp$ and calculation of C_L, C_D and L/D can begin.

3.3 Pressure Ratio Across Lower Surface Shock

An attached shock will not be possible if the leading edge is subsonic or $\Gamma_{max}\left\{M\ (M_\infty,\Theta,\Phi)\right\} < \Gamma_\perp(\delta,\Theta,\Phi)$. $M_\perp\ (M_\infty,\Theta,\Phi)$ is given by Equations (3.2.12), (3.2.4) and (3.2.5). If $M_\perp < 1$, the leading edge is subsonic and calculation of the aerodynamic coefficients for the current values of the independent variables is aborted. Otherwise $\Gamma_{max}\ (M_\perp)$ is calculated using Equations (3.2.24) and (3.2.25) and $\Gamma_\perp$ is calculated from Equations (3.2.21) and (3.2.4-6). Again, if $\Gamma_{max} < \Gamma_\perp$ further calculation is terminated. However, if $\Gamma_{max} \geq \Gamma_\perp$, a weak shock is attached to the leading edge and the pressure ratio can be found as follows.

No simple expression for the pressure ratio in terms of $M_\perp$ and $\Gamma_\perp$ exists so it is necessary to calculate the shock angle, ω, as an intermediate step. There is a cubic equation for $\sin^2\omega$ with coefficients that depend on $M_\perp$ and $\Gamma_\perp$; however, it was found to be easier to search for the value of ω between $\sin^{-1}\ (1/M_\infty)$ and $\omega|_{\Gamma_{max}}$, which gives the correct value of $\Gamma_\perp$ using the formula

$$\Gamma_{\perp} = \cot^{-1}\left[\tan\omega\left[\frac{6\,M^2}{5(M^2\sin^2\omega-1)} - 1\right]\right] . \qquad (3.3.1)$$

Once ω is known, the pressure ratio across the shock, ξ_{ℓ}, is given by

$$\xi_{\ell} = \frac{p_{\ell}}{p_{\infty}} = \frac{7\,M^2\sin^2\omega - 1}{6} \qquad (3.3.2)$$

where p_{∞} and p_{ℓ} are the static pressures upstream and downstream of the shock.

3.4 Pressure Ratio Across Upper Surface Expansion

The expansion angle normal to the leading edge, $\Gamma_{\perp}'$, through which the upper surface flow turns is calculated in the same manner as $\Gamma_{\perp}$ except that δ', C' and c_2' replace δ, C and c_2 in Equations (3.2.3), (3.2.6) and (3.2.21). These equations become

$$C' = (1, c_2', 0) \qquad (3.4.1)$$

$$c_2' = -\tan\delta' \qquad (3.4.2)$$

$$\Gamma_{\perp}' = \sin^{-1}\left[\frac{-c_2'\,(1 + b_2^2 + b_3^2}{\sqrt{c'^2_2+1+\left(\frac{c_2-b_2}{b_3}\right)^2}\ \sqrt{b_2^4+2b_2^2b_3^2+b_3^4+b_2^2+b_3^2}}\right]. \qquad (3.4.3)$$

In order to calculate the pressure ratio across the upper surface expansion, ξ_u, the Mach number normal to the leading edge and downstream of the expansion, $M_{u\perp}$, must be found. To find $M_{u\perp}$ the Prandtl-Meyer angle, ν, through which a stream would turn in expanding from M=1 to $M=M_{u\perp}$ is needed and is given by

$$\nu=2.4495\ \tan^{-1}(.40825\sqrt{M_\perp^2-1})-\tan^{-1}\sqrt{M_\perp^2-1}+\Gamma_\perp'. \qquad (3.4.4)$$

$M_{u\perp}$ is found using the following equation by searching for the value which gives the correct Prandtl-Meyer angle, ν.

$$\nu=2.4495\ \tan^{-1}(.40825\sqrt{M_{u\perp}^2-1})-\tan^{-1}\sqrt{M_{u\perp}^2-1} \qquad (3.4.5)$$

Once $M_{u\perp}$ is known, the pressure ratio can be determined with the formula

$$\xi_u = \frac{p_u}{p_\infty} = \left[\frac{5+M_u^2}{5+M^2}\right]^{-3.5} \qquad (3.4.6)$$

where p_∞ and p_u are the static pressures upstream and downstream of the expansion.

3.5 Average Skin Friction Coefficient

The calculation of four quantities will be described in this section. They are the average laminar and turbulent skin friction coefficients on the caret wing's lower surface, $C_{f\ell\ell}$ and $C_{ft\ell}$, and the average laminar and turbulent skin friction coefficients on the upper surface, $C_{f\ell u}$ and C_{ftu}.

Reynolds numbers based on length downstream of the lower surface shock and upper surface expansion are required for the calculation of the skin friction coefficients. A power law for the variation of viscosity with temperature of the form

$$\frac{\mu}{\mu_r} = \left(\frac{T}{T_r}\right)^{0.76}, \quad 300^{\circ}R < T < 900^{\circ}R \tag{3.5.1}$$

will be used in their determination. The Reynolds number ratio across the lower surface shock is given by

$$\frac{Re_{\ell_2}}{Re_\infty} = \frac{\ell_2}{\sqrt{S}} \frac{\rho_\ell}{\rho_\infty} \frac{V_\ell}{V_\infty} \frac{\mu_\infty}{\mu_\ell} \tag{3.5.2}$$

where ℓ_2 is the length of the internal rib and the subscript ℓ refers to a property of the lower surface flow downstream of the shock. Expressions for the ratios in Equation (3.5.2) are

$$\frac{\ell_2}{\sqrt{S}} = \frac{1}{\cos\delta\sqrt{\tan\Theta\tan\frac{\Phi}{2}}} \tag{3.5.3}$$

$$\frac{\rho_\ell}{\rho_\infty} = \frac{6\,\xi_\ell + 1}{\xi_\ell + 6} \tag{3.5.4}$$

$$\frac{V_\ell}{V_\infty} = \left[1 - \frac{5(\xi_\ell^2-1)}{M_\infty^2(6\,\xi_\ell+1)}\right]^{1/2} \tag{3.5.5}$$

$$\frac{\mu_\infty}{\mu_\ell} = \left(\frac{T_\infty}{T_\ell}\right)^{0.76} = \left[\frac{6\,\xi_\ell+1}{\xi_\ell(\xi_\ell+6)}\right]^{0.76} \tag{3.5.6}$$

Substituting Equations (3.5.3-6) into Equation (3.5.2) gives

$$\frac{Re_{\ell_2}}{Re_\infty} = \frac{\left[\frac{6\xi_\ell+1}{\xi_\ell+6}\right]\left[1 - \frac{5(\xi_\ell^2-1)}{M_\infty^2(6\xi_\ell+1)}\right]^{1/2}\left[\frac{6\xi_\ell+1}{\xi_\ell(\xi_\ell+6)}\right]^{0.76}}{\cos\delta\sqrt{\tan\Theta\tan\frac{\Phi}{2}}} \tag{3.5.7}$$

The Reynolds number ratio across the upper surface expansion is given by

$$\frac{Re_{\ell_3}}{Re_\infty} = \frac{\ell_3}{\sqrt{S}} \frac{\rho_u}{\rho_\infty} \frac{M_u}{M_\infty} \frac{a_u}{a_\infty} \frac{\mu_\infty}{\mu_u} \tag{3.5.8}$$

where ℓ_3 is the length of the upper surface rib and the subscript u refers to a property of the upper surface flow downstream of the expansion. Expressions for the ratios in Equation (3.5.8) are

$$\frac{\ell_3}{\sqrt{S}} = \frac{1}{\cos \delta' \sqrt{\tan \Theta \tan \frac{\Phi}{2}}} \tag{3.5.9}$$

$$\frac{\rho_u}{\rho_\infty} = \left[\frac{5 + M_u^2}{5 + M_\infty^2}\right]^{-\frac{5}{2}} \tag{3.5.10}$$

$$\frac{a_u}{a_\infty} = \left[\frac{5 + M_u^2}{5 + M_\infty^2}\right]^{-\frac{1}{2}} \tag{3.5.11}$$

$$\frac{\mu_\infty}{\mu_u} = \left(\frac{T_\infty}{T_u}\right)^{0.76} = \left[\frac{5 + M_u^2}{5 + M_\infty^2}\right]^{0.76} \tag{3.5.12}$$

where

$$M_u^2 = (5 + M_\infty^2)\left[\xi_u\right]^{-2/7} - 5 \qquad (3.5.13)$$

Substituting Equations (3.5.9-13) into Equation (3.5.8) gives

$$\frac{Re_{\ell_3}}{Re_\infty} = \frac{\sqrt{(5+M_\infty^2)\ \xi_u^{-2/7} - 5}}{M_\infty \cos\delta' \sqrt{\tan\Theta \tan\frac{\Phi}{2}}} (\xi_u)^{\frac{4.48}{7}} \qquad (3.5.14)$$

The Mach number of the lower surface flow downstream of the shock is given by

$$M_\ell^2 = \frac{M_\infty^2(6\xi_\ell+1) - 5(\xi_\ell^2-1)}{\xi_\ell(\xi_\ell+6)} \qquad (3.5.15)$$

The four average skin friction coefficients can now be calculated. The local, laminar, incompressible skin friction coefficient is

$$C_{f\ell}(x) = \frac{.664}{\sqrt{Re_x}} \qquad (3.5.16)$$

where x is the distance from the leading edge in the streamwise direction. The average over the lower wetted surface is given by

$$(C_{f\ell\ell})_i = \frac{1}{h}\int_0^h dz \, \frac{1}{\ell(z)} \int_0^{\ell(z)} dx \, C_{f\ell}(x) = \frac{2.656}{\sqrt{Re_{\ell_2}}} \qquad (3.5.17)$$

where h is the semi-span, $\ell(z) = \frac{\ell_2}{h} z$ (Figure 10) and the subscript i indicates incompressible flow. For the upper surface

$$(C_{f\ell u})_i = \frac{2.656}{\sqrt{Re_{\ell_3}}}. \qquad (3.5.18)$$

Multiplying Equations (3.5.17) and (3.5.18) by the ratio of compressible-to-incompressible laminar skin friction coefficients gives

$$C_{f\ell\ell} = \frac{2.656-.0718M_\ell}{\sqrt{Re_{\ell_2}}}, \; 0 < M_\ell < 10 \qquad (3.5.19)$$

$$C_{f\ell u} = \frac{2.656-.0718M_u}{\sqrt{Re_{\ell_3}}}, \; 0 < M_u < 10. \qquad (3.5.20)$$

The average turbulent, incompressible skin friction coefficient between the leading edge and a point a distance ℓ from it is

$$C_{ft}(\ell) = \frac{.455}{(\log_{10} Re_\ell)^{2.58}}, \quad 5\times10^5 < Re_\ell < 10^9. \qquad (3.5.21)$$

The average over the lower wetted surface is

$$(C_{ft\ell})_i = \frac{1}{h}\int_0^h C_{ft}(\ell(z))\, dz$$

$$= \frac{.455}{h}\int_0^h \left[\log Re_{\ell_2} + \log \frac{z}{h}\right]^{-2.58} dz \qquad (3.5.22)$$

where $\ell(z) = \frac{\ell_2}{h} z$ and h is the semi-span (Figure 10).

Using the binomial expansion

$$(C_{ft\ell})_i \approx \frac{.455}{h}\int_0^h \left[(\log Re_{\ell_2})^{-2.58} - 2.58(\log Re_{\ell_2})^{-3.58} \log \frac{z}{h}\right] dz$$

$$= .455\left[(\log Re_{\ell_2})^{-2.58} + \frac{2.58}{\ell n_e 10}(\log Re_{\ell_2})^{-3.58}\right]. \qquad (3.5.23)$$

For the upper surface

$$(C_{ftu})_i \simeq .455 \left[(\log Re_{\ell_3})^{-2.58} + \frac{2.58}{\ell n_e 10} (\log Re_{\ell_3})^{-3.58}\right]. \tag{3.5.24}$$

Multiplying Equations (3.5.23) and (3.5.24) by the ratio of compressible-to-incompressible turbulent skin friction coefficients gives

$$C_{ft\ell} = \begin{cases} (1.0-0.1186\ M_\ell)(C_{ft\ell})_i, & 0 \leq M_\ell \leq 5.36 \\ (0.5962-0.0430\ M_\ell)(C_{ft\ell})_i, & 5.36 \leq M_\ell \leq 10 \end{cases} \tag{3.5.25}$$

$$C_{ftu} = \begin{cases} (1.0-0.1186\ M_u)(C_{ftu})_i, & 0 \leq M_u \leq 5.36 \\ (0.5962-0.0430\ M_u)(C_{ftu})_i, & 5.36 \leq M_u \leq 10 \end{cases} \tag{3.5.26}$$

3.6 Base Pressure Ratio

The ratio of base pressure to free stream static pressure is calculated for two cases. ξ_{bt} is the pressure ratio for a turbulent boundary layer approaching the trailing edge and $\xi_{b\ell}$ is the pressure ratio for a laminar boundary layer.

Base pressure ratio is correlated to the ratio of boundary layer thickness at the trailing edge to trailing edge thickness. This parameter depends on the thickness ratio and Reynolds number based on chord length. The thickness ratio, τ, is given by

$$\tau = (\tan \delta - \tan \delta') \cos \left(\frac{\delta'+\delta}{2}\right) \qquad (3.6.1)$$

The average Reynolds number based on chord length over the span is

$$Re_{ave} = \frac{Re_{\infty}}{2 \cos \left(\frac{\delta'+\delta}{2}\right) \sqrt{\tan \Theta \tan \frac{\Phi}{2}}} \qquad (3.6.2)$$

For a turbulent boundary layer the correlation parameter, η_t, is given over the range $0 \leq \eta_t \leq 5$ by

$$\eta_t = \frac{1}{\tau (Re_{ave})^{1/5}} \qquad (3.6.3)$$

and the lines fit to Chapman's (11) and Goecke's (12) data are

$$\xi_{bt} = \begin{cases} 0.5+0.0125\ (\eta_t-0.5), & M_\infty = 1.5 \\ 0.35+0.025\ (\eta_t-0.5), & M_\infty = 2.0 \\ 0.2+0.062\ (\eta_t-0.65), & M_\infty = 3.1 \\ 0.14+0.062\ (\eta_t-0.22), & M_\infty = 5.0\ . \end{cases} \tag{3.6.4}$$

At intermediate Mach numbers linear interpolation between the lines is used.

For a laminar boundary layer the correlation parameter, η_ℓ, is given over the range $0 \leq \eta_\ell \leq 0.2$ by

$$\eta_\ell = \frac{1}{\tau\ (R_{\ell_{ave}})^{1/2}}\ . \tag{3.6.5}$$

Data taken from Chapman's (11) curves at M_∞=1.5, 2.0 and 3.1 is presented in Table 1. The base pressure ratio at these three Mach numbers is found by parabolic interpolation. At intermediate Mach numbers linear interpolation between the curves is used.

3.7 Lift Coefficient, Drag Coefficient and Lift-to-Drag Ratio

Formulas for the aerodynamic coefficients are developed in this section. These expressions depend on the pressure ratios and skin friction coefficients determined in the preceding sections, the ratio of free stream static pressure to

dynamic pressure, p_∞/q_∞, and several area ratios described in this section.

Let ℓ_1 be the caret wing length measured from the apex to the plane containing the base (Figure 4). Then the plan area, S, is given by

$$S = \ell_1^2 \tan \Theta \tan \frac{\Phi}{2} . \qquad (3.7.1)$$

The area of the projection of the lower surface onto a plane perpendicular to the free stream E_ℓ, is used to calculate the contribution of the lower surface pressure to the drag. It is given by

$$E_\ell = \ell_1^2 \tan \Theta \tan \frac{\Phi}{2} \tan \delta \quad . \qquad (3.7.2)$$

Similarly, the area of the projection of the upper surface onto a plane perpendicular to the free stream, E_u, is used to calculate the contribution of the upper surface pressure to the drag. Changing δ to δ' in Equation (3.7.2) gives the following expression for E_u.

$$E_u = \ell_1^2 \tan \Theta \tan \frac{\Phi}{2} \tan \delta' \qquad (3.7.3)$$

The base area, B, is just the difference of these two and is given by

$$B=E_{\ell}-E_{u}=\ell_1^2 \tan\Theta \tan\frac{\Phi}{2} (\tan\delta - \tan\delta') \ . \qquad (3.7.4)$$

The area of a triangle with sides of length a, b and c is given by

$$\text{Area} = \sqrt{s(s-a)(s-b)(s-c)} \qquad (3.7.5)$$

where the semi-perimeter, s, is

$$s = \frac{1}{2} (a + b + c) \ . \qquad (3.7.6)$$

The wetted areas of the lower and upper surfaces, A_{ℓ} and A_u, are each composed of two triangles. For the lower surface, the two triangles have sides whose lengths are given by

$$a = \frac{\ell_1}{\cos\delta} \qquad (3.7.7)$$

$$b = \ell_1\sqrt{\tan^2\Theta\tan^2\frac{\Phi}{2} + (\tan\Theta-\tan\delta)^2} \qquad (3.7.8)$$

$$c = \ell_1\sqrt{\tan^2\Theta\tan^2\frac{\Phi}{2} + \tan^2\Theta+1} \ . \qquad (3.7.9)$$

The wetted area of the lower surface is

$$A_\ell = 2\sqrt{s(s-a)(s-b)(s-c)} \tag{3.7.10}$$

Changing δ to δ' in Equations (3.7.6-10) gives the wetted area of the upper surface.

Only ratios of areas appear in the formulas for C_L, C_D and L/D, so ℓ_1 drops out.

These ratios are

$$\frac{E_\ell}{S} = \tan\delta \tag{3.7.11}$$

$$\frac{E_u}{S} = \tan\delta' \tag{3.7.12}$$

$$\frac{B}{S} = \tan\delta - \tan\delta' \tag{3.7.13}$$

$$\frac{A_\ell}{S} = \frac{2\sqrt{s'(s'-a')(s'-b')(s'-c')}}{\tan\Theta\,\tan\frac{\Phi}{2}} \tag{3.7.14}$$

where

$$a' = \frac{1}{\cos\delta} \tag{3.7.15}$$

$$b' = \sqrt{\tan^2\Theta\,\tan^2\frac{\Phi}{2} + (\tan\Theta - \tan\delta)^2} \tag{3.7.16}$$

$$c' = \sqrt{\tan^2\Theta\,\tan^2\frac{\Phi}{2} + \tan^2\Theta + 1} \tag{3.7.17}$$

$$s' = \frac{1}{2}(a'+b'+c') \tag{3.7.18}$$

Changing δ to δ' in Equations (3.7.14-18) gives the ratio A_u/S.

The final quantity needed in the formulas for the aerodynamic coefficients is the ratio of free stream static pressure to dynamic pressure. It is given by

$$\frac{p_\infty}{q_\infty} = \frac{1}{0.7\ M_\infty^2} \tag{3.7.19}$$

Expressions for C_L, C_D and L/D can now be derived. The lift, L, is given by

$$L = (p_\ell - p_u)S - \tau_\ell A_\ell \sin\delta - \tau_u A_u \sin\delta' \tag{3.7.20}$$

where τ_ℓ and τ_u are the boundary layer shear stresses on the lower and upper surfaces. The lift coefficient is given by

$$C_L = \frac{L}{q_\infty S} = \frac{(p_\ell - p_u)}{p_\infty}\frac{p_\infty}{q_\infty} - \frac{\tau_\ell}{q_\infty}\frac{A_\ell}{S}\sin\delta - \frac{\tau_u}{q_\infty}\frac{A_u}{S}\sin\delta'$$

$$= (\xi_\ell - \xi_u)\frac{p_\infty}{q_\infty} - (C_f)_\ell \frac{A_\ell}{S}\sin\delta - (C_f)_u \frac{A_u}{S}\sin\delta'. \tag{3.7.21}$$

The drag, D, is given by

$$D = p_\ell E_\ell - p_u E_u - p_b B + \tau_\ell A_\ell \cos\delta + \tau_u A_u \cos\delta' \quad (3.7.22)$$

where p_b is the base pressure.

The drag coefficient is given by

$$C_D = \frac{D}{q_\infty S}$$

$$= \left(\xi_\ell \frac{E_\ell}{S} - \xi_u \frac{E_u}{S} - \xi_b \frac{B}{S}\right) \frac{p_\infty}{q_\infty} + (C_f)_\ell \frac{A_\ell}{S} \cos\delta + (C_f)_u \frac{A_u}{S} \cos\delta' \quad (3.7.23)$$

The lift-to-drag ratio is given by

$$L/D = C_L/C_D \quad . \quad (3.7.24)$$

In the case of a laminar boundary layer, $C_{f\ell\ell}$, $C_{f\ell u}$ and $\xi_{b\ell}$ are used for $(C_f)_\ell$, $(C_f)_u$ and ξ_b in Equations (3.7.21), (3.7.23) and (3.7.24). For a turbulent boundary layer case, $C_{ft\ell}$, C_{ftu} and ξ_{bt} are used for $(C_f)_\ell$, $(C_f)_u$ and ξ_b. For the case of zero skin friction, $(C_f)_\ell$ and $(C_f)_u$ are set to zero. For zero base drag ξ_b is set equal to 1.0.

3.8 Computer Program

The calculations described in this chapter are straightforward but quite lengthy. Therefore, a computer program was

written for the calculation of the aerodynamic coefficients using the FORTRAN IV language. Execution of this program was carried out at M.I.T.'s Information Processing Center on their IBM System 370/168 computer. Graphical output was produced on a CalComp 563 Drum Plotter using a CalComp 905 Controller.

The computer program is broken up into subroutines along the lines of the sectional division of this chapter. Subroutine CARET coordinates the basic process of calculating C_L, C_D and L/D as functions of $\delta,\delta',\Theta,\Phi,M_\infty$ and Re_∞. Depending on the test matrix desired, a main program is written to feed subroutine CARET with a sequence of values for the independent variables. The form in which the results are recorded, either tabular or graphical, is also controlled by the main program. A flow chart of the interaction between the main program and subroutines appears in Figure 11. Appendix I contains listings of the main programs and subroutines and a short description of each.

CHAPTER IV

RESULTS

4.1 Test Matrix

Testing all possible combinations of the six independent variables throughout their entire ranges would yield an enormous and unmanageable amount of data. Therefore, a test matrix was devised which would elucidate most of the relationships with a reasonable amount of computation. One of the independent variables, δ', was eliminated entirely by setting it equal to $\delta-3^{o}$. Essentially, this restricts the study to wings which are approximately five per cent thick. The remaining independent variables can be broken into two groups, those which specify the caret wing's geometry and incidence and those which specify the flight conditions. The test matrix was divided along these lines into two parts, the variable geometry test and the fixed geometry test.

In the variable geometry test the flight conditions, M_{∞} and Re_{∞}, were held fixed while the geometric parameters, δ, Θ and Φ, were allowed to vary. This test is composed of three parts according to which of the geometric parameters is being examined. When the dependence of the aerodynamic coefficients on δ is being considered, δ is varied from 3^{o}

to 13° in steps of two tenths of a degree. When Θ is being considered, it is varied from 4° to 80° in steps of two degrees. When Φ is being considered, it is varied from 24° to 178° in steps of two degrees. In each of the three parts of the variable geometry test, the other two geometric parameters are allowed to take on all combinations of the following values: $\delta = 4^{\circ}, 6^{\circ}, 8^{\circ}$ and 10°; $\Theta = 30^{\circ}$, 50° and 70°; and $\Phi = 60^{\circ}$, 90°, 120° and 150°.

The entire variable geometry test was carried out at two different flight conditions. First at low Mach number and high Reynolds number with a turbulent boundary layer: $M_{\infty} = 2.0$ and $Re_{\infty} = 10^{7}$. Second at high Mach number and low Reynolds number with a laminar boundary layer: $M_{\infty} = 3.1$ and $Re_{\infty} = 10^{5}$.

In the fixed geometry test the geometric parameters, δ, Θ and Φ, were held fixed and the effects of Mach number and Reynolds number on the aerodynamic coefficients were examined. This test is composed of two parts according to whether the skin friction and base drag calculations are based on a laminar or turbulent boundary layer. For the laminar boundary layer case the Mach number is varied from 1.5 to 3.1 by tenths. For the turbulent boundary layer case the Mach number is varied from 1.5 to 5.0 by tenths. Each part of the fixed geometry test is repeated for Reynolds numbers of 10^{5}, 10^{6}, 10^{7} and 10^{8}.

The particular caret wings selected for the fixed geometry test were chosen for their high L/D based on the results of the variable geometry test. For the laminar boundary layer case the caret wing $\delta = 8.3^{\circ}$, $\Theta = 30.0^{\circ}$ and $\Phi = 120.0^{\circ}$ was used. For the turbulent boundary layer case the caret wing $\delta = 6.5^{\circ}$, $\Theta = 30.0^{\circ}$ and $\Phi = 120.0^{\circ}$ was used.

Many of the combinations of the independent variables which occur in the above test matrix do not correspond to caret wings that belong to the restricted class considered in this study. They may be disqualified for any of the following reasons. No design Mach number exists, the design point shock is strong with respect to the free stream, Φ is less than Φ_{trans}, the leading edge is subsonic or Γ_{max} is less than $\Gamma_{\perp}$. Such cases are dropped from the test matrix by the computer program when they are found.

The test matrix is summarized in Table 2.

4.2 Variable Geometry Test

4.2.1 Dependence on δ

The dependence of the aerodynamic coefficients on δ is illustrated in three types of graphs. Graphs of the first type indicate the effect of a second geometric parameter. This is done with a family of curves for four different values of Φ (60°, 90°, 120° and 150°). The curves, like those on

all graphs described in this chapter, are distinguished from each other by symbols plotted at every tenth data point. There are eighteen graphs of this type, one for each combination of the three aerodynamic coefficients, two flight conditions and three values of Θ (30°, 50° and 70°). Graphs of C_L vs. δ, C_D vs. δ and L/D vs. δ appear in Figures 12-17, 24-29 and 36-41 respectively.

Graphs of the second type illustrate the contribution of skin friction and base drag to the overall lift, drag and L/D. The three curves on each graph correspond to inclusion of all the forces, no base drag and no base drag or skin friction. There are twelve graphs of this type, one for each combination of the three aerodynamic coefficients, two flight conditions and two values of Θ (30° and 50°). The value of Φ is 120° in all of them. Graphs of C_L vs. δ, C_D vs. δ and L/D vs. δ appear in Figures 18-21, 30-33 and 42-45.

Graphs of the third type illustrate the effect of boundary layer type. The two curves on each graph correspond to laminar and turbulent boundary layers. There is a graph for each combination of the three aerodynamic coefficients and two values of Θ (30° and 50°). All six of these graphs are for the low Mach number, high Reynolds number flight condition and ϕ equal to 120°. The high Mach number, low

Reynolds number flight condition is excluded because the Reynolds number is outside the range of validity of the formula for the turbulent skin friction coefficient. Graphs of C_L vs. δ, C_D vs. δ and L/D vs. δ appear in Figures 22-23, 34-35 and 46-47.

The graphs of C_L vs. δ appear in Figures 12-23. As one would certainly expect, all these graphs show that C_L increases with δ. The greater the value of δ, the greater will be the deflection of the free stream. Consequently, the pressure ratio across the lower surface shock will increase with δ while the pressure ratio across the upper surface expansion decreases. As a result the lift coefficient increases with δ.

Since the base of the caret wing was constructed perpendicular to the free stream, the base pressure ratio should have absolutely no effect on the lift coefficient. This is confirmed by Figures 18-21 in which the curves for all forces and no base drag lie directly on top of each other.

Because the skin friction shear stress acts tangent to the caret wing's surface and the wing is at fairly low angle of attack, skin friction should have only a small effect, which increases slightly with δ, on the lift coefficient. Exactly this behavior is observed in Figures 18-21. Since the skin friction has only a small effect on C_L, the boundary

layer type (laminar or turbulent) should not make a significant difference in the lift coefficient. This, too, is confirmed by Figures 22 and 23.

Since base pressure and skin friction do not play an important role in the behavior of C_L, the only forces which make a significant contribution are those due to the upper and lower surface pressures. In Figure 7 the pressure ratio across the lower surface shock of the caret wing family $\delta = 5.0^\circ$, $\Theta = 34.0^\circ$ is plotted for several off design Mach numbers as a function of Φ. When $M_{des} < M_\infty$, the pressure ratio increases with Φ and when $M_{des} > M_\infty$, the pressure ratio decreases with increasing Φ. On this basis one might predict that C_L will increase with Φ when $M_{des} < M_\infty$ and decrease with increasing Φ when $M_{des} > M_\infty$. This trend is precisely confirmed by Figures 12-17. In Figure 12, M_{des} ranges from 2.158 at $\delta = 3.0^\circ$ to 3.031 at $\delta = 13.0^\circ$, always greater than the free stream Mach number of 2.0. The family of curves in this graph shows that C_L decreases with increasing Φ. In Figures 13-17 M_{des} is always less than M_∞ and C_L increases with Φ.

For the first flight condition, $M_\infty = 2.0$ and $Re_\infty = 10^7$, the lift coefficient ranges from a minimum of 0.036 to a maximum of 0.535. For the second flight condition, $M_\infty = 3.1$ and $Re_\infty = 10^5$, C_L ranges from a minimum of 0.019 to a maximum of 0.313.

The graphs of C_D vs. δ appear in Figures 24-35. Many of the comments made about the dependence of C_L on δ also apply to C_D. Again, as expected, all the graphs show that C_D increases with δ.

Unlike the situation for C_L, the base pressure and skin friction do have an important effect on C_D. For the flight condition $M_\infty = 2.0$, $Re_\infty = 10^7$ and a turbulent boundary layer, Figures 30 and 31 show that the base drag is about twice the skin friction drag. For the flight condition $M_\infty = 3.1$, $Re_\infty = 10^5$ and a laminar boundary layer, Figures 32 and 33 show that the skin friction drag is about ten times the base drag. This change in relative importance makes sense because base drag is lower for a laminar boundary layer than for a turbulent boundary layer and skin friction drag is higher for a lower Reynolds number. For both flight conditions, Figures 30-33 show that base drag and skin friction drag are

the principle sources of drag at low values of δ but that pressure drag takes over at higher δ. Figures 34 and 35 show that C_D is higher for a turbulent boundary layer than for a laminar boundary layer but that the difference is small.

At the larger values of δ, where pressure drag is more significant than base drag or skin friction drag, C_D displays the same dependence on Φ as discussed for C_L (see Figures 24-29). At lower values of δ, the pressure drag becomes insignificant compared to the other sources of drag and the arguments which explain the dependence of C_L on Φ can no longer be applied to C_D. As Φ increases, there is less wetted area for a given plan area and therefore, the skin friction drag goes down with increasing Φ. This effect is observed in Figures 25, 27 and 28 where the dependence of C_D on Φ reverses as δ decreases and skin friction drag becomes more important than pressure drag.

For the first flight condition, $M_\infty = 2.0$ and $Re_\infty = 10^7$, the drag coefficient ranges from a minimum of 0.021 to a maximum of 0.133. For the second flight condition, $M_\infty = 3.1$ and $Re_\infty = 10^5$, C_D ranges from a minimum of 0.022 to a maximum of 0.093.

The graphs of L/D vs. δ appear in Figures 36-47. Since the angle δ is closely related to the angle of attack, these curves would be expected to exhibit a maximum. Those curves which cover a large enough range of δ have the expected maximum.

Figures 42-45 show the contribution of skin friction and base drag to L/D. The relative importance of skin friction and base drag is the same here as described for the drag coefficient. For $M_\infty = 2.0$ and $Re_\infty = 10^7$, base drag is significant compared to skin friction. For $M_\infty = 3.1$ and $Re_\infty = 10^5$, base drag is insignificant compared to skin friction. Figures 46 and 47 show that the higher drag associated with a turbulent boundary layer leads to a lower L/D than for a laminar boundary layer.

Figures 37-41, in which $M_{des} < M_\infty$, show a predominant tendency for L/D to increase with Φ. However, there are some exceptions in Figures 39 and 40. Figure 36, in which $M_{des} > M_\infty$, shows the opposite trend. In this figure L/D decreases with increasing Φ.

For the first flight condition, $M_\infty = 2.0$ and $Re_\infty = 10^7$, the maximum L/D occurs at $\delta = 6.4^\circ$ on the curve $\Phi = 120^\circ$ and is equal to 5.679. For the second flight condition, $M_\infty = 3.1$ and $Re_\infty = 10^5$, the maximum L/D occurs at $\delta = 8.4^\circ$ on the curve $\Phi = 120^\circ$ and is equal to 4.057.

4.2.2 Dependence on Θ

The dependence of the aerodynamic coefficients on Θ is illustrated in Figures 48-65. These figures also indicate the dependence on δ with a family of curves corresponding to four values of that parameter (4°, 6°, 8° and 10°). There is a graph for every combination of the three aerodynamic coefficients, two flight conditions and three values of Φ (90°, 120° and 150°). The design point has been marked on the four curves of Figure 48 and occurs at the same values of Θ in Figures 49-65.

In Section 4.2.1 it was established that the lift coefficient is primarily influenced by upper and lower surface pressure rather than skin friction or base pressure. Examining the expression for C_L, Equation (3.7.21), these pressures enter in terms of the pressure ratios across the lower surface shock and upper surface expansion in such a way that C_L increases with increasing ξ_ℓ and/or decreasing ξ_u. The pressure ratios are functions of $M_\perp$, $\Gamma_\perp$ and $\Gamma_\perp'$, which in turn depend on Θ.

Sample calculations within the ranges of δ, δ' and Φ of interest show that $\Gamma_\perp$ and $\Gamma_\perp'$ increase with decreasing Θ. Since ξ_ℓ increases with $\Gamma_\perp$ and ξ_u decreases with

increasing $\Gamma_\perp'$, it follows that C_L will tend to increase with decreasing Θ due to changes in the stream deflection angles.

Combining Equations (3.2.4), (3.2.5) and (3.2.12) gives an expression for $M_\perp$ as a function of Θ. The derivative of $M_\perp$ with respect to Θ is always positive, so $M_\perp$ increases with Θ. However, the pressure ratios across the shock and expansion may increase or decrease with increasing $M_\perp$ depending on the values of $M_\perp$, $\Gamma_\perp$ and $\Gamma_\perp'$. Thus the dependence of C_L on Θ due to changes in the normal component of the Mach number will vary with the situation.

In light of these results, the overall dependence of C_L on Θ has not been anticipated. Looking at the graphs of C_L vs. Θ which appear in Figures 48-53, it can be seen that C_L increases with decreasing Θ throughout the range of the present test matrix. The graphs are also consistent with the previous finding that C_L increases with δ. For the flight condition $M_\infty = 2.0$, $Re_\infty = 10^7$, the lift coefficient ranges from a minimum of 0.077 to a maximum of 0.484. For the flight condition $M_\infty = 3.1$, $Re_\infty = 10^5$, the lift coefficient ranges from 0.045 to 0.263.

The remarks made about the dependence of C_L on Θ due to upper and lower surface pressure also apply to the drag coefficient. The changes in ξ_ℓ and ξ_u which cause C_L to decrease with increasing Θ will also cause the pressure drag to decrease with increasing Θ.

Besides pressure drag, skin friction and base drag also influence the drag coefficient. The ratio of base area to plan area given by Equation (3.7.13) does not depend on Θ. However, the Reynolds number based on length decreases with increasing Θ leading to a higher base pressure ratio and lower base drag. Thus base drag reinforces the effect of pressure drag, driving the drag coefficient down when Θ increases.

Equations (3.7.14-18) show that the ratio of wetted area to plan area increases with Θ. This means that skin friction drag and its importance relative to the other sources of drag increase with Θ. At large enough values of Θ skin friction drag might predominate and reverse the dependence of C_D on Θ.

This reversal is observed clearly at the high Mach number, low Reynolds number flight condition in Figures 57-59. The curves of C_D vs. Θ have a negative slope at low values of Θ and positive slope at high values of Θ. It was shown in Section 4.2.1 that the magnitude of the pressure

drag relative to skin friction drag increases with δ. This accounts for the shift of the minimum in these curves to the right with increasing δ.

It was also shown in Section 4.2.1 that base drag is greater than skin friction drag at the low Mach number, high Reynolds number flight condition. Most of the curves corresponding to this flight condition, Figures 54-56, do not have a minimum. Except for a few cases at low δ and high Θ, the drag coefficient decreases with increasing Θ.

The graphs for both flight conditions are consistent with the previous finding that C_D increases with δ. For $M_\infty = 2.0$ and $Re_\infty = 10^7$ the drag coefficient ranges from a minimum of 0.024 to a maximum of 0.097. For $M_\infty = 3.1$ and $Re_\infty = 10^5$ the drag coefficient ranges from 0.021 to 0.066.

The dependence of the lift-to-drag ratio on Θ is shown in Figures 60-65. Due to the effect of skin friction, C_D does not fall off as rapidly as C_L when Θ is increased. As a result, the lift-to-drag ratio decreases with increasing Θ. For the $M_\infty = 2.0$, $Re_\infty = 10^7$ flight condition, the maximum L/D occurs at $\delta = 6^\circ$, $\Theta = 14^\circ$ and $\Phi = 150^\circ$ and has the value 6.483. For the $M_\infty = 3.1$, $Re_\infty = 10^5$ flight condition, the maximum L/D occurs at

$\delta = 6^{\circ}$, $\Theta = 16^{\circ}$ and $\Phi = 120^{\circ}$ and has the value 4.973. Figures 60-65 are consistent with the previous finding that the lift-to-drag ratio goes through a maximum as δ increases.

4.2.3 Dependence on Φ

The dependence of the aerodynamic coefficients on Φ is illustrated in Figures 66-83. These figures also indicate the dependence on δ with a family of curves corresponding to four values of that parameter (4°, 6°, 8° and 10°). There is a graph for every combination of the three aerodynamic coefficients, two flight conditions and three values of Θ (30°, 50° and 70°).

Figures 12-17, 24-29 and 36-41 discussed in Section 4.2.1 have already indicated the dependence of C_L, C_D and L/D on Φ. Essentially the same dependence is observed in Figures 66-83. It was established in Section 4.2.1 that the lift coefficient increases with Φ when $M_{des} < M_{\infty}$ and decreases with increasing Φ when $M_{des} > M_{\infty}$. In Figures 67-71 M_{des} is less than M_{∞} and C_L is observed to increase with Φ in most cases. A few exceptions are present in which C_L begins to decrease as Φ approaches 180°. In Figure 66 M_{des} is greater than M_{∞} and C_L decreases with increasing Φ.

At $M_\infty = 2.0$ and $Re_\infty = 10^7$ the lift coefficient ranges from 0.051 to 0.484. At $M_\infty = 3.1$ and $Re_\infty = 10^5$ C_L ranges from 0.026 to 0.225.

The drag coefficient shows the same dependence on Φ as C_L except at low enough values of δ and Φ where the effect of skin friction can reverse the behavior (Figures 72-77). C_D ranges from 0.024 to 0.097 for the first flight condition and from 0.023 to 0.091 for the second flight condition.

The increase in lift-to-drag ratio with Φ when $M_{des} < M_\infty$ observed in Section 4.2.1 is confirmed by Figures 79-83. Exceptions to this trend which were noted in that section are seen here as a sharp decrease in L/D as Φ approaches 180°. Figure 78 is consistent with the previously observed decrease in L/D with increasing Φ when $M_{des} > M_\infty$. The maximum L/D for the first flight condition occurs at $\delta = 6^\circ$, $\Theta = 30^\circ$ and $\Phi = 100^\circ$ and has the value 6.006. The maximum L/D for the second flight condition occurs at $\delta = 8^\circ$, $\Theta = 30^\circ$ and $\Phi = 124^\circ$ and has the value 4.050.

The dependence of C_L, C_D and L/D on δ in Figures 66-83 is the same as described in Sections 4.2.1 and 4.4.4.

4.3 Fixed Geometry Test

The dependence of the aerodynamic coefficients on Mach number and Reynolds number is illustrated in Figures 84-89. Mach number is the abscissa and Reynolds number a parameter in these figures. There is a graph for every combination of the three aerodynamic coefficients and two boundary layer types. The caret wing used in the turbulent boundary layer case is on design at $M_\infty = 2.38$ and the one used in the laminar boundary layer case is on design at $M_\infty = 2.53$.

In linearized thin airfoil theory (18) the dependence of the pressure coefficient on free stream Mach number is proportional to $(M_\infty^2 - 1)^{-1/2}$. Since the deflection of the streamlines in the caret wing flow field is small, the dependence of the lift and drag coefficients on Mach number should be fairly similar to this. As a further indication of the influence of Mach number, consider the terms in the expressions for C_L and C_D, Equations (3.7.21) and (3.7.23). The difference between the pressure ratios across the shock and expansion, multiplied by the ratio of free stream static-to-dynamic pressure is proportional to the difference in pressure coefficient between the upper and lower surfaces. For small stream deflection

angles this term is proportional to $(M_\infty^2 - 1)^{-1/2}$, corresponding to thin airfoil theory. As described in Sections 2.4 and 3.5, a linear approximation to the decrease in skin friction coefficient with increasing Mach number is used. The contribution of base drag to C_D is proportional to $(1 - \xi_b)p_\infty/q_\infty$. The factor $(1 - \xi_b)$ increases slowly with M_∞ but the ratio of static-to-dynamic pressure falls off with M_∞^{-2}. Overall, this term decreases as M_∞ increases.

These remarks are consistent with the dependence of C_L and C_D on M_∞ shown in Figures 84-87. The curves of L/D vs. M_∞ for the turbulent boundary layer case, Figure 88, have a minimum near $M_\infty = 3.2$. The highest L/D on each curve occurs at the low end of the Mach number range. For the laminar boundary layer case, Figure 89, the maximum L/D on each curve also occurs at the low end of the Mach number range. Two of the curves decrease throughout the range and two have a minimum.

Reynolds number influences the aerodynamic coefficients through the skin friction coefficients and base pressure ratio. The skin friction drag decreases and the base drag increases as Re_∞ increases. In most cases the skin friction effect is the primary one.

Changes in skin friction have little effect on the lift coefficient and changes in base drag have no effect so C_L should be nearly independent of Re_∞. The curves for different Reynolds numbers in Figures 84 and 85 confirm this by lying virtually on top of each other.

For a turbulent boundary layer, Figure 86 shows that the drag coefficient decreases as Re_∞ increases. This is also true in the laminar boundary layer case for Mach numbers above 2.3 (Figure 87). For lower Mach numbers there is a narrow range of Reynolds numbers, between 10^6 and 10^7, in which the effect of base drag dominates and the dependence of C_D on Re_∞ reverses. This coincides with the steepest portion of the laminar base pressure curves in Figure 9.

The dependence of the lift-to-drag ratio on Re_∞ is just the inverse of the drag coefficient's behavior. For a turbulent boundary layer L/D increases with Re_∞ (Figure 88). This is also true in the laminar boundary layer case above $M_\infty = 2.3$ (Figure 89). At lower Mach numbers, the lift-to-drag ratio decreases over some range of Reynolds numbers between 10^6 and 10^7.

CHAPTER V

CONCLUSIONS and RECOMMENDATIONS

A clear picture of the way the lift coefficient, drag coefficient and lift-to-drag ratio vary with caret wing geometry and flight condition has emerged. The influence of δ, Θ, Φ, M_∞ and Re_∞ on each of the aerodynamic coefficients is summarized below.

The lift coefficient increases with δ under all conditions and with Φ when $M_{des} < M_\infty$. It decreases as Θ or M_∞ increase and, when $M_{des} > M_\infty$, as Φ increases. Reynolds number has no appreciable effect on C_L.

The drag coefficient also increases with δ under all conditions. Drag due to upper and lower surface pressure decreases as Θ increases. However, skin friction drag increases with Θ and can be the dominant factor at some flight conditions. Depending on whether M_{des} is greater than or less than M_∞, the drag coefficient will decrease or increase, respectively, as Φ increases. This dependence on Φ arises through the influence of upper and lower surface pressure. At low values of δ and Φ the effects of skin friction may override this dependence and, in such cases, C_D will decrease as Φ increases regardless of the relative magnitudes of M_{des} and M_∞. Finally, the

drag coefficient decreases as M_∞ or Re_∞ increase. The exception to this dependence on Re_∞ noted in Section 4.3 is a consequence of the rapid rise in laminar base drag over a narrow Reynolds number range. This result must be viewed with suspicion because the two-dimensional base pressure data gives, at best, only a rough indication of the base drag.

The lift-to-drag ratio goes through a maximum as δ is varied and, when $M_{des} < M_\infty$, there is a maximum in its dependence on Φ. When $M_{des} > M_\infty$, L/D decreases as Φ increases. The lift-to-drag ratio also decreases with increasing Θ. For cases where the Mach number range extended up to 5.0, a minimum was found in the dependence of L/D on M_∞. Finally, the lift-to-drag ratio increases with Re_∞. The remarks made about the exception to the dependence of C_D on Re_∞ also apply here.

The best lift-to-drag ratio found in the variable geometry test was 6.483 for the caret wing $\delta = 6^o$, $\Theta = 14^o$ and $\Phi = 150^o$ and the flight condition $M_\infty = 2.0$, $Re_\infty = 10^7$. The corresponding lift coefficient and design Mach number are 0.285 and 5.989. Taking the best L/D from each of the graphs of L/D vs. δ, Θ and Φ, two other cases were found in which the lift-to-drag ratio exceeded 6.0 and many were found between 5.0 and 6.0.

The best L/D found in the fixed geometry test was 6.391 for the caret wing $\delta = 6.5^{\circ}$, $\Theta = 30^{\circ}$ and $\Phi = 120^{\circ}$ and flight condition $M_{\infty} = 1.8$, $Re_{\infty} = 10^{8}$. The corresponding lift coefficient and design Mach number are 0.324 and 2.384.

These examples of high L/D are only the best cases from the test matrix considered in this study. Some improvement can be expected by searching in the neighborhood of these cases, using the behavior of L/D described above as a guide. Additional improvement in L/D could be achieved by adding some type of afterbody and thereby reducing the base drag. The curves for zero base drag in Figures 42-45 give an indication of the room for improvement. In Figure 42, for example, the L/D goes from 5.679 to 8.945 when base drag is eliminated.

The performance of caret wings is compared to that of delta wings in Figure 90. Wind tunnel tests of 8 percent thick delta wings with double wedge profiles at $M_{\infty} = 1.92$ and Reynolds number based on two-thirds the root chord, $Re_{\bar{c}}$, covering the range 0.57×10^{6} to 1.25×10^{6} were made by Love (19). A thinner series of delta wings, 1.3 to 1.8 percent thick, constructed from flat plate with sharpened leading and trailing edges are also included in his tests.

The boundary layer over most of the wetted surface was shown to be turbulent by a liquid-film method. Love measured the aerodynamic coefficients through an angle of attack range of $\pm 6^{o}$. The maximum L/D of these delta wings is plotted as a function of apex half-angle in Figure 90.

The free stream conditions in the first part of the variable geometry test, $M_{\infty} = 2.0$ and $Re_{\infty} = 10^{7}$, are nearly the same as the conditions in Love's experiment. Caret wings with high L/D from this part of the study are plotted alongside the delta wing data in Figure 90 using the apex half-angle of the planform for the abscissa. The Mach number and average Reynolds number of Love's experiment were duplicated exactly at one point of the test matrix in the fixed geometry test and this case is also included in the figure. The caret wing data does not represent the maximum L/D for any given planform, only the best to occur in the test matrix. Geometric properties, M_{∞} and $Re_{\bar{c}}$ are listed in tabular form on the figure.

The thickness ratio of the caret wings is .052, about midway between the two groups of delta wings. As shown in Figure 90, the lift-to-drag ratios of the caret wings also lie between the two groups of delta wings, indicating that

caret and delta wings have comparable lifting efficiencies. However, the delta wings considered here have sharp trailing edges while the caret wings have blunt bases. If the addition of an afterbody to the caret wings could significantly reduce their base drag, the resulting lift-to-drag ratios would be superior to those for delta wings.

One objective of further research should be the determination of the accuracy and range of applicability of the method of calculation presented in this thesis. This could be accomplished through experimental measurements or calculations based on a more sophisticated model of the caret wing flow field.

The work of Ziph (7) mentioned in the Introduction could be used as a starting point in the latter approach. Ziph treated the case of a reentrant pyramid with surface curvature in the transverse plane. His numerical solution of the equations of conical flow is restricted to flow fields in which the shock is attached to the apex but detached from the leading edges. This restriction is the result of a transformation of the region of computation into a square. The computational region is bounded by the shock, the body and two symmetry lines extending radially from the leading edge and internal rib to the shock. If the shock were attached, the length of one side of the

computational region would go to zero and the transformation would have a singularity.

As shown in Chapter II, the leading edge shock can be calculated correctly by treating the caret wing as a swept wedge. One way of extending Ziph's method to the attached shock case would be to modify the computational region so that the part near the leading edge is no longer included. The leading edge shock of Chapter II would then be used in this region and would give the boundary conditions necessary for the new computational region. Neglecting boundary layer effects, this procedure would yield the correct shock shape and pressure distribution over the caret wing's lower surface. The error incurred by approximating the average pressure over the lower surface with the pressure downstream of the leading edge shock could then be assessed. If found to be unacceptably large, this approximation could be abandoned in favor of Ziph's lengthier, but more accurate method.

Another objective of further research would be the inclusion of caret wings whose design point shocks are strong with respect to flow normal to the leading edge ($\Phi < \Phi_{trans}$) in the search for high lift-to-drag ratios.

If these "strong" shocks actually occur, the high lower surface pressure that could be generated at low angle of attack would yield lift-to-drag ratios much higher than those found in this study. An experimental investigation of this possibility would be very interesting.

APPENDIX I

COMPUTER PROGRAM LISTING

A short description of the subroutines precedes the listing.

Subroutine HEAD prints a heading for data printed by subroutine PRINT. There are no arguments.

Subroutine CARET calculates M_{des}, design point shock type with respect to flow normal to the leading edge, ξ_ℓ, ξ_u, $\xi_{b\ell}$, ξ_{bt}, C_L, C_D and L/D given δ, δ', Θ, Φ, M_∞ and Re_∞.

Subroutine PRINT prints data under the heading produced by subroutine head. Input arguments are δ, δ', Θ, Φ, M_∞, Re_∞, M_{des}, shock type, ξ_ℓ, ξ_u, $\xi_{b\ell}$, ξ_{bt}, C_L, C_D and L/D.

Subroutine LOWER calculates M_{des}, ξ_ℓ, shock type, $C_{f\ell\ell}$ and $C_{ft\ell}$ given δ, Θ, Φ, M_∞ and Re_∞.

Subroutine DESIGN calculates M_{des} and Φ_{trans} given δ and Θ.

Subroutine DG calculates Γ_{max}, $\Gamma_\perp$, $\Gamma_{max} - \Gamma_\perp$ and $M_\perp$ given δ, Θ, Φ and M_∞. It also calculates $\Gamma_\perp'$ when given δ' instead of δ.

Subroutine SHOCKW calculates the pressure ratio across a weak shock given the upstream Mach number and stream deflection angle.

Subroutine SHOCKS calculates the pressure ratio across a strong shock given the upstream Mach number and stream deflection angle.

Subroutine SFL calculates $C_{f\ell\ell}$ and $C_{ft\ell}$ given δ, Θ, Φ, M_∞, Re_∞ and ξ_ℓ.

Subroutine UPPER calculates ξ_u, $C_{f\ell u}$ and C_{ftu} given δ', Θ, Φ, M_∞ and Re_∞.

Subroutine PM calculates the pressure ratio across a Prandtl-Meyer expansion given the upstream Mach number and angle through which the stream turns.

Subroutine SFU calculates $C_{f\ell u}$ and C_{ftu} given δ', Θ, Φ, M_∞, Re_∞ and ξ_u.

Subroutine BASE calculates $\xi_{b\ell}$ and ξ_{bt} given δ, δ', Θ, Φ, M_∞ and Re_∞.

Subroutine COEFF calculates C_L, C_D and L/D given δ, δ', Θ, Φ, M_∞, ξ_ℓ, ξ_u, $\xi_{b\ell}$, ξ_{bt}, $C_{f\ell\ell}$, $C_{ft\ell}$, $C_{f\ell u}$ and C_{ftu}.

Subroutine PICTR draws labeled axes, title and subtitle and plots up to four curves identified by symbols.

```
/*SETUP UNIT=TAPE9,ID=(001022,RING,SAVE,SL),DDNAME=FT09F001,A=DMP
//STEP1 EXEC FORCGO,LIBRARY='SYS5.PLOT.SUBR'
//C.SYSIN DD *,DCB=BLKSIZE=2000
C       MAIN - CL, CD & LD VS. DELTA - GRAPHS I, II & III
        INTEGER TYPE,XLABEL(7),YLABEL(7),TITLE(7),SUBTTL(7),VAR(5,4),SYMTT
       1L(8,4)
        INTEGER YLAB(7,3),TIT(7,3),SUBT(7,3),SYMT(8,4,3)
        REAL LD(5)
        DIMENSION CL(5),CD(5),X(320),Y(320),NUM(5),VAL(4),XX(320),NUM2(5),
       1NUM3(5)
        DIMENSION YX(3,5,320),NCY(3)
        DATA IS/'S'/
        DATA NUM/0,0,0,0,0/
C       READ X-AXIS LABEL & NO. CHARACTERS IN XLABEL, THEN 3 PAIRS OF Y-AXIS
C        LABEL & NO. CHARACTERS IN YLAB (CL,CD,LD)
        READ(5,1000) XLABEL,NCX,((YLAB(I,J),I=1,7),NCY(J),J=1,3)
 1000   FORMAT(7A4,2X,I10)
C       READ 3 TITLES, THEN 3 SUBTITLES (CL,CD,LD;TURBULENT,LAMINAR,BLANK)
        READ(5,1001) TIT,SUBT
 1001   FORMAT(7A4)
C       READ VARIABLE NAMES (XM,RE,THETA,PHI)
        READ(5,1002) VAR
 1002   FORMAT(5A4)
C       READ 3 SETS OF SYMBOL TITLES (PHI=60,90,120,150;NO SKIN FRICTION OR BASE
C        DRAG,NO BASE DRAG,ALL FORCES,BLANK;LAMINAR,TURBULENT,BLANK,BLANK)
        READ(5,1003) SYMT
 1003   FORMAT(8A4)
        ICASE=5
        XM=2.
        RE=1.0E+07
        CALL PLOTS(IDUM,IDUM,9)
        CALL PLOT(0.,2.,-3)
    2   VAL(1)=XM
        VAL(2)=RE/1.0E+05
        DO 40 I=30,70,20
        THETA=I
```

```
      VAL(3)=THETA
      I=0
      DO 41 J=1,4
      IND=0
      PHI=60+(J-1)*30
      WRITE(6,100) THETA,PHI,XM,RE
  100 FORMAT(1H1,'THETA =',F10.5,10X,'PHI =',F10.5,10X,'XM =',F10.5,10X,
     1'RE =',E10.3//1X,'   L  DELTA  XMDES  CL(1)  CL(2)  CL(3)  CL(4)
     2CL(5)  CD(1)  CD(2)  CD(3)  CD(4)  CD(5)  LD(1)  LD(2)  LD(3)  LD(
     34)  LD(5)'//)
      DO 42 K=30,130,2
      XK=K
      DELTA=XK/10.
      DELTU=DELTA-3.
      CALL CARET(DELTA,DELTU,THETA,PHI,XM,RE,XMDES,TYPE,PRATIO,ERATIO,BR
     1ATL,BRATT,CL,CD,LD)
      IF(XMDES.EQ.0..OR.PRATIO.LE.0..OR.ERATIO.LE.0..OR.TYPE.EQ.IS) GO
     1 TO 39
      IND=1
      L=L+1
      X(L)=DELTA
      DO 50 II=1,5
      YX(1,II,L)=CL(II)
      YX(2,II,L)=CD(II)
   50 YX(3,II,L)=LD(II)
      WRITE(6,200) L,X(L),XMDES,((YX(II,JJ,I),JJ=1,5),II=1,3)
  200 FORMAT(1X,I4,17F7.3)
      GO TO 42
   39 IF(IND.EQ.1) GO TO 41
   42 CONTINUE
   41 NUM(J+1)=L
      NPTS=NUM(5)
      NPT=NUM(4)-NUM(3)
      NP=NUM(3)
      DO 51 II=1,4
      NUM2(II)=NPT*(II-1)
```

```
 51 NUM3(II)=NPT*(II-1)
    NUM2(5)=NUM2(4)
    NUM3(4)=NUM3(3)
    NUM3(5)=NUM3(3)
    DO 52 II=1,NPT
    XX(II)=X(NP+II)
    XX(NPT+II)=X(NP+II)
 52 XX(2*NPT+II)=X(NP+II)
    DO 53 II=1,3
    DO 54 JJ=1,7
    YLABEL(JJ)=YLAB(JJ,II)
 54 TITLE(JJ)=TIT(JJ,II)
    IF(XM.EQ.3.1) GO TO 3
    DO 55 JJ=1,7
 55 SUBTTL(JJ)=SUBT(JJ,1)
    GO TO 4
  3 DO 56 JJ=1,7
 56 SUBTTL(JJ)=SUBT(JJ,2)
  4 VAL(4)=0.
    DO 57 JJ=1,8
    DO 57 KK=1,4
 57 SYMTTL(JJ,KK)=SYMT(JJ,KK,1)
    DO 58 JJ=1,NPTS
 58 Y(JJ)=YX(II,ICASE,JJ)
    CALL PICTR(5.,5.,XLABEL,NCX,YLABEL,NCY(II),TITLE,SUBTTL,VAR,VAL,SY
   1MTTL,X,Y,NUM,4,10)
    WRITE(6,300) II
300 FORMAT(1X,'PLOT I -',I2,' COMPLETE')
    IF(THETA.EQ.70.) GO TO 53
    VAL(4)=120.
    DO 59 JJ=1,8
    DO 59 KK=1,4
 59 SYMTTL(JJ,KK)=SYMT(JJ,KK,2)
    DO 60 JJ=1,NPT
    Y(JJ)=YX(II,1,NP+JJ)
    Y(NPT+JJ)=YX(II,ICASE-2,NP+JJ)
```

```
   60 Y(2*NPT+JJ)=YX(II,ICASE,NP+JJ)
      CALL PICTR(5.,5.,XLABEL,NCX,YLABEL,NCY(II),TITLE,SUBTTL,VAR,VAL,SY
     1MTTL,XX,Y,NUM2,3,10)
      WRITE(6,400) II
  400 FORMAT(1X,'PLOT II -',I2,' COMPLETE')
      DO 63 JJ=1,7
   63 SUBTTL(JJ)=SUBT(JJ,3)
      DO 64 JJ=1,8
      DO 64 KK=1,4
   64 SYMTTL(JJ,KK)=SYMT(JJ,KK,3)
      DO 65 JJ=1,NPT
      Y(JJ)=YX(II,4,NP+JJ)
   65 Y(NPT+JJ)=YX(II,5,NP+JJ)
      CALL PICTR(5.,5.,XLABEL,NCX,YLABEL,NCY(II),TITLE,SUBTTL,VAR,VAL,SY
     1MTTL,XX,Y,NUM3,2,10)
      WRITE(6,500) II
  500 FORMAT(1X,'PLOT III -',I2,' COMPLETE')
   53 CONTINUE
   40 CONTINUE
      IF(XM.EQ.3.1) GO TO 1
      XM=3.1
      RE=1.0E+05
      ICASE=4
      GO TO 2
    1 CALL ENDPLT(0.,-2.,999)
      STOP
      END
//G.OBJECT DD DSNAME=U.M12280.13637.SUBLIB.OBJ,DISP=OLD
//G.FT09F001 DD UNIT=TAPE9,LABEL=(1,NL),DISP=(NEW,PASS),
//     DCB=(DEN=2,RECFM=VS,LRECL=504,BLKSIZE=508)
//G.FT04F001 DD DSN=&&CALDATA,DISP=(NEW,PASS),UNIT=SCRATCH,
//     SPACE=(22,1)
//G.SYSIN DD *,DCB=BLKSIZE=2000
DELTA IN DEGREES                    16
LIFT COEFFICIENT                    16
DRAG COEFFICIENT                    16
```

```
LIFT TO DRAG RATIO
LIFT COEFFICIENT VS. DELTA
DRAG COEFFICIENT VS. DELTA
LIFT TO DRAG RATIO VS. DELTA
TURBULENT BOUNDARY LAYER
LAMINAR BOUNDARY LAYER

MACH NUMBER =
REYNOLDS NO./10 5  =
THETA IN DEGREES =
PHI IN DEGREES =
PHI =  60 DEGREES
PHI =  90 DEGREES
PHI = 120 DEGREES
PHI = 150 DEGREES
NO SKIN FRICTION OR BASE DRAG
NO BASE DRAG
ALL FORCES

LAMINAR BOUNDARY LAYER
TURBULENT BOUNDARY LAYER


/*EOJ ********
```

```
/*SETUP UNIT=TAPE9,ID=(000470,RING,SAVE,NL),DDNAME=FT09F001,A=OJH
//STEP1 EXEC FORCGO,LIBRARY='SYS5.PLOT.SUBR'
//C.SYSIN DD *,DCB=BLKSIZE=2000
C      MAIN - CL, CD & LD VS. THETA - GRAPHS IV
       INTEGER TYPE,XLABEL(7),YLABEL(7),TITLE(7),SUBTTL(7),VAR(5,4),SYMTT
      1L(8,4)
       INTEGER YLAB(7,3),TIT(7,3),SUBT(7,3),SYMT(8,4,3)
       REAL LD(5)
       DIMENSION CL(5),CD(5),X(320),Y(320),NUM(5),VAL(4),XX(320),NUM2(5),
      1NUM3(5)
       DIMENSION YY(3,5,320),NCY(3)
       DATA IS/'S'/
       DATA NUM/0,0,0,0,0/
C      READ X-AXIS LABEL & NO. CHARACTERS IN XLABEL, THEN 3 PAIRS OF Y-AXIS
C       LABEL & NO. CHARACTERS IN YLAB (CL,CD,LD)
       READ(5,1000) XLABEL,NCX,((YLAB(I,J),I=1,7),NCY(J),J=1,3)
 1000  FORMAT(7A4,2X,I10)
C      READ 3 TITLES, THEN 3 SUBTITLES (CL,CD,LD;TURBULENT,LAMINAR,BLANK)
       READ(5,1001) TIT,SUBT
 1001  FORMAT(7A4)
C      READ VARIABLE NAMES (XM,RE,THETA,PHI)
       READ(5,1002) VAR
 1002  FORMAT(5A4)
C      READ 3 SETS OF SYMBOL TITLES (PHI=60,90,120,150;NO SKIN FRICTION OR BASE
C       DRAG,NO BASE DRAG,ALL FORCES,BLANK;LAMINAR,TURBULENT,BLANK,BLANK)
       READ(5,1003) SYMT
 1003  FORMAT(8A4)
       ICASE=5
       XM=2.
       RE=1.0E+07
       CALL PLOTS(IDUM,IDUM,9)
       CALL PLOT(0.,2.,-3)
     2 VAL(1)=XM
       VAL(2)=RE/1.0E+05
       DO 40 I=90,150,30
       PHI=I
```

```
      VAL(3)=PHI
      L=0
      DO 41 J=1,4
      IND=0
      DELTA=4+(J-1)*2
      DELTU=DELTA-3.
      WRITE(6,100) PHI,DELTA,XM,RE
  100 FORMAT(1H1,'PHI =',F10.5,10X,'DELTA =',F10.5,10X,'XM =',F10.5,10X,
     1'RE =',E10.3//1X,'   L  THETA  XMDES  CL(1)  CL(2)  CL(3)  CL(4)
     2CL(5)  CD(1)  CD(2)  CD(3)  CD(4)  CD(5)  LD(1)  LD(2)  LD(3)  LD(
     34)  LD(5)'//)
      KKK=4+(J-1)*2
      DO 42 K=KKK,80,2
      THETA=K
      CALL CARET(DELTA,DELTU,THETA,PHI,XM,RE,XMDES,TYPE,PRATIO,ERATIO,BR
     1ATIL,BRATT,CL,CD,LD)
      IF(XMDES.EQ.0..OR.PRATIO.LE.0..OR.ERATIO.LE.0..OR.TYPE.EQ.IS) GO
     1 TO 39
      IND=1
      L=L+1
      X(L)=THETA
      DO 50 II=1,5
      YY(1,II,L)=CL(II)
      YY(2,II,L)=CD(II)
   50 YY(3,II,L)=LD(II)
      WRITE(6,200) L,X(L),XMDES,((YY(II,JJ,L),JJ=1,5),II=1,3)
  200 FORMAT(1X,I4,17F7.3)
      GO TO 42
   39 IF(IND.EQ.1) GO TO 41
   42 CONTINUE
   41 NUM(J+1)=L
      NETS=NUM(5)
      NPT=NUM(4)-NUM(3)
      NP=NUM(3)
      DO 53 II=1,3
      DO 54 JJ=1,7
```

```
      YLABEL(JJ)=YLAB(JJ,II)
   54 TITLE(JJ)=TIT(JJ,II)
      IF(XM.EQ.3.1) GO TO 3
      DO 55 JJ=1,7
   55 SUBTTL(JJ)=SUBT(JJ,1)
      GO TO 4
    3 DO 56 JJ=1,7
   56 SUBTTL(JJ)=SUBT(JJ,2)
    4 VAL(4)=0.
      DO 57 JJ=1,8
      DO 57 KK=1,4
   57 SYMTTL(JJ,KK)=SYMT(JJ,KK,1)
      DO 58 JJ=1,NPTS
   58 Y(JJ)=YX(II,ICASE,JJ)
      CALL PICTR(5.,5.,XLABEL,NCX,YLABEL,NCY(II),TITLE,SUBTTL,VAR,VAL,SY
     1MTTL,X,Y,NUM,4,10)
   53 WRITE(6,300) II
  300 FORMAT(1X,'PLOT IV -',I2,' COMPLETE')
   40 CONTINUE
      IF(XM.EQ.3.1) GO TO 1
      XM=3.1
      RR=1.0E+05
      ICASE=4
      GO TO 2
    1 CALL ENDPLT(0.,-2.,999)
      STOP
      END
//G.OBJECT DD DSNAME=U.M12280.13637.SUBLIB.OBJ,DISP=OLD
//G.FT09F001 DD UNIT=TAPE9,LABEL=(1,NL),DISP=(NEW,PASS),
//     DCB=(DEN=2,RECFM=VS,LRECL=504,BLKSIZE=508)
//G.FT64F001 DD DSN=&&CALDATA,DISP=(NEW,PASS),UNIT=SCRATCH,
//     SPACE=(22,1)
//G.SYSIN DD *,DCB=BLKSIZE=2000
THETA IN DEGREES                    16
LIFT COEFFICIENT                    16
DRAG COEFFICIENT                    16
```

LIFT TO DRAG RATIO
LIFT COEFFICIENT VS. THETA
DRAG COEFFICIENT VS. THETA
LIFT TO DRAG RATIO VS. THETA
TURBULENT BOUNDARY LAYER
LAMINAR BOUNDARY LAYER

MACH NUMBER =
REYNOLDS NO./10 5 =
PHI IN DEGREES =
THETA IN DEGREES =
DELTA = 4 DEGREES
DELTA = 6 DEGREES
DELTA = 8 DEGREES
DELTA = 10 DEGREES
NO SKIN FRICTION OR BASE DRAG
NO BASE DRAG
ALL FORCES

LAMINAR BOUNDARY LAYER
TURBULENT BOUNDARY LAYER

/*EOJ ********

```
/*SETUP UNIT=TAPE9,ID=(001029,RING,SAVE,SL),DDNAME=FT09F001,A=OSS
//STEP1 EXEC FORCGO,LIBRARY='SYS5.PLOT.SUBR'
//C.SYSIN DD *,DCB=BLKSIZE=2000
C      MAIN - CL, CD & LD VS. PHI - GRAPHS V
       INTEGER TYPE,XLABEL(7),YLABEL(7),TITLE(7),SUBTTL(7),VAR(5,4),SYMTT
      1I(8,4)
       INTEGER YLAB(7,3),TIT(7,3),SUBT(7,3),SYMT(8,4,3)
       REAL LD(5)
       DIMENSION CL(5),CD(5),X(320),Y(320),NUM(5),VAL(4),XX(320),NUM2(5),
      1NUM3(5)
       DIMENSION YX(3,5,320),NCY(3)
       DATA IS/'S'/
       DATA NUM/0,0,0,0,0/
C      READ X-AXIS LABEL & NO. CHARACTERS IN XLABEL, THEN 3 PAIRS OF Y-AXIS
C       LABEL & NO. CHARACTERS IN YLAB (CL,CD,LD)
       READ(5,1000) XLABEL,NCX,((YLAB(I,J),I=1,7),NCY(J),J=1,3)
 1000  FORMAT(7A4,2X,I10)
C      READ 3 TITLES, THEN 3 SUBTITLES (CL,CD,LD;TURBULENT,LAMINAR,BLANK)
       READ(5,1001) TIT,SUBT
 1001  FORMAT(7A4)
C      READ VARIABLE NAMES (XM,RE,THETA,PHI)
       READ(5,1002) VAR
 1002  FORMAT(5A4)
C      READ 3 SETS OF SYMBOL TITLES (PHI=60,90,120,150;NO SKIN FRICTION OR BASE
C       DRAG,NO BASE DRAG,ALL FORCES,BLANK;LAMINAR,TURBULENT,BLANK,BLANK)
       READ(5,1003) SYMT
 1003  FORMAT(8A4)
       ICASE=5
       XM=2.
       RE=1.0E+07
       CALL PLOTS(IDUM,IDUM,9)
       CALL PLOT(0.,2.,-3)
    2  VAL(1)=XM
       VAL(2)=RE/1.0E+05
       DO 40 I=30,70,20
       THETA=I
```

```
      VAL(3)=THETA
      I=0
      DO 41 J=1,4
      IND=0
      DELTA=4+(J-1)*2
      DELTU=DELTA-3.
      WRITE(6,100) THETA,DELTA,XM,RE
  100 FORMAT(1H1,'THETA =',F10.5,10X,'DELTA =',F10.5,10X,'XM =',F10.5,10
     1X,'RE =',E10.3//1X,'   L     PHI   XMDES   CL(1)   CL(2)   CL(3)   CL(4)
     2  CL(5)   CD(1)   CD(2)   CD(3)   CD(4)   CD(5)   LD(1)   LD(2)   LD(3)   L
     3D(4)   LD(5)'//)
      DO 42 K=24,178,2
      PHI=K
      CALL CARET(DELTA,DELTU,THETA,PHI,XM,RE,XMDES,TYPE,PRATIO,ERATIO,BR
     1ATL,BRATT,CL,CD,LD)
      IF(XMDES.EQ.0..OR.PRATIO.LE.0..OR.ERATIO.LE.0..OR.TYPE.EQ.IS) GO
     1 TO 39
      IND=1
      I=I+1
      X(I)=PHI
      DO 50 II=1,5
      YY(1,II,I)=CL(II)
      YY(2,II,I)=CD(II)
   50 YY(3,II,I)=LD(II)
      WRITE(6,200) I,X(I),XMDES,((YY(II,JJ,I),JJ=1,5),II=1,3)
  200 FORMAT(1X,I4,17F7.3)
      GO TO 42
   39 IF(IND.EQ.1) GO TO 41
   42 CONTINUE
   41 NUM(J+1)=I
      NPTS=NUM(5)
      NPT=NUM(4)-NUM(3)
      NP=NUM(3)
      DO 53 II=1,3
      DO 54 JJ=1,7
      YLABEL(JJ)=YLAB(JJ,II)
```

```
      TITLE(JJ)=TIT(JJ,II)
      IF(XM.EQ.3.1) GO TO 3
      DO 55 JJ=1,7
   55 SUBTTL(JJ)=SUBT(JJ,1)
      GO TO 4
    3 DO 56 JJ=1,7
   56 SUBTTL(JJ)=SUBT(JJ,2)
    4 VAL(4)=0.
      DO 57 JJ=1,8
      DO 57 KK=1,4
   57 SYMTTL(JJ,KK)=SYMT(JJ,KK,1)
      DO 58 JJ=1,NPTS
   58 Y(JJ)=YY(II,ICASE,JJ)
      CALL PICTR(5.,5.,XLABEL,NCX,YLABEL,NCY(II),TITLE,SUBTTL,VAR,VAL,SY
     1MTTL,X,Y,NUM,4,10)
   59 WRITE(6,300) II
  300 FORMAT(1X,'PLOT  V -',I2,' COMPLETE')
   60 CONTINUE
      IF(XM.EQ.3.1) GO TO 1
      XM=3.1
      RE=1.0E+05
      ICASE=4
      GO TO 2
    1 CALL ENDPLT(0.,-2.,999)
      STOP
      END
//G.OBJECT DD DSNAME=U.M12280.13637.SUBLIB.OBJ,DISP=OLD
//G.FT09F001 DD UNIT=TAPE9,LABEL=(1,SL),DISP=(NEW,PASS),
//     DCB=(DEN=2,RECFM=VS,LRECL=504,BLKSIZE=508)
//G.FT04F001 DD DSN=&&CALDATA,DISP=(NEW,PASS),UNIT=SCRATCH,
//     SPACE=(22,1)
//G.SYSIN DD *,DCB=BLKSIZE=2000
```

```
INI IN ENGINES                          14
LIFT COEFFICIENT                        16
DRAG COEFFICIENT                        16
LIFT TO DRAG RATIO                      18
```

LIFT COEFFICIENT VS. PHI
DRAG COEFFICIENT VS. PHI
LIFT TO DRAG RATIO VS. PHI
TURBULENT BOUNDARY LAYER
LAMINAR BOUNDARY LAYER

MACH NUMBER =
REYNOLDS NO./10 5 =
THETA IN DEGREES =
PHI IN DEGREES =
DELTA = 4 DEGREES
DELTA = 6 DEGREES
DELTA = 8 DEGREES
DELTA = 10 DEGREES
NO SKIN FRICTION OR BASE DRAG
NO BASE DRAG
ALL FORCES

LAMINAR BOUNDARY LAYER
TURBULENT BOUNDARY LAYER

/FREE ********

AD-A053 691 MASSACHUSETTS INST OF TECH CAMBRIDGE AEROPHYSICS LAB F/G 20/4
A STUDY OF THE LIFT-TO-DRAG RATIO CAPABILITY OF CARET WING WAVE--ETC(U)
MAR 78 M D SOLOMON F44620-76-C-0049
UNCLASSIFIED TR-200 AFOSR-TR-78-0758 NL

2 OF 3
AD
A053691

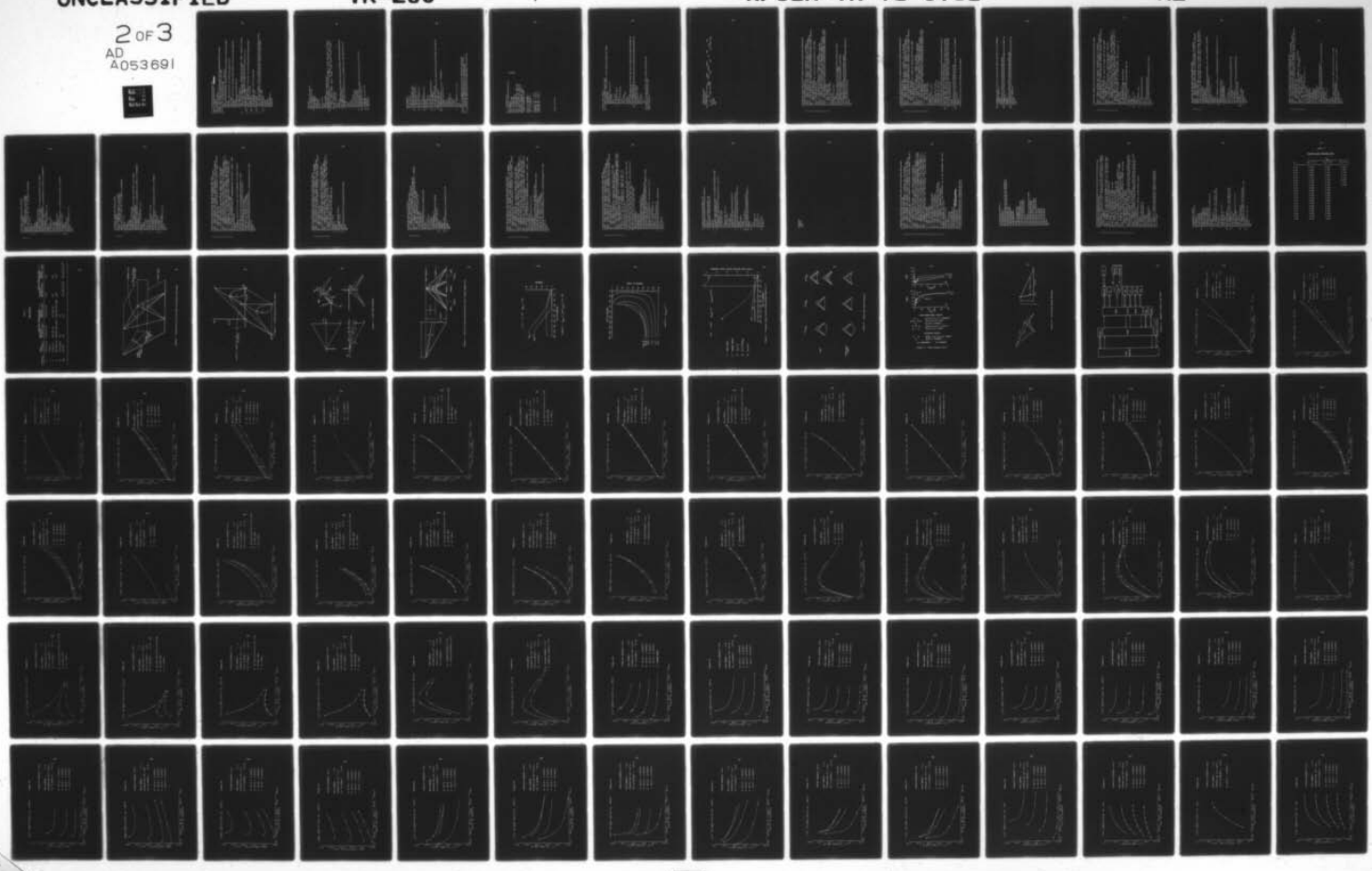

```
// 'SOLOMON',CLASS=C,REGION=150K
/*MITID USER=(M12280,13637,,[redacted])
/*SRI STANDARD
/*MAIN TIME=3,LINES=3
/*SETUP UNIT=TAPE9,ID=(001028,RING,SAVE,SL),DDNAME=FT09F001,A=HQH
//STEP1 EXEC FORCGO,LIBRARY='SYS5.PLOT.SUBR'
//C.SYSIN DD *,DCB=BLKSIZE=2000
C     MAIN - CL, CD & LD VS. XM - GRAPHS VI
      INTEGER TYPE,XLABEL(7),YLABEL(7),TITLE(7),SUBTTL(7),VAR(5,4),SYMTT
     1L(8,4)
      INTEGER YLAB(7,3),TIT(7,3),SUBT(7,3),SYMT(8,4,3)
      REAL LD(5)
      DIMENSION CL(5),CD(5),X(320),Y(320),NUM(5),VAL(4),XX(320),NUM2(5),
     1NUM3(5)
      DIMENSION YX(3,5,320),NCY(3)
      DATA IS/'S'/
      DATA NUM/0,0,0,0,0/
C     READ X-AXIS LABEL & NO. CHARACTERS IN XLABEL, THEN 3 PAIRS OF Y-AXIS
C      LABEL & NO. CHARACTERS IN YLAB (CL,CD,LD)
      READ(5,1000) XLABEL,NCX,((YLAB(I,J),I=1,7),NCY(J),J=1,3)
 1000 FORMAT(7A4,2X,I10)
C     READ 3 TITLES, THEN 3 SUBTITLES (CL,CD,LD;TURBULENT,LAMINAR,BLANK)
      READ(5,1001) TIT,SUBT
 1001 FORMAT(7A4)
C     READ VARIABLE NAMES (XM,RE,THETA,PHI)
      READ(5,1002) VAR
 1002 FORMAT(5A4)
C     READ 3 SETS OF SYMBOL TITLES (PHI=60,90,120,150;NO SKIN FRICTION OR BASE
C      DRAG,NO BASE DRAG,ALL FORCES,BLANK;LAMINAR,TURBULENT,BLANK,BLANK)
      READ(5,1003) SYMT
 1003 FORMAT(8A4)
      ICASE=5
      MLIM=50
      DELTA=6.5
      DELTU=DELTA-3.
      THETA=30.
```

```
      PHI=120.
      CALL PLOTS(IDUM,IDUM,9)
      CALL PLOT(0.,2.,-3)
    2 VAL(1)=DELTA
      VAL(2)=THETA
      VAL(3)=PHI
      VAL(4)=0.
      L=0
      DO 41 J=1,4
      IND=0
      RE=10.**(J+4)
      WRITE(6,100) DELTA,THETA,PHI,RE
  100 FORMAT(1H1,'DELTA =',F10.5,10X,'THETA =',F10.5,10X,'PHI =',F10.5,1
     10X,'RE =',E10.3//1X,'   L      XM  XMDES  CL(1)  CL(2)  CL(3)  CL(4
     2)  CL(5)  CD(1)  CD(2)  CD(3)  CD(4)  CD(5)  LD(1)  LD(2)  LD(3)
     3LD(4)  LD(5)'//)
      DO 42 K=15,MLIM
      XK=K
      XM=XK/10.
      CALL CARET(DELTA,DELTU,THETA,PHI,XM,RE,XMDES,TYPE,PRATIO,ERATIO,BR
     1ATL,BRATT,CL,CD,LD)
      IF(XMDES.EQ.0..OR.PRATIO.LE.0..OR.ERATIO.LE.0..OR.TYPE.EQ.IS) GO
     1 TO 39
      IND=1
      L=L+1
      X(L)=XM
      DO 50 II=1,5
      YX(1,II,L)=CL(II)
      YX(2,II,L)=CD(II)
   50 YX(3,II,L)=LD(II)
      WRITE(6,200) L,X(L),XMDES,((YX(II,JJ,L),JJ=1,5),II=1,3)
  200 FORMAT(1X,I4,17F7.3)
      GO TO 42
   39 IF(IND.EQ.1) GO TO 41
   42 CONTINUE
   41 NUM(J+1)=L
```

```
      NPTS=NUM(5)
      DO 53 II=1,3
      DO 54 JJ=1,7
      YLABEL(JJ)=YLAB(JJ,II)
   54 TITLE(JJ)=TIT(JJ,II)
      IF(ICASE.EQ.4) GO TO 3
      DO 55 JJ=1,7
   55 SUBTTL(JJ)=SUBT(JJ,1)
      GO TO 4
    3 DO 56 JJ=1,7
   56 SUBTTL(JJ)=SUBT(JJ,2)
    4 CONTINUE
      DO 57 JJ=1,8
      DO 57 KK=1,4
   57 SYMTTL(JJ,KK)=SYMT(JJ,KK,1)
      DO 58 JJ=1,NPTS
   58 Y(JJ)=YX(II,ICASE,JJ)
      CALL PICTR(5.,5.,XLABEL,NCX,YLABEL,NCY(II),TITLE,SUBTTL,VAR,VAL,SY
     1MTTL,X,Y,NUM,4,10)
   53 WRITE(6,300) II
  300 FORMAT(1X,'PLOT VI -',I2,' COMPLETE')
      IF(ICASE.EQ.4) GO TO 1
      ICASE=4
      MLIM=31
      DELTA=8.3
      DELTU=DELTA-3.
      THETA=30.
      PHI=120.
      GO TO 2
    1 CALL ENDPLT(0.,-2.,999)
      STOP
      END
//G.OBJFCT DD DSNAME=U.M12280.13637.SUBLIB.OBJ,DISP=OLD
//G.FT09F001 DD UNIT=TAPE9,LABEL=(1,SL),DISP=(NEW,PASS),
//     DCB=(DEN=2,RECFM=VS,LRECL=504,BLKSIZE=508)
//G.FT64F001 DD DSN=&&CALDATA,DISP=(NEW,PASS),UNIT=SCRATCH,
```

```
//     SPACE=(22,1)
//G.SYSIN DD *,DCB=BLKSIZE=2000
MACH NUMBER                              11
LIFT COEFFICIENT                         16
DRAG COEFFICIENT                         16
LIFT TO DRAG RATIO                       18
LIFT COEFFICIENT VS. MACH NO
DRAG COEFFICIENT VS. MACH NO
LIFT/DRAG RATIO VS. MACH NO.
TURBULENT BOUNDARY LAYER
LAMINAR BOUNDARY LAYER

DELTA IN DEGREES =
THETA IN DEGREES =
PHI IN DEGREES =

REYNOLDS NO. = 10 5
REYNOLDS NO. = 10 6
REYNOLDS NO. = 10 7
REYNOLDS NO. = 10 8
```



```
/*EOJ ********
```

```
//STEP3 EXEC FORCGO
//C.SYSIN DD *,DCB=BLKSIZE=2000
C      MAIN PROGRAM - TEST MATRIX I WITH REFINED RANGE FOR DELTA
       INTEGER TYPE
       DIMENSION CL(5),CD(5)
       REAL LD(5)
       XM=2.
       RE=1.0E+07
     1 DO 40 I=10,70,20
       THETA=I
       DO 40 J=60,150,30
       PHI=J
       CALL HEAD
       DO 40 K=3,10
       DELTA=K
       DELTU=K-3
       CALL CARET(DELTA,DELTU,THETA,PHI,XM,RE,XMDES,TYPE,PRATIO,ERATIO,BR
      1ATL,BRATT,CL,CD,LD)
    40 CALL PRINT(DELTA,DELTU,THETA,PHI,XM,RE,XMDES,TYPE,PRATIO,ERATIO,BR
      1ATL,BRATT,CL,CD,LD)
       IF(XM.NE.2.) STOP
       XM=3.1
       RE=1.0E+05
       GO TO 1
       END
//G.OBJECT DD DSN=U.M12280.13637.SUBLIB.OBJ,DISP=OLD
//G.SYSIN DD *,DCB=BLKSIZE=2000
/*EOJ ********
```

```
      SUBROUTINE HEAD
      WRITE(6,100)
  100 FORMAT(1H1,1X,'DELTA      DELTU      THETA         PHI         XM
     1       RE          XMDES  TYPE    BRATL         CL          CD
     2  L/D    CASE'/3X,'DEG         DEG         DEG           DEG',46X,'BRA
     3TT'//)
      RETURN
      END
```

```
      SUBROUTINE CARET(DELTA,DELTU,THETA,PHI,XM,RE,XMDES,TYPE,PRATIO,ERA
     1TIO,BRATL,BRATT,CL,CD,LD)
C     DELTA = ANGLE BETWEEN FREE STREAM & INTERNAL RIB, IN DEGREES
C     DELTU = ANGLE BETWEEN FREE STREAM & UPPER SURFACE RIB, IN DEGREES
C     THETA = ANGLE BETWEEN FREE STREAM & PLANE SPANNING L.E.'S, IN DEGREES
C     PHI = ANGLE BETWEEN FREE STREAM SURFACES CONTAINING LEADING EDGES, DEGREES
C     XM = FREE STREAM MACH NO.
C     RE = FREE STREAM REYNOLDS NO. BASED ON SQUARE ROOT OF PLAN AREA
C     XMDES = DESIGN MACH NO.
C     TYPE = W, IF SHOCK IS WEAK; S, IF SHOCK IS STRONG
C     PRATIO = LOWER SURFACE PRESSURE / FREE STREAM STATIC PRESSURE
C     ERATIO = STATIC PRESSURE RATIO ACROSS P-M EXPANSION NORMAL TO L.E.
C     BRATL = BASE PRESSURE / FREE STREAM STATIC PRESSURE,LAMINAR BOUNDARY LAYER
C     BRATT = BASE PRESSURE/FREE STREAM STATIC PRESSURE,TURBULENT BOUNDARY LAYER
C     CL = LIFT COEFFICIENT
C     CD = DRAG COEFFICIENT
C     LD = LIFT TO DRAG RATIO
      INTEGER TYPE
      DIMENSION CL(5),CD(5)
      REAL LD(5)
      CALL LOWER(DELTA,THETA,PHI,XM,RE,XMDES,PRATIO,TYPE,CFLL,CFTL)
      IF(XMDES.EQ.0..OR.PRATIO.LE.0.) RETURN
      CALL UPPER(DELTU,THETA,PHI,XM,RE,ERATIO,CFLU,CFTU)
      IF(ERATIO.LE.0.) RETURN
      CALL BASE(DELTA,DELTU,THETA,PHI,XM,RE,BRATL,BRATT)
      CALL COEFF(DELTA,DELTU,THETA,PHI,XM,PRATIO,ERATIO,BRATL,BRATT,CFLL
     1,CFTL,CFLU,CFTU,CL,CD,LD)
      RETURN
      END
```

```
      SUBROUTINE PRINT(DELTA,DELTU,THETA,PHI,XM,RE,XMDES,TYPE,PRATIO,ERA
     1TIO,BRATL,BRATT,CL,CD,LD)
C     DELTA = ANGLE BETWEEN FREE STREAM & INTERNAL RIB, IN DEGREES
C     DELTU = ANGLE BETWEEN FREE STREAM & UPPER SURFACE RIB, IN DEGREES
C     THETA = ANGLE BETWEEN FREE STREAM & PLANE SPANNING L.E.'S, IN DEGREES
C     PHI = ANGLE BETWEEN FREE STREAM SURFACES CONTAINING LEADING EDGES, DEGREES
C     XM = FREE STREAM MACH NO.
C     RE = FREE STREAM REYNOLDS NO. BASED ON SQUARE ROOT OF PLAN AREA
C     XMDES = DESIGN MACH NO.
C     TYPE = W, IF SHOCK IS WEAK; S, IF SHOCK IS STRONG
C     PRATIO = LOWER SURFACE PRESSURE / FREE STREAM STATIC PRESSURE
C     ERATIO = STATIC PRESSURE RATIO ACROSS P-M EXPANSION NORMAL TO L.E.
C     BRATL = BASE PRESSURE / FREE STREAM STATIC PRESSURE,LAMINAR BOUNDARY LAYER
C     BRATT = BASE PRESSURE/FREE STREAM STATIC PRESSURE,TURBULENT BOUNDARY LAYER
C     CL = LIFT COEFFICIENT
C     CD = DRAG COEFFICIENT
C     LD = LIFT TO DRAG RATIO
      INTEGER TYPE
      DIMENSION CL(5),CD(5)
      REAL LD(5)
      IF(XMDES.EQ.0.) GO TO 1
      IF(PRATIO.EQ.-1.) GO TO 2
      IF(PRATIO.EQ.0.) GO TO 3
      IF(ERATIO.LE.0.) GO TO 4
      WRITE(6,500) DELTA,DELTU,THETA,PHI,XM,RE,XMDES,TYPE,BRATL,CL(1),CD
     1(1),LD(1),BRATT,(CL(I),CD(I),LD(I),I=2,5)
  500 FORMAT(1X,3(F6.2,5X),F7.2,5X,F5.2,5X,1PE9.2,5X,0PF6.2,4X,A1,5X,F5.
     12,5X,2(F6.3,5X),F6.2,5X,'(1)'/86X,F5.2,5X,2(F6.3,5X),F6.2,5X,'(2)'
     2/96X,2(F6.3,5X),F6.2,5X,'(3)'/96X,2(F6.3,5X),F6.2,5X,'(4)'/96X,2(F
     36.3,5X),F6.2,5X,'(5)'//)
      RETURN
    1 WRITE(6,100) DELTA,DELTU,THETA,PHI,XM,RE
  100 FORMAT(1X,3(F6.2,5X),F7.2,5X,F5.2,5X,1PE9.2,5X,'THERE IS NO DESIGN
     1 MACH NO.'//)
      RETURN
    2 WRITE(6,200) DELTA,DELTU,THETA,PHI,XM,RE,XMDES
```

```
200 FORMAT(1X,3(F6.2,5X),F7.2,5X,F5.2,5X,1PE9.2,5X,0PF6.2,5X,'SUBSONIC
   1 LEADING EDGE'//)
     RETURN
   3 WRITE(6,300) DELTA,DELTU,THETA,PHI,XM,RE,XMDES
300 FORMAT(1X,3(F6.2,5X),F7.2,5X,F5.2,5X,1PE9.2,5X,0PF6.2,5X,'SHOCK DE
   1TACHED'//)
     RETURN
   4 WRITE(6,400) DELTA,DELTU,THETA,PHI,XM,RE,XMDES,TYPE
400 FORMAT(1X,3(F6.2,5X),F7.2,5X,F5.2,5X,1PE9.2,5X,0PF6.2,4X,A1,5X,'ER
   1ATIO NOT FOUND'//)
     RETURN
     END
```

```
      SUBROUTINE LOWER(DELTA,THETA,PHI,XM,RE,XMDES,PRATIO,TYPE,CFLL,CFTL
     1)
C     DELTA = ANGLE BETWEEN FREE STREAM & INTERNAL RIB, IN DEGREES
C     THETA = ANGLE BETWEEN FREE STREAM & PLANE SPANNING L.E.'S, IN DEGREES
C     PHI = ANGLE BETWEEN FREE STREAM SURFACES CONTAINING LEADING EDGES, DEGREES
C     XM = FREE STREAM MACH NO.
C     RE = FREE STREAM REYNOLDS NO. BASED ON SQUARE ROOT OF PLAN AREA
C     XMDES = DESIGN MACH NO.
C     PRATIO = LOWER SURFACE PRESSURE / FREE STREAM STATIC PRESSURE
C     TYPE = W, IF SHOCK IS WEAK; S, IF SHOCK IS STRONG
C     CFLL = LAMINAR FRICTION COEFF. FOR LOWER SURFACE = WALL SHEAR STRESS / Q
C     CFTL = TURBULENT FRICTION COEFF. FOR LOWER SURFACE = WALL SHEAR STRESS / Q
C     IF DELTA & THETA DO NOT REPRESENT A WEAK OBLIQUE SHOCK, XMDES IS SET = 0.
C     IF LEADING EDGE IS SUBSONIC, PRATIO IS SET = -1.
C     IF MAX DEFLECTION ANGLE IS .LT. WEDGE ANGLE, PRATIO IS SET = 0.
      INTEGER TYPE
      DATA IW,IS/'W','S'/
      CALL DESIGN(DELTA,THETA,XMDES,PHIB)
      IF(XMDES.EQ.0.) RETURN
      CALL DG(DELTA,THETA,PHI,XM,DM,GAMMA,DMG,XN)
      IF(XN-1.) 1,1,2
    1 PRATIO=-1.
      RETURN
    2 IF(DMG) 3,4,4
    3 PRATIO=0.
      RETURN
    4 IF(PHI-PHIB) 5,6,6
    5 TYPE=IS
      CALL SHOCKS(XN,GAMMA,PRATIO)
      GO TO 7
    6 TYPE=IW
      CALL SHOCKW(XN,GAMMA,PRATIO)
    7 CALL SFL(DELTA,THETA,PHI,XM,RE,PRATIO,CFLL,CFTL)
      RETURN
      END
```

```
      SUBROUTINE DESIGN(DELTA,THETA,XMDES,PHIB)
C     DELTA = ANGLE BETWEEN FREE STREAM & INTERNAL RIB, IN DEGREES
C     THETA = ANGLE BETWEEN FREE STREAM & PLANE SPANNING L.E.'S, IN DEGREES
C     XMDES = DESIGN MACH NO.
C     PHIB = VALUE OF PHI WHICH DIVIDES WEAK & STRONG SHOCK CASES (ON DESIGN)
C     IF DELTA & THETA DO NOT REPRESENT A WEAK SHOCK, XMDES & PHIB ARE SET = 0.
      RD=57.29577951308
      DELTAR=DELTA/RD
      THETAR=THETA/RD
      XMDES2=10.*(COTAN(THETAR)+TAN(DELTAR))/(5.*SIN(2.*THETAR)-TAN(DELT
     1AR)*(7.+5.*COS(2.*THETAR)))
      IF(XMDES2-1.) 1,1,2
    1 XMDES=0.
      PHIB=0.
      RETURN
    2 STH2=(3.*XMDES2-5.+SQRT(3.*(3.*XMDES2*XMDES2+4.*XMDES2+20.)))/7./X
     1MDES2
      THMAXR=ARSIN(SQRT(STH2))
      IF(THETAR-THMAXR) 3,1,1
    3 XMDES=SQRT(XMDES2)
      PHI=1.
      DO 40 I=1,3
      XINC=10./10.**I
      CALL DG(DELTA,THETA,PHI,XMDES,DM,GAMMA,DMG,XN)
      DO 41 J=1,178
      PHI=PHI+XINC
      CALL DG(DELTA,THETA,PHI,XMDES,DM,GAMMA,DMGP,XN)
      IF(DMGP-DMG) 41,40,40
   41 DMG=DMGP
   40 PHI=PHI-2.*XINC
      PHIB=PHI+XINC
      RETURN
      END
```

```
      SUBROUTINE DG(DELTA,THETA,PHI,XM,DM,GAMMA,DMG,XN)
C     DELTA = ANGLE BETWEEN FREE STREAM & INTERNAL RIB, IN DEGREES
C     THETA = ANGLE BETWEEN FREE STREAM & PLANE SPANNING L.E.'S, IN DEGREES
C     PHI = ANGLE BETWEEN FREE STREAM SURFACES CONTAINING LEADING EDGES, DEGREES
C     XM = FREE STREAM MACH NO.
C     DM = MAX DEFLECTION ANGLE NORMAL TO L.E., IN DEGREES
C     GAMMA = WEDGE ANGLE NORMAL TO L.E., IN DEGREES
C     DMG = DM - GAMMA, IN DEGREES
C     XN = MACH NO. NORMAL TO L.E.
C     IF XN .LE. 1., DM & DMG ARE SET = 0.
      RD=57.29577951308
      DELTAR=DELTA/RD
      THETAR=THETA/RD
      PHIR=PHI/RD
      B2=-TAN(THETAR)
      C2=-TAN(DELTAR)
      B3=-B2*TAN(PHIR/2.)
      X=1.+B2**2+B3**2
      Y=B2**4+2.*B2**2*B3**2+B3**4+B2**2+B3**2
      GAMMA=ARSIN(-C2*X/SQRT(Y)/SQRT(C2**2+1.+((C2-B2)/B3)**2))*RD
      XN2=XM*XM*Y/X**2
      XN=SQRT(XN2)
      IF(XN-1.) 1,1,2
    1 DM=0.
      DMG=0.
      RETURN
    2 STH2=(3.*XN2-5.+SQRT(3.*(3.*XN2**2+4.*XN2+20.)))/7./XN2
      THR=ARSIN(SQRT(STH2))
      DM=ATAN(1./(TAN(THR)*(6.*XN2/5./(XN2*STH2-1.)-1.)))*RD
      DMG=DM-GAMMA
      RETURN
      END
```

```
      SUBROUTINE SHOCKW(XN,GAMMA,PRATIO)
C     XN = MACH NUMBER
C     GAMMA = DEFLECTION ANGLE, IN DEGREES
C     PRATIO = PRESSURE RATIO ACROSS SHOCK
C     PRATIO SET = 0. IF XN .LE. 1. OR SHOCK IS DETACHED
      IF(XN-1.) 3,3,8
    3 PRATIO=0.
      RETURN
    8 XN2=XN*XN
      XN4=XN2*XN2
      GR=GAMMA/57.29577951308
      SA2MAX=(3.*XN2-5.+SQRT(3.*(3.*XN4+4.*XN2+20.)))/(7.*XN2)
      AMAXR=ARSIN(SQRT(SA2MAX))
      GMAXR=ATAN(5.*(XN2*SA2MAX-1.)/TAN(AMAXR)/(5.+XN2*(6.-5.*SA2MAX)))
      IF(GR-GMAXR) 1,2,3
    2 PRATIO=(7.*XN2*SA2MAX-1.)/6.
      RETURN
    1 AR=ARSIN(1./XN)
      DO 40 I=1,4
      XINC=.1**I
    6 AR=AR+XINC
      IF(AR-AMAXR) 4,40,5
    4 SA2=SIN(AR)**2
      TEST=ATAN(5.*(XN2*SA2-1.)/TAN(AR)/(5.+XN2*(6.-5.*SA2)))
      IF(TEST-GR) 6,7,40
    5 AR=AMAXR
   40 AR=AR-XINC
      SA2=SIN(AR)**2
    7 PRATIO=(7.*XN2*SA2-1.)/6.
      RETURN
      END
```

```
      SUBROUTINE SHOCKS(XN,GAMMA,PRATIO)
C     XN = MACH NUMBER
C     GAMMA = DEFLECTION ANGLE, IN DEGREES
C     PRATIO = PRESSURE RATIO ACROSS SHOCK
C     PRATIO SET = 0. IF XN .LE. 1. OR SHOCK IS DETACHED
      IF(XN-1.) 3,3,8
    3 PRATIO=0.
      RETURN
    8 XN2=XN*XN
      XN4=XN2*XN2
      GR=GAMMA/57.29577951308
      SA2MAX=(3.*XN2-5.+SQRT(3.*(3.*XN4+4.*XN2+20.)))/(7.*XN2)
      AMAXR=ARSIN(SQRT(SA2MAX))
      GMAXR=ATAN(5.*(XN2*SA2MAX-1.)/TAN(AMAXR)/(5.+XN2*(6.-5.*SA2MAX)))
      IF(GR-GMAXR) 1,2,3
    2 PRATIO=(7.*XN2*SA2MAX-1.)/6.
      RETURN
    1 AR=AMAXR
      DO 40 I=1,4
      XINC=.1**I
    6 AR=AR+XINC
      IF(AR-1.570796327) 4,40,5
    4 SA2=SIN(AR)**2
      TEST=ATAN(5.*(XN2*SA2-1.)/TAN(AR)/(5.+XN2*(6.-5.*SA2)))
      IF(GR-TEST) 6,7,40
    5 AR=1.570796327
   40 AR=AR-XINC
      SA2=SIN(AR)**2
    7 PRATIO=(7.*XN2*SA2-1.)/6.
      RETURN
      END
```

```
      SUBROUTINE SFI(DELTA,THETA,PHI,XM,RE,PRATIO,CFLL,CFTL)
C     DELTA = ANGLE BETWEEN FREE STREAM & INTERNAL RIB, IN DEGREES
C     THETA = ANGLE BETWEEN FREE STREAM & PLANE SPANNING L.E.'S, IN DEGREES
C     PHI = ANGLE BETWEEN FREE STREAM SURFACES CONTAINING LEADING EDGES, DEGREES
C     XM = FREE STREAM MACH NO.
C     RE = FREE STREAM REYNOLDS NO. BASED ON SQUARE ROOT OF PLAN AREA
C     PRATIO = LOWER SURFACE PRESSURE / FREE STREAM STATIC PRESSURE
C     CFLL = LAMINAR FRICTION COEFF. FOR LOWER SURFACE = WALL SHEAR STRESS / Q
C     CFTL = TURBULENT FRICTION COEFF. FOR LOWER SURFACE = WALL SHEAR STRESS / Q
C     REL = REYNOLDS NO. ON LOWER SURFACE BASED ON SQUARE ROOT OF PLAN AREA
C     RELL = REYNOLDS NO. ON LOWER SURFACE BASED ON LENGTH OF INTERNAL RIB
C     XML = MACH NO. DOWNSTREAM OF SHOCK
C     CRATIO = RATIO OF COMPRESSIBLE TO INCOMPRESSIBLE SKIN FRIC. COEFF., TURB.
      RD=57.29577951308
      X=PRATIO
      REL=RE*X**(-.76)*((6.*X+1.)/(X+6.))**1.76*SQRT(1.-5.*(X*X-1.)/XM/X
     1M/(6.*X+1.))
      RELL=REL/COS(DELTA/RD)/SQRT(TAN(THETA/RD)*TAN(PHI/2./RD))
      XML=SQRT((XM*XM*(6.*X+1.)-5.*(X*X-1.))/X/(X+6.))
      CFLL=(2.656-.0718*XML)/SQRT(RELL)
      IF(XML.LE.5.36) CRATIO=1.-.1186*XML
      IF(XML.GT.5.36) CRATIO=.5962-.043*XML
      CFTL=CRATIO*.455*(ALOG10(RELL)**(-2.58)+2.58*ALOG10(RELL)**(-3.58)
     1/ALOG(10.))
      RETURN
      END
```

```
      SUBROUTINE UPPER(DELTU,THETA,PHI,XM,RE,ERATIO,CFLU,CFTU)
C     DELTU = ANGLE BETWEEN FREE STREAM & UPPER SURFACE RIB, IN DEGREES
C     THETA = ANGLE BETWEEN FREE STREAM & PLANE SPANNING L.E.'S, IN DEGREES
C     PHI = ANGLE BETWEEN FREE STREAM SURFACES CONTAINING LEADING EDGES, DEGREES
C     XM = FREE STREAM MACH NO.
C     RE = FREE STREAM REYNOLDS NO. BASED ON SQUARE ROOT OF PLAN AREA
C     ERATIO = STATIC PRESSURE RATIO ACROSS P-M EXPANSION NORMAL TO L.E.
C     CFLU = LAMINAR FRICTION COEFF. FOR UPPER SURFACE = WALL SHEAR STRESS / Q
C     CFTU = TURBULENT FRICTION COEFF. FOR UPPER SURFACE = WALL SHEAR STRESS / Q
C     IF LEADING EDGE IS SUBSONIC, ERATIO IS SET = -1.
C     IF ERATIO NOT FOUND, IT IS SET = 0.
      CALL DG(DELTU,THETA,PHI,XM,DM,GAMMA,DMG,XN)
      IF(XN-1.) 1,1,2
    1 ERATIO=-1.
      RETURN
    2 CALL PM(XN,GAMMA,ERATIO)
      IF(ERATIO) 3,3,4
    3 RETURN
    4 CALL SFU(DELTU,THETA,PHI,XM,RE,ERATIO,CFLU,CFTU)
      RETURN
      END
```

```
      SUBROUTINE PM(XM1,TA,ERATIO)
C     XM1 = MACH NO. UPSTREAM OF EXPANSION
C     TA = TURNING ANGLE OF EXPANSION, IN DEGREES
C     ERATIO = STATIC PRESSURE RATIO ACROSS P-M EXPANSION
C     XNU = EXPANSION ANGLE FROM M=1 TO DOWNSTREAM MACH NO., RADIANS
C     XM2 = MACH NO. DOWNSTREAM OF EXPANSION
C     IF ERATIO NOT FOUND, IT IS SET = 0.
      RD=57.29577951308
      X=SQRT(XM1*XM1-1.)
      XNU=2.4495*ATAN(.40825*X)-ATAN(X)+TA/RD
      XM2=XM1
      DO 40 I=1,5
      XINC=10./10.**I
      DO 41 J=1,11
      XM2=XM2+XINC
      X=SQRT(XM2*XM2-1.)
      TEST=2.4495*ATAN(.40825*X)-ATAN(X)
      IF(TEST-XNU) 41,1,40
   41 CONTINUE
      ERATIO=0.
      RETURN
   40 XM2=XM2-XINC
    1 ERATIO=((5.+XM2*XM2)/(5.+XM1*XM1))**(-3.5)
      RETURN
      END
```

```
      SUBROUTINE SFU(DELTU,THETA,PHI,XM,RE,ERATIO,CFLU,CFTU)
C     DELTU = ANGLE BETWEEN FREE STREAM & UPPER SURFACE RIB, IN DEGREES
C     THETA = ANGLE BETWEEN FREE STREAM & PLANE SPANNING L.E.'S, IN DEGREES
C     PHI = ANGLE BETWEEN FREE STREAM SURFACES CONTAINING LEADING EDGES, DEGREES
C     XM = FREE STREAM MACH NO.
C     RE = FREE STREAM REYNOLDS NO. BASED ON SQUARE ROOT OF PLAN AREA
C     ERATIO = STATIC PRESSURE RATIO ACROSS P-M EXPANSION NORMAL TO L.E.
C     CFLU = LAMINAR FRICTION COEFF. FOR UPPER SURFACE = WALL SHEAR STRESS / Q
C     CFTU = TURBULENT FRICTION COEFF. FOR UPPER SURFACE = WALL SHEAR STRESS / Q
C     REU = REYNOLDS NO. ON UPPER SURFACE BASED ON SQUARE ROOT OF PLAN AREA
C     REUL = REYNOLDS NO. ON UPPER SURFACE BASED ON LENGTH OF UPPER SURFACE RIB
C     XMU = MACH NO. DOWNSTREAM OF P-M EXPANSION
C     CRATIO = RATIO OF COMPRESSIBLE TO INCOMPRESSIBLE SKIN FRIC. COEFF., TURB.
      PD=57.29577951308
      XMU2=(5.+XM*XM)/ERATIO**(1./3.5)-5.
      XMU=SQRT(XMU2)
      REU=RE*XMU/XM*((5.+XMU2)/(5.+XM*XM))**(-2.24)
      REUL=REU/COS(DELTU/RD)/SQRT(TAN(THETA/RD)*TAN(PHI/2./RD))
      CFLU=(2.656-.0178*XMU)/SQRT(REUL)
      IF(XMU.LE.5.36) CRATIO=1.-.1186*XMU
      IF(XMU.GT.5.36) CRATIO=.5962-.043*XMU
      CFTU=CRATIO*.455*(ALOG10(REUL)**(-2.58)+2.58*ALOG10(REUL)**(-3.58)
     1/ALOG(10.))
      RETURN
      END
```

```
      SUBROUTINE BASE(DELTA,DELTU,THETA,PHI,XM,RE,BRATL,BRATT)
C     DELTA = ANGLE BETWEEN FREE STREAM & INTERNAL RIB, IN DEGREES
C     DELTU = ANGLE BETWEEN FREE STREAM & UPPER SURFACE RIB, IN DEGREES
C     THETA = ANGLE BETWEEN FREE STREAM & PLANE SPANNING L.E.'S, IN DEGREES
C     PHI = ANGLE BETWEEN FREE STREAM SURFACES CONTAINING LEADING EDGES, DEGREES
C     XM = FREE STREAM MACH NO.
C     RE = FREE STREAM REYNOLDS NO. BASED ON SQUARE ROOT OF PLAN AREA
C     REC = FREE STREAM REYNOLDS NO. BASED ON HALF THE LENGTH
C     BRATL = BASE PRESSURE / FREE STREAM STATIC PRESSURE,LAMINAR BOUNDARY LAYER
C     BRATT = BASE PRESSURE/FREE STREAM STATIC PRESSURE,TURBULENT BOUNDARY LAYER
C     TRATIO = THICKNESS RATIO OF WING
C     IF XM.LT.1.5 OR .GT.3.1 OR PARAML.GT..2, BRATL IS SET = 0.
C     IF XM.LT.1.5 OR .GT.5.0 OR PARAMT.GT.5., BRATT IS SET = 0.
      DIMENSION X(21),Y(21),Z(7)
      DATA X/.49375,.444,.557,.647,.704,.738,.764,.782,.8,.809,.822,.825
     X,.831,.838,.844,.844,.844,.847,.847,.847,.847/
      DATA Y/.3375,.357,.570,.669,.716,.742,.764,.779,.789,.795,.8,.8,.8
     X06,.809,.813,.813,.816,.819,.819,.819,.819/
      DATA Z/.16,.257,.376,.472,.554,.631,.697/
      RD=57.29577951308
      DELTAR=DELTA/RD
      DELTUR=DELTU/RD
      A=COS(DELTUR+(DELTAR-DELTUR)/2.)
      TRATIO=(TAN(DELTAR)-TAN(DELTUR))*A
      REC=RE/A/SQRT(TAN(THETA/RD)*TAN(PHI/RD/2.))/2.
C     CALCULATE BASE PRESSURE RATIO FOR TURBULENT BOUNDARY LAYER
      PARAMT=1./(TRATIO*REC**.2)
      IF(PARAMT.GT.5..OR.XM.LT.1.5.OR.XM.GT.5.) GO TO 1
      IF(XM.GT.3.1) GO TO 2
      RATIO2=.35+.025*(PARAMT-.5)
      IF(XM-2.) 3,4,5
    3 RATIO1=.5+.0125*(PARAMT-.5)
      BRATT=RATIO1+(RATIO2-RATIO1)/.5*(XM-1.5)
      GO TO 6
    4 BRATT=RATIO2
      GO TO 6
```

```
    5 RATIO3=.2+.0615385*(PARAMT-.65)
      BRATT=RATIO2+(RATIO3-RATIO2)/1.1*(XM-2.)
      GO TO 6
    2 RATIO3=.2+.0615385*(PARAMT-.65)
      BRATT=RATIO3-.01765181*(XM-3.1)
      GO TO 6
    1 BRATT=0.
C     CALCULATE BASE PRESSURE RATIO FOR LAMINAR BOUNDARY LAYER
    6 PARAML=1./(TRATIO*SQRT(REC))
      IF(PARAML.GT..2.OR.XM.LT.1.5.OR.XM.GT.3.1) GO TO 7
      I=PARAML*100.+1.5
      IF(I.GT.20) I=20
      XI=I
      O=PARAML*100.-(XI-1.)
      X1=O*(O-1.)/2.
      X2=1.-O*O
      X3=O*(O+1.)/2.
      RATIO2=X1*Y(I-1)+X2*Y(I)+X3*Y(I+1)
      IF(XM-2.) 8,9,10
    8 RATIO1=X1*X(I-1)+X2*X(I)+X3*X(I+1)
      BRATL=RATIO1+(RATIO2-RATIO1)/.5*(XM-1.5)
      RETURN
    9 BRATL=RATIO2
      RETURN
   10 IF(I-7) 11,12,13
   11 RATIO3=X1*Z(I-1)+X2*Z(I)+X3*Z(I+1)
   14 BRATL=RATIO2+(RATIO3-RATIO2)/1.1*(XM-2.)
      RETURN
   12 I=6
      O=O+1.
      X1=O*(O-1.)/2.
      X2=1.-O*O
      X3=O*(O+1.)/2.
      GO TO 11
   13 RATIO3=.726
      GO TO 14
```

```
7 BRATL=0.
  RETURN
  END
```

```
      SUBROUTINE COEFF(DELTA,DELTU,THETA,PHI,XM,PRATIO,ERATIO,BRATL,BRAT
     1T,CFLL,CFTL,CFLU,CFTU,CL,CD,LD)
C     DELTA = ANGLE BETWEEN FREE STREAM & INTERNAL RIB, IN DEGREES
C     DELTU = ANGLE BETWEEN FREE STREAM & UPPER SURFACE RIB, IN DEGREES
C     THETA = ANGLE BETWEEN FREE STREAM & PLANE SPANNING L.E.'S, IN DEGREES
C     PHI = ANGLE BETWEEN FREE STREAM SURFACES CONTAINING LEADING EDGES, DEGREES
C     XM = FREE STREAM MACH NO.
C     PRATIO = LOWER SURFACE PRESSURE / FREE STREAM STATIC PRESSURE
C     ERATIO = STATIC PRESSURE RATIO ACROSS P-M EXPANSION NORMAL TO L.E.
C     BRATL = BASE PRESSURE / FREE STREAM STATIC PRESSURE,LAMINAR BOUNDARY LAYER
C     BRATT = BASE PRESSURE/FREE STREAM STATIC PRESSURE,TURBULENT BOUNDARY LAYER
C     CFLL = LAMINAR FRICTION COEFF. FOR LOWER SURFACE = WALL SHEAR STRESS / Q
C     CFTL = TURBULENT FRICTION COEFF. FOR LOWER SURFACE = WALL SHEAR STRESS / Q
C     CFLU = LAMINAR FRICTION COEFF. FOR UPPER SURFACE = WALL SHEAR STRESS / Q
C     CFTU = TURBULENT FRICTION COEFF. FOR UPPER SURFACE = WALL SHEAR STRESS / Q
C     CL = LIFT COEFFICIENT
C     CD = DRAG COFFFICIENT
C     LD = LIFT TO DRAG RATIO
C     (1) = NO SKIN FRICTION OR BASE DRAG
C     (2) = WITH LAMINAR SKIN FRICTION
C     (3) = WITH TURBULENT SKIN FRICTION
C     (4) = WITH LAMINAR SKIN FRICTION & BASE DRAG
C     (5) = WITH TURBULENT SKIN FRICTION & BASE DRAG
C     PQ = STATIC PRESSURE / DYNAMIC PRESSURE
C     IF BRATL OR BRATT ARE ZERO, THEN CONDITIONS (4) OR (5) REPRESENT ZERO BASE
C     PRESSURE (MAXIMUM BASE DRAG)
      DIMENSION CL(5),CD(5)
      REAL LD(5)
      RD=57.29577951308
      PQ=10./(7.*XM*XM)
      T2TH=TAN(THETA/RD)**2
      T2THP2=T2TH*TAN(PHI/2./RD)**2
      AL=1./COS(DELTA/RD)
      AU=1./COS(DELTU/RD)
      BL=SQRT(T2THP2+(TAN(THETA/RD)-TAN(DELTA/RD))**2)
      BU=SQRT(T2THP2+(TAN(THETA/RD)-TAN(DELTU/RD))**2)
```

```
CC=SQRT(T2THP2+T2TH+1.)
SL=(AI+BL+CC)/2.
SU=(AU+BU+CC)/2.
ALS=SQRT(SL*(SL-AL)*(SL-BL)*(SL-CC)/T2THP2)*2.
AUS=SQRT(SU*(SU-AU)*(SU-BU)*(SU-CC)/T2THP2)*2.
A=ALS*SIN(DELTA/RD)
B=AUS*SIN(DELTU/RD)
C=TAN(DELTA/RD)
D=TAN(DELTU/RD)
F=C-D
F=ALS*COS(DELTA/RD)
G=AUS*COS(DELTU/RD)
CI(1)=(PRATIO-ERATIO)*PQ
CL(2)=CL(1)-CFLL*A-CFLU*B
CL(3)=CL(1)-CFTL*A-CFTU*B
CL(4)=CL(2)
CL(5)=CL(3)
CD(1)=(PRATIO*C-ERATIO*D)*PQ-PQ*F
CD(2)=CD(1)+CFLL*F+CFLU*G
CD(3)=CD(1)+CFTL*F+CFTU*G
CD(4)=CD(2)+(1.-ERATL)*PQ*E
CD(5)=CD(3)+(1.-BRATT)*PQ*E
LD(1)=CL(1)/CD(1)
LD(2)=CL(2)/CD(2)
LD(3)=CL(3)/CD(3)
LD(4)=CL(2)/CD(4)
LD(5)=CL(3)/CD(5)
RETURN
END
```

```
      SUBROUTINE PICTR(XDIM,YDIM,XLABEL,NCX,YLABEL,NCY,TITLE,SUBTTL,VAR,
     1VAL,SYMTTL,X,Y,NUM,NBR,LINTYP)
C     PICTR DRAWS & LABELS AXES; DRAWS UP TO 4 CURVES IDENTIFIED BY SYMBOLS;
C      PRINTS TITLE, SUBTITLE, UP TO 4 PARAMETERS AND THEIR VALUES, & LABELS
C      UP TO 4 SYMBOLS
C     XDIM = LENGTH OF X-AXIS BEFORE SCALING OF PLOT TO 5 INCH SQUARE AREA
C     YDIM = LENGTH OF Y-AXIS BEFORE SCALING OF PLOT TO 5 INCH SQUARE AREA
C     XLABEL = UP TO 28 CHARACTERS TO LABEL X-AXIS
C     NCX = NUMBER OF CHARACTERS IN XLABEL
C     YLABEL = UP TO 28 CHARACTERS TO LABEL Y-AXIS
C     NCY = NUMBER OF CHARACTERS IN YLABEL
C     TITLE = UP TO 28 CHARACTERS FOR TITLE OF PLOT
C     SUBTTL = UP TO 28 CHARACTERS FOR SUBTITLE (EG. LAMINAR B. L.)
C     VAR = UP TO 20 CHARACTERS FOR PARAMETER NAME (ARRAY OF 4 NAMES)
C     VAL = NUMERICAL VALUE OF PARAMETER (ARRAY OF 4 VALUES)
C     SYMTTL = UP TO 4 LABELS TO IDENTIFY MEANING OF SYMBOLS ON CURVES
C     X = ARRAY CONTAINING ABSCISSA VALUES
C     Y = ARRAY CONTAINING ORDINATE VALUES
C     NUM = ARRAY WHOSE FIRST ELEMENT IS ZERO AND NEXT FOUR ELEMENTS CONTAIN
C      NUMBER OF THE ELEMENT OF X OR Y WHICH IS THE LAST POINT OF CURVES 1-4
C     NBR = NUMBER OF CURVES TO BE PLOTTED
C     LINTYP = INTERVAL BETWEEN PLOTTED SYMBOLS (SAME MEANING AS FOR SUB LINE)
      INTEGER XLABEL(7),YLABEL(7),TITLE(7),SUBTTL(7),VAR(5,4),SYMTTL(8,4
     1),VARX(5),SYMTTX(8)
      DIMENSION X(320),Y(320),XA(80),YA(80),NUM(5),VAL(4)
      NPTS=NUM(5)
      CALL SCALE(X,XDIM,NPTS,1)
      CALL SCALE(Y,YDIM,NPTS,1)
      XFCT=5./XDIM
      YFCT=5./YDIM
      FACT=AMIN1(XFCT,YFCT)
      CALL FACTOR(FACT)
      NCXX=-NCX
      CALL AXIS(0.,0.,XLABEL,NCXX,XDIM,0.,X(NPTS+1),X(NPTS+2))
      CALL AXIS(0.,0.,YLABEL,NCY,YDIM,90.,Y(NPTS+1),Y(NPTS+2))
      DO 40 N=1,NBR
```

```
      NPT=NUM(N+1)-NUM(N)
      IF(NPT.EQ.0) GO TO 40
      NPX=NUM(N)
      DO 41 M=1,NPT
      XA(M)=X(NPX+M)
   41 YA(M)=Y(NPX+M)
      XA(NPT+1)=X(NPTS+1)
      XA(NPT+2)=X(NPTS+2)
      YA(NPT+1)=Y(NPTS+1)
      YA(NPT+2)=Y(NPTS+2)
      CALL LINE(XA,YA,NPT,1,LINTYP,N-1)
   40 CONTINUE
      CALL FACTOR(1.)
      CALL SYMBOL(.5,5.25,.14,TITLE,0.,28)
      CALL SYMBOL(5.2,4.3,.105,SUBTTL,0.,28)
      YPAGE=4.05
      DO 42 N=1,4
      IF(VAL(N).EQ.0.) GO TO 1
      YPAGE=YPAGE-.35
      DO 43 M=1,5
   43 VARX(M)=VAR(M,N)
      CALL SYMBOL(5.2,YPAGE,.105,VARX,0.,20)
   42 CALL NUMBER(999.,999.,.105,VAL(N),0.,2)
    1 YPAGE=YPAGE-.25
      DO 44 N=1,NBR
      IF(NUM(N+1)-NUM(N).EQ.0) GO TO 44
      YPAGE=YPAGE-.35
      DO 45 M=1,8
   45 SYMTTX(M)=SYMTTL(M,N)
      CALL SYMBOL(5.25,YPAGE,.105,N-1,0.,-1)
      CALL SYMBOL(5.55,YPAGE-.05,.105,SYMTTX,0.,32)
   44 CONTINUE
    2 CALL PLOT(17.,0.,-3)
      RETURN
      END
```

Table 1

LAMINAR BASE PRESSURE DATA

η_ℓ	$\xi_{b\ell}$		
	$M_\infty = 1.5$	$M_\infty = 2.0$	$M_\infty = 3.1$
0.00	0.494	0.338	0.160
0.01	0.444	0.357	0.257
0.02	0.557	0.570	0.376
0.03	0.647	0.669	0.472
0.04	0.704	0.716	0.554
0.05	0.738	0.742	0.631
0.06	0.764	0.764	0.697
0.07	0.782	0.779	0.726
0.08	0.800	0.789	
0.09	0.809	0.795	
0.10	0.822	0.800	
0.11	0.825	0.800	
0.12	0.831	0.806	
0.13	0.838	0.809	
0.14	0.844	0.813	
0.15	0.844	0.813	
0.16	0.844	0.816	
0.17	0.847	0.819	
0.18	0.847	0.819	
0.19	0.847	0.819	
0.20	0.847	0.819	

Table 2

TEST MATRIX

Parameter	Range, Increment	Variable Geometry Test		Fixed Geometry Test	
		Turbulent Boundary Layer	Laminar Boundary Layer	Turbulent Boundary Layer	Laminar Boundary Layer
δ	3^{o}-13^{o},0.2^{o}	4^{o},6^{o},8^{o},10^{o}	4^{o},6^{o},8^{o},10^{o}	6.5^{o}	8.3^{o}
δ'	$\delta'=\delta-3^{o}$				
Θ	4^{o}-80^{o},2^{o}	30^{o},50^{o},70^{o}	30^{o},50^{o},70^{o}	30^{o}	30^{o}
Φ	24^{o}-178^{o},2^{o}	60^{o},90^{o},120^{o},150^{o}	60^{o},90^{o},120^{o},150^{o}	120^{o}	120^{o}
M_{∞}	1.5-5.0,0.1	2.0	3.1		
Re_{∞}	10^{5}-10^{8}	10^{7}	10^{5}	10^{5},10^{6},10^{7},10^{8}	10^{5},10^{6},10^{7},10^{8}

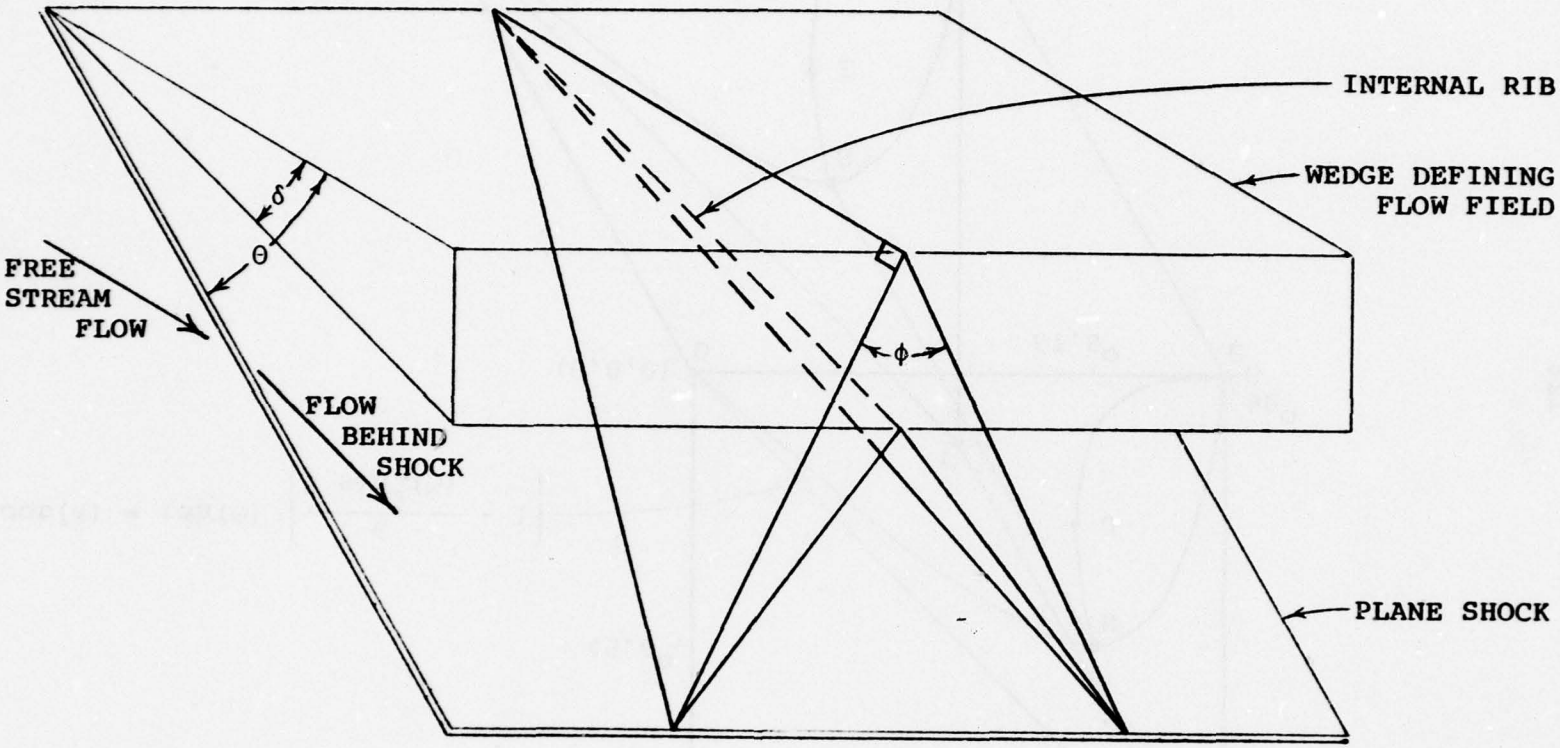

Figure 1. Construction of Caret Wing from Known Flow Field

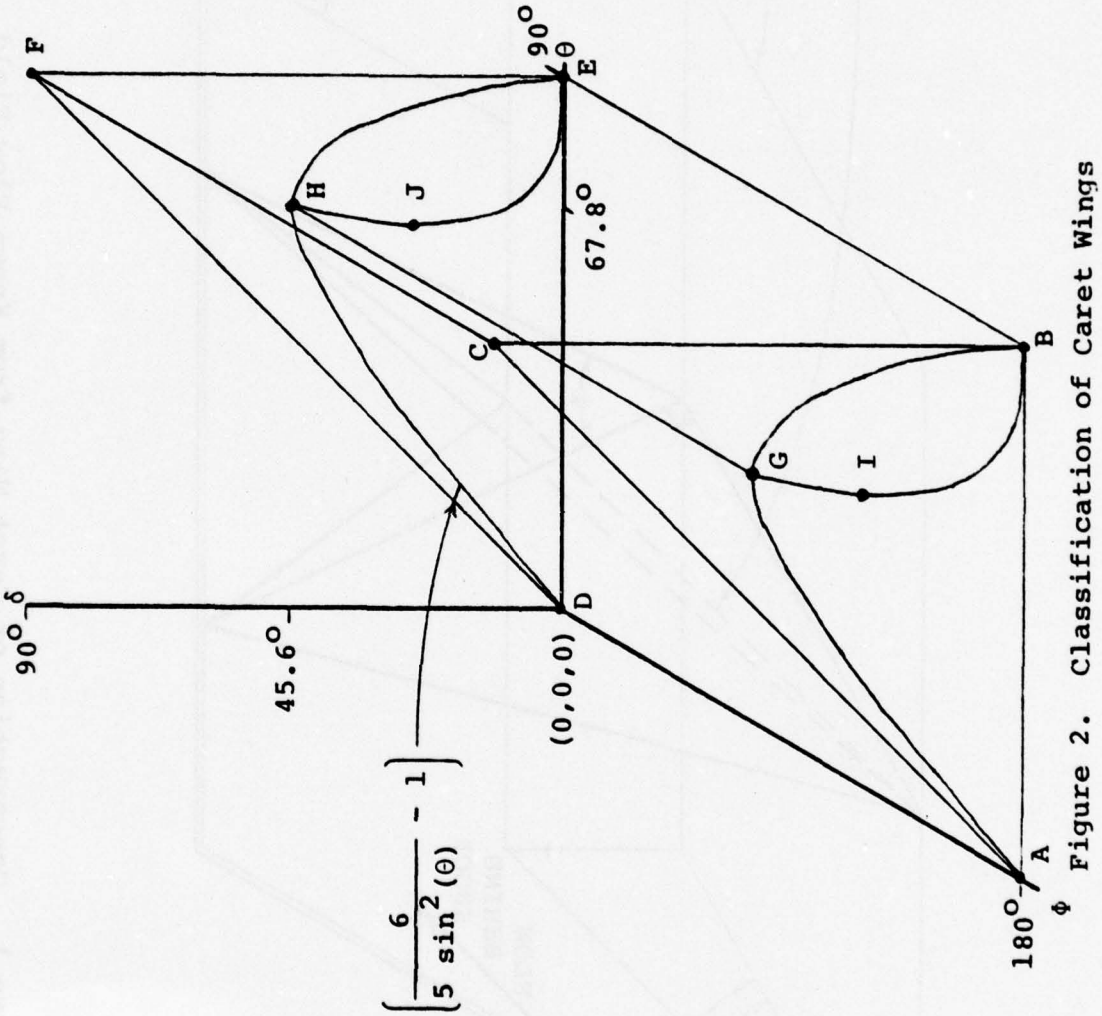

Figure 2. Classification of Caret Wings

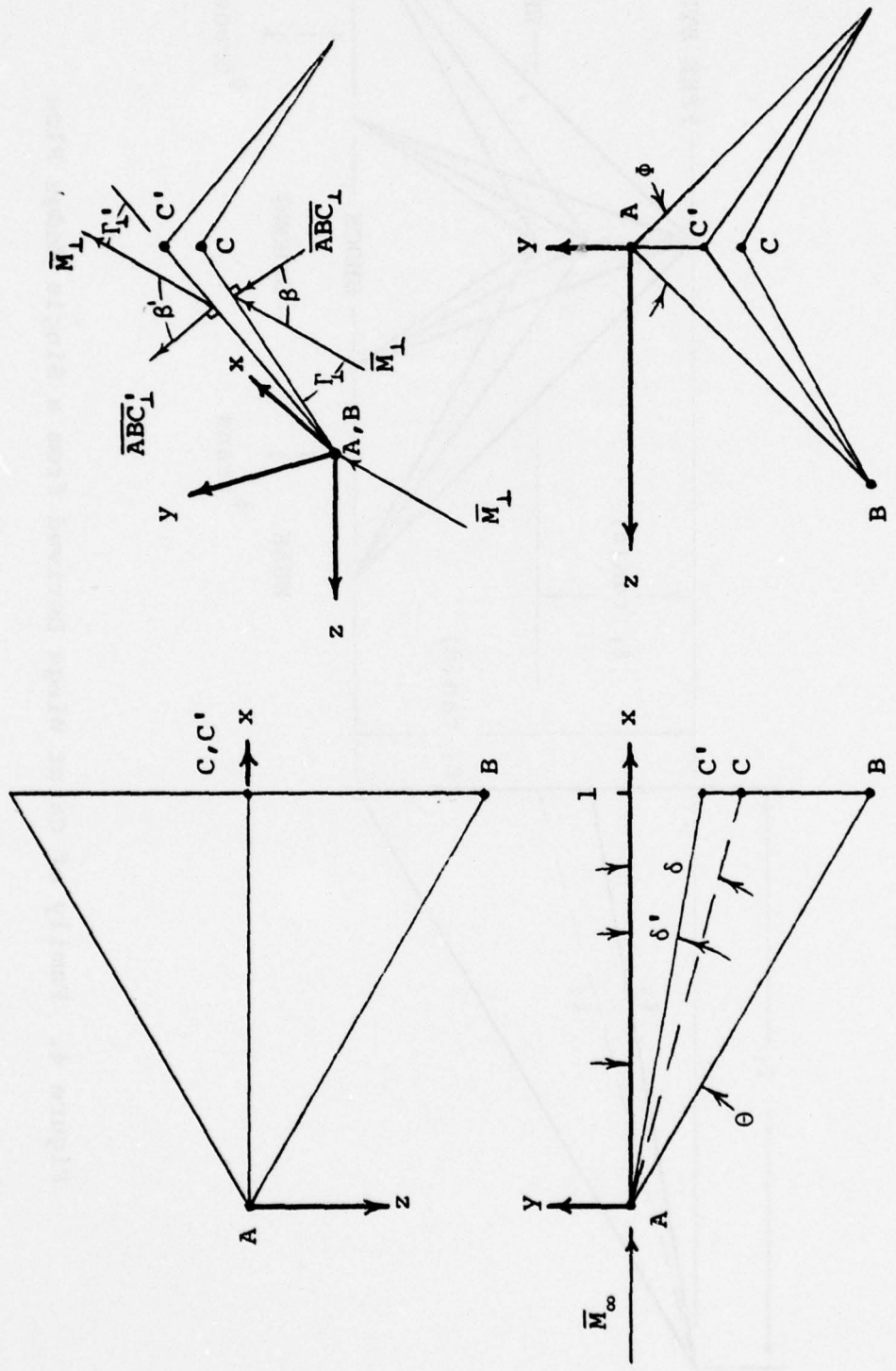

Figure 3. Caret Wing Geometry

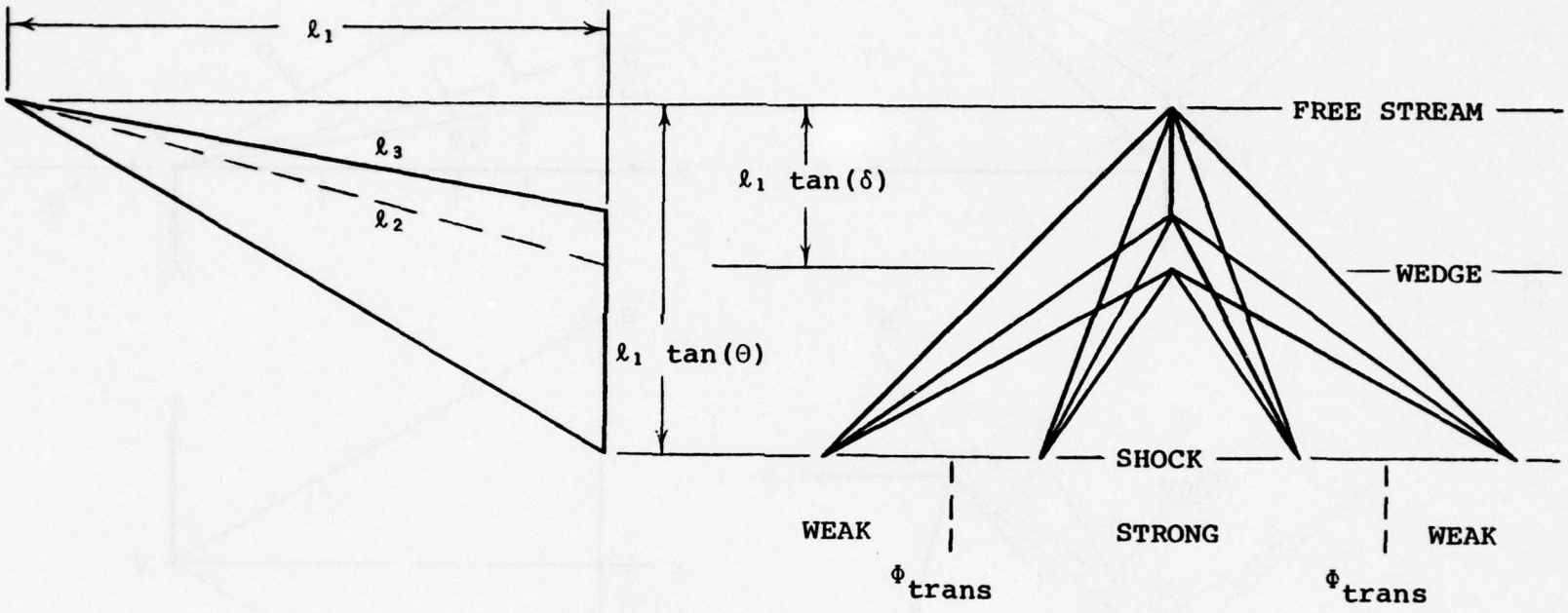

Figure 4. Family of Caret Wings Derived from a Single Wedge Flow

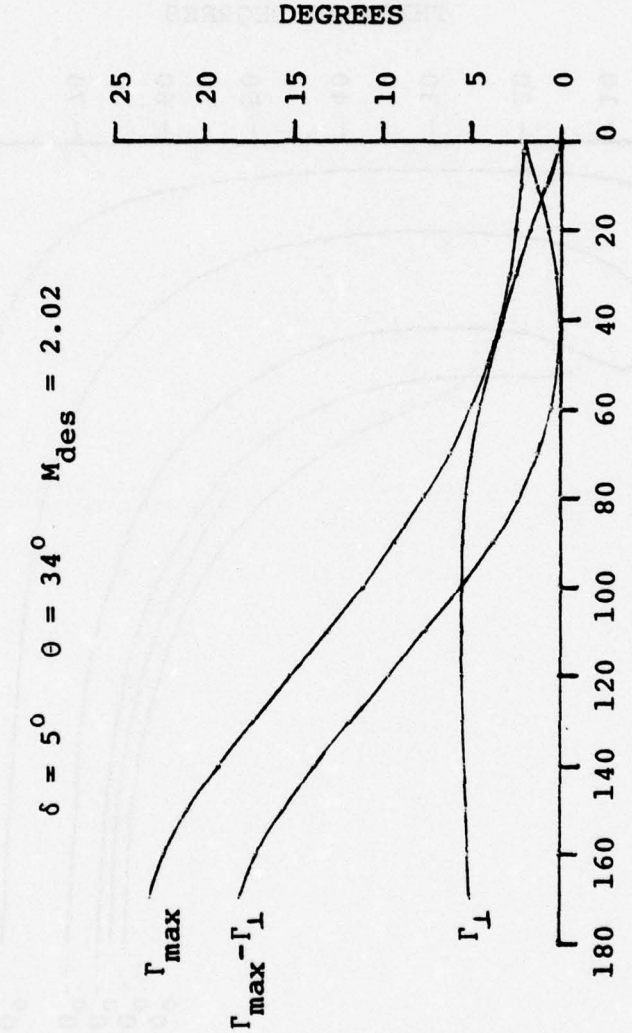

Figure 5. Γ_{max}, $\Gamma_\perp$ and $\Gamma_{max}-\Gamma_\perp$ vs. Phi

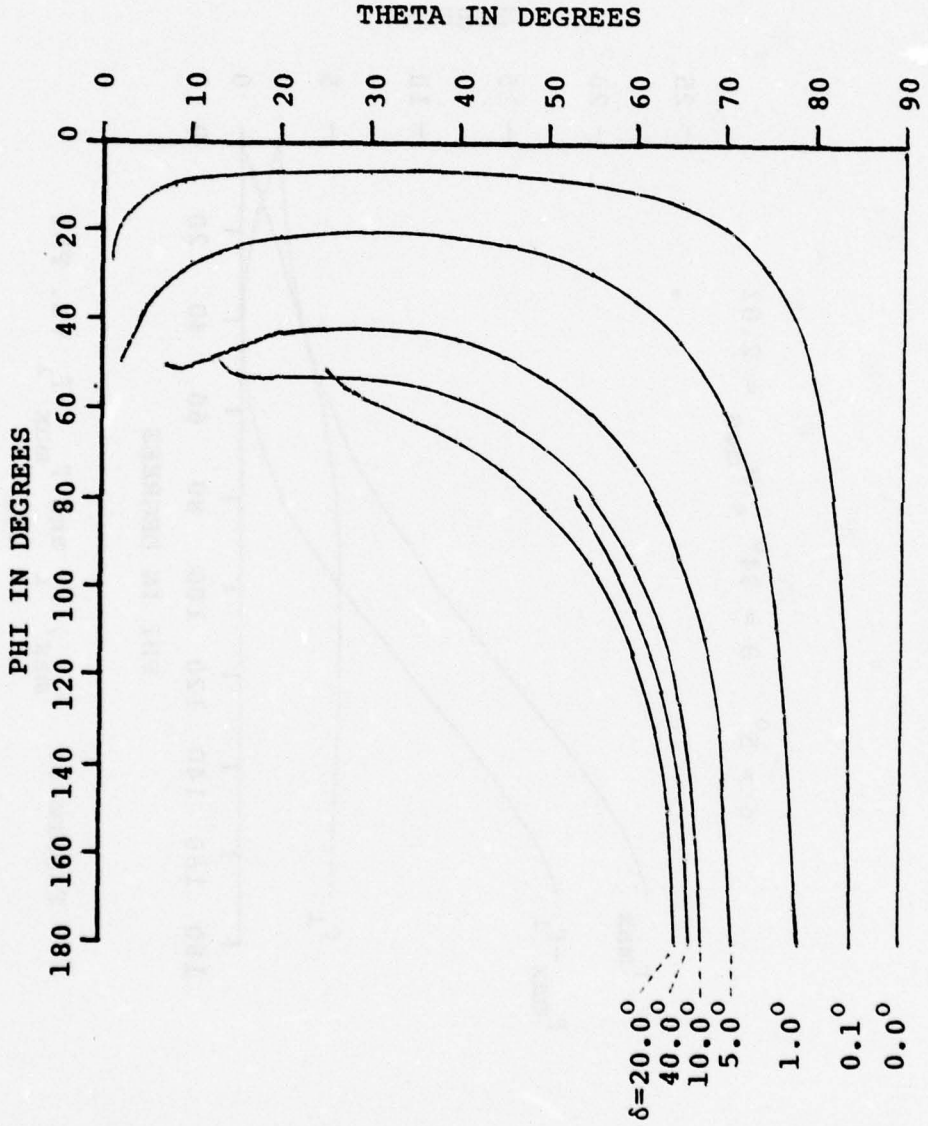

Figure 6. Φ_{trans} vs. Θ

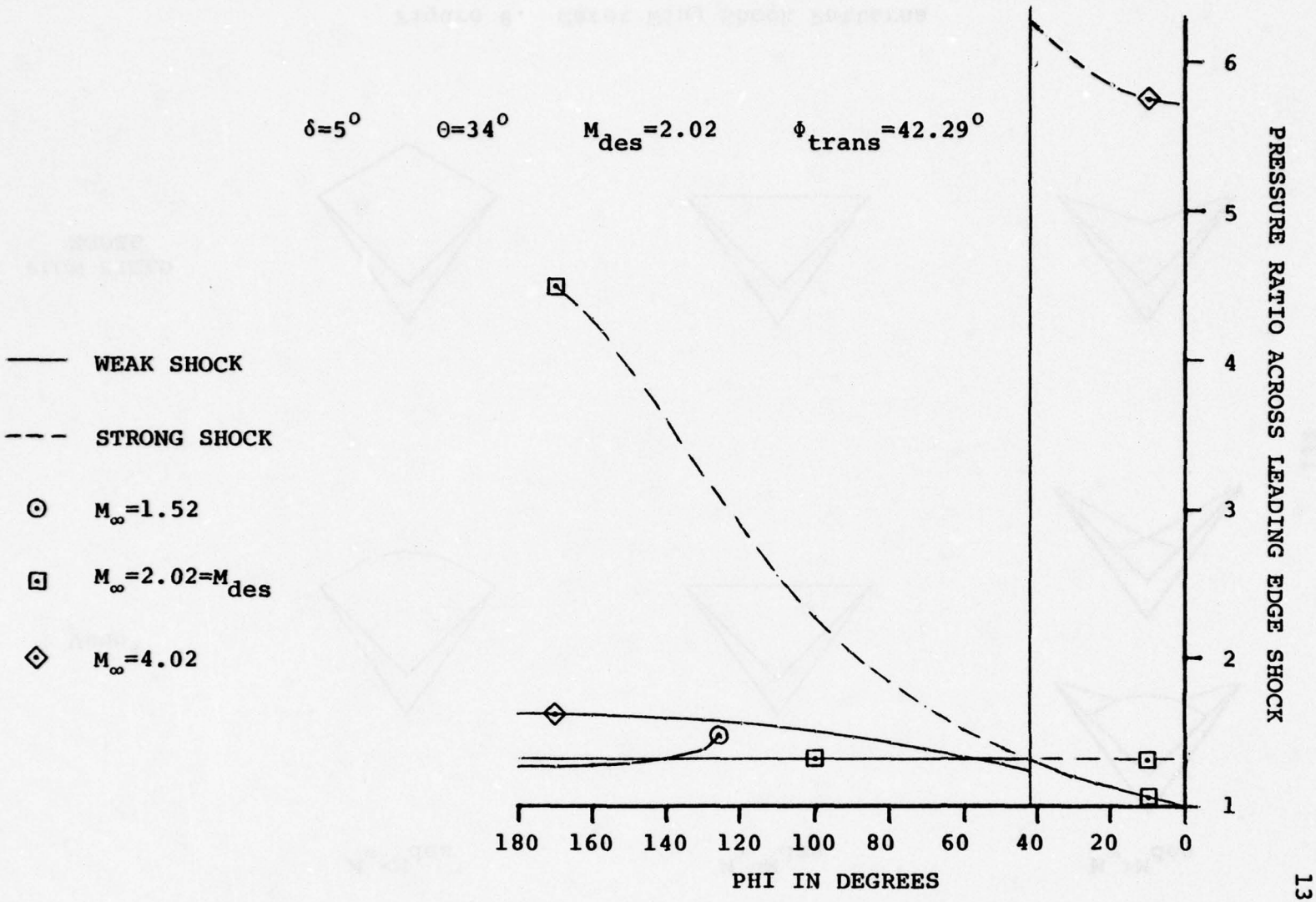

Figure 7. Pressure Ratio Across Leading Edge Shock vs. Φ

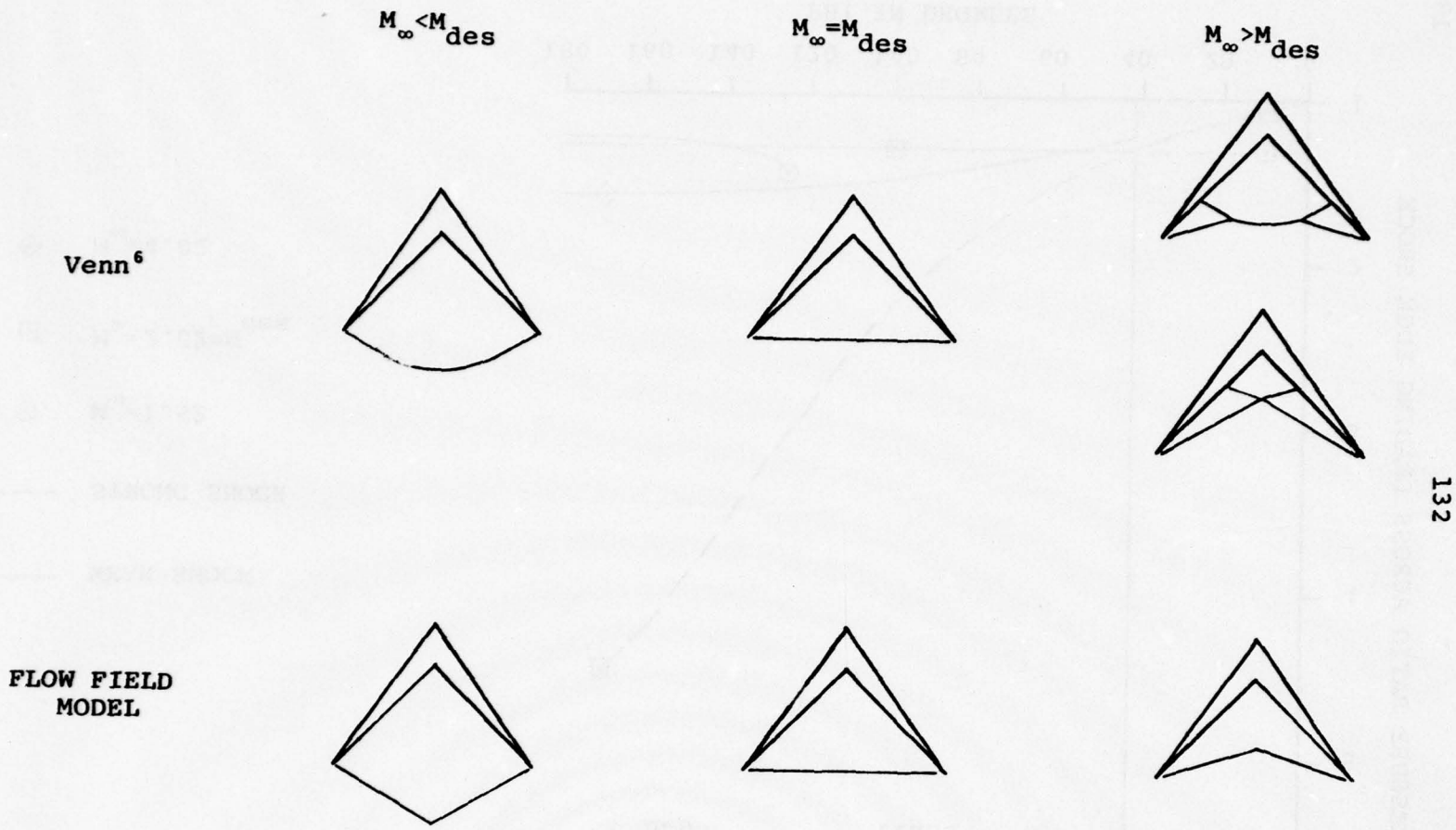

Figure 8. Caret Wing Shock Patterns

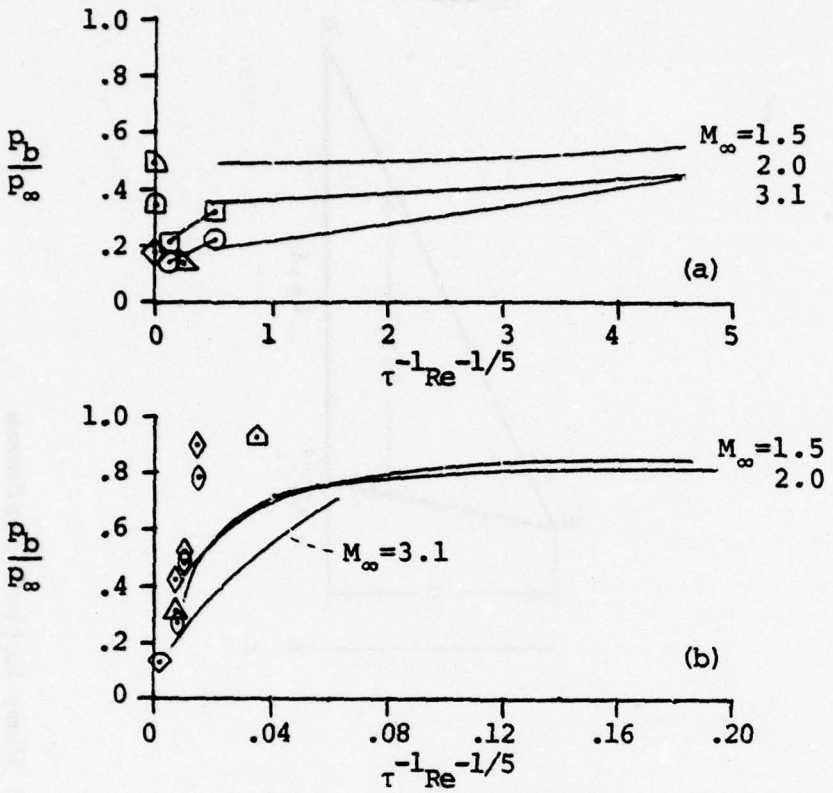

TWO-DIMENSIONAL BODIES

M_∞=1.5,2.0,3.1; Chapman[11]

M_∞=2.25,3.5; Rom[13]

M_∞=5.0; Goecke[12]

M_∞=1.5,2.0,3.1; Korst[15]

M_∞=2.0,3.0; Gadd[14]

MAIKAPAR BODIES

Model 3,4; M_∞=4.0; Adams[16]

M_∞=6.3; Solomon[17]

(a) TURBULENT (b) LAMINAR

Figure 9. Base Pressure Data

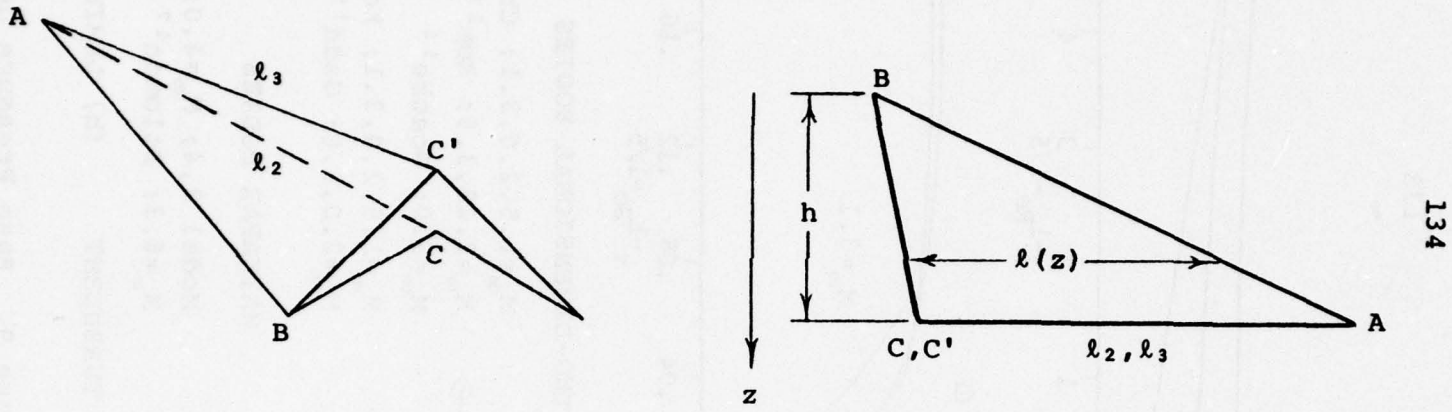

Figure 10. Caret Wing Wetted Surfaces

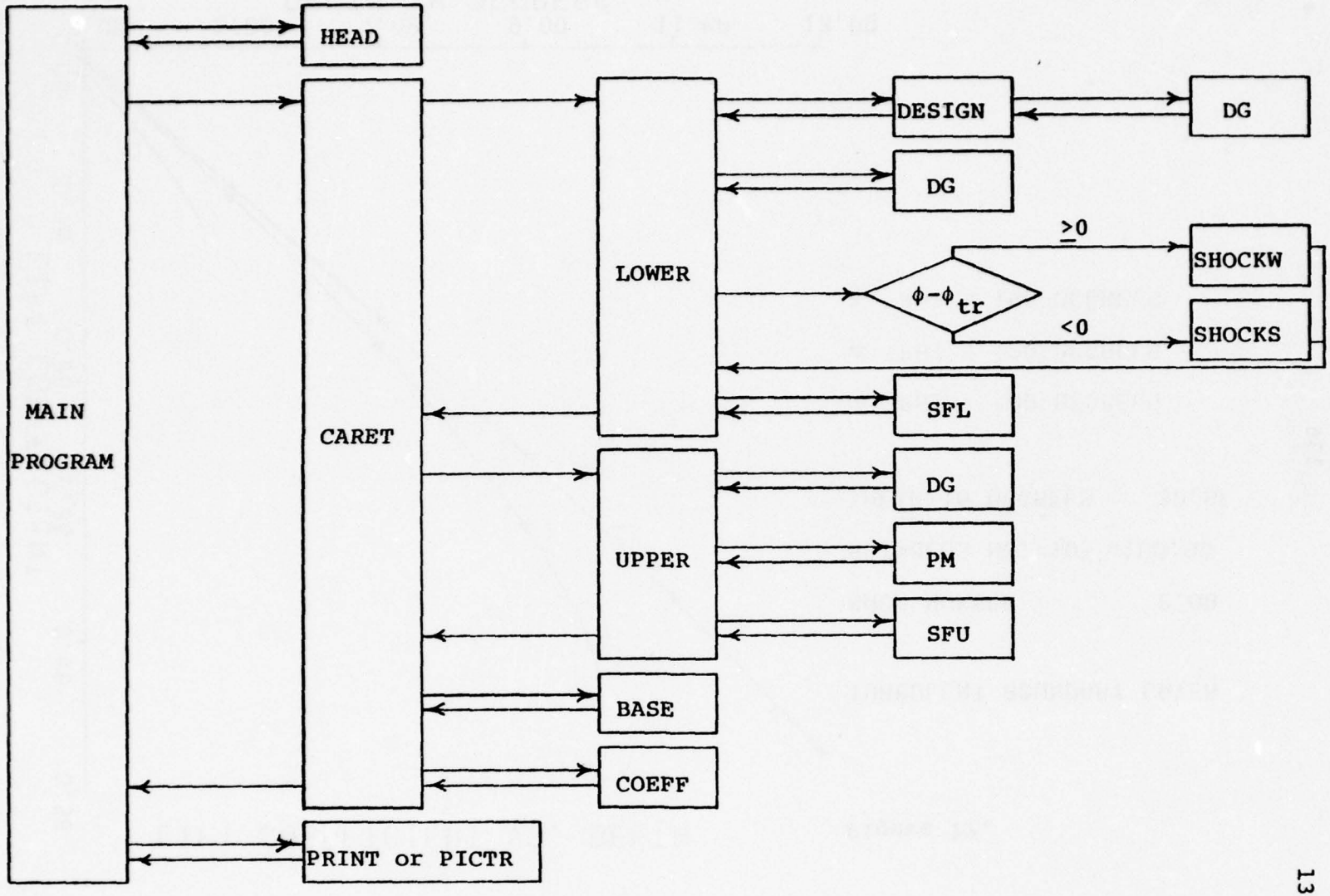

Figure 11. Computer Program Flow Chart

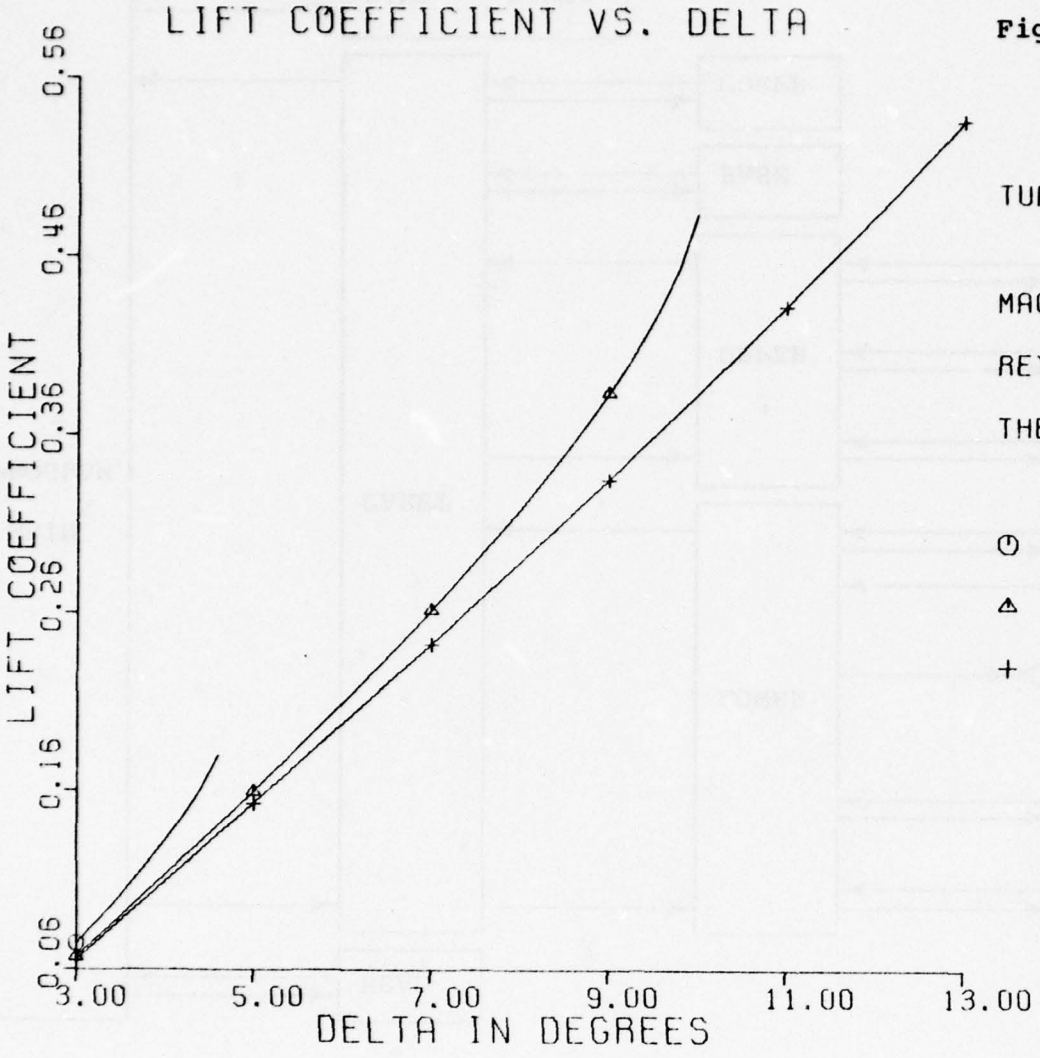

Figure 12.

TURBULENT BOUNDARY LAYER

MACH NUMBER = 2.00

REYNOLDS NO./10^5 =100.00

THETA IN DEGREES = 30.00

⊙ PHI = 90 DEGREES

△ PHI = 120 DEGREES

\+ PHI = 150 DEGREES

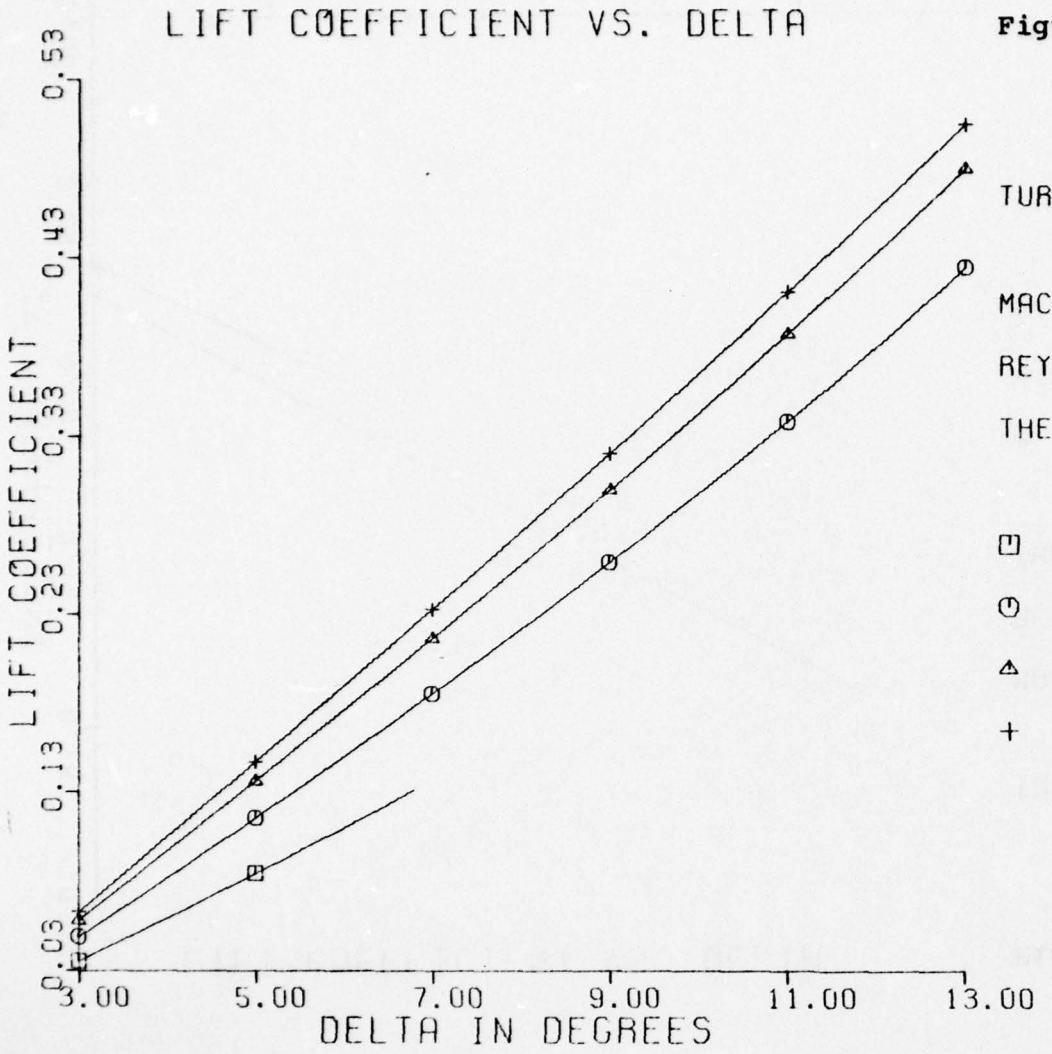

Figure 13.

TURBULENT BOUNDARY LAYER

MACH NUMBER = 2.00

REYNOLDS NO./10^5 =100.00

THETA IN DEGREES = 50.00

□ PHI = 60 DEGREES

○ PHI = 90 DEGREES

△ PHI = 120 DEGREES

\+ PHI = 150 DEGREES

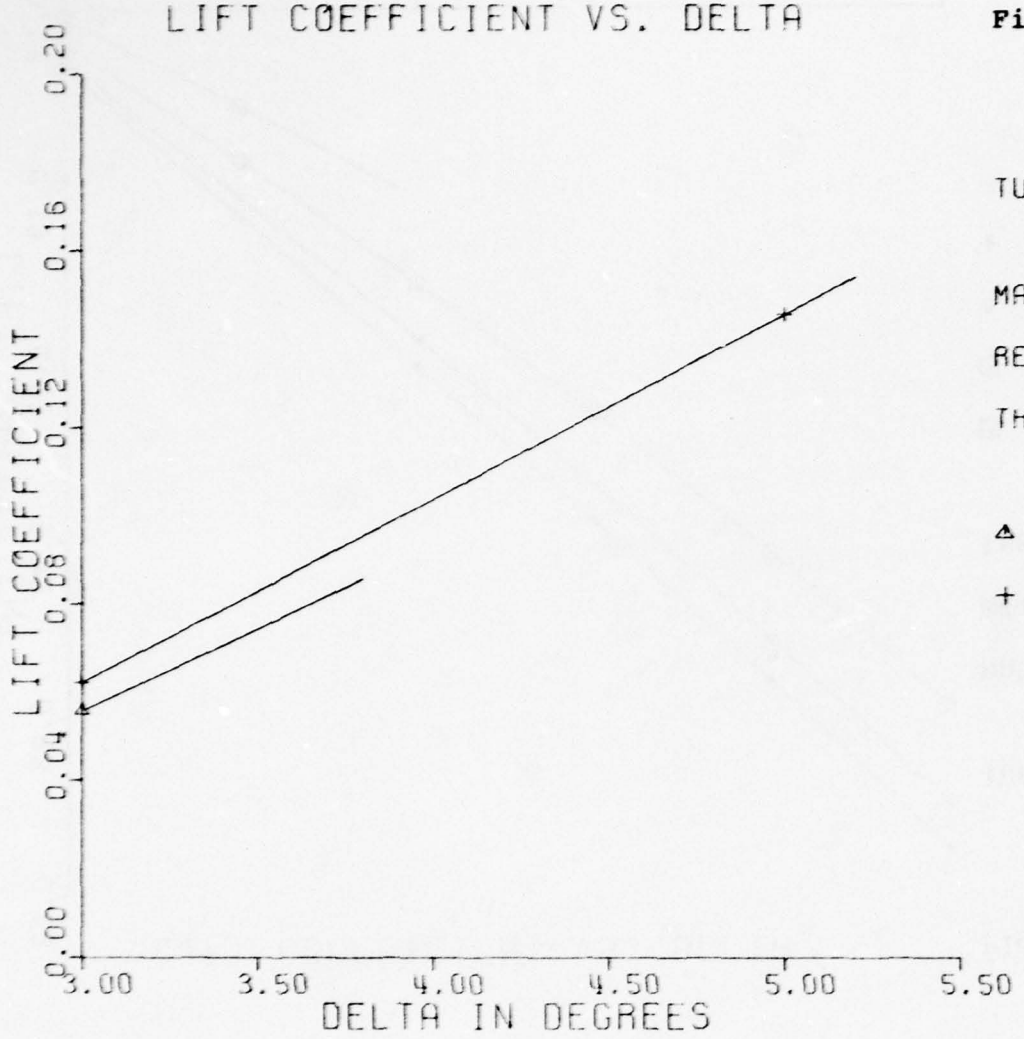

Figure 14.

TURBULENT BOUNDARY LAYER

MACH NUMBER = 2.00

REYNOLDS NO./10^5 =100.00

THETA IN DEGREES = 70.00

△ PHI = 120 DEGREES

\+ PHI = 150 DEGREES

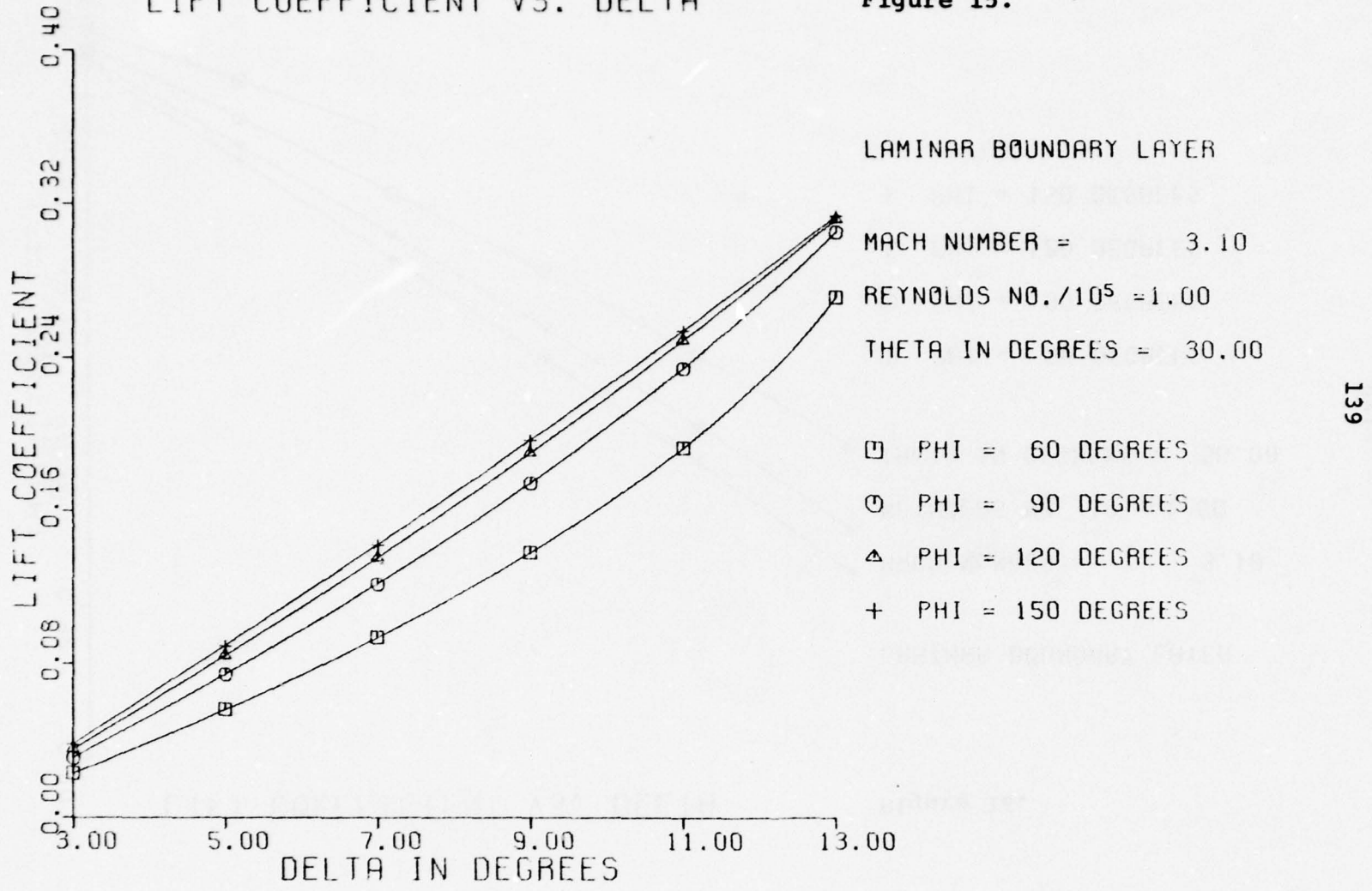
LIFT COEFFICIENT VS. DELTA
LIFT COEFFICIENT
0.00
0.08
0.16
0.24
0.32
0.40
3.00
5.00
7.00
9.00
11.00
13.00
DELTA IN DEGREES
LAMINAR BOUNDARY LAYER
MACH NUMBER = 3.10
REYNOLDS NO./10^5 = 1.00
THETA IN DEGREES = 30.00
PHI = 60 DEGREES
PHI = 90 DEGREES
PHI = 120 DEGREES
PHI = 150 DEGREES

Figure 15.

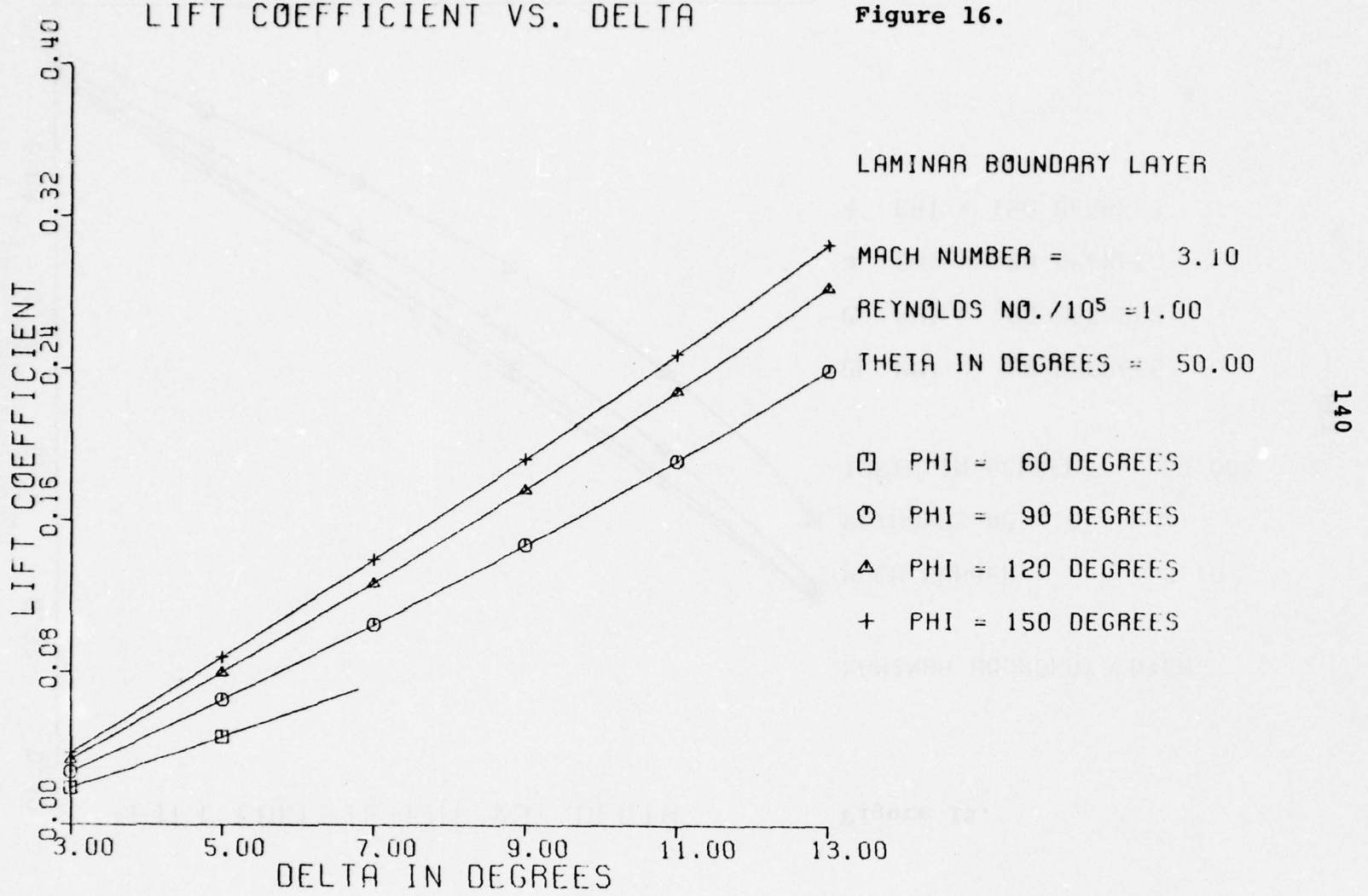
LIFT COEFFICIENT VS. DELTA
LIFT COEFFICIENT
0.00
0.08
0.16
0.24
0.32
0.40
3.00
5.00
7.00
9.00
11.00
13.00
DELTA IN DEGREES
LAMINAR BOUNDARY LAYER
MACH NUMBER = 3.10
REYNOLDS NO./10^5 = 1.00
THETA IN DEGREES = 50.00
PHI = 60 DEGREES
PHI = 90 DEGREES
PHI = 120 DEGREES
PHI = 150 DEGREES

Figure 16.

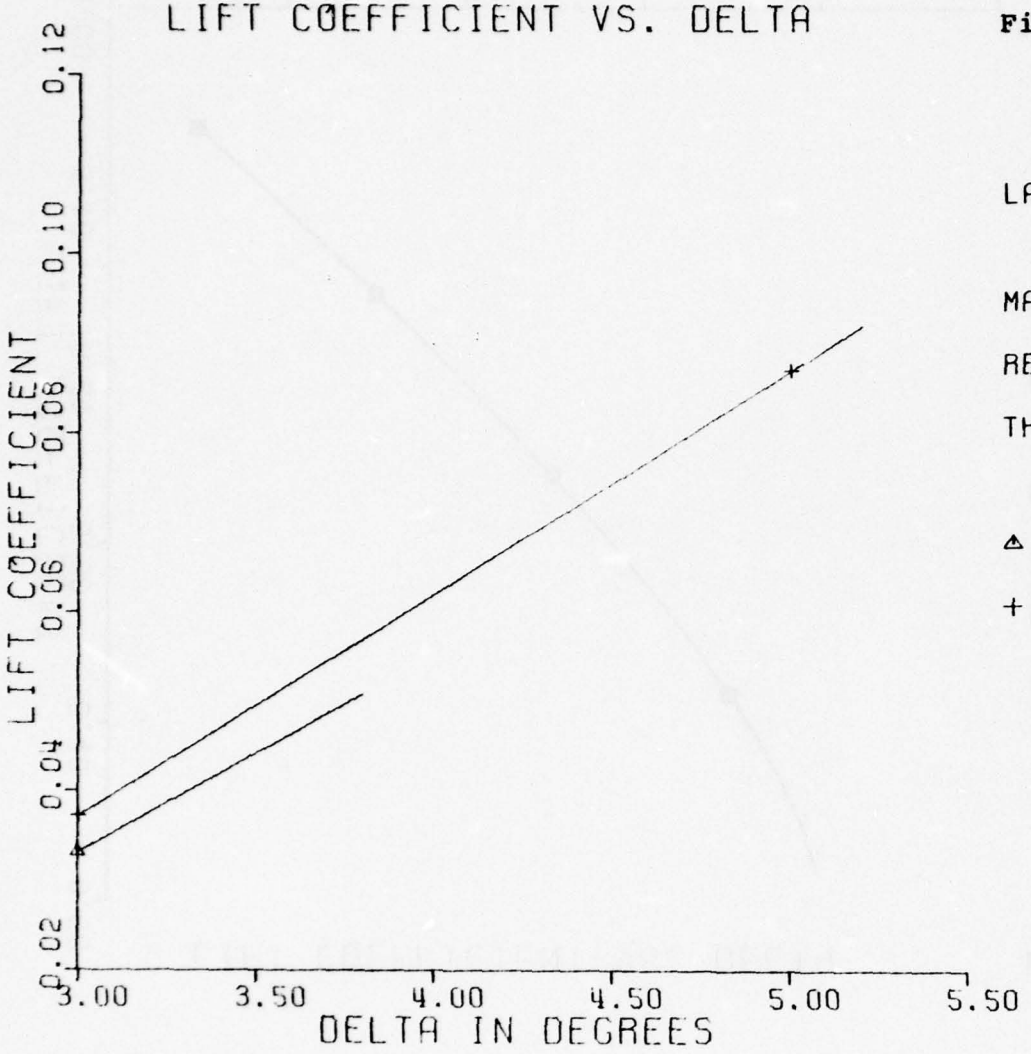

Figure 17.

LAMINAR BOUNDARY LAYER

MACH NUMBER = 3.10

REYNOLDS NO./10^5 =1.00

THETA IN DEGREES = 70.00

△ PHI = 120 DEGREES

\+ PHI = 150 DEGREES

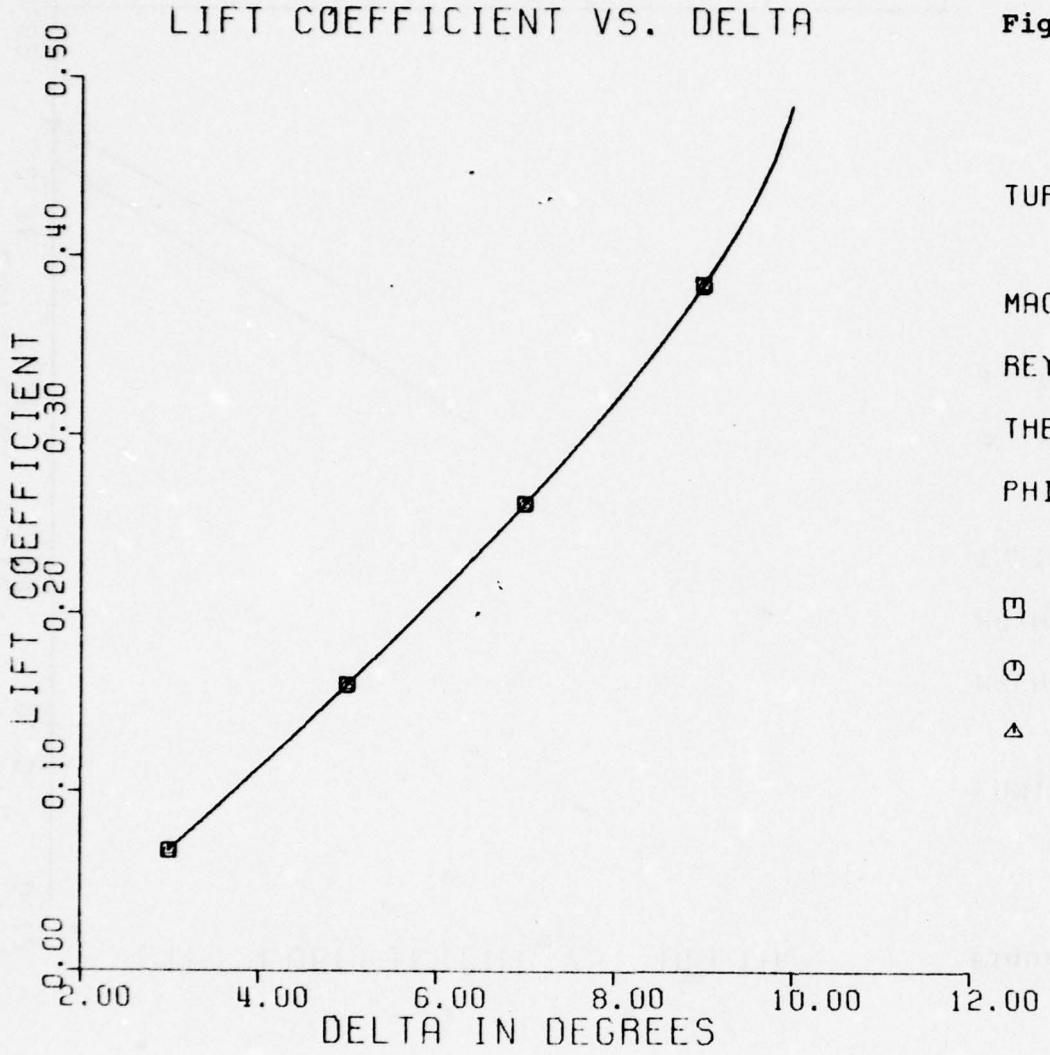

Figure 18.

TURBULENT BOUNDARY LAYER

MACH NUMBER = 2.00

REYNOLDS NO./10^5 =100.00

THETA IN DEGREES = 30.00

PHI IN DEGREES = 120.00

□ NO SKIN FRICTION OR BASE DRAG

○ NO BASE DRAG

△ ALL FORCES

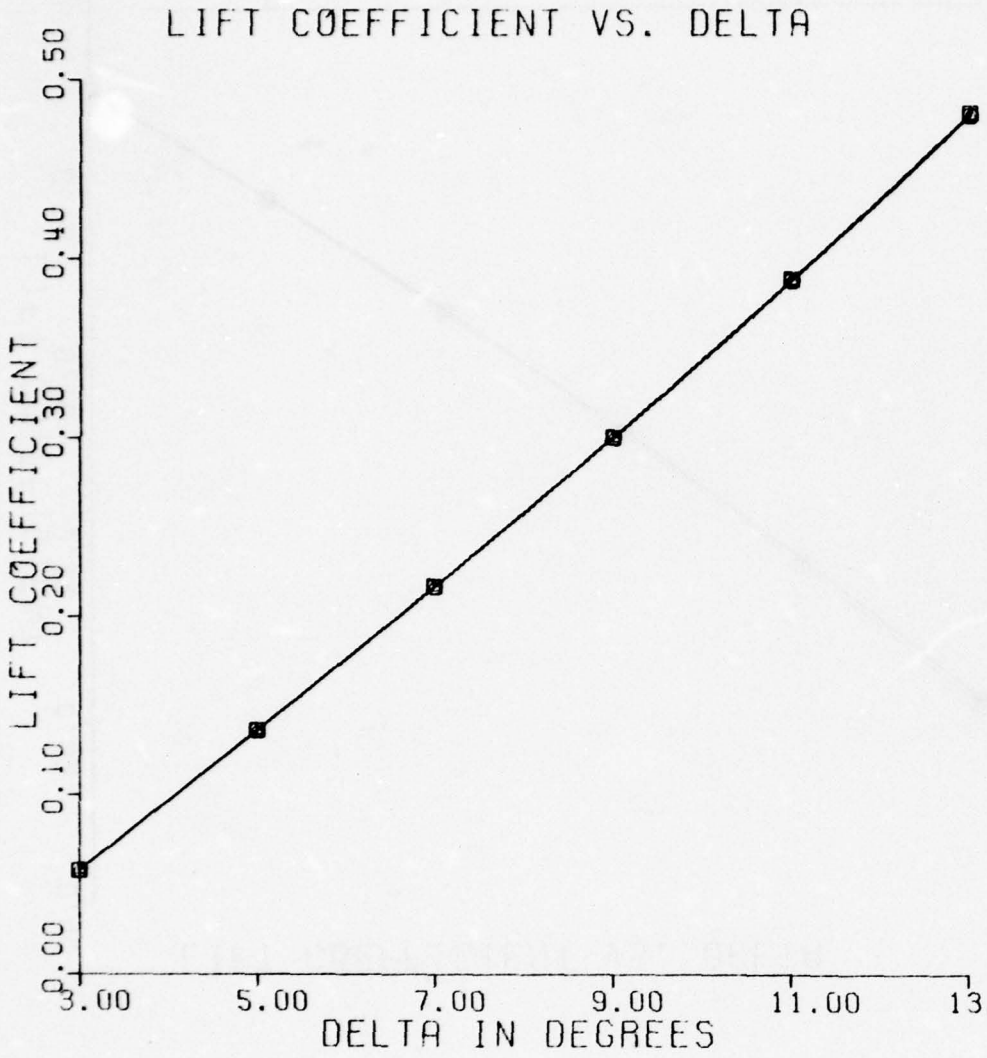

Figure 19.

TURBULENT BOUNDARY LAYER

MACH NUMBER = 2.00

REYNOLDS NO./10^5 =100.00

THETA IN DEGREES = 50.00

PHI IN DEGREES = 120.00

□ NO SKIN FRICTION OR BASE DRAG

○ NO BASE DRAG

△ ALL FORCES

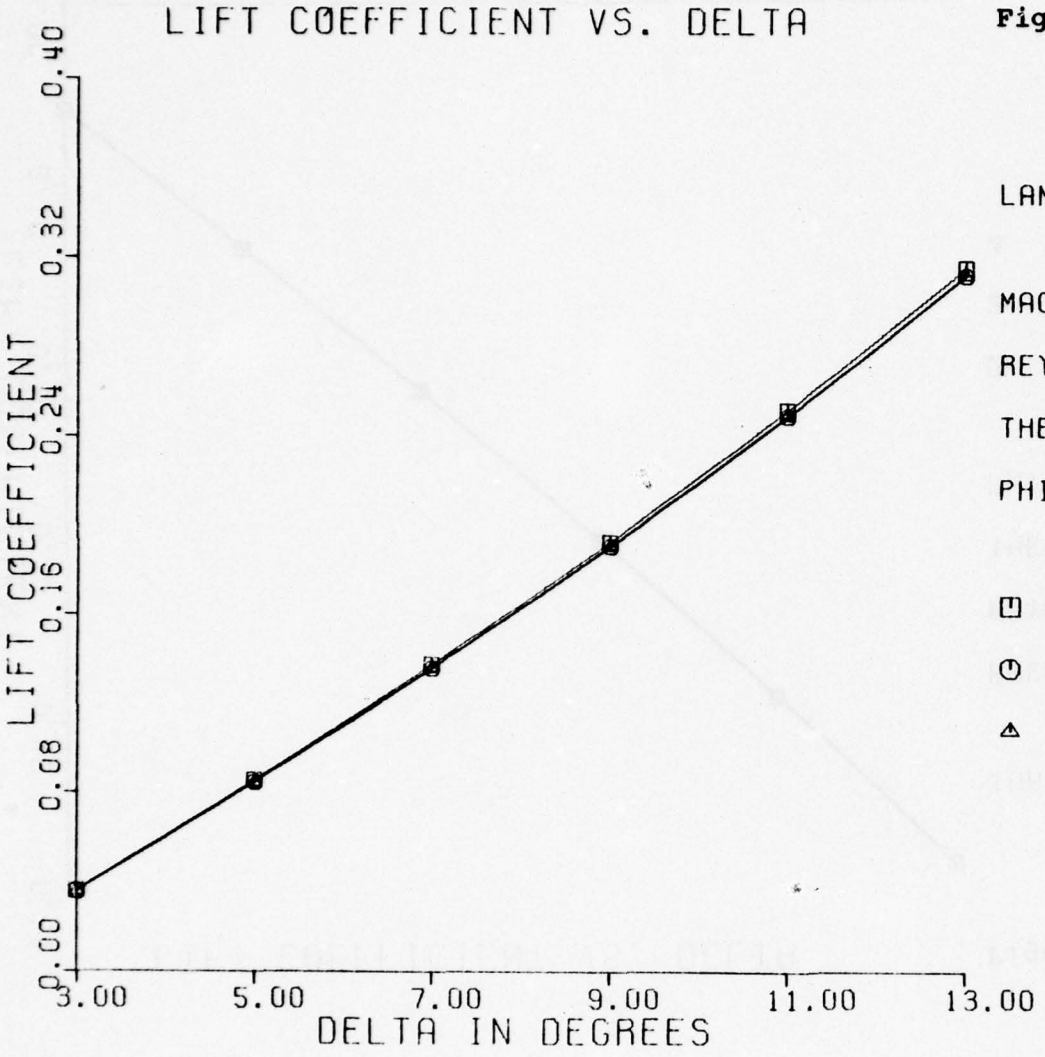

Figure 20.

LAMINAR BOUNDARY LAYER

MACH NUMBER = 3.10

REYNOLDS NO./10^5 =1.00

THETA IN DEGREES = 30.00

PHI IN DEGREES = 120.00

□ NO SKIN FRICTION OR BASE DRAG

○ NO BASE DRAG

△ ALL FORCES

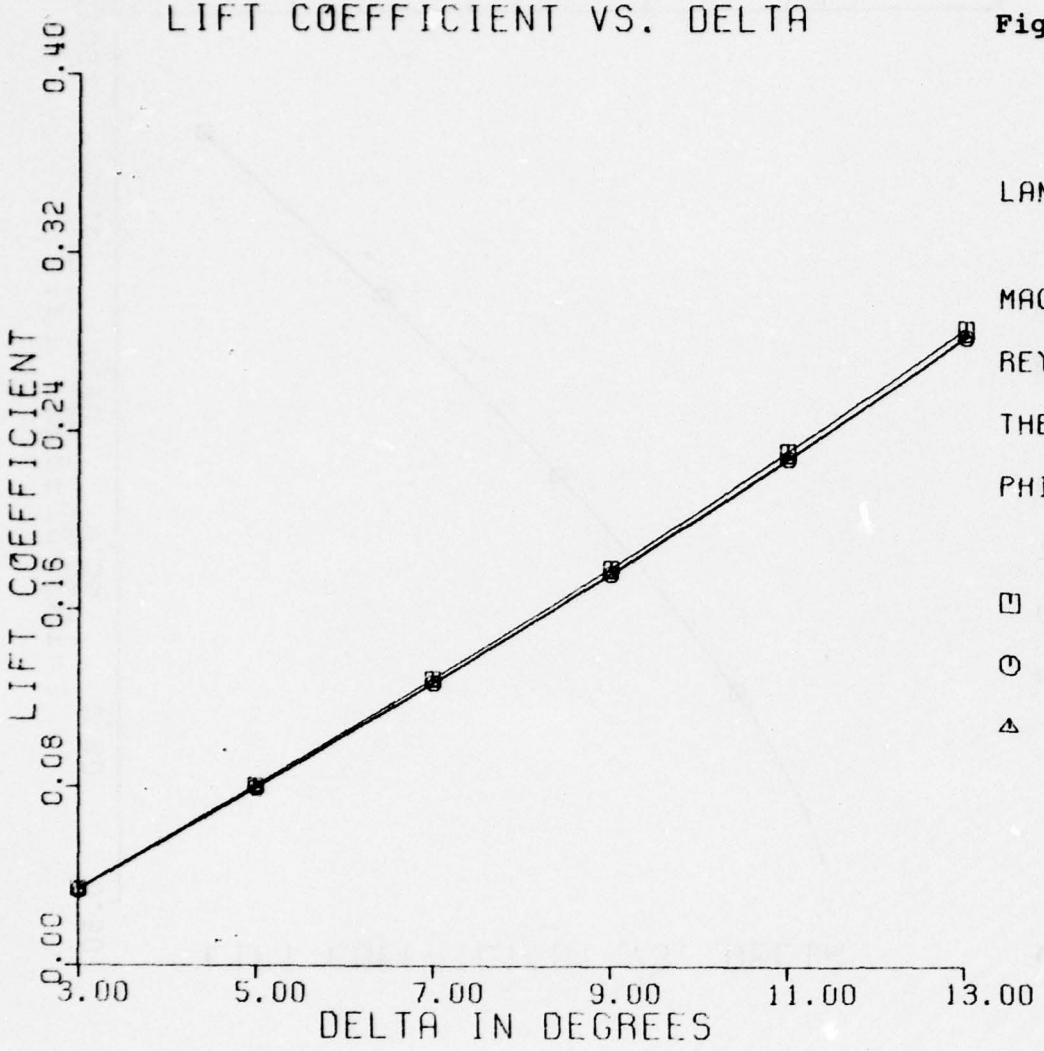

Figure 21.

LAMINAR BOUNDARY LAYER

MACH NUMBER = 3.10

REYNOLDS NO./10^5 =1.00

THETA IN DEGREES = 50.00

PHI IN DEGREES = 120.00

□ NO SKIN FRICTION OR BASE DRAG

○ NO BASE DRAG

△ ALL FORCES

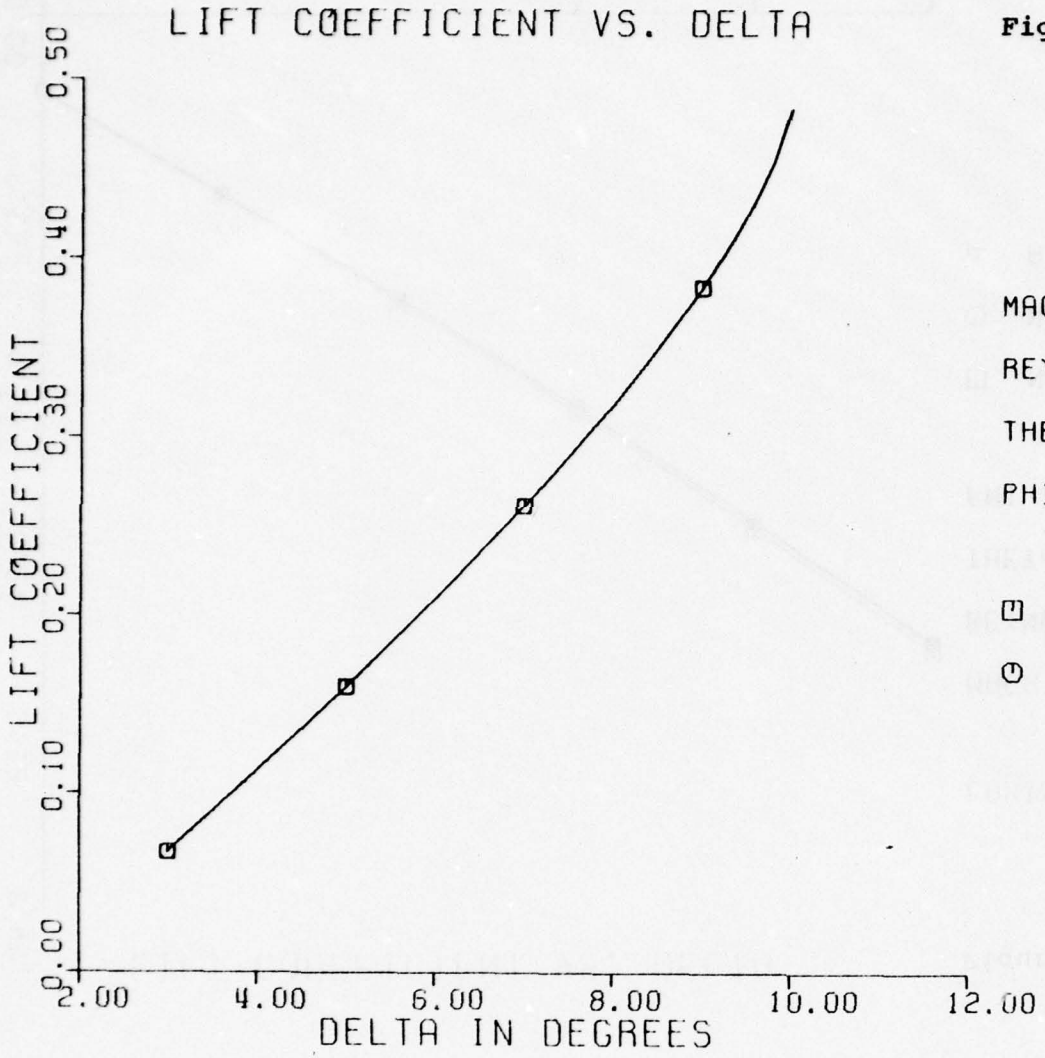

Figure 22.

MACH NUMBER = 2.00

REYNOLDS NO./10^5 =100.00

THETA IN DEGREES = 30.00

PHI IN DEGREES = 120.00

□ LAMINAR BOUNDARY LAYER

○ TURBULENT BOUNDARY LAYER

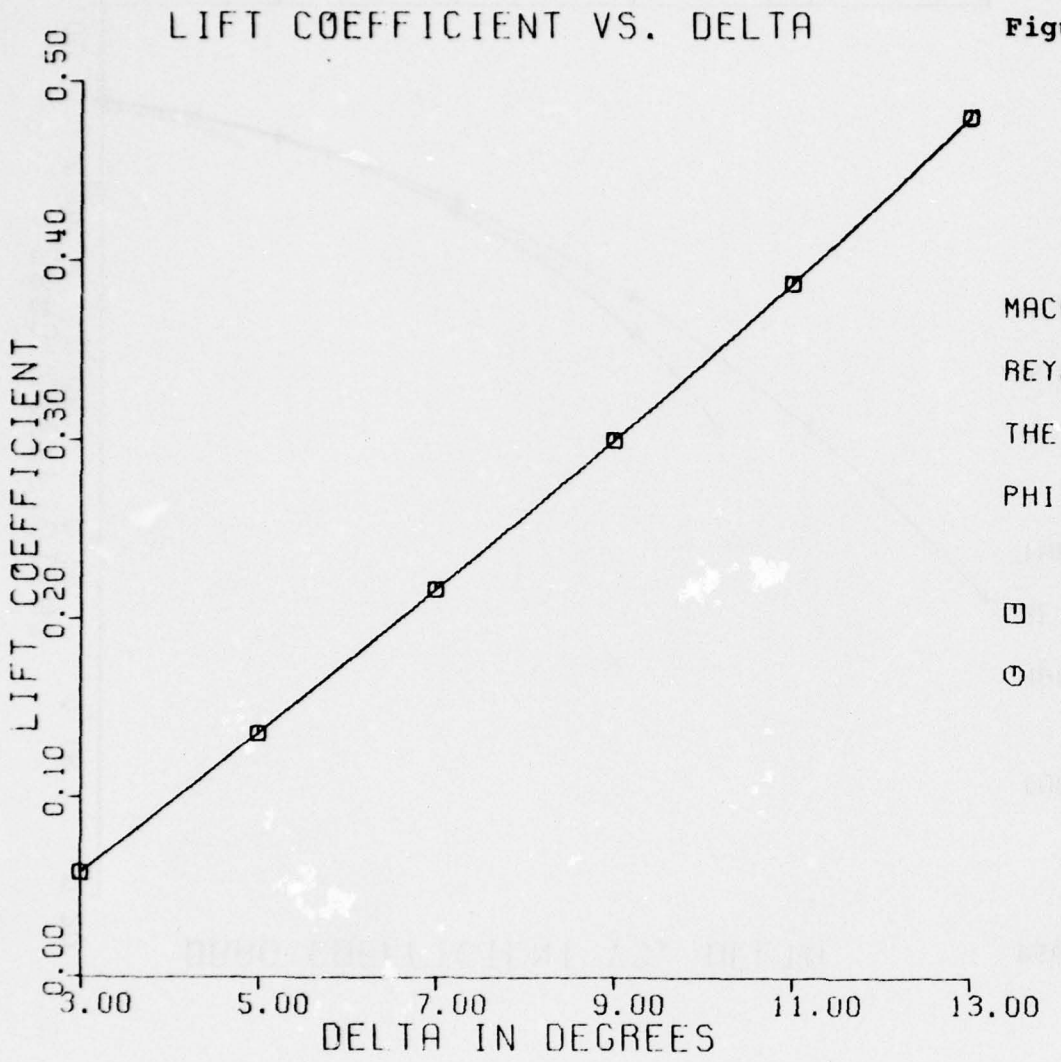

Figure 23.

MACH NUMBER = 2.00

REYNOLDS NO./10^5 =100.00

THETA IN DEGREES = 50.00

PHI IN DEGREES = 120.00

□ LAMINAR BOUNDARY LAYER

○ TURBULENT BOUNDARY LAYER

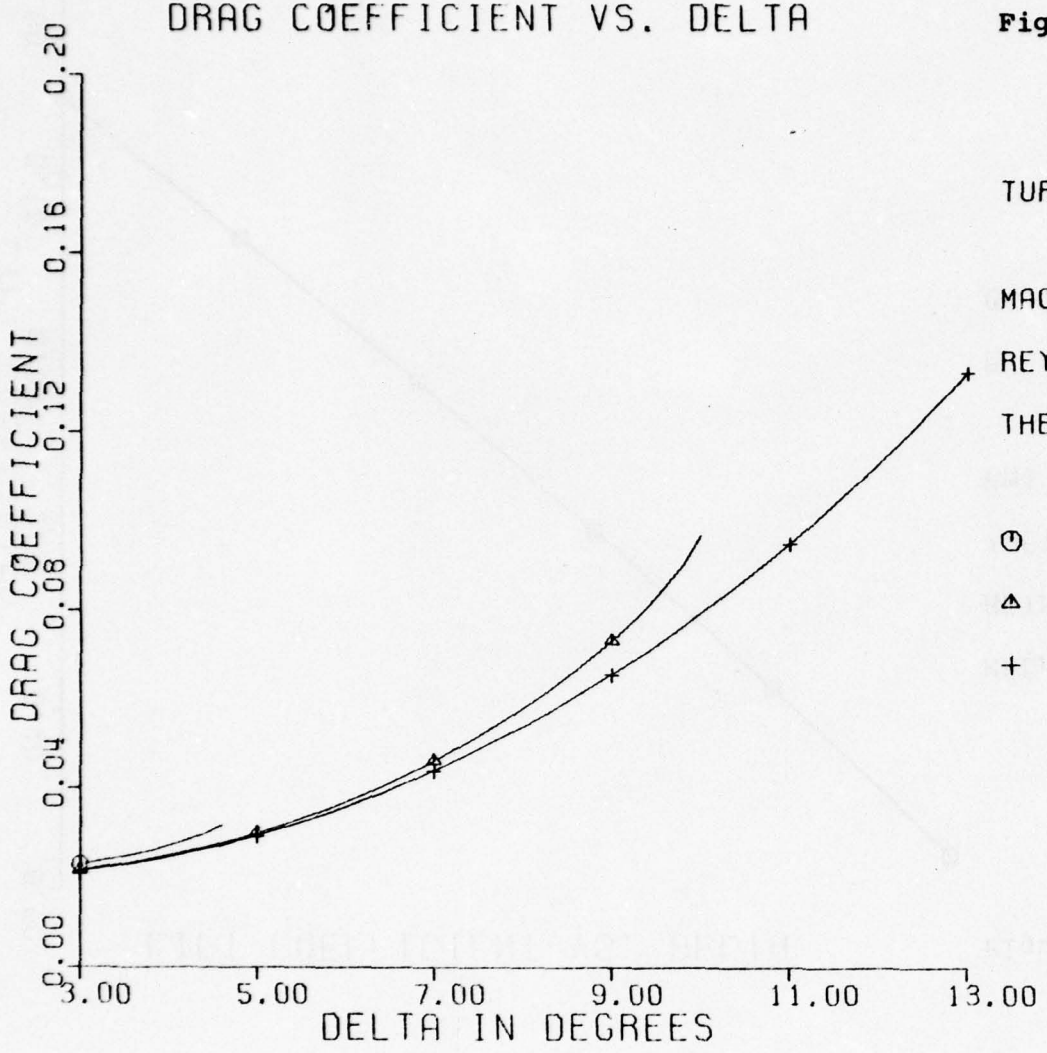

Figure 24.

TURBULENT BOUNDARY LAYER

MACH NUMBER = 2.00

REYNOLDS NO./10^5 =100.00

THETA IN DEGREES = 30.00

⊙ PHI = 90 DEGREES

△ PHI = 120 DEGREES

\+ PHI = 150 DEGREES

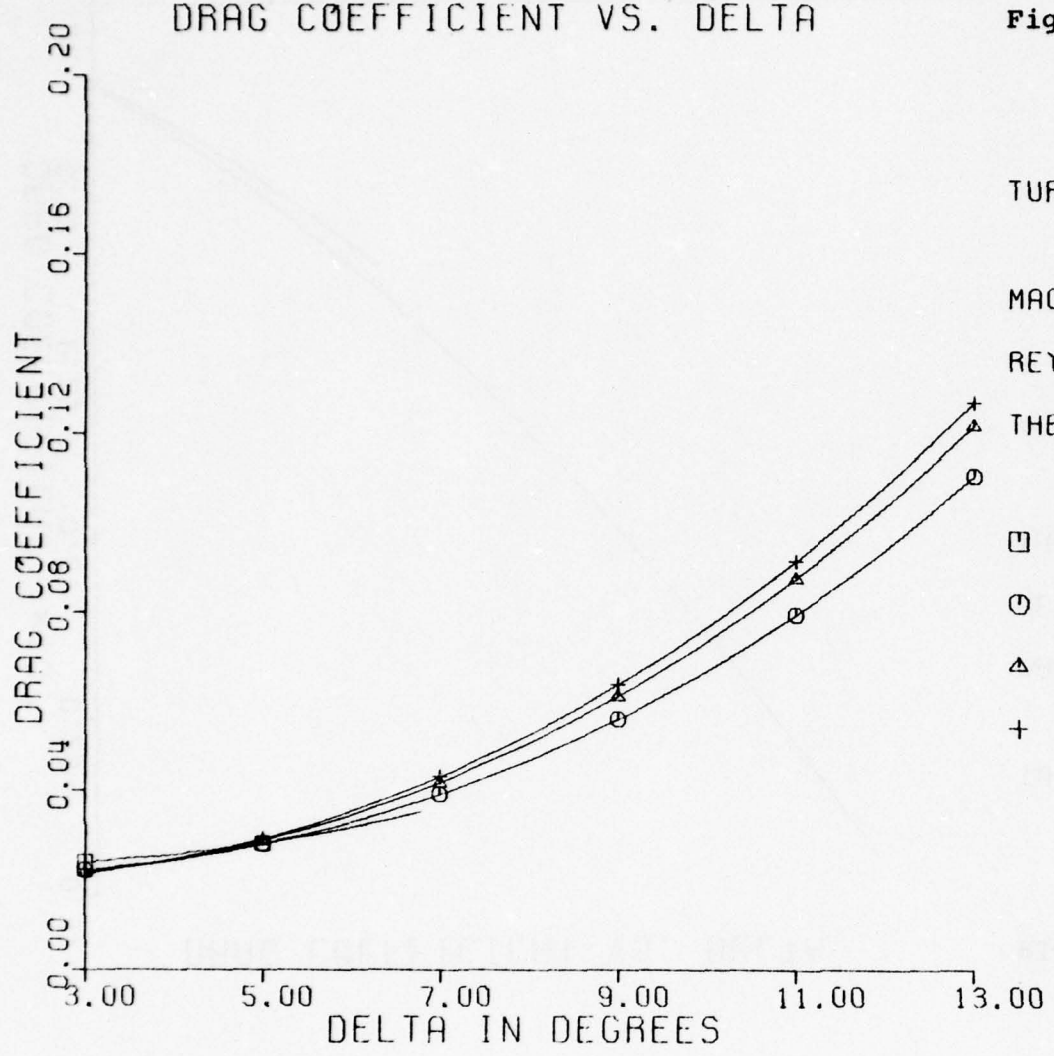
DRAG COEFFICIENT VS. DELTA
DRAG COEFFICIENT
0.00
0.04
0.08
0.12
0.16
0.20
3.00
5.00
7.00
9.00
11.00
13.00
DELTA IN DEGREES
TURBULENT BOUNDARY LAYER
MACH NUMBER = 2.00
REYNOLDS NO./10^5 =100.00
THETA IN DEGREES = 50.00
PHI = 60 DEGREES
PHI = 90 DEGREES
PHI = 120 DEGREES
PHI = 150 DEGREES

Figure 25.

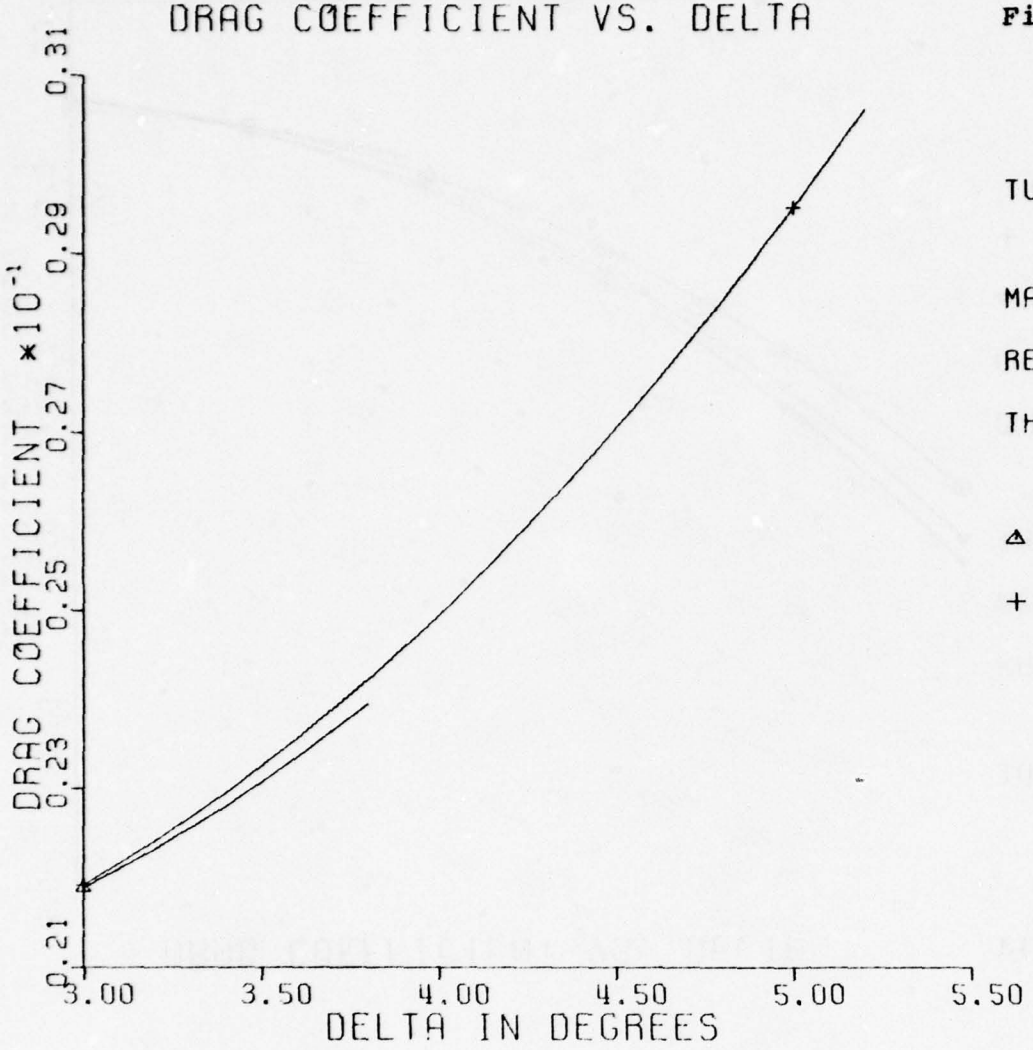

Figure 26.

TURBULENT BOUNDARY LAYER

MACH NUMBER = 2.00

REYNOLDS NO./10^5 =100.00

THETA IN DEGREES = 70.00

△ PHI = 120 DEGREES

\+ PHI = 150 DEGREES

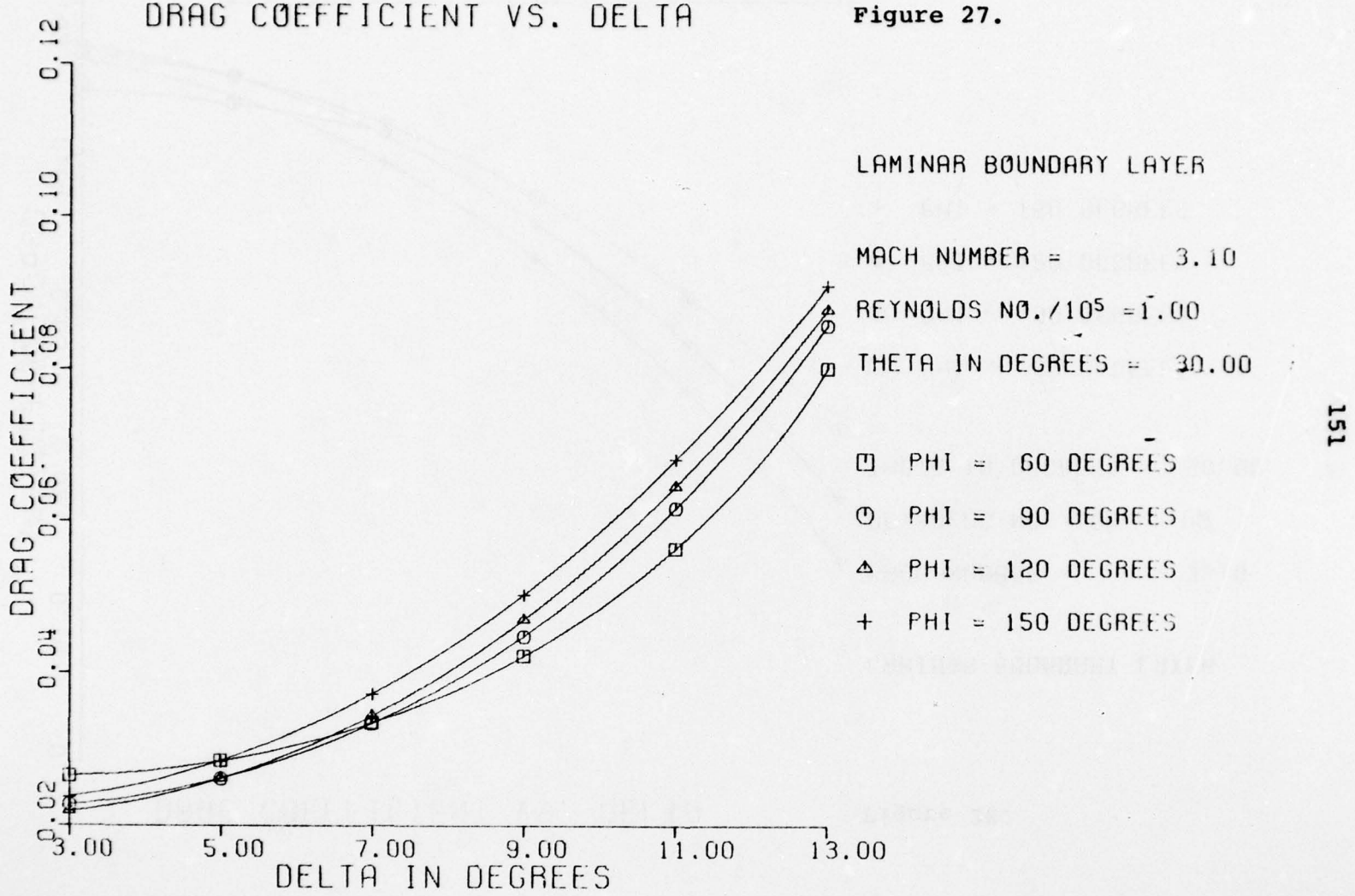
DRAG COEFFICIENT VS. DELTA
DRAG COEFFICIENT
0.02
0.04
0.06
0.08
0.10
0.12
3.00
5.00
7.00
9.00
11.00
13.00
DELTA IN DEGREES
LAMINAR BOUNDARY LAYER
MACH NUMBER = 3.10
REYNOLDS NO./10^5 = 1.00
THETA IN DEGREES = 30.00
PHI = 60 DEGREES
PHI = 90 DEGREES
PHI = 120 DEGREES
PHI = 150 DEGREES

Figure 27.

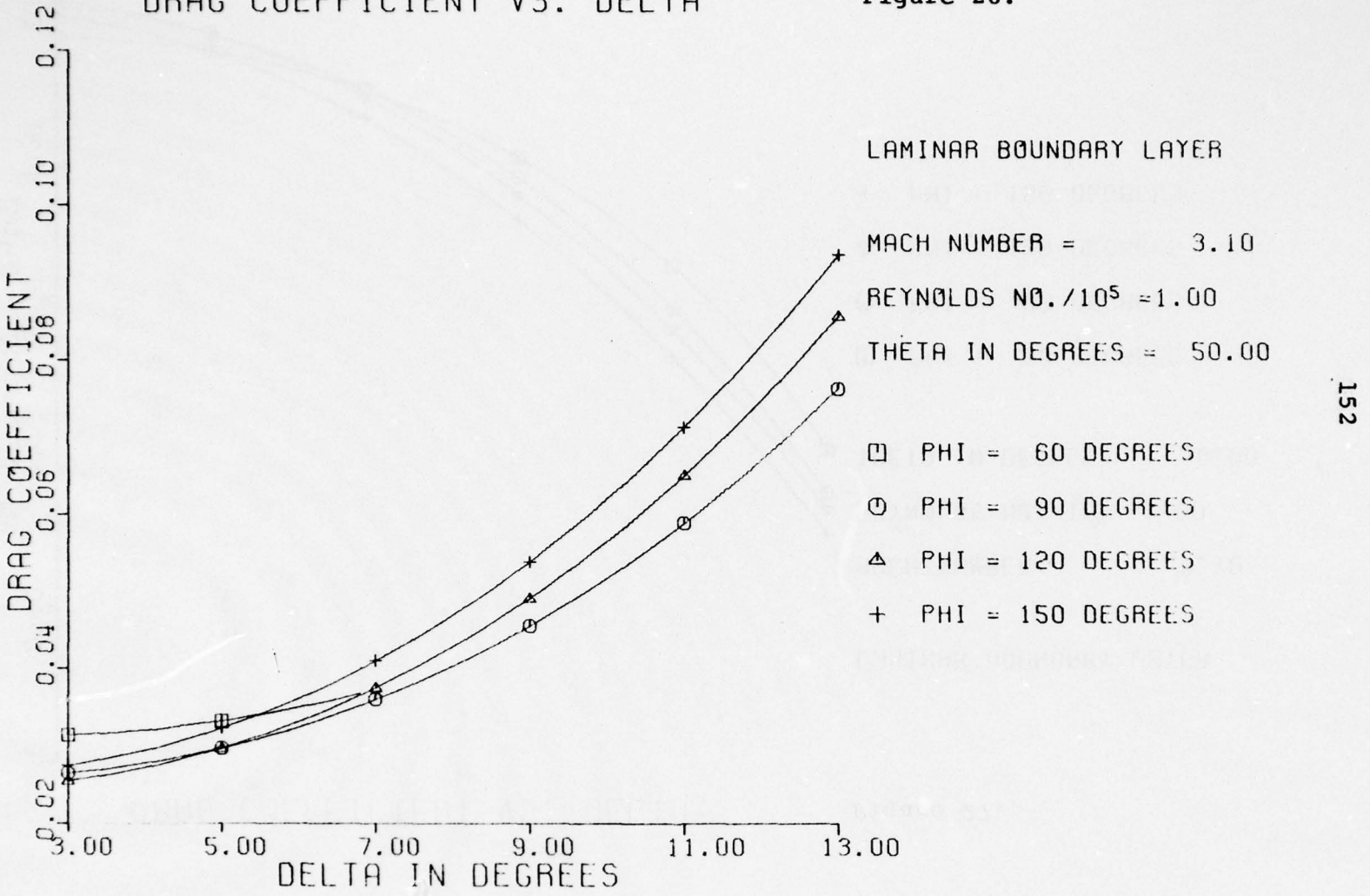
DRAG COEFFICIENT VS. DELTA
DRAG COEFFICIENT
0.02
0.04
0.06
0.08
0.10
0.12
3.00
5.00
7.00
9.00
11.00
13.00
DELTA IN DEGREES
LAMINAR BOUNDARY LAYER
MACH NUMBER = 3.10
REYNOLDS NO./10^5 =1.00
THETA IN DEGREES = 50.00
PHI = 60 DEGREES
PHI = 90 DEGREES
PHI = 120 DEGREES
PHI = 150 DEGREES

Figure 28.

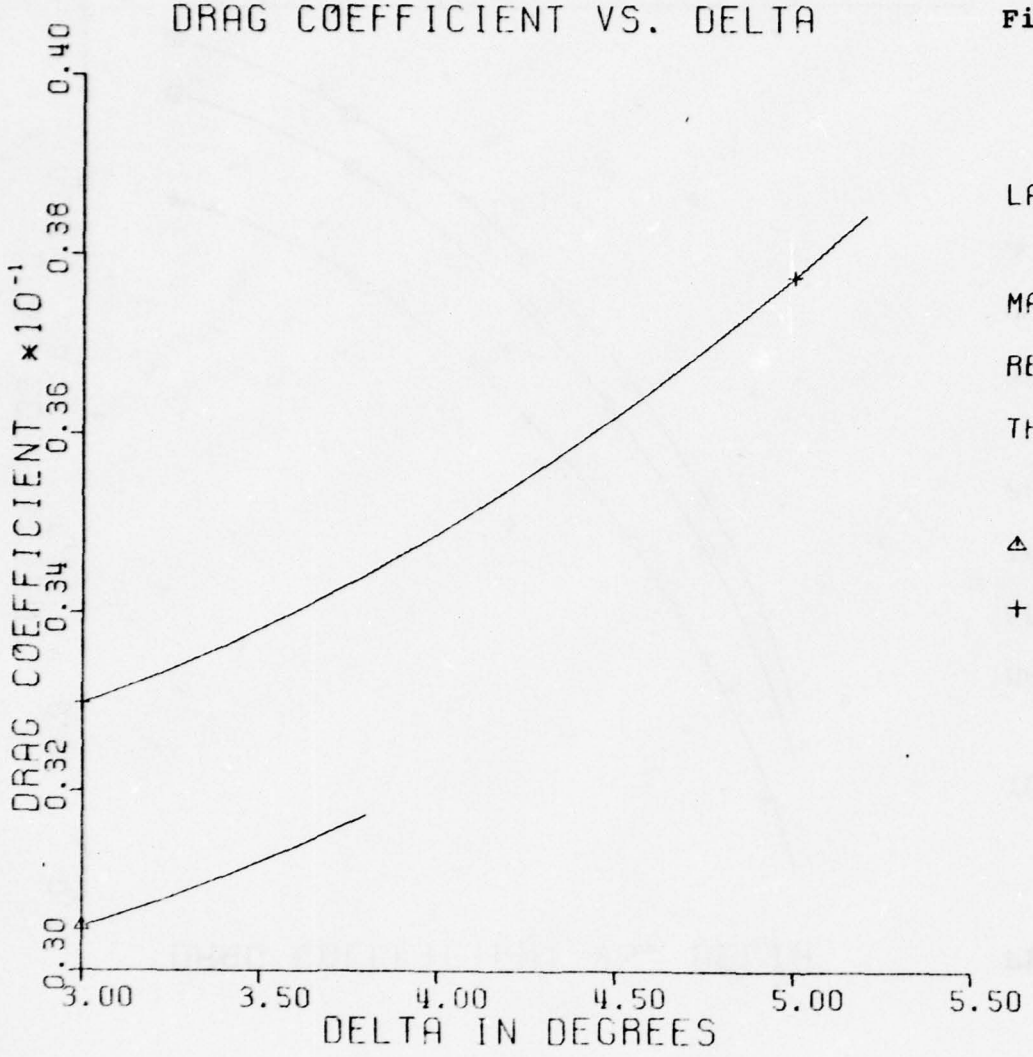

Figure 29.

LAMINAR BOUNDARY LAYER

MACH NUMBER = 3.10

REYNOLDS NO./10^5 =1.00

THETA IN DEGREES = 70.00

△ PHI = 120 DEGREES

\+ PHI = 150 DEGREES

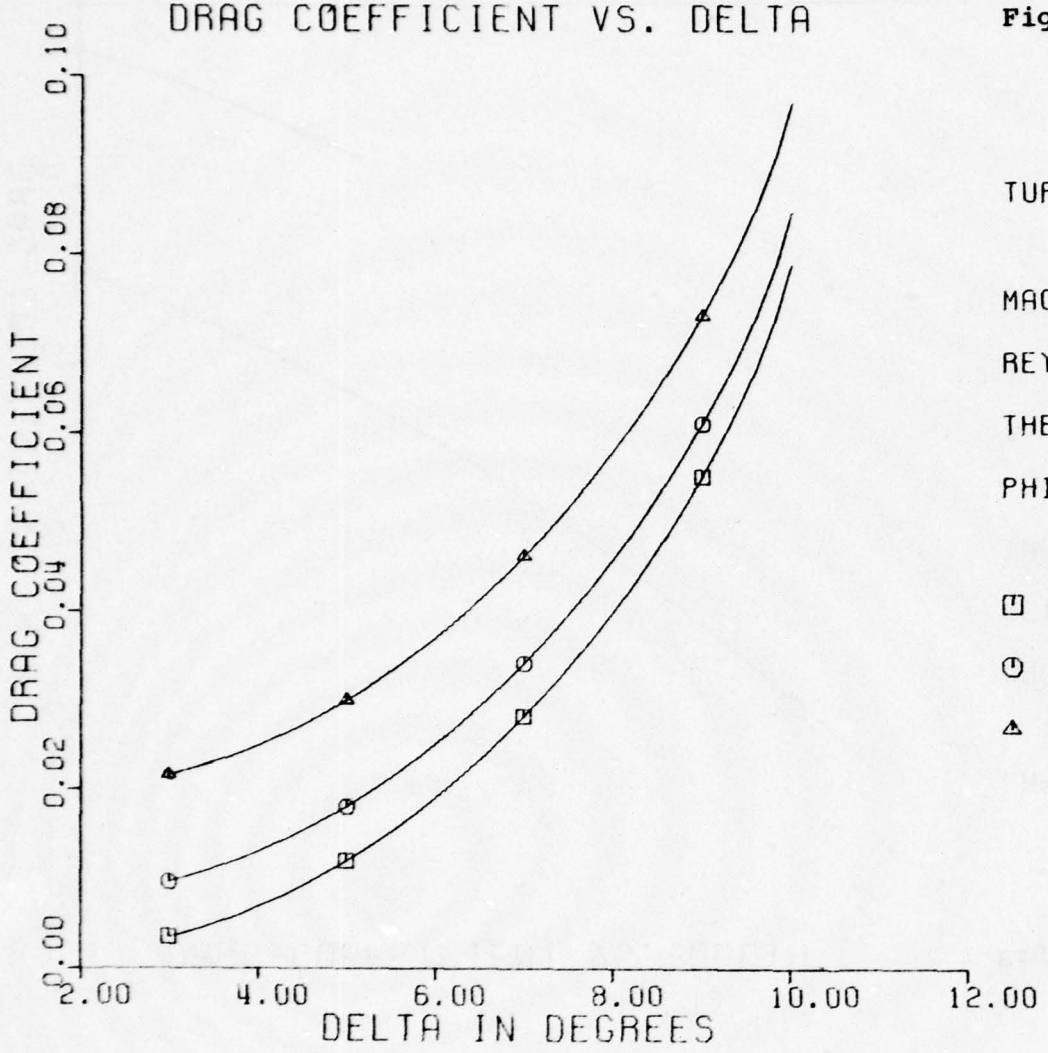

Figure 30.

TURBULENT BOUNDARY LAYER

MACH NUMBER = 2.00

REYNOLDS NO./10^5 =100.00

THETA IN DEGREES = 30.00

PHI IN DEGREES = 120.00

□ NO SKIN FRICTION OR BASE DRAG

○ NO BASE DRAG

△ ALL FORCES

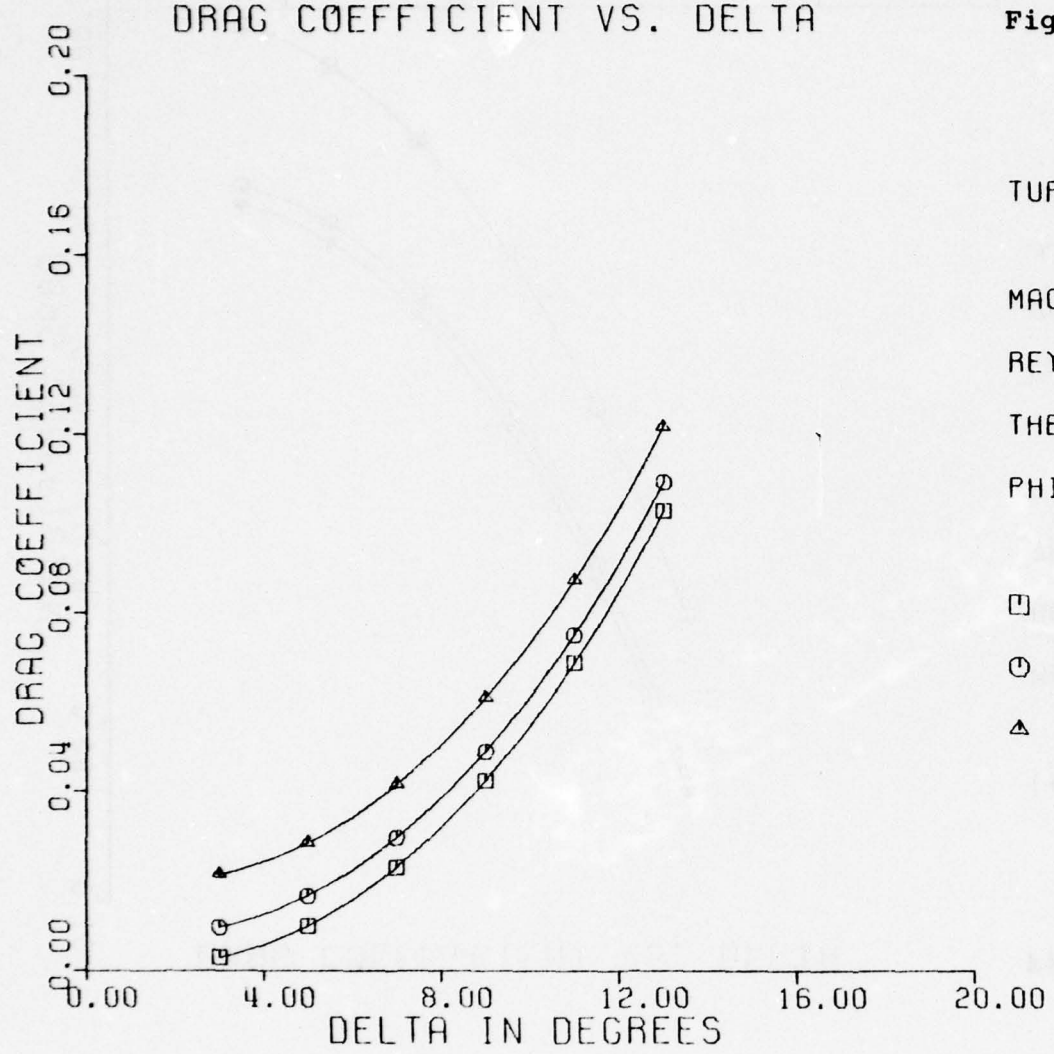

Figure 31.

TURBULENT BOUNDARY LAYER

MACH NUMBER = 2.00

REYNOLDS NO./10^5 =100.00

THETA IN DEGREES = 50.00

PHI IN DEGREES = 120.00

□ NO SKIN FRICTION OR BASE DRAG

○ NO BASE DRAG

△ ALL FORCES

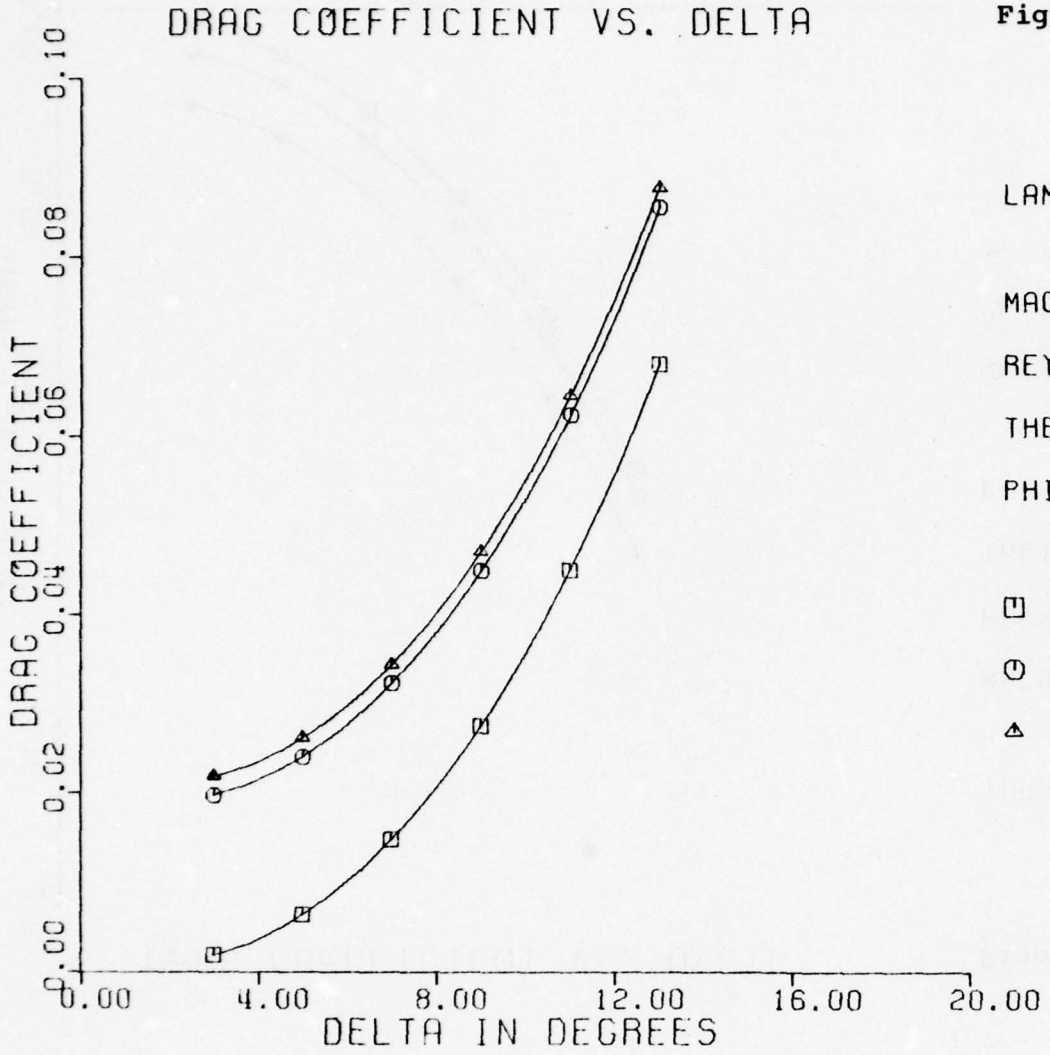

Figure 32.

LAMINAR BOUNDARY LAYER

MACH NUMBER = 3.10

REYNOLDS NO./10^5 =1.00

THETA IN DEGREES = 30.00

PHI IN DEGREES = 120.00

□ NO SKIN FRICTION OR BASE DRAG

○ NO BASE DRAG

△ ALL FORCES

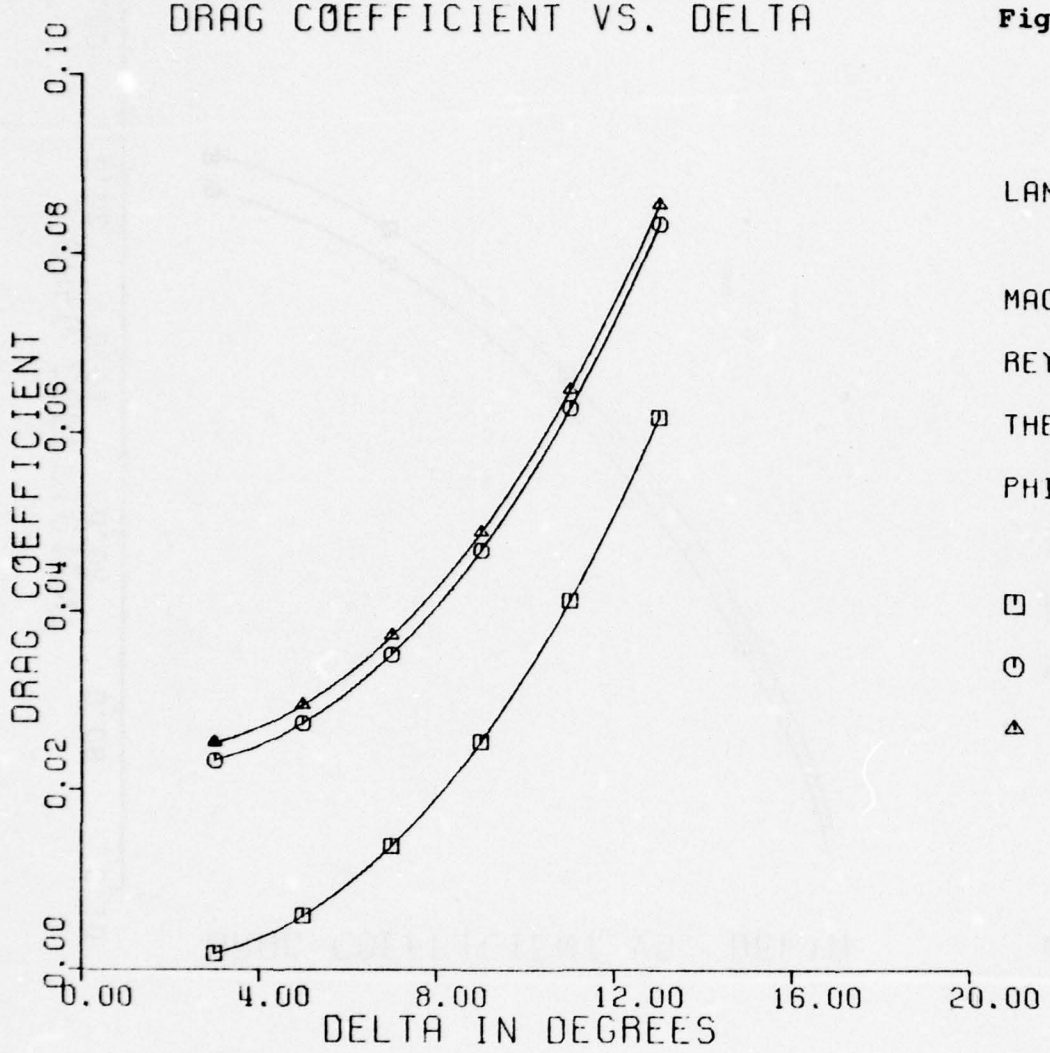

Figure 33.

LAMINAR BOUNDARY LAYER

MACH NUMBER = 3.10

REYNOLDS NO./10^5 =1.00

THETA IN DEGREES = 50.00

PHI IN DEGREES = 120.00

□ NO SKIN FRICTION OR BASE DRAG

○ NO BASE DRAG

△ ALL FORCES

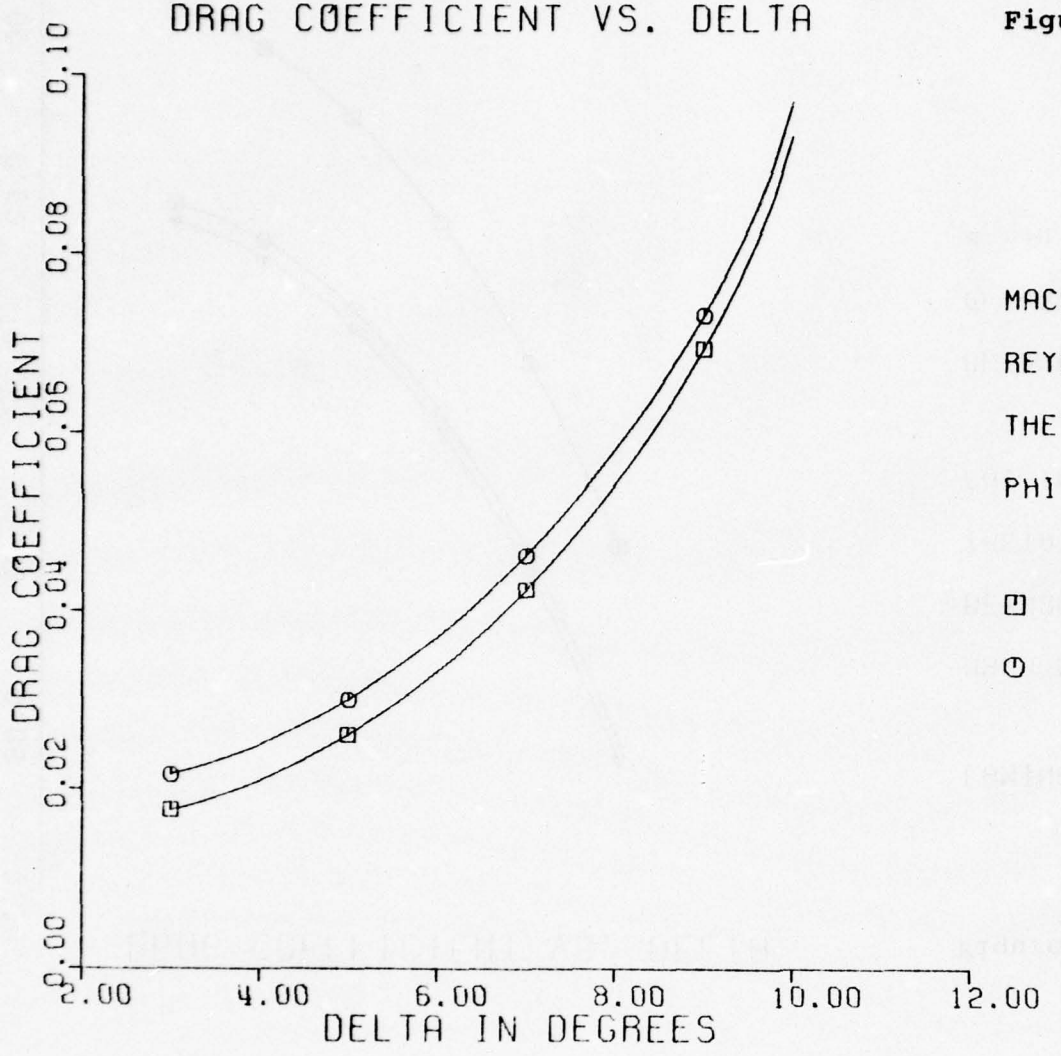

Figure 34.

MACH NUMBER = 2.00

REYNOLDS NO./10^5 =100.00

THETA IN DEGREES = 30.00

PHI IN DEGREES = 120.00

□ LAMINAR BOUNDARY LAYER

○ TURBULENT BOUNDARY LAYER

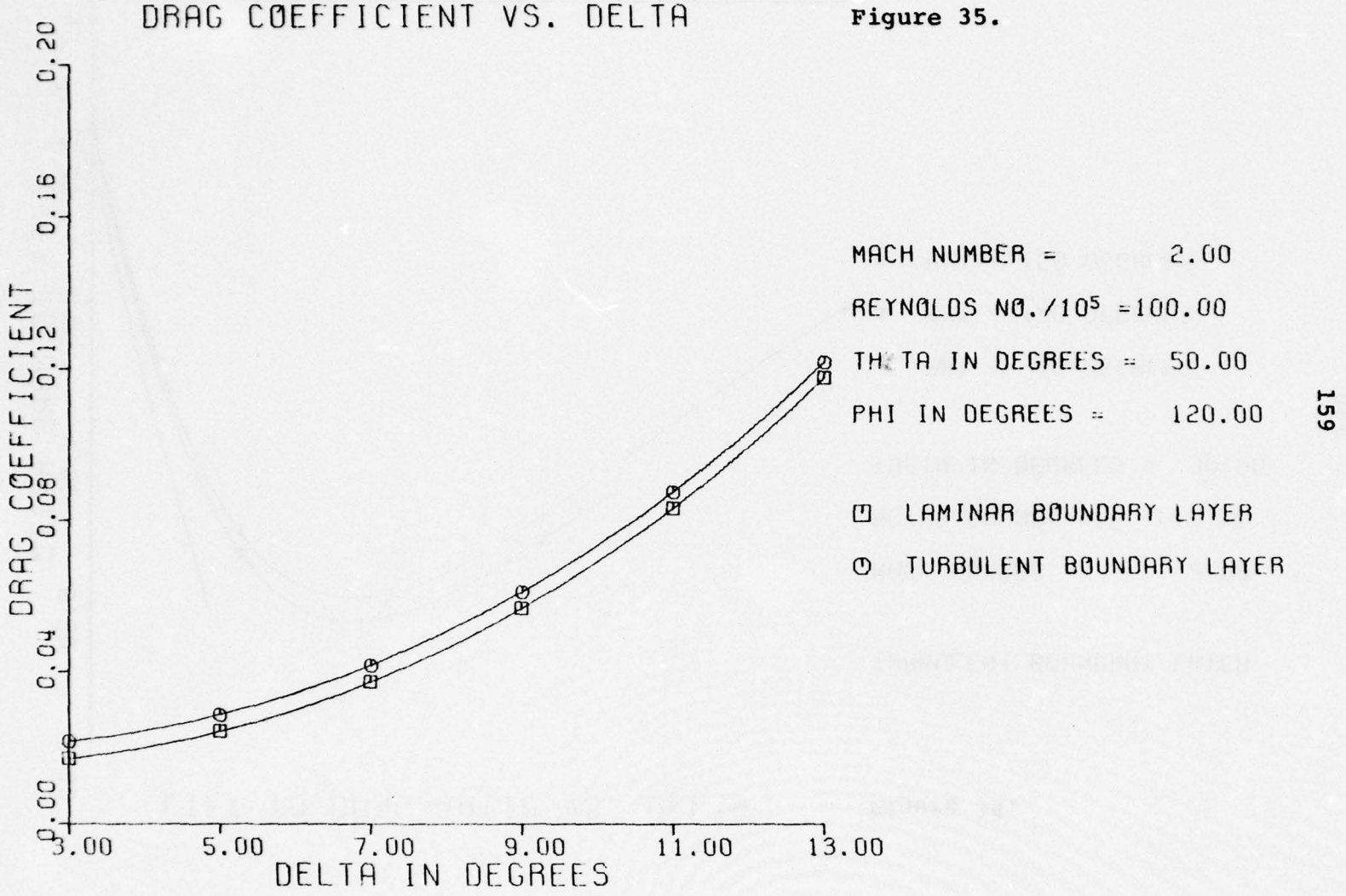
DRAG COEFFICIENT VS. DELTA
DRAG COEFFICIENT
0.00
0.04
0.08
0.12
0.16
0.20
3.00
5.00
7.00
9.00
11.00
13.00
DELTA IN DEGREES
MACH NUMBER = 2.00
REYNOLDS NO./10^5 =100.00
THETA IN DEGREES = 50.00
PHI IN DEGREES = 120.00
LAMINAR BOUNDARY LAYER
TURBULENT BOUNDARY LAYER

Figure 35.

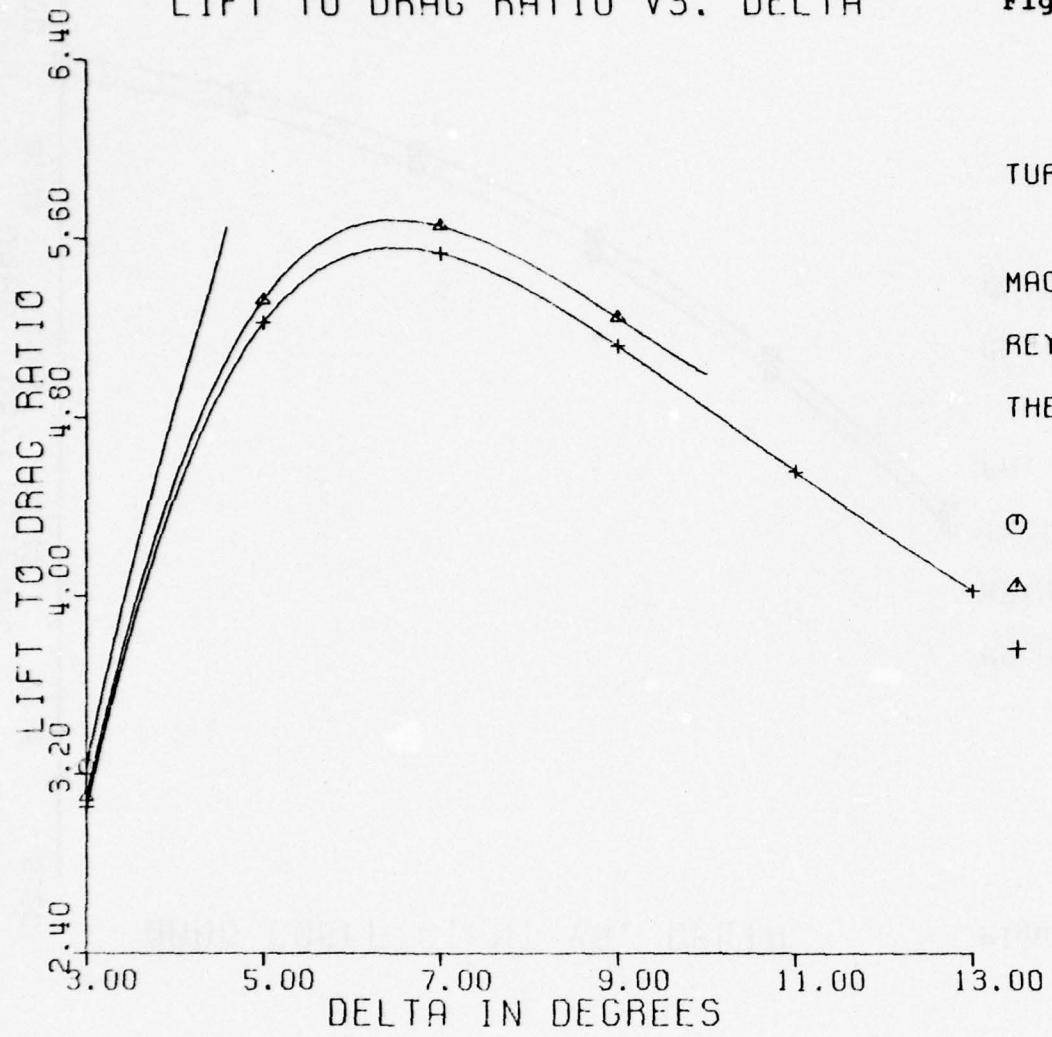

Figure 36.

TURBULENT BOUNDARY LAYER

MACH NUMBER = 2.00

REYNOLDS NØ./10^5 =100.00

THETA IN DEGREES = 30.00

⊙ PHI = 90 DEGREES

△ PHI = 120 DEGREES

\+ PHI = 150 DEGREES

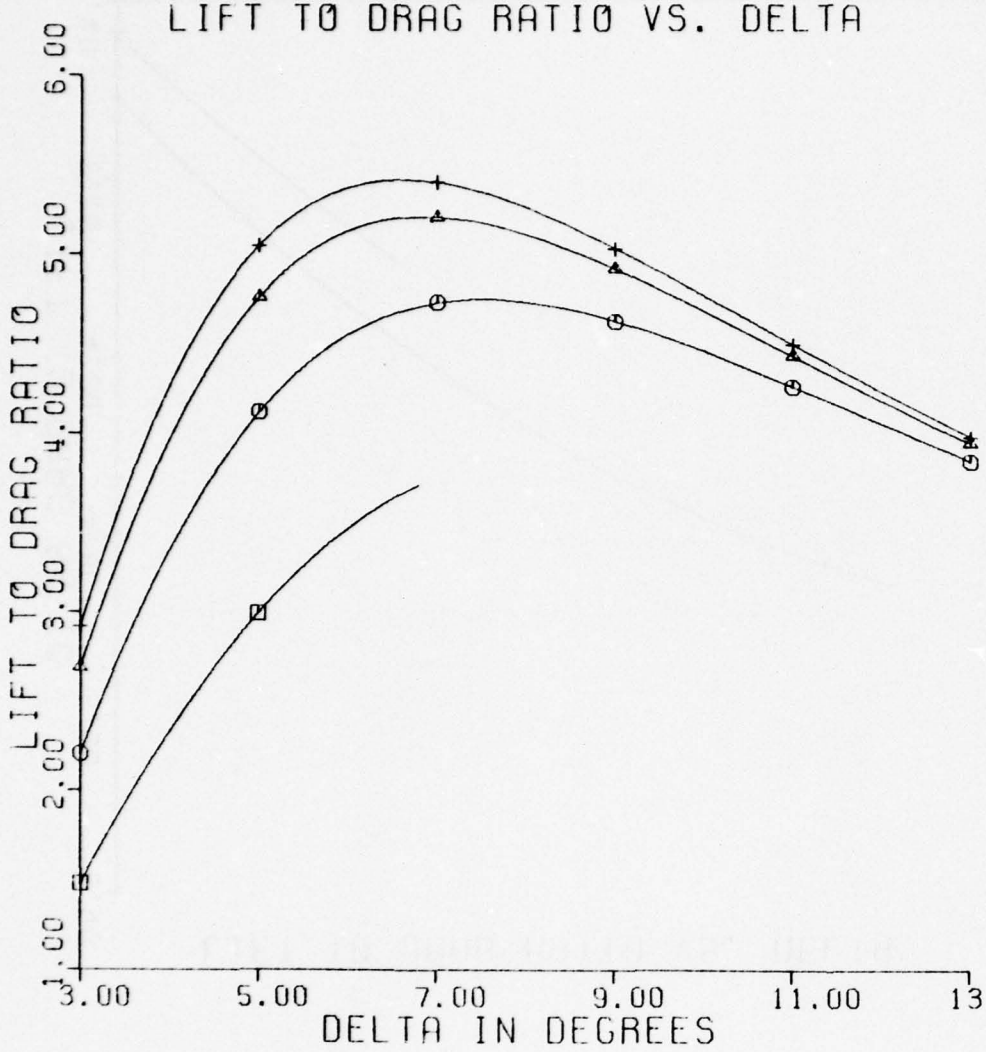

Figure 37.

TURBULENT BOUNDARY LAYER

MACH NUMBER = 2.00

REYNOLDS NO./10^5 =100.00

THETA IN DEGREES = 50.00

□ PHI = 60 DEGREES

○ PHI = 90 DEGREES

△ PHI = 120 DEGREES

\+ PHI = 150 DEGREES

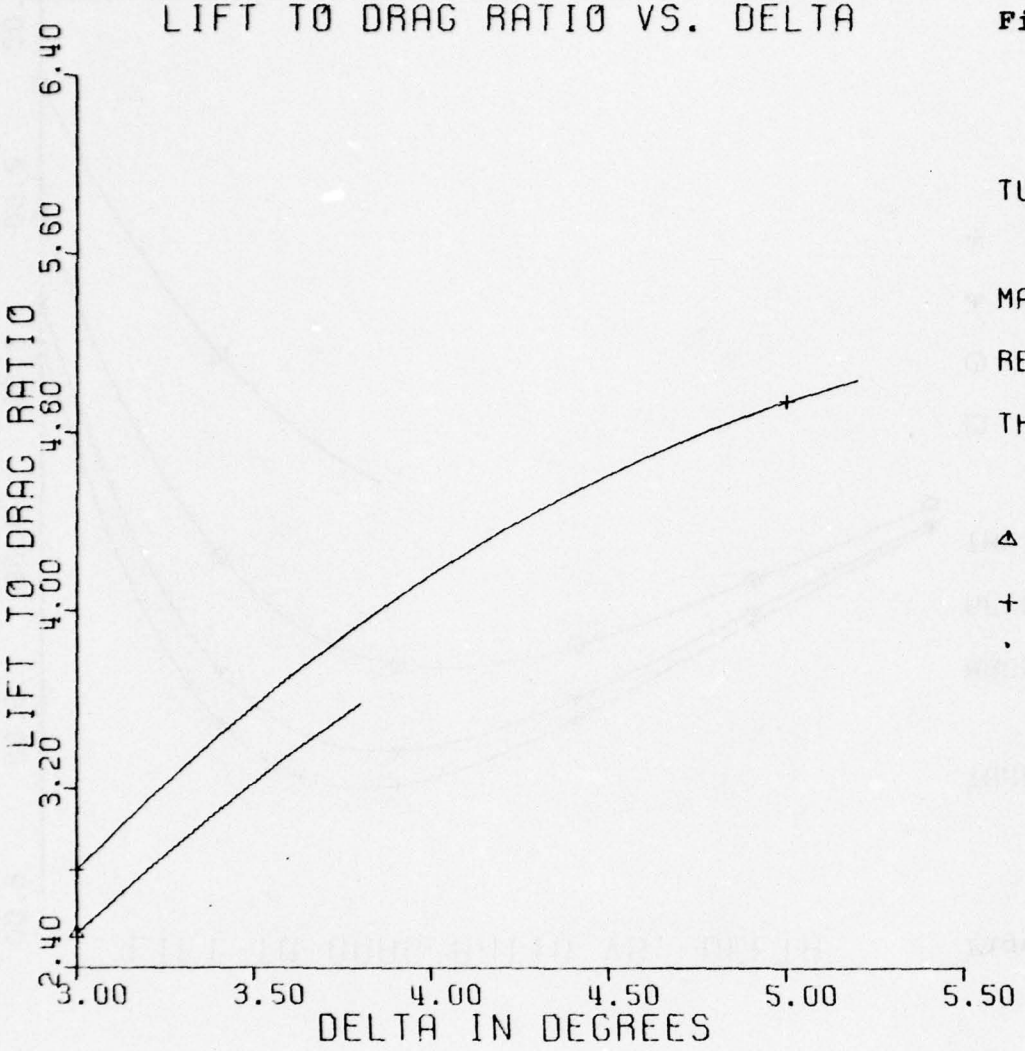

Figure 38.

TURBULENT BØUNDARY LAYER

MACH NUMBER = 2.00

REYNØLDS NØ./10^5 =100.00

THETA IN DEGREES = 70.00

△ PHI = 120 DEGREES

\+ PHI = 150 DEGREES

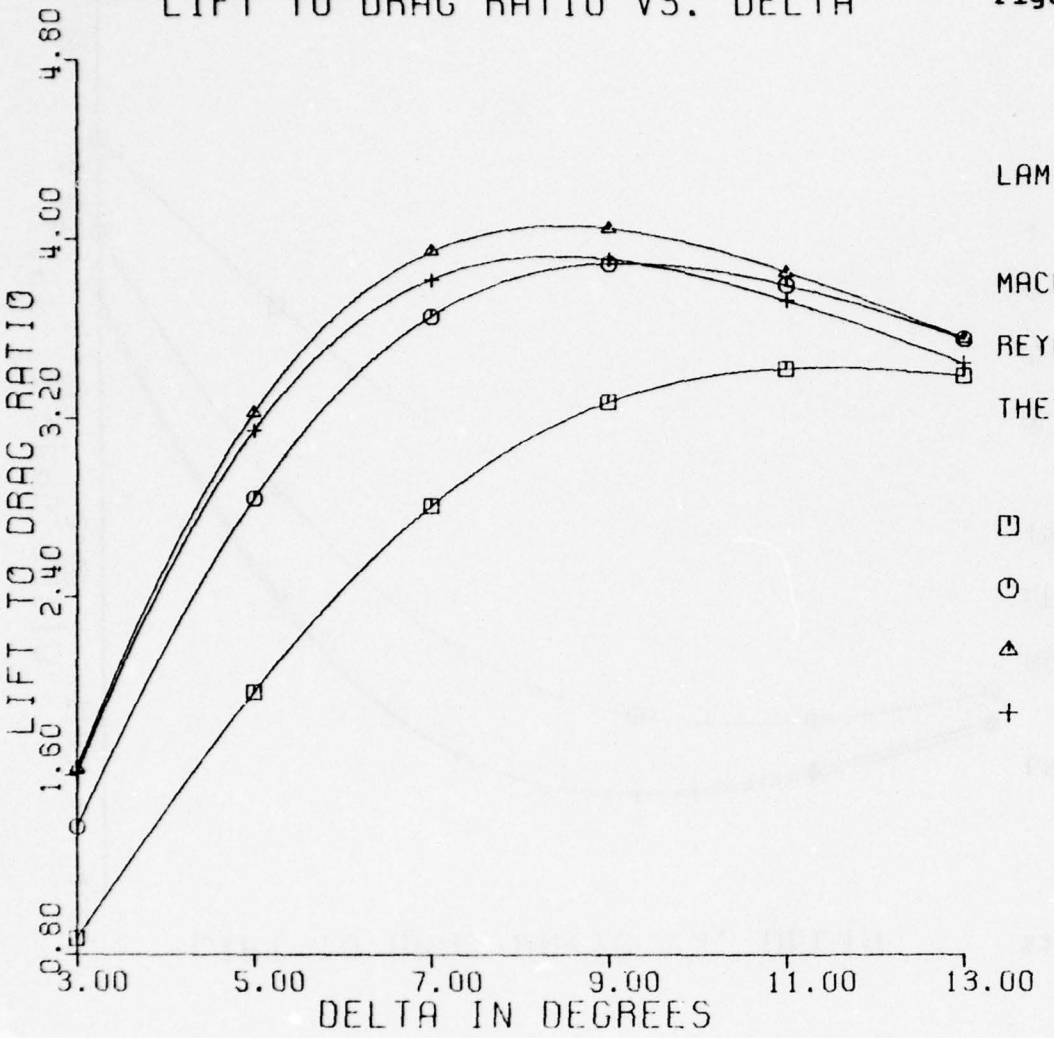

Figure 39.

LAMINAR BOUNDARY LAYER

MACH NUMBER = 3.10

REYNOLDS NO./10^5 =1.00

THETA IN DEGREES = 30.00

□ PHI = 60 DEGREES

○ PHI = 90 DEGREES

△ PHI = 120 DEGREES

\+ PHI = 150 DEGREES

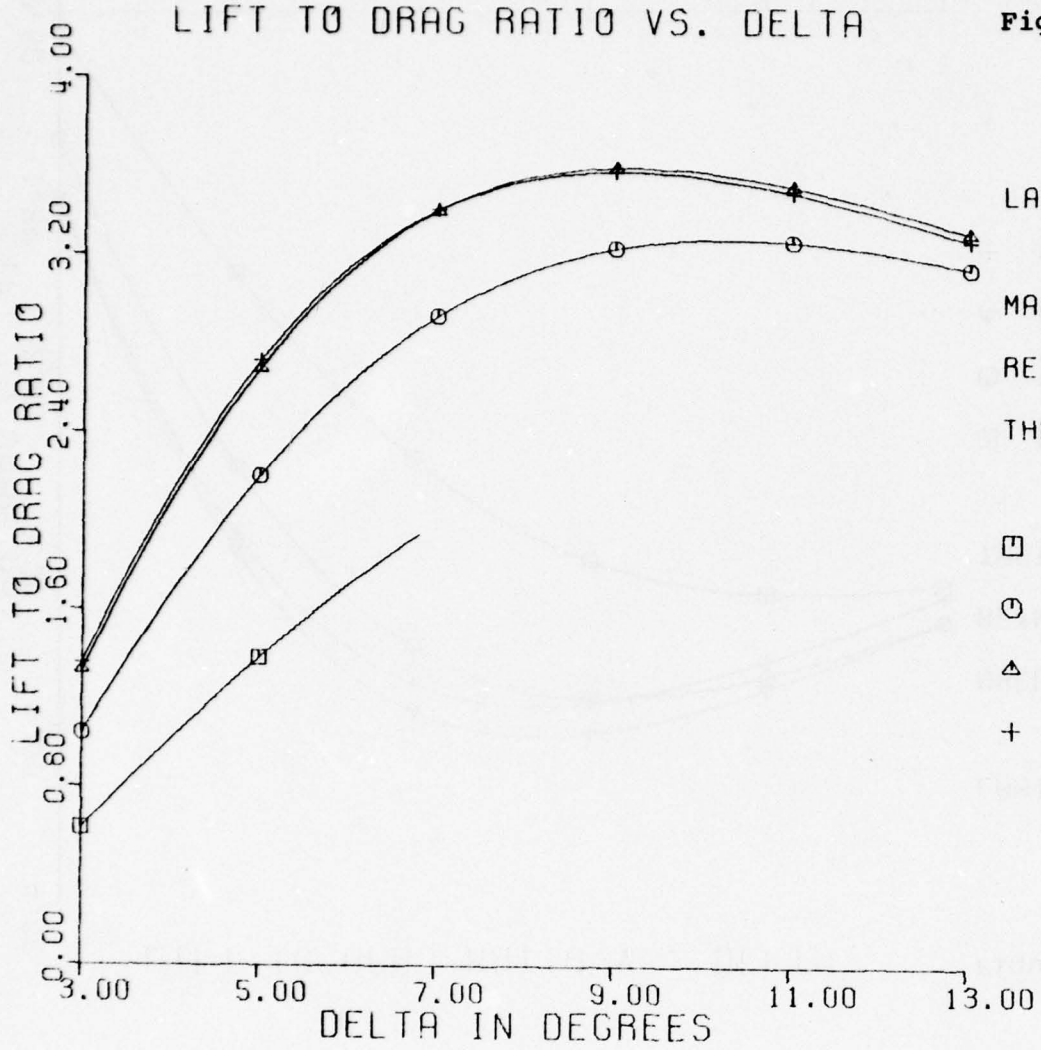

Figure 40.

LAMINAR BOUNDARY LAYER

MACH NUMBER = 3.10

REYNOLDS NO./10^5 =1.00

THETA IN DEGREES = 50.00

□ PHI = 60 DEGREES

○ PHI = 90 DEGREES

△ PHI = 120 DEGREES

\+ PHI = 150 DEGREES

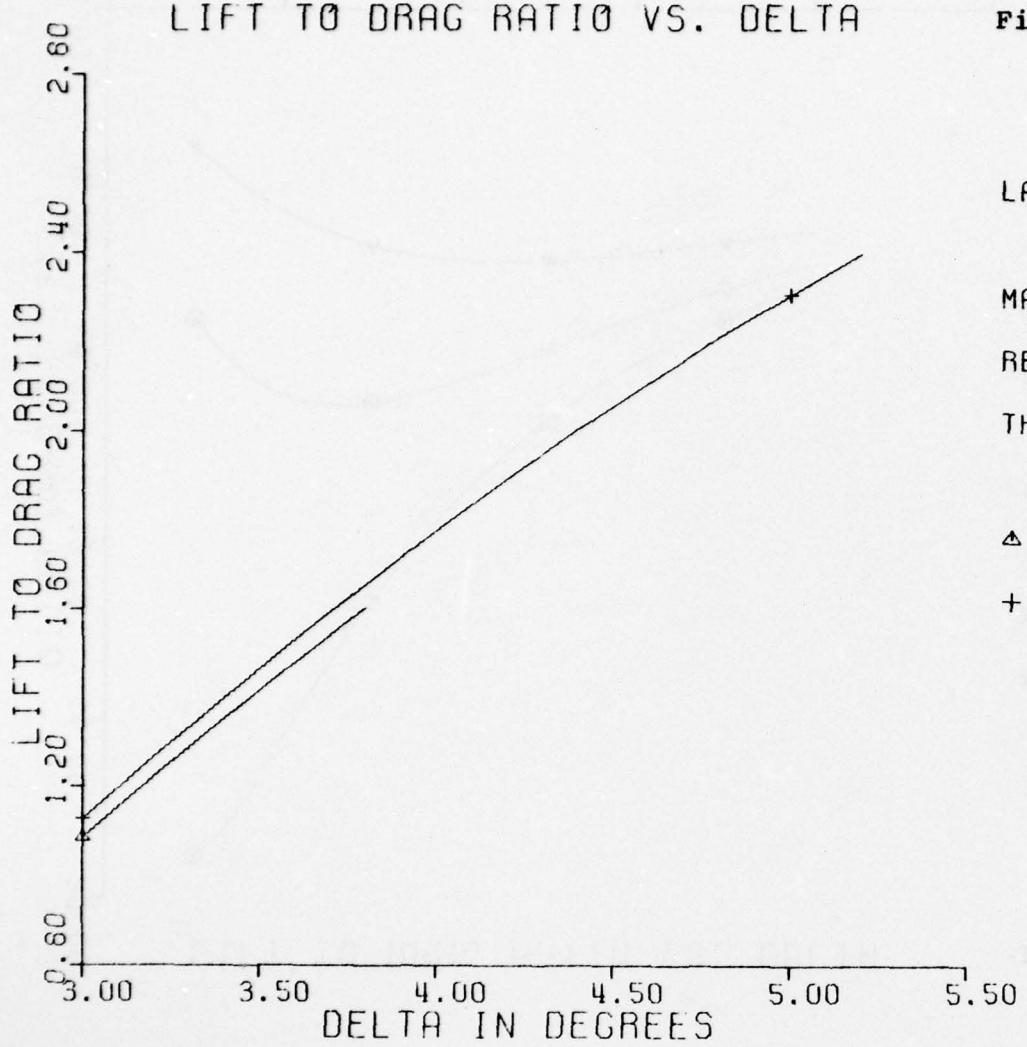

Figure 41.

LAMINAR BOUNDARY LAYER

MACH NUMBER = 3.10

REYNOLDS NO./10^5 =1.00

THETA IN DEGREES = 70.00

△ PHI = 120 DEGREES

\+ PHI = 150 DEGREES

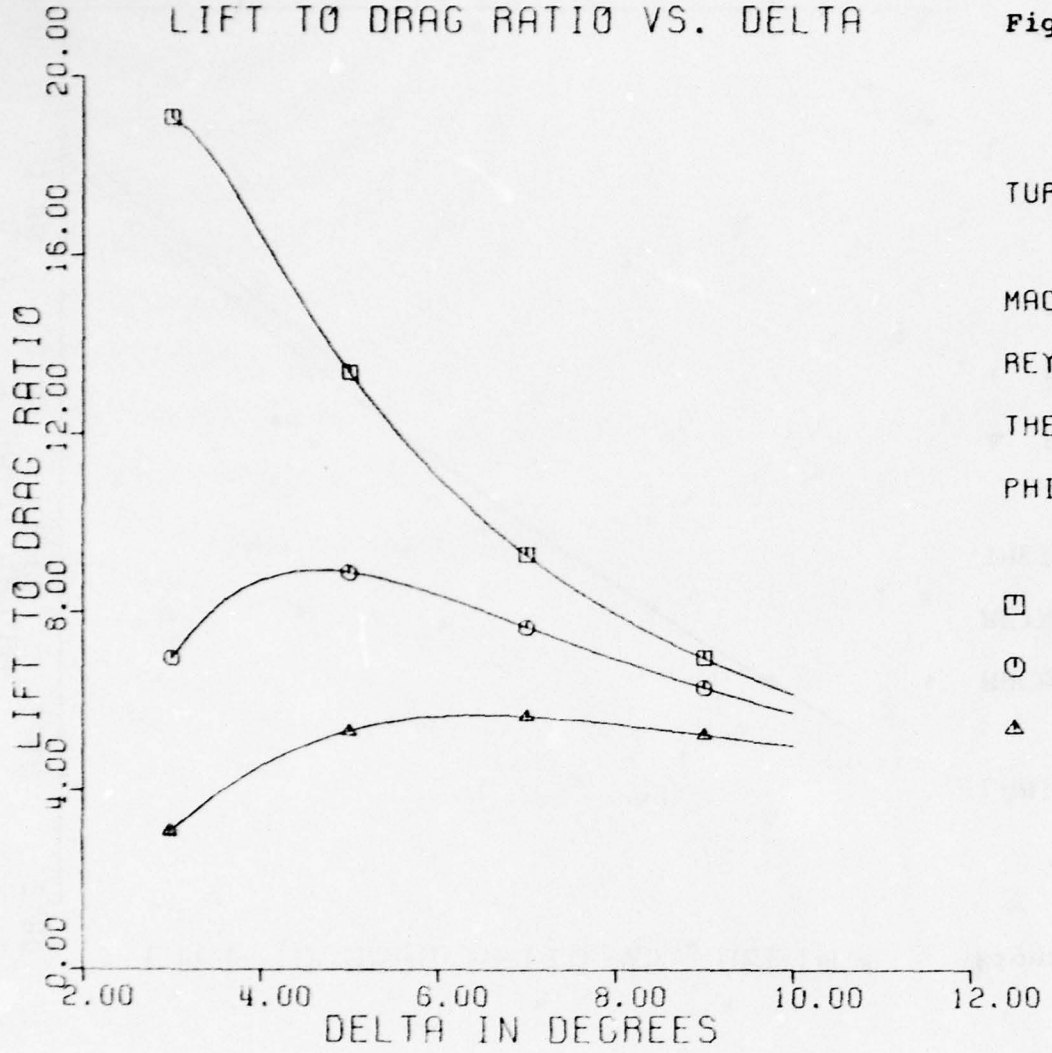

Figure 42.

TURBULENT BOUNDARY LAYER

MACH NUMBER = 2.00

REYNOLDS NO./10^5 =100.00

THETA IN DEGREES = 30.00

PHI IN DEGREES = 120.00

□ NO SKIN FRICTION OR BASE DRAG

○ NO BASE DRAG

△ ALL FORCES

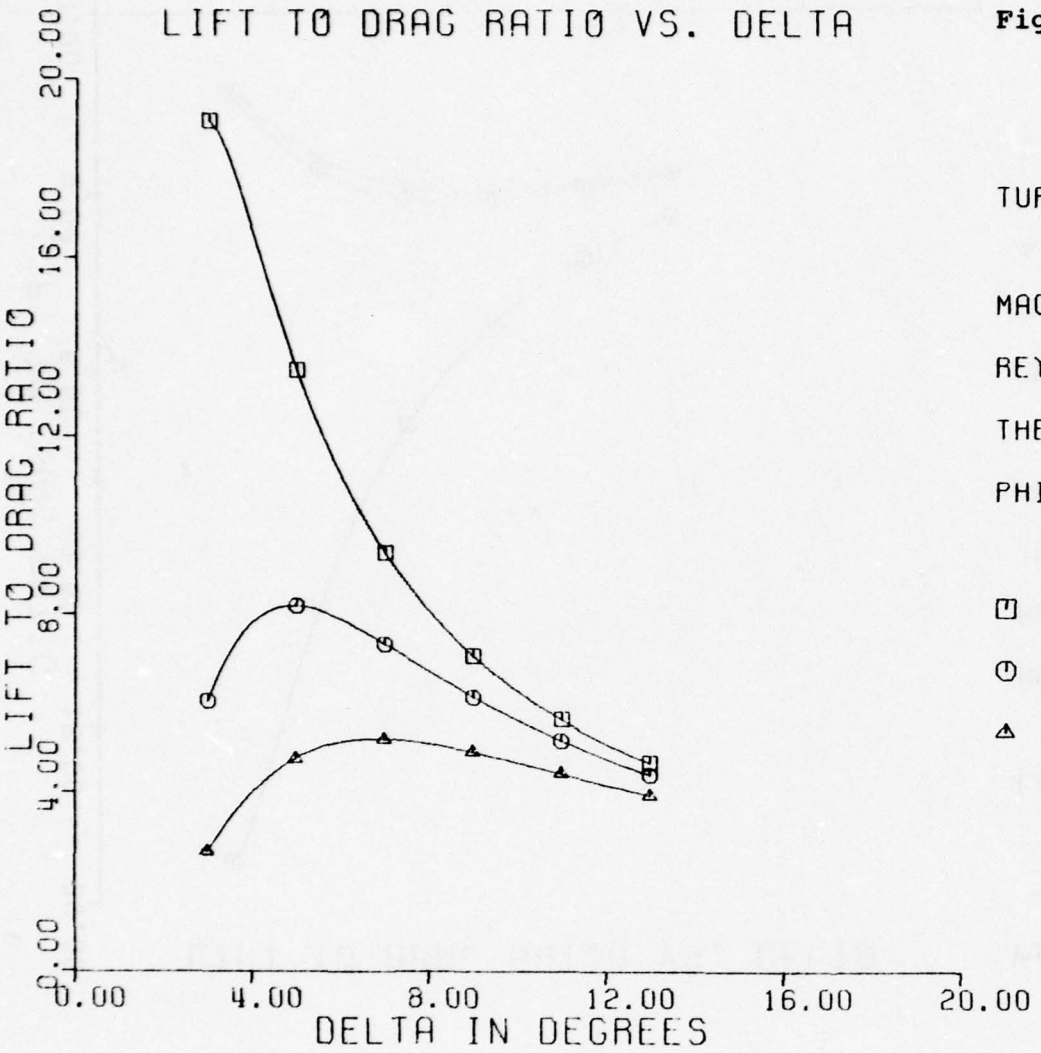

Figure 43.

TURBULENT BOUNDARY LAYER

MACH NUMBER = 2.00

REYNOLDS NO./10^5 =100.00

THETA IN DEGREES = 50.00

PHI IN DEGREES = 120.00

□ NO SKIN FRICTION OR BASE DRAG

○ NO BASE DRAG

△ ALL FORCES

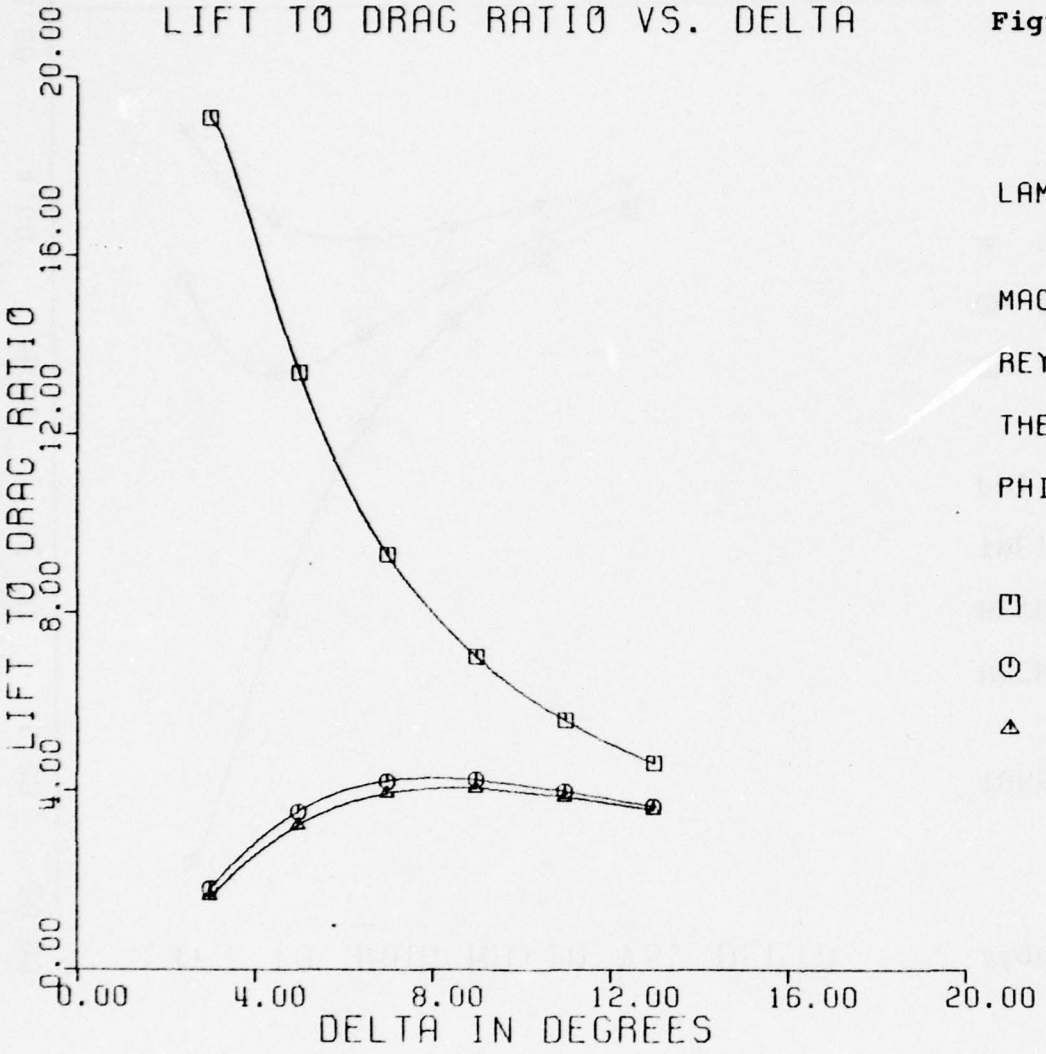

Figure 44.

LAMINAR BØUNDARY LAYER

MACH NUMBER = 3.10

REYNØLDS NØ./10^5 =1.00

THETA IN DEGREES = 30.00

PHI IN DEGREES = 120.00

168

□ NØ SKIN FRICTIØN ØR BASE DRAG

○ NØ BASE DRAG

△ ALL FØRCES

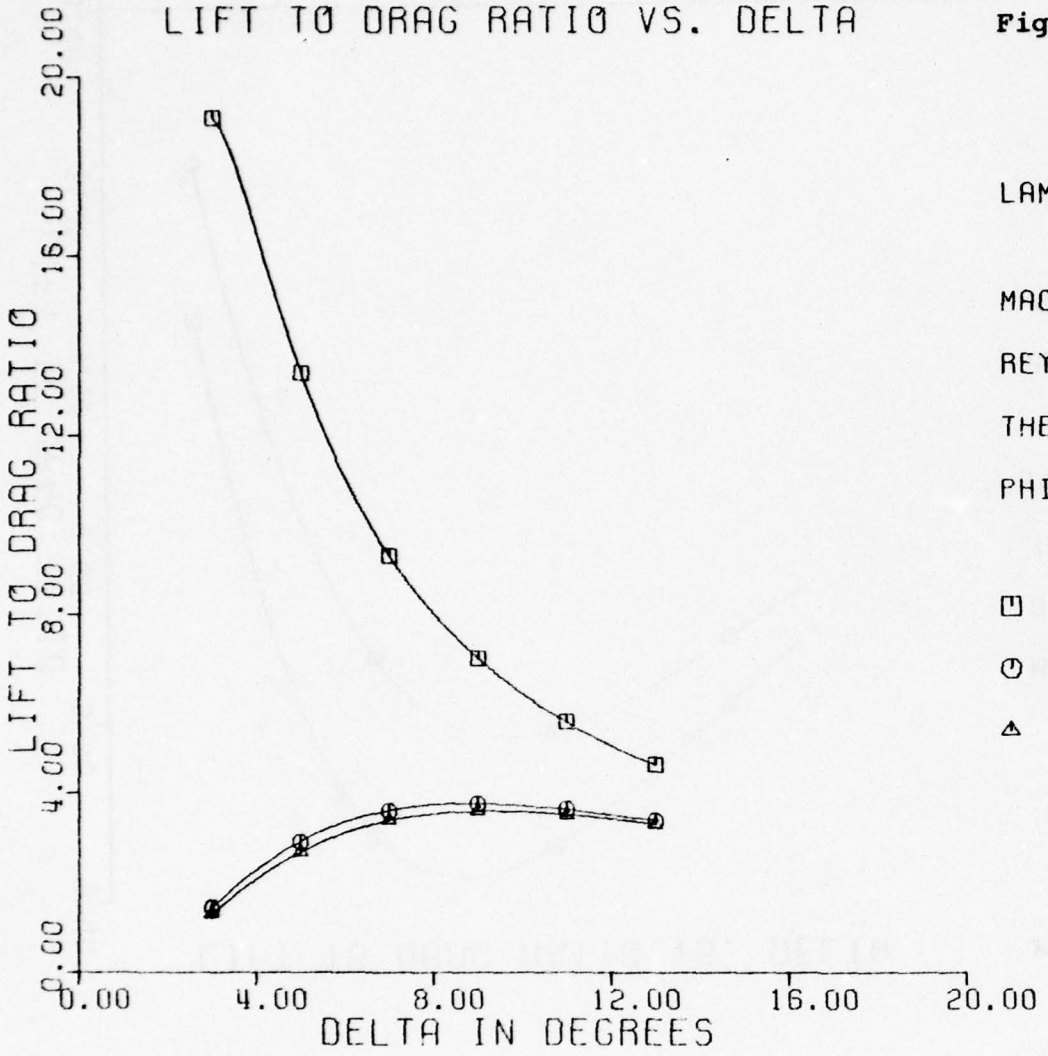

Figure 45.

LAMINAR BØUNDARY LAYER

MACH NUMBER = 3.10

REYNØLDS NØ./10^5 =1.00

THETA IN DEGREES = 50.00

PHI IN DEGREES = 120.00

□ NØ SKIN FRICTION ØR BASE DRAG

○ NØ BASE DRAG

△ ALL FØRCES

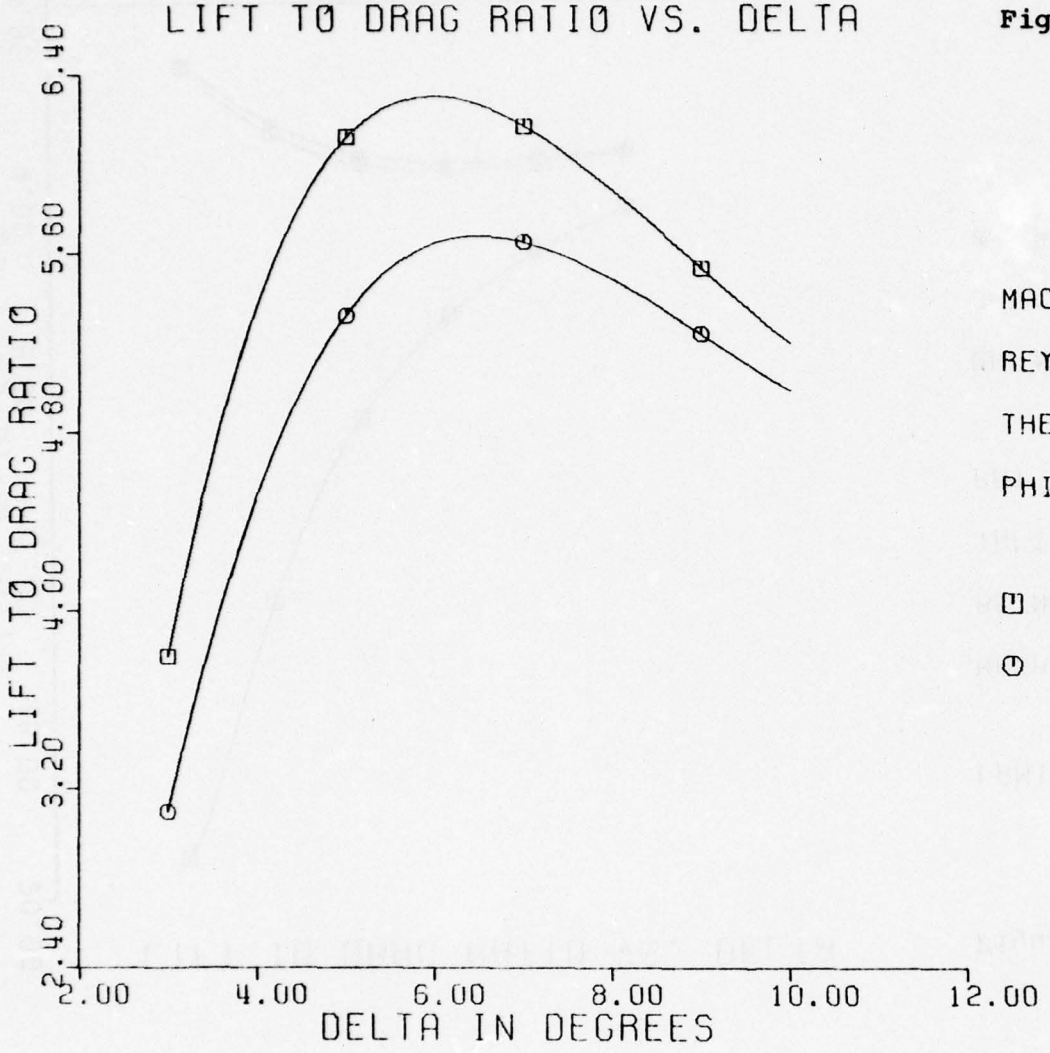

Figure 46.

MACH NUMBER = 2.00

REYNØLDS NØ./10^5 =100.00

THETA IN DEGREES = 30.00

PHI IN DEGREES = 120.00

□ LAMINAR BØUNDARY LAYER

○ TURBULENT BØUNDARY LAYER

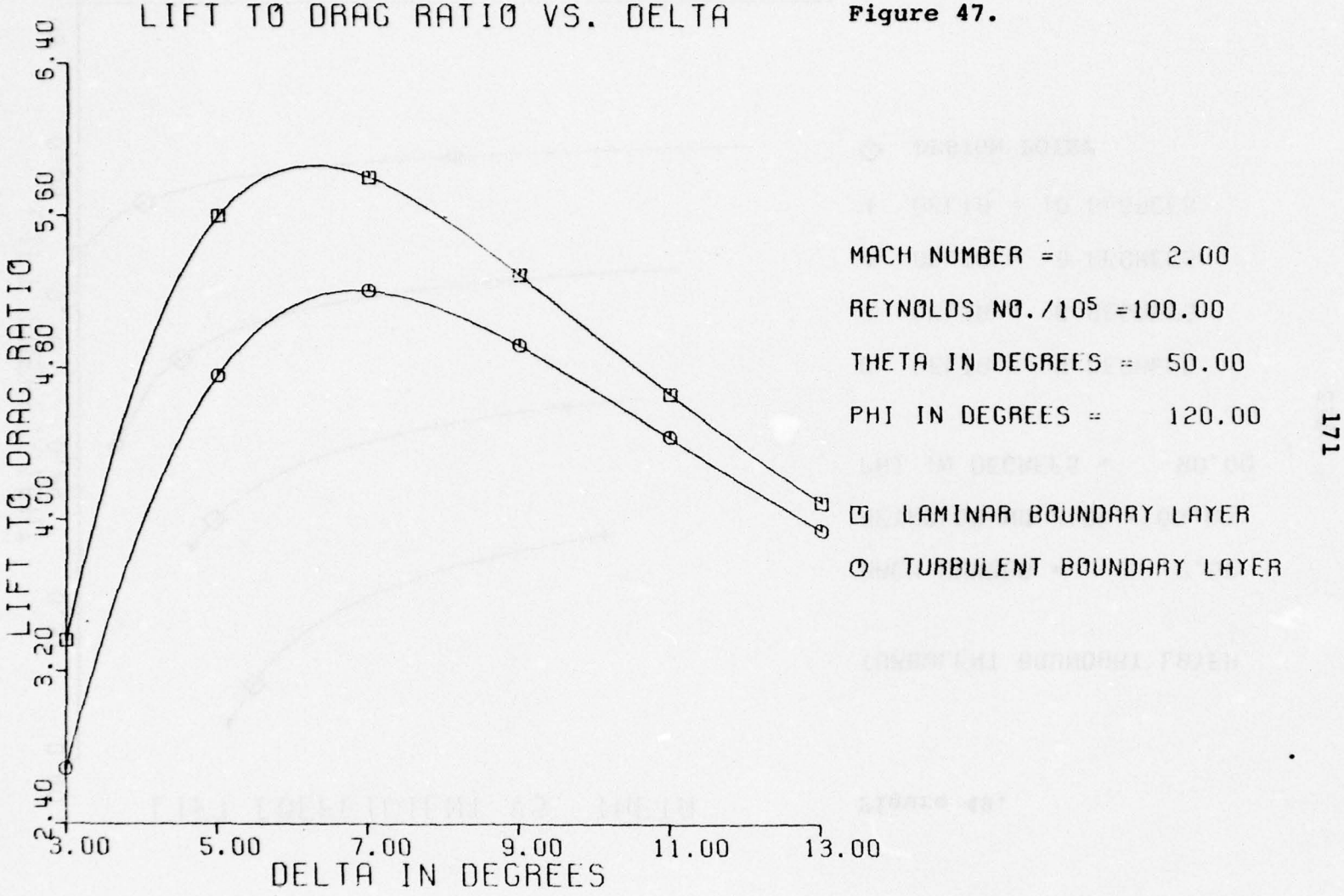
LIFT TO DRAG RATIO VS. DELTA
LIFT TO DRAG RATIO
6.40
5.60
4.80
4.00
3.20
2.40
3.00
5.00
7.00
9.00
11.00
13.00
DELTA IN DEGREES
MACH NUMBER = 2.00
REYNOLDS NO./10^5 =100.00
THETA IN DEGREES = 50.00
PHI IN DEGREES = 120.00
LAMINAR BOUNDARY LAYER
TURBULENT BOUNDARY LAYER

Figure 47.

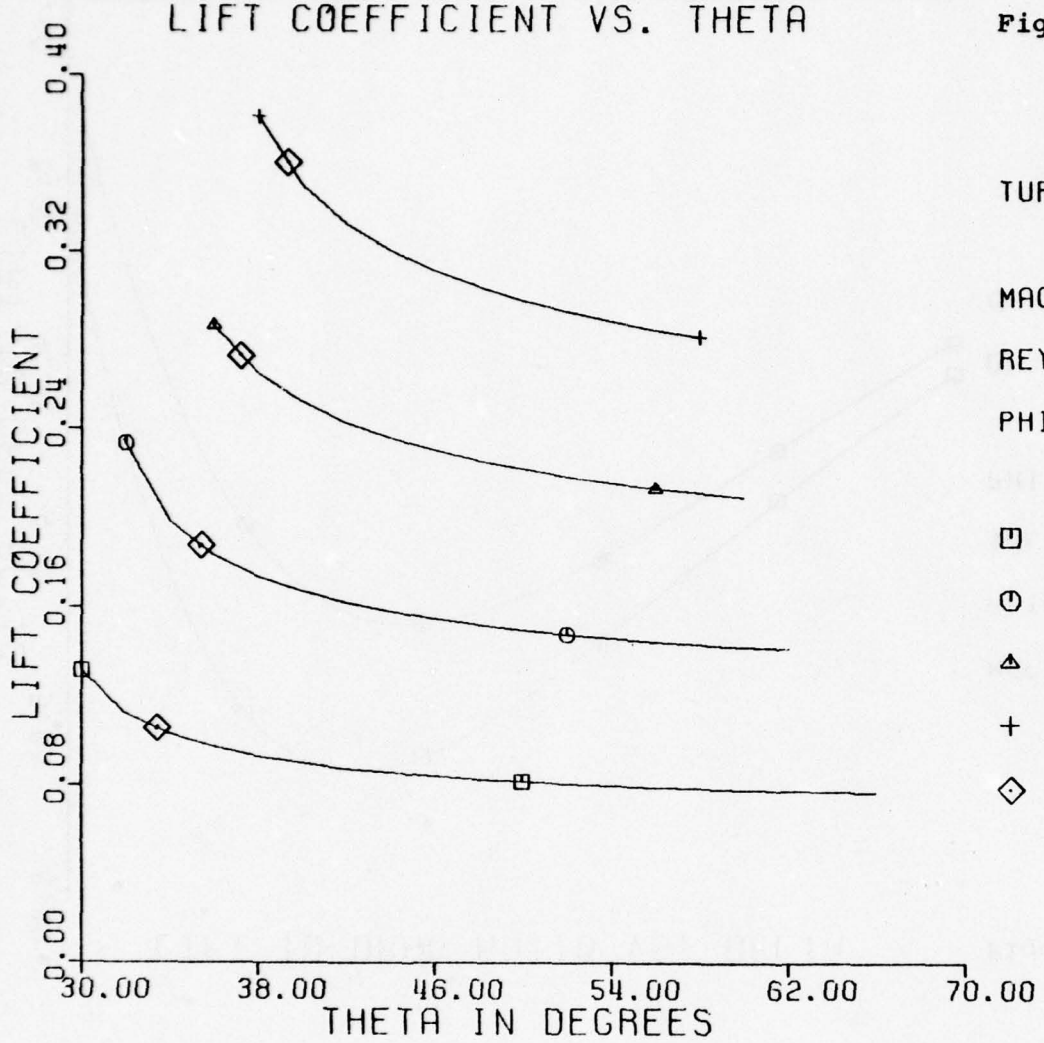

Figure 48.

TURBULENT BOUNDARY LAYER

MACH NUMBER = 2.00

REYNOLDS NO./10^5 =100.00

PHI IN DEGREES = 90.00

□ DELTA = 4 DEGREES

○ DELTA = 6 DEGREES

△ DELTA = 8 DEGREES

\+ DELTA = 10 DEGREES

◇ **DESIGN POINT**

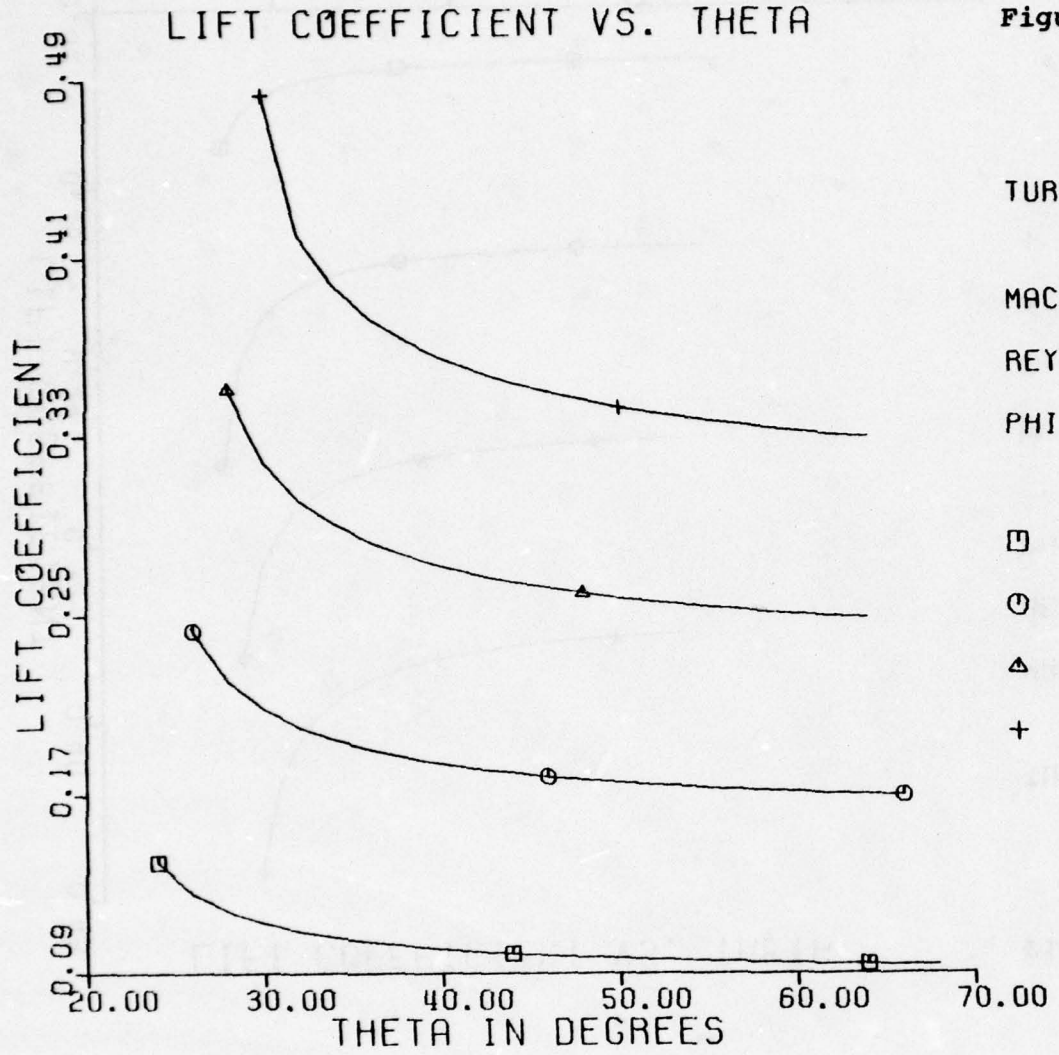

Figure 49.

TURBULENT BOUNDARY LAYER

MACH NUMBER = 2.00

REYNOLDS NO./10^5 =100.00

PHI IN DEGREES = 120.00

□ DELTA = 4 DEGREES

⊙ DELTA = 6 DEGREES

△ DELTA = 8 DEGREES

\+ DELTA = 10 DEGREES

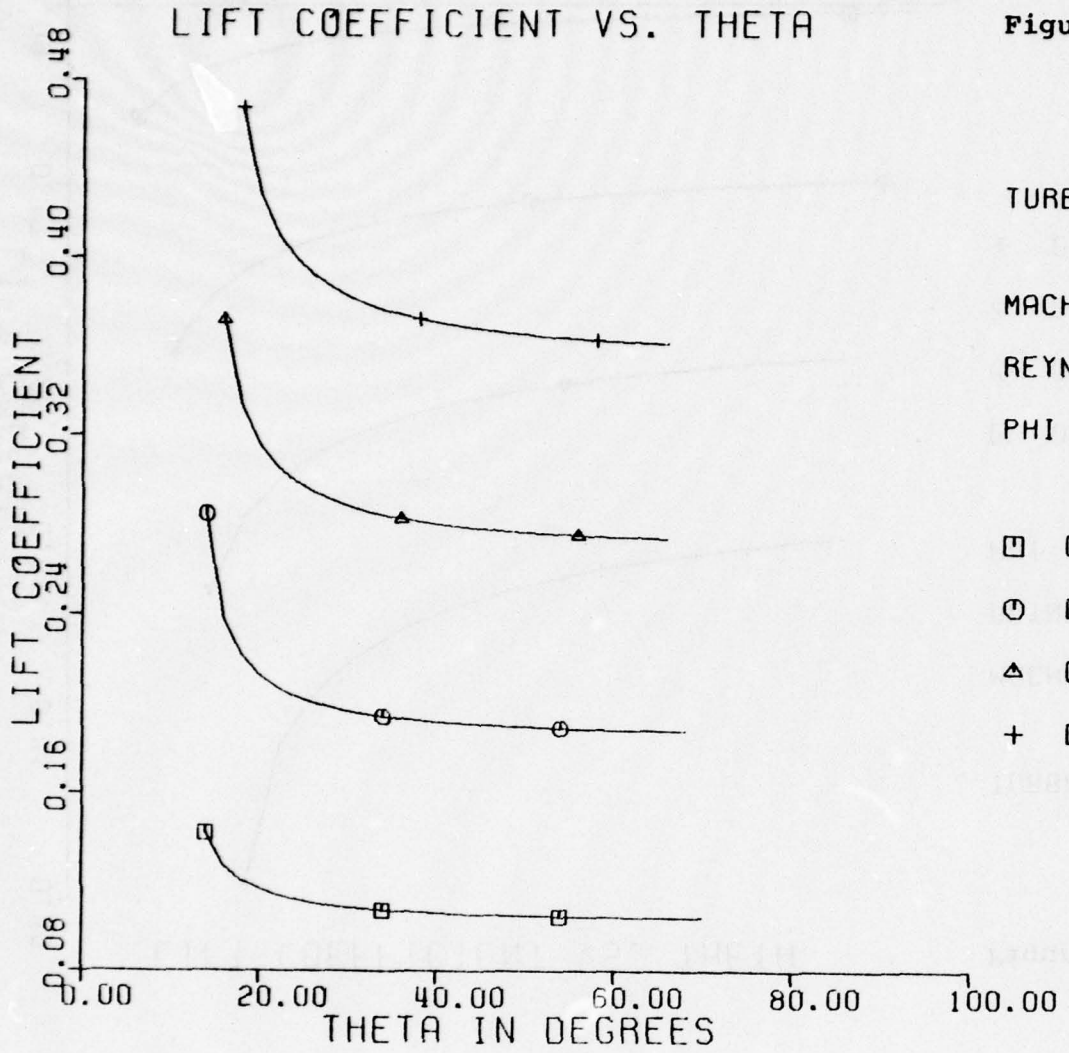

Figure 50.

TURBULENT BOUNDARY LAYER

MACH NUMBER = 2.00

REYNOLDS NO./10^5 =100.00

PHI IN DEGREES = 150.00

□ DELTA = 4 DEGREES

⊙ DELTA = 6 DEGREES

△ DELTA = 8 DEGREES

\+ DELTA = 10 DEGREES

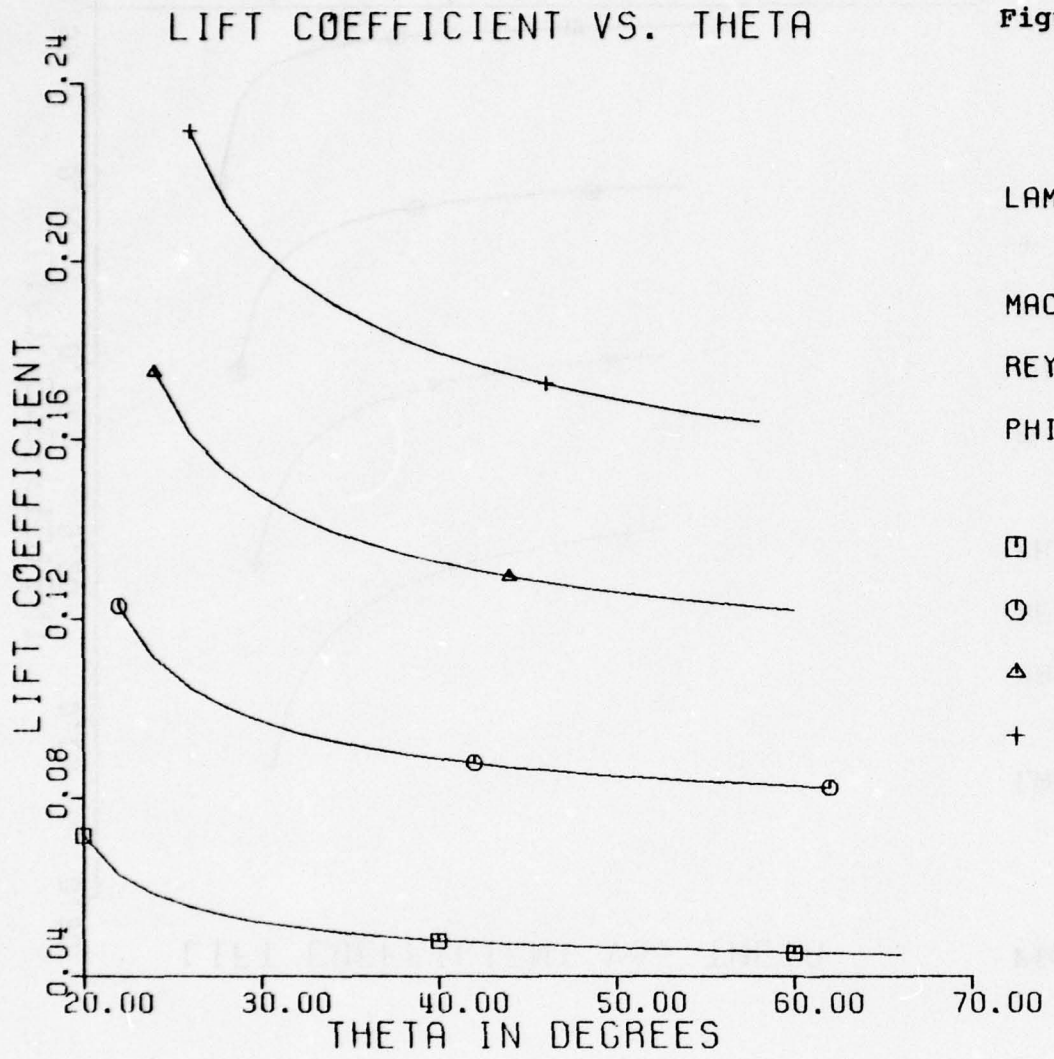

Figure 51.

LAMINAR BOUNDARY LAYER

MACH NUMBER = 3.10

REYNOLDS NO./10^5 =1.00

PHI IN DEGREES = 90.00

⊡ DELTA = 4 DEGREES

⊙ DELTA = 6 DEGREES

△ DELTA = 8 DEGREES

\+ DELTA = 10 DEGREES

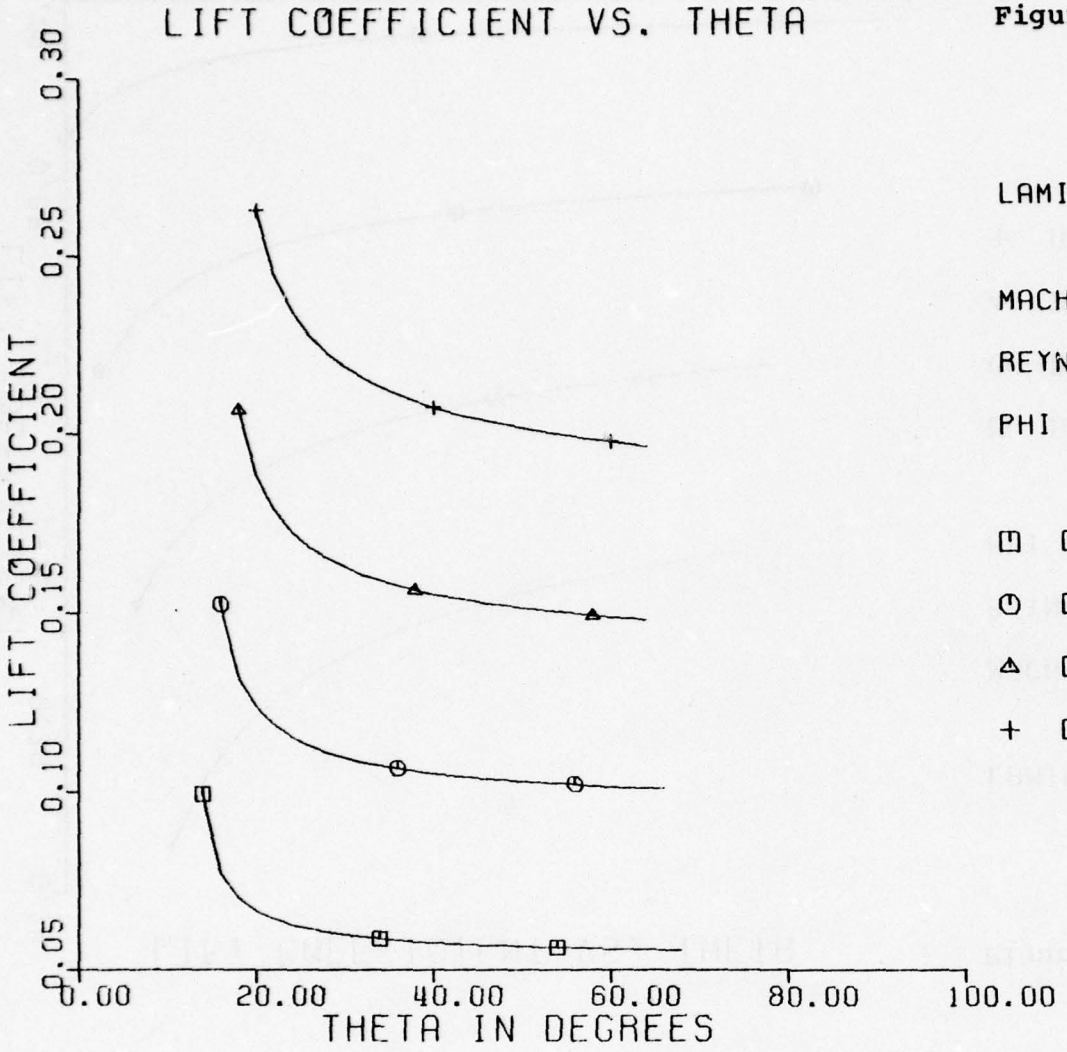

Figure 52.

LAMINAR BOUNDARY LAYER

MACH NUMBER = 3.10

REYNOLDS NO./10^5 =1.00

PHI IN DEGREES = 120.00

□ DELTA = 4 DEGREES

⊖ DELTA = 6 DEGREES

△ DELTA = 8 DEGREES

\+ DELTA = 10 DEGREES

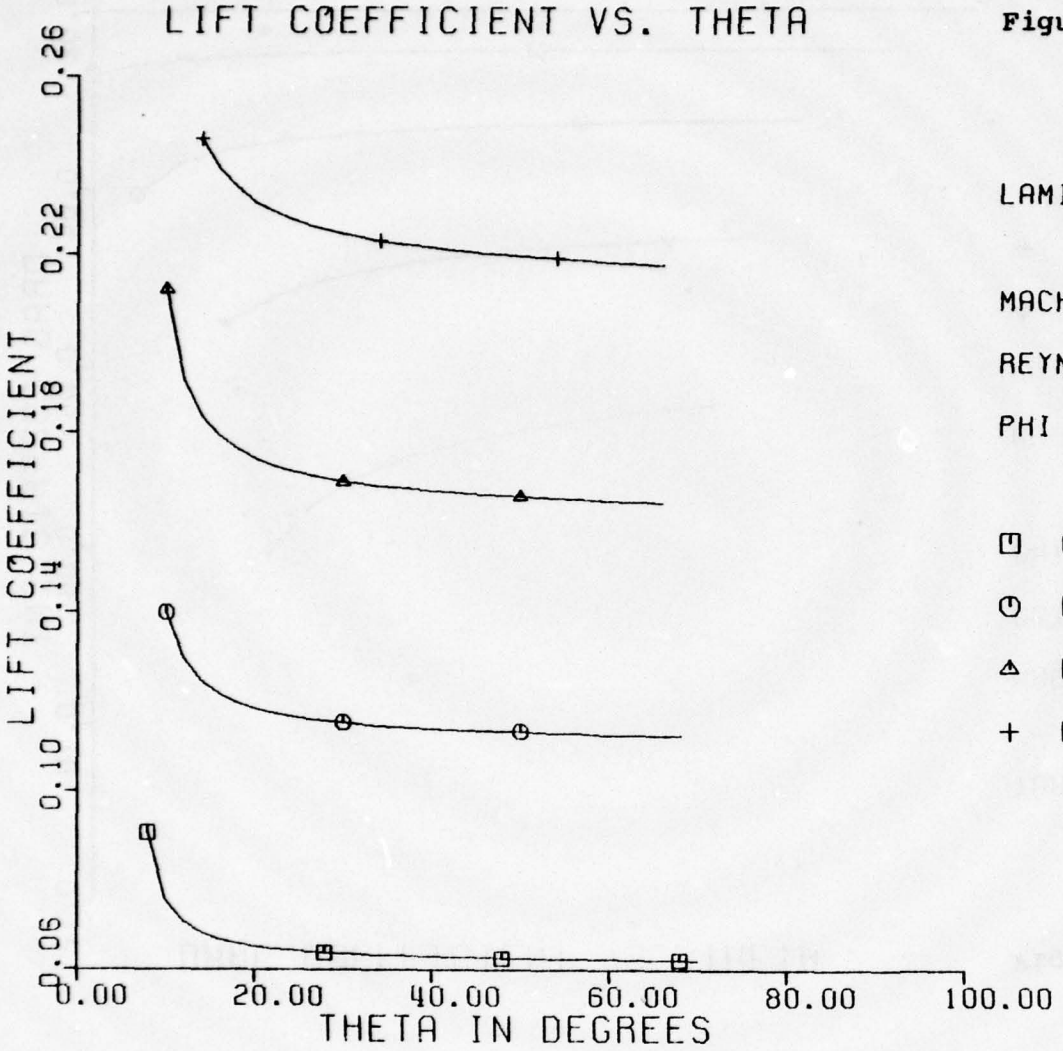

Figure 53.

LAMINAR BOUNDARY LAYER

MACH NUMBER = 3.10

REYNOLDS NO./10^5 =1.00

PHI IN DEGREES = 150.00

□ DELTA = 4 DEGREES

○ DELTA = 6 DEGREES

△ DELTA = 8 DEGREES

\+ DELTA = 10 DEGREES

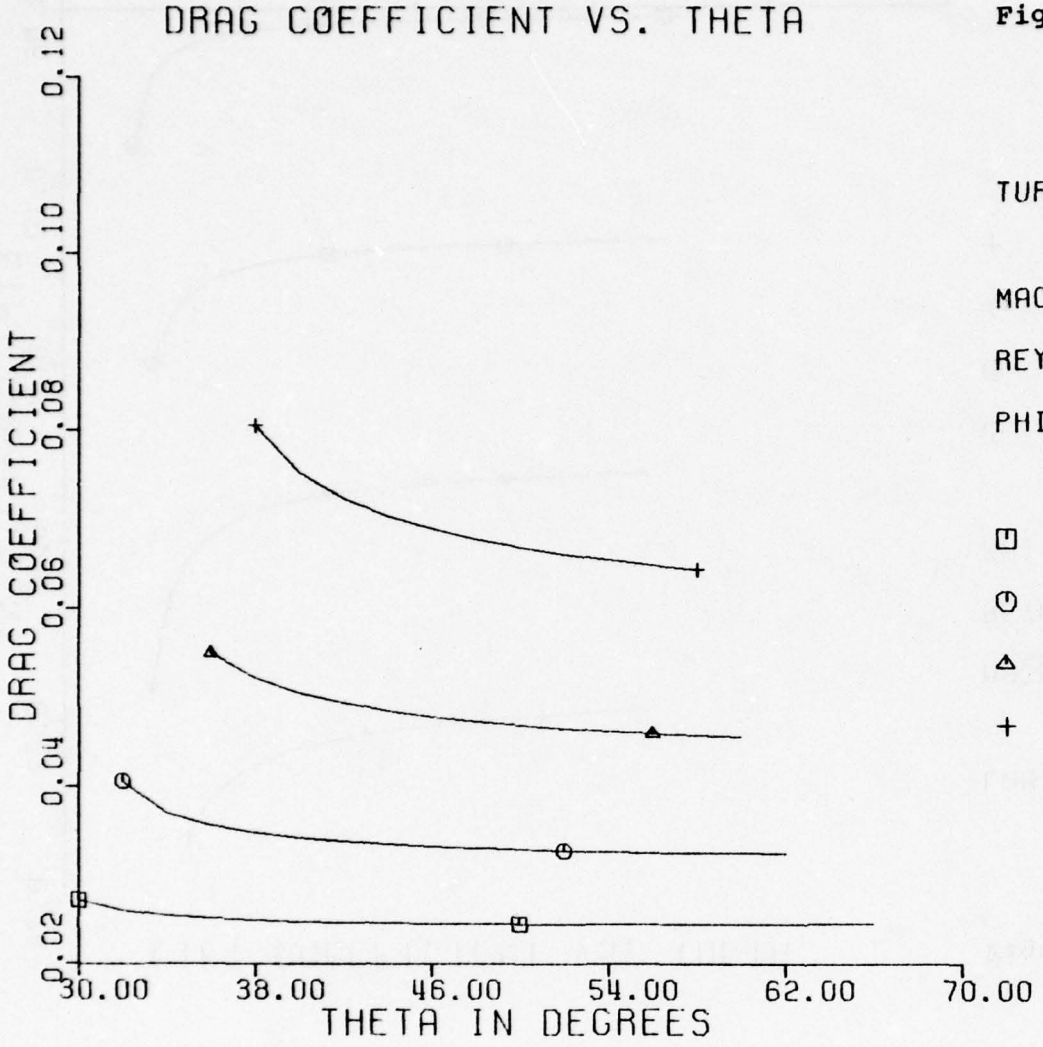

Figure 54.

TURBULENT BOUNDARY LAYER

MACH NUMBER = 2.00

REYNOLDS NO./10^5 =100.00

PHI IN DEGREES = 90.00

□ DELTA = 4 DEGREES

○ DELTA = 6 DEGREES

△ DELTA = 8 DEGREES

\+ DELTA = 10 DEGREES

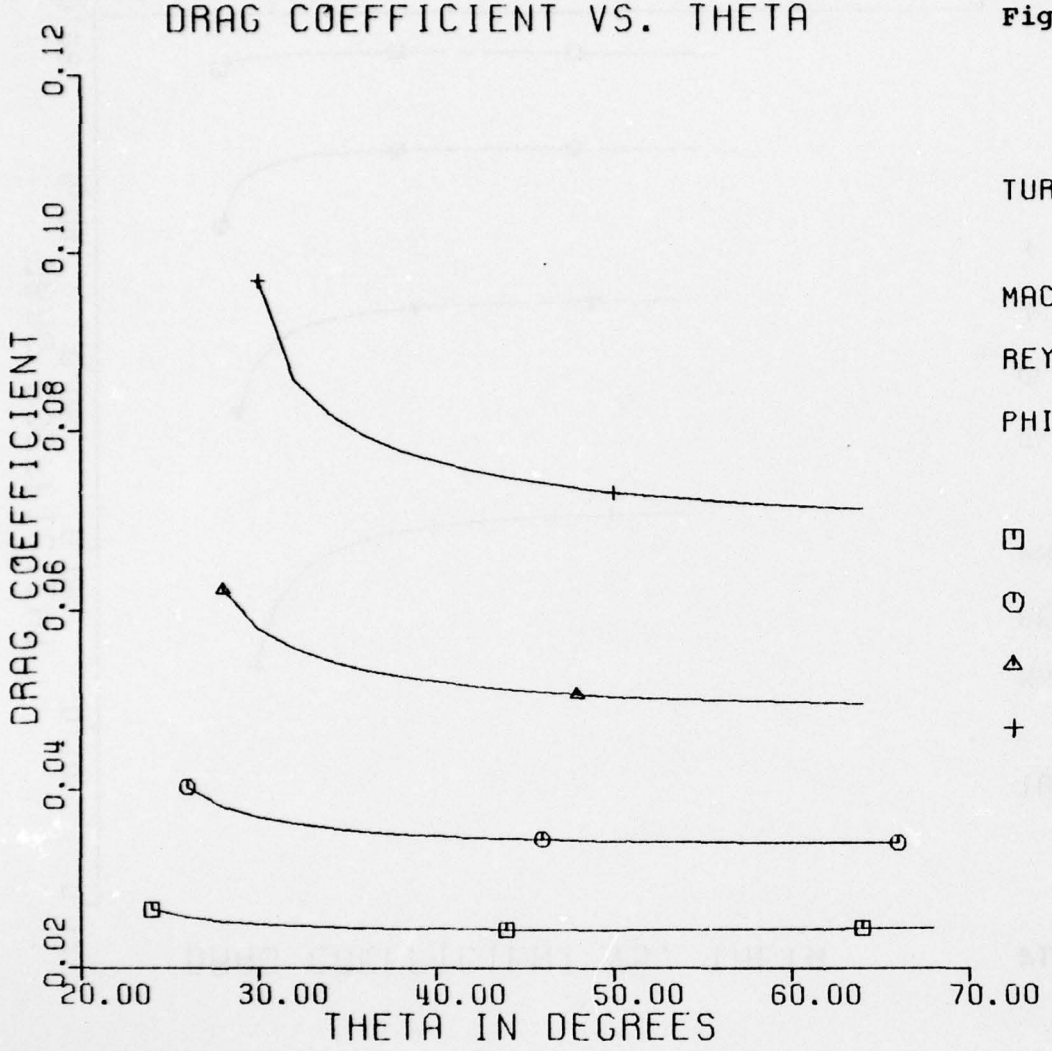

Figure 55.

TURBULENT BOUNDARY LAYER

MACH NUMBER = 2.00

REYNOLDS NO./10^5 =100.00

PHI IN DEGREES = 120.00

□ DELTA = 4 DEGREES

⊙ DELTA = 6 DEGREES

△ DELTA = 8 DEGREES

\+ DELTA = 10 DEGREES

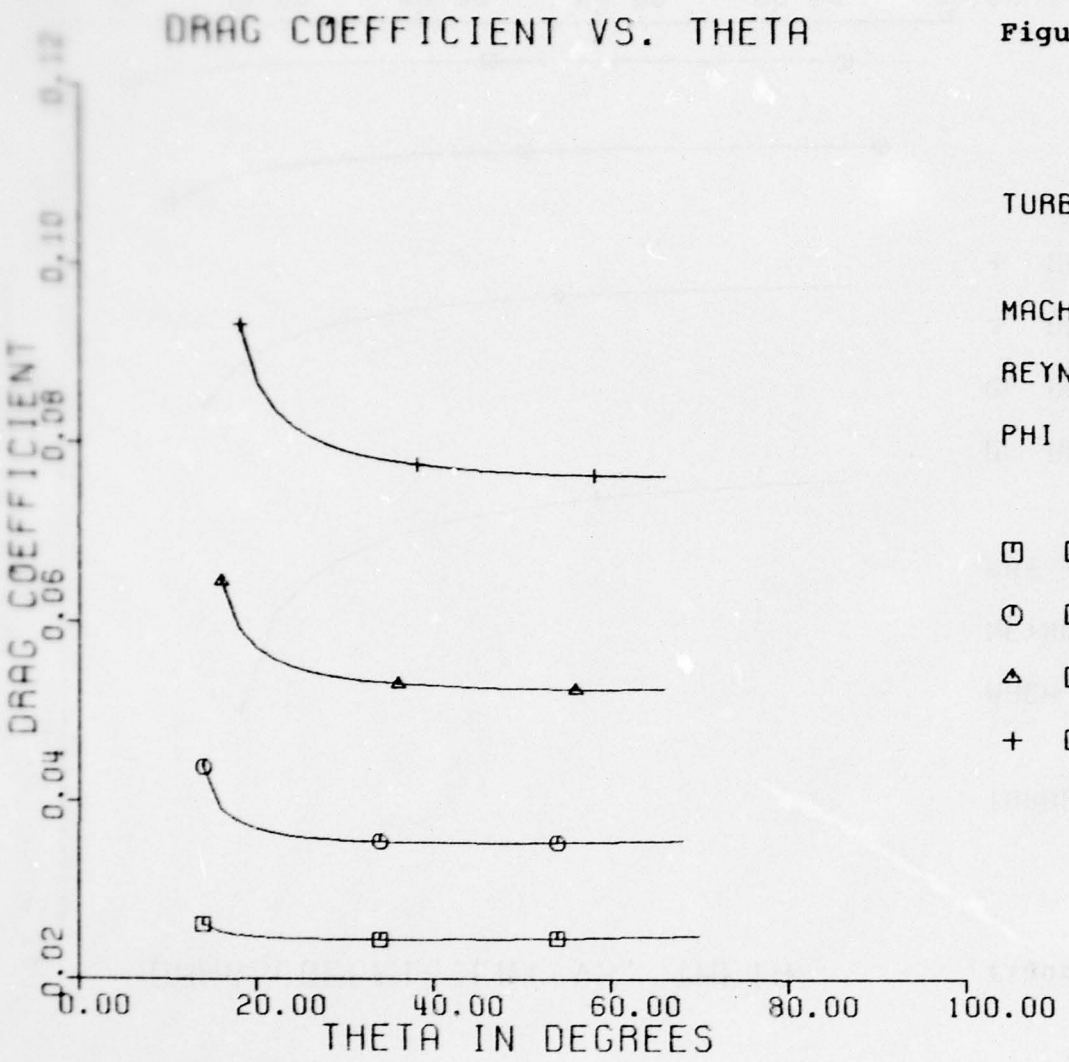

Figure 56.

TURBULENT BOUNDARY LAYER

MACH NUMBER = 2.00

REYNOLDS NO./10^5 =100.00

PHI IN DEGREES = 150.00

180

□ DELTA = 4 DEGREES

○ DELTA = 6 DEGREES

△ DELTA = 8 DEGREES

\+ DELTA = 10 DEGREES

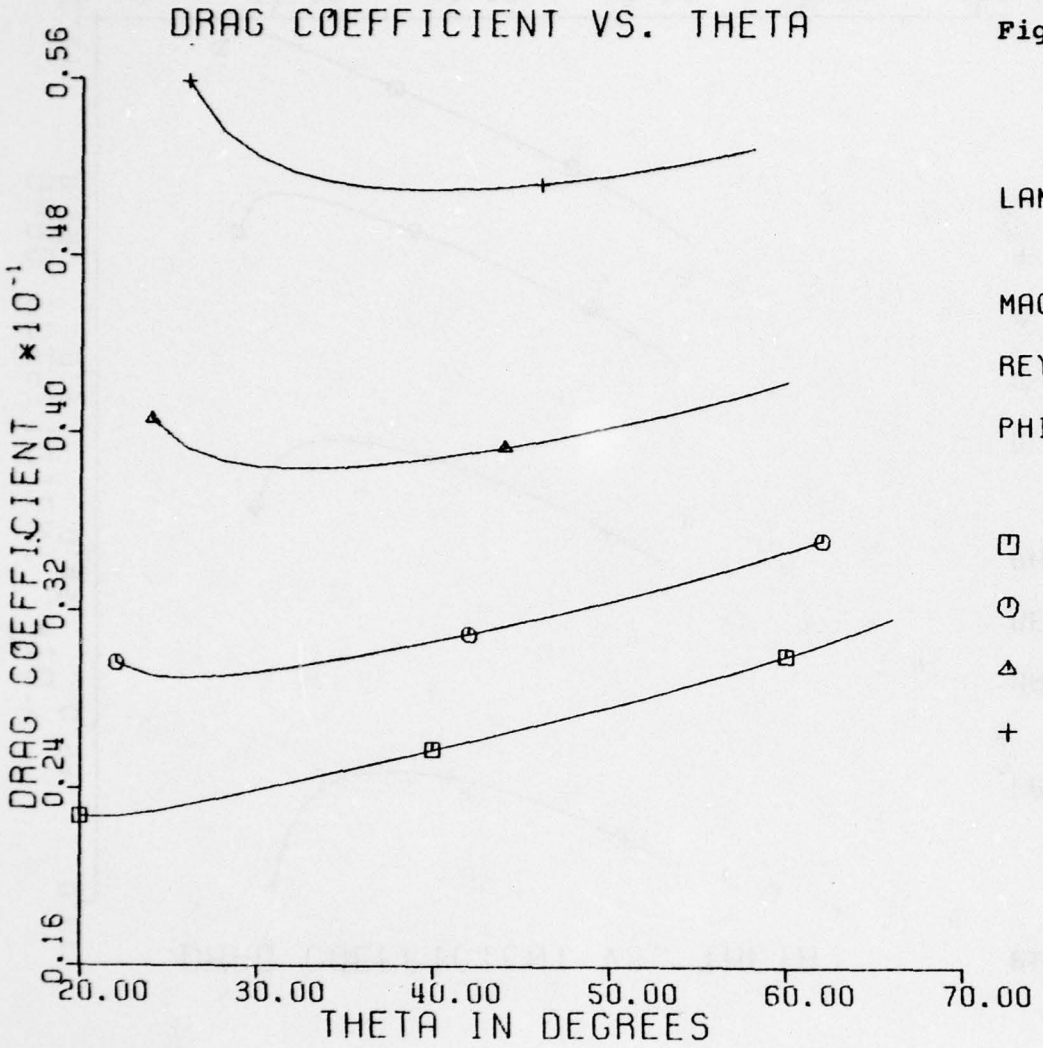

Figure 57.

LAMINAR BOUNDARY LAYER

MACH NUMBER = 3.10

REYNOLDS NO./10^5 =1.00

PHI IN DEGREES = 90.00

□ DELTA = 4 DEGREES

⊙ DELTA = 6 DEGREES

△ DELTA = 8 DEGREES

\+ DELTA = 10 DEGREES

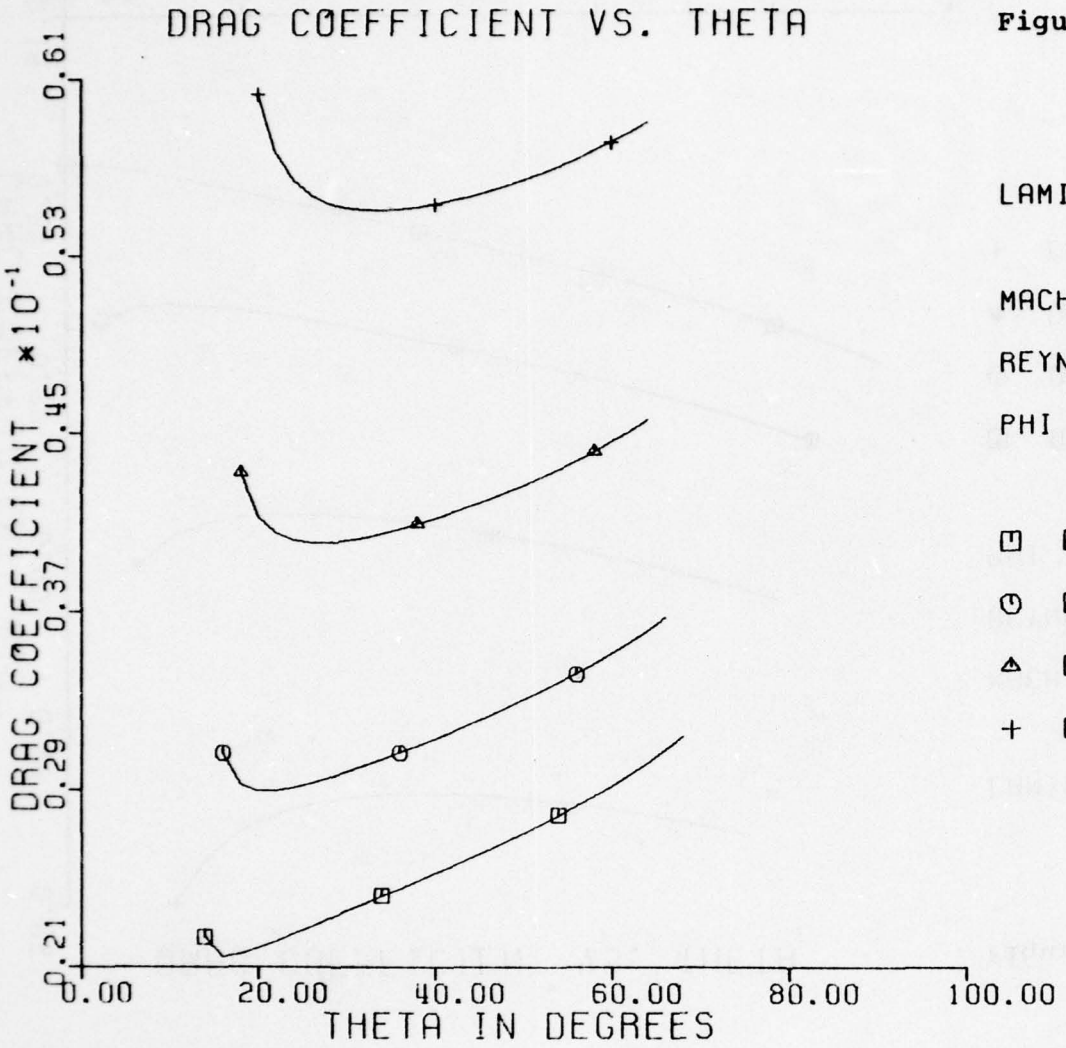

Figure 58.

LAMINAR BOUNDARY LAYER

MACH NUMBER = 3.10

REYNOLDS NO./10^5 =1.00

PHI IN DEGREES = 120.00

□ DELTA = 4 DEGREES

⊙ DELTA = 6 DEGREES

△ DELTA = 8 DEGREES

\+ DELTA = 10 DEGREES

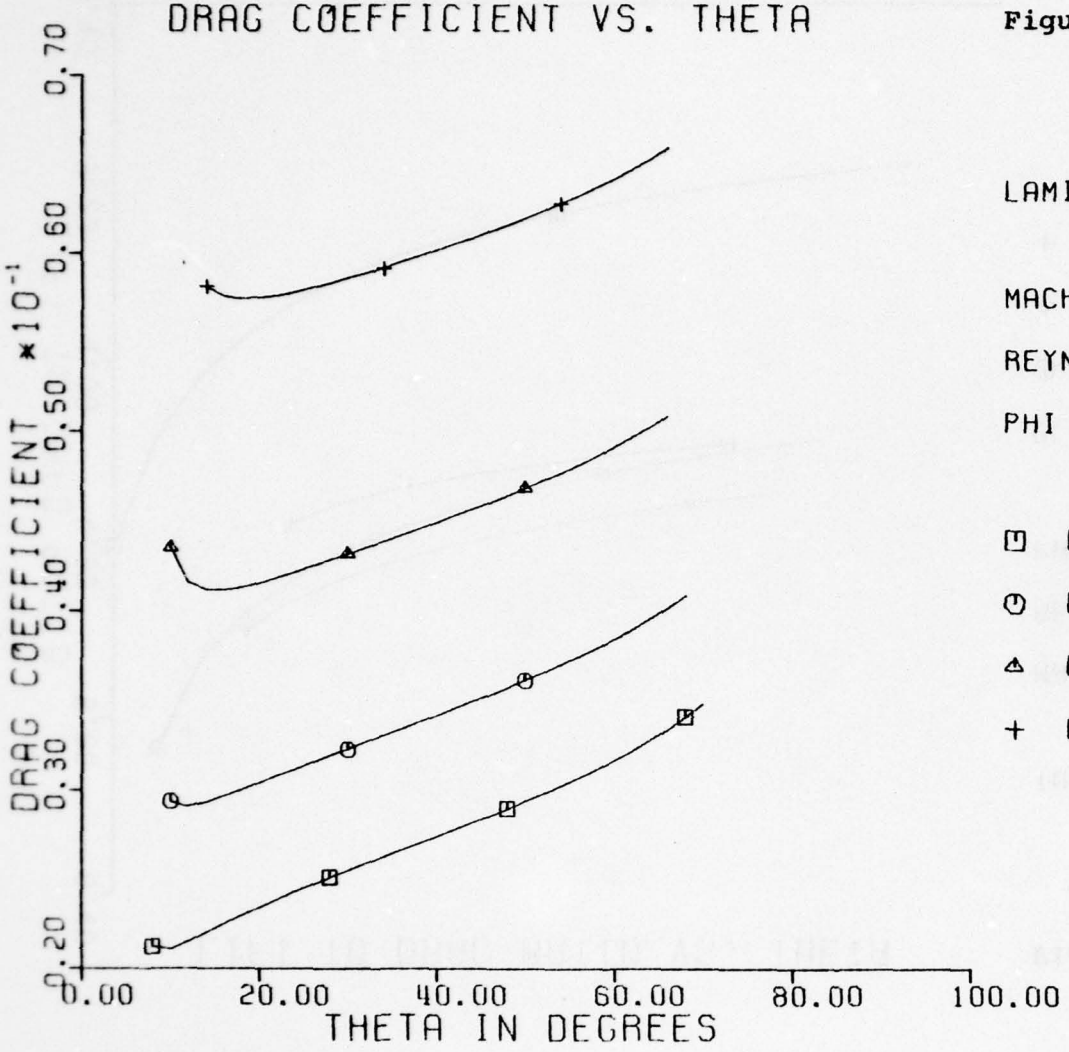

Figure 59.

LAMINAR BOUNDARY LAYER

MACH NUMBER = 3.10

REYNOLDS NO./10^5 =1.00

PHI IN DEGREES = 150.00

□ DELTA = 4 DEGREES

○ DELTA = 6 DEGREES

△ DELTA = 8 DEGREES

\+ DELTA = 10 DEGREES

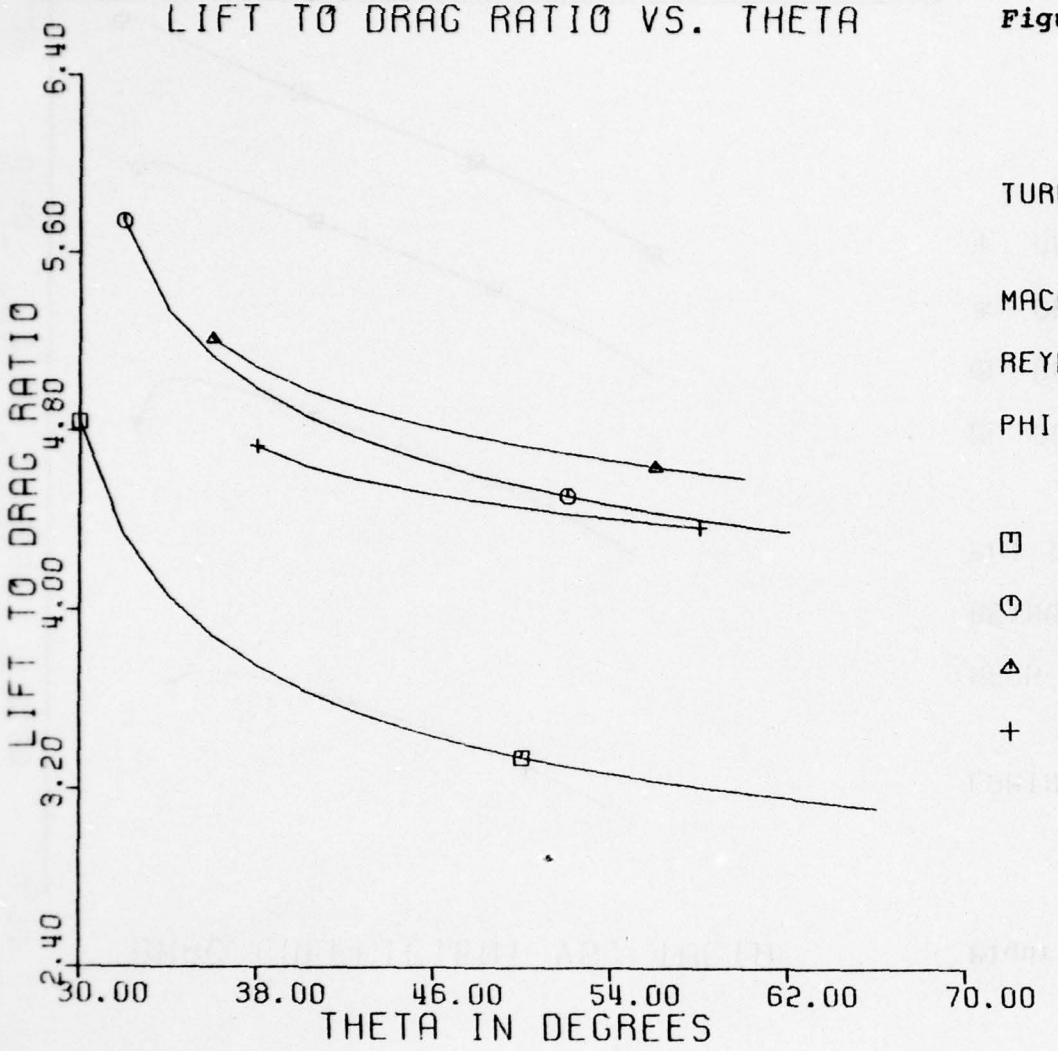

Figure 60.

TURBULENT BOUNDARY LAYER

MACH NUMBER = 2.00

REYNOLDS NO./10^5 =100.00

PHI IN DEGREES = 90.00

□ DELTA = 4 DEGREES

⊙ DELTA = 6 DEGREES

△ DELTA = 8 DEGREES

\+ DELTA = 10 DEGREES

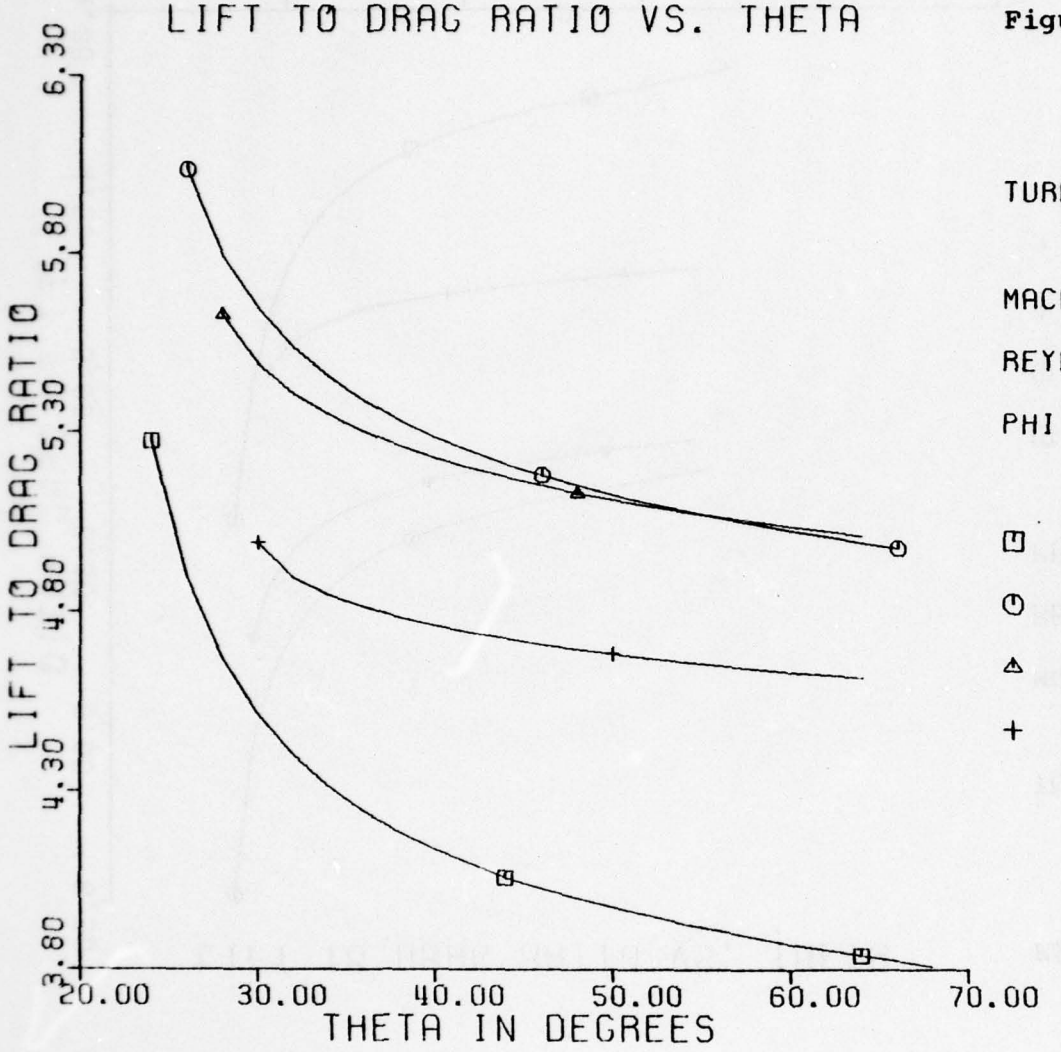

Figure 61.

TURBULENT BOUNDARY LAYER

MACH NUMBER = 2.00

REYNOLDS NO./10^5 =100.00

PHI IN DEGREES = 120.00

□ DELTA = 4 DEGREES

○ DELTA = 6 DEGREES

△ DELTA = 8 DEGREES

\+ DELTA = 10 DEGREES

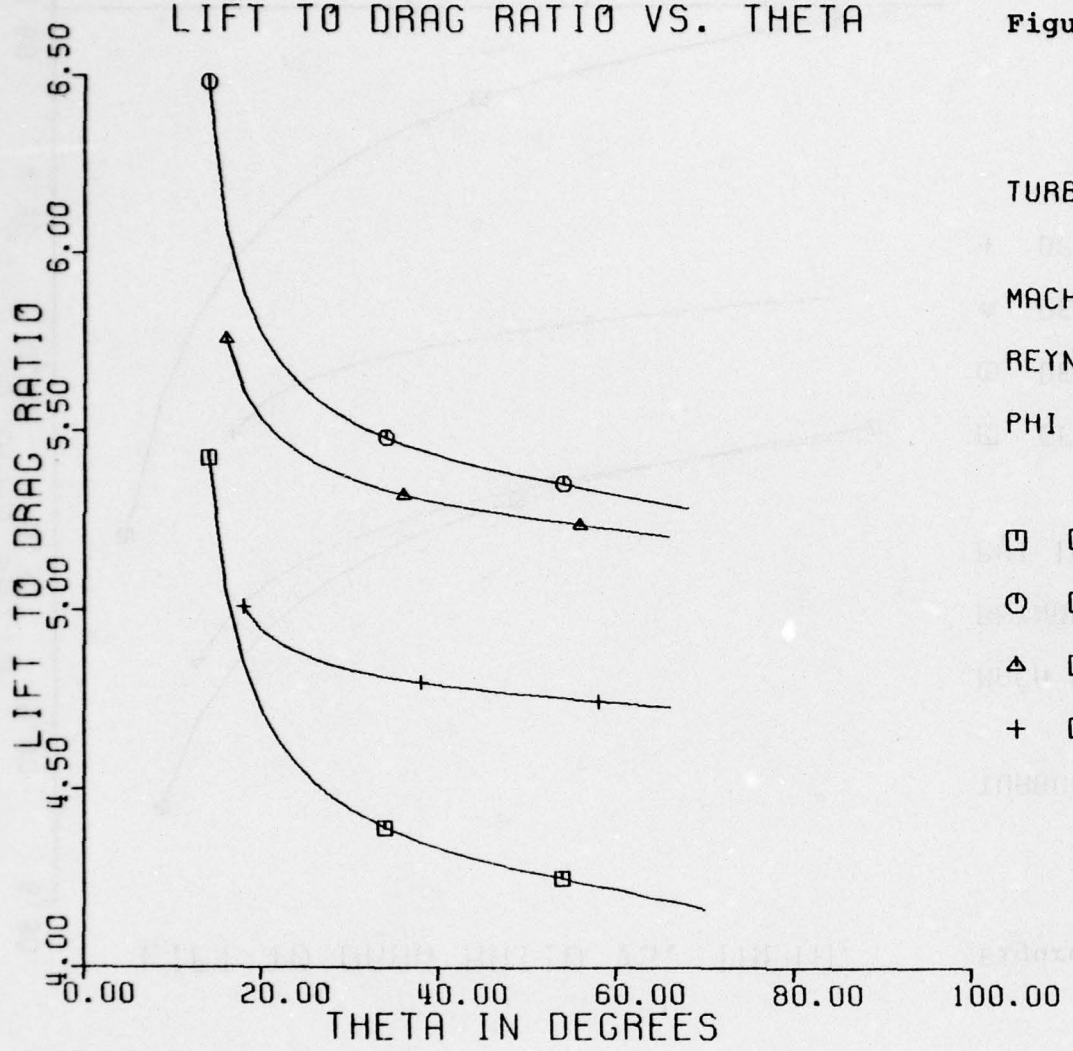

Figure 62.

TURBULENT BOUNDARY LAYER

MACH NUMBER = 2.00

REYNOLDS NO./10^5 =100.00

PHI IN DEGREES = 150.00

□ DELTA = 4 DEGREES

○ DELTA = 6 DEGREES

△ DELTA = 8 DEGREES

\+ DELTA = 10 DEGREES

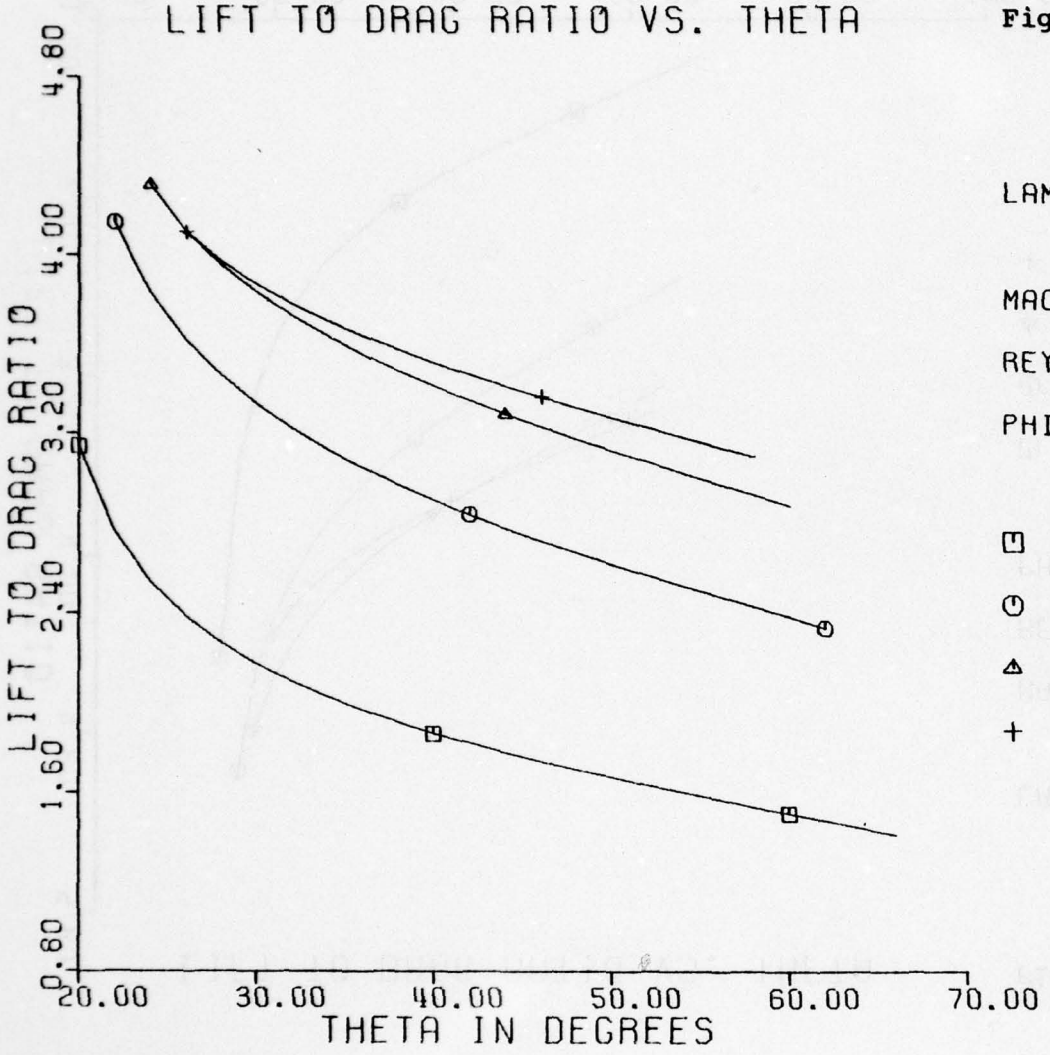

Figure 63.

LAMINAR BOUNDARY LAYER

MACH NUMBER = 3.10

REYNOLDS NO./10^5 =1.00

PHI IN DEGREES = 90.00

□ DELTA = 4 DEGREES

○ DELTA = 6 DEGREES

△ DELTA = 8 DEGREES

\+ DELTA = 10 DEGREES

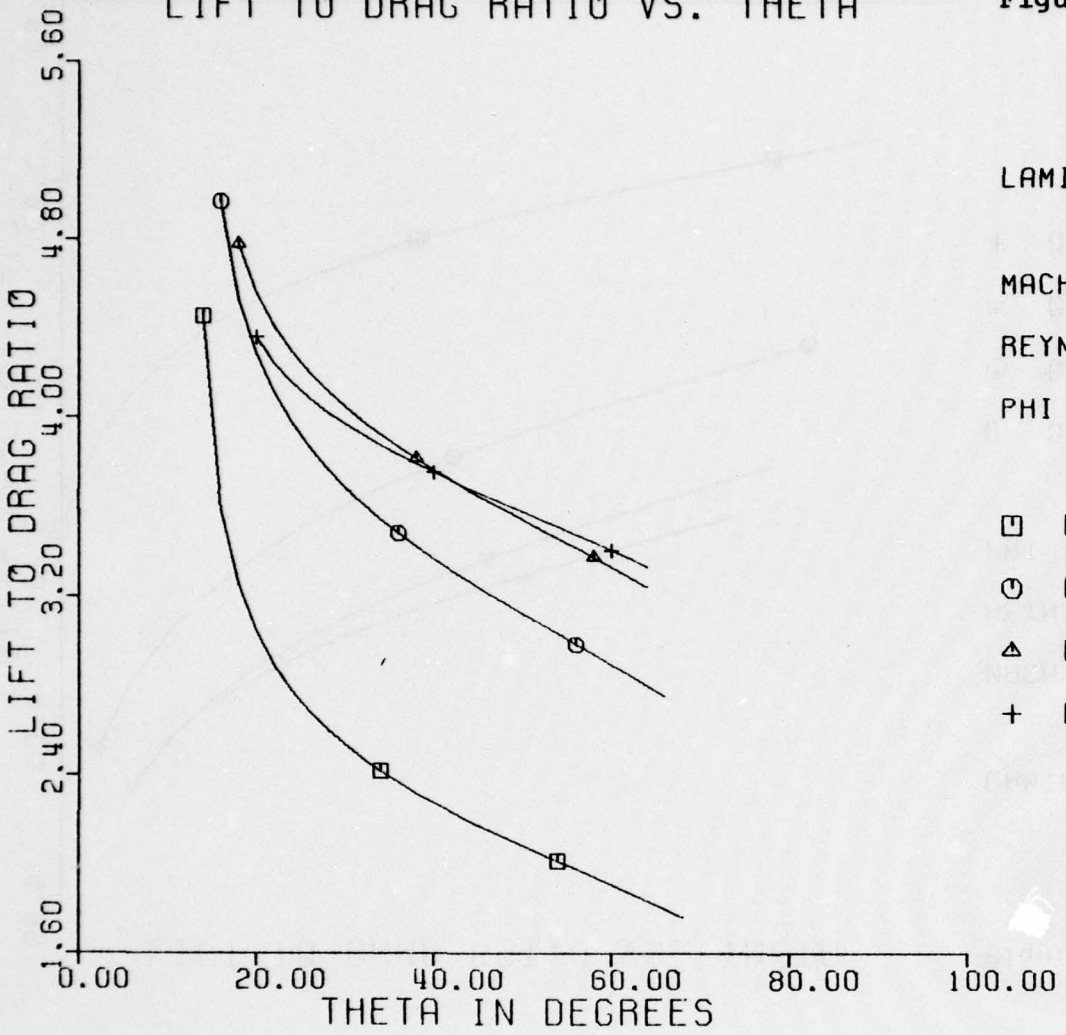

Figure 64.

LAMINAR BOUNDARY LAYER

MACH NUMBER = 3.10

REYNOLDS NO./10^5 =1.00

PHI IN DEGREES = 120.00

□ DELTA = 4 DEGREES

○ DELTA = 6 DEGREES

△ DELTA = 8 DEGREES

\+ DELTA = 10 DEGREES

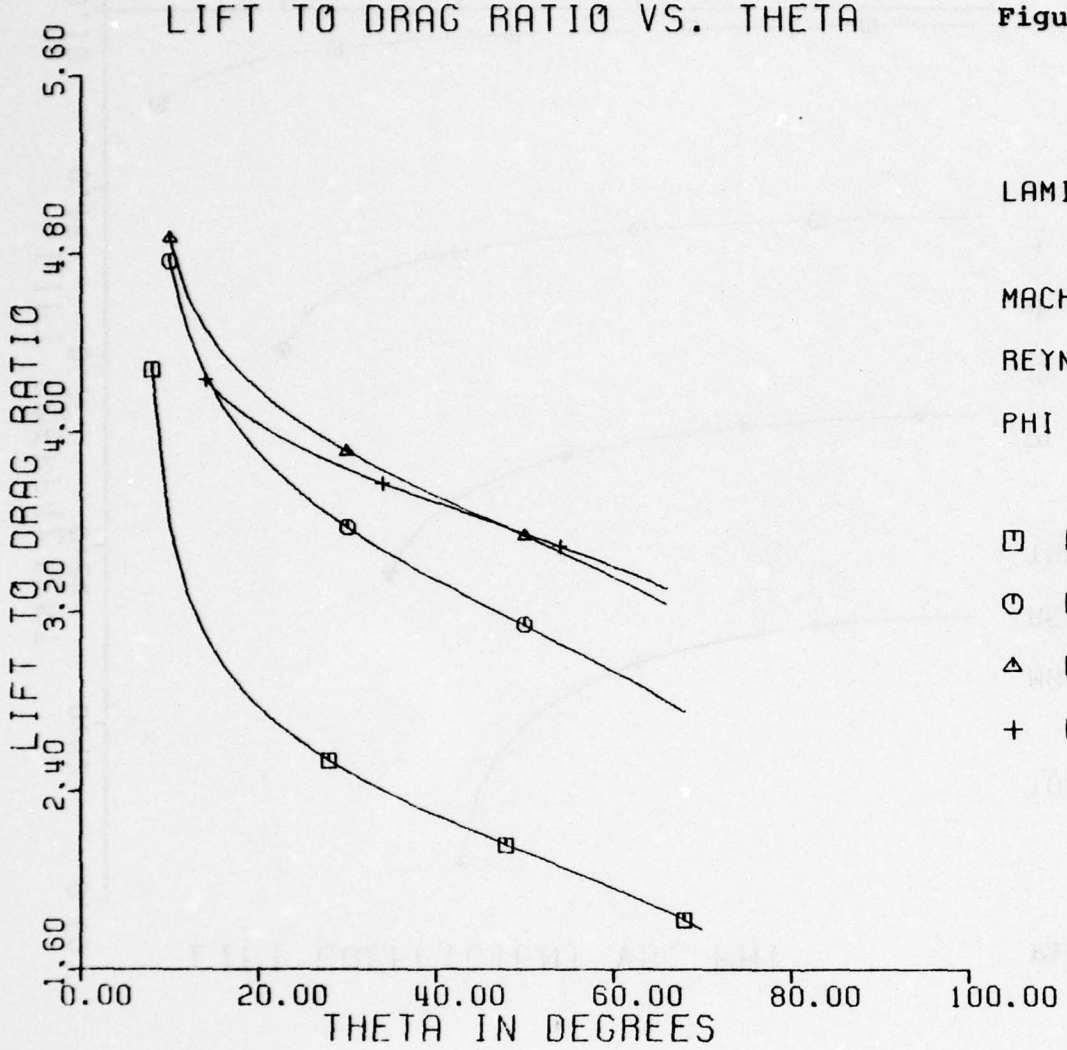

Figure 65.

LAMINAR BOUNDARY LAYER

MACH NUMBER = 3.10

REYNOLDS NO./10^5 =1.00

PHI IN DEGREES = 150.00

□ DELTA = 4 DEGREES

○ DELTA = 6 DEGREES

△ DELTA = 8 DEGREES

\+ DELTA = 10 DEGREES

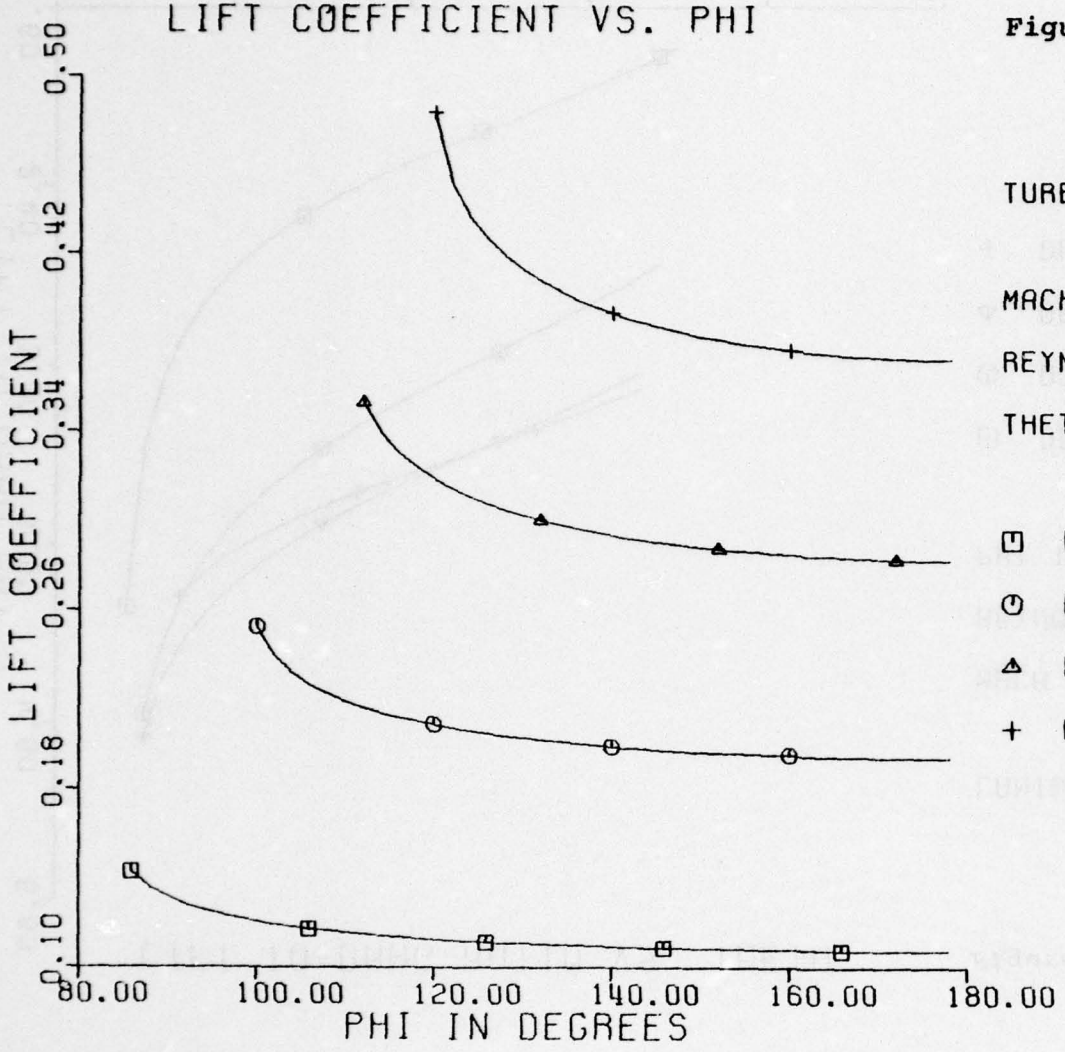
LIFT COEFFICIENT VS. PHI
LIFT COEFFICIENT
0.10
0.18
0.26
0.34
0.42
0.50
80.00
100.00
120.00
140.00
160.00
180.00
PHI IN DEGREES
TURBULENT BOUNDARY LAYER
MACH NUMBER = 2.00
REYNOLDS NO./10^5 =100.00
THETA IN DEGREES = 30.00
DELTA = 4 DEGREES
DELTA = 6 DEGREES
DELTA = 8 DEGREES
DELTA = 10 DEGREES

Figure 66.

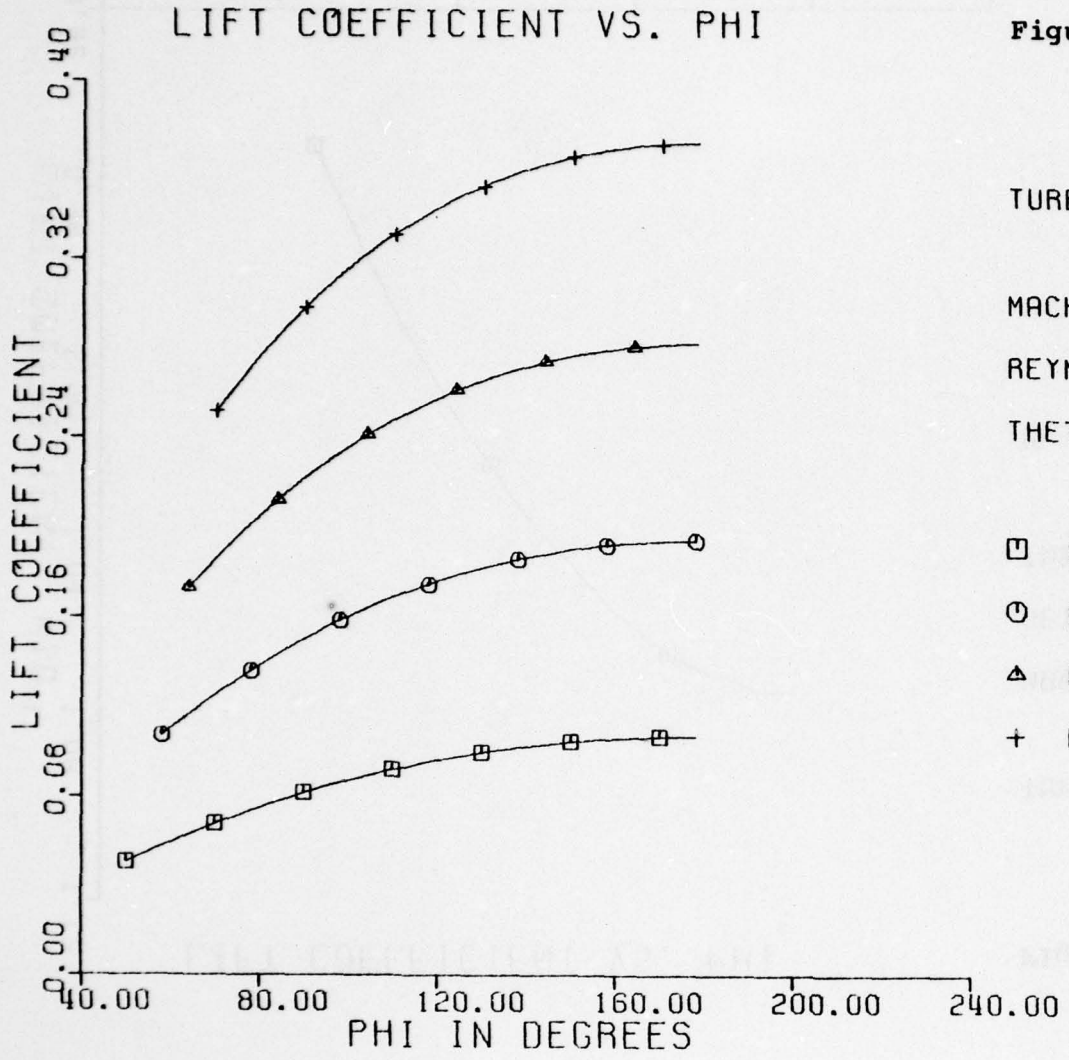

Figure 67.

TURBULENT BOUNDARY LAYER

MACH NUMBER = 2.00

REYNOLDS NO./10^5 =100.00

THETA IN DEGREES = 50.00

□ DELTA = 4 DEGREES

○ DELTA = 6 DEGREES

△ DELTA = 8 DEGREES

\+ DELTA = 10 DEGREES

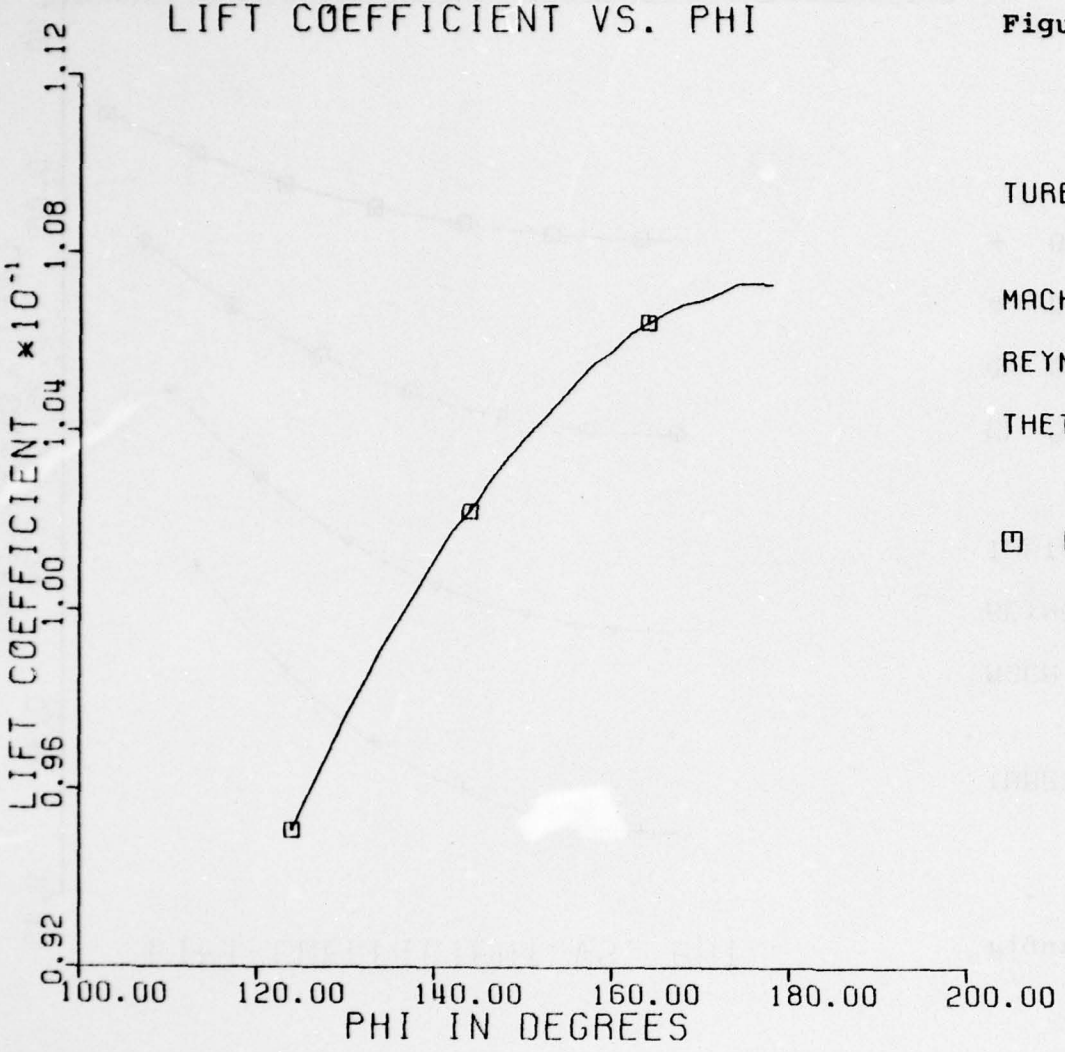

Figure 68.

TURBULENT BOUNDARY LAYER

MACH NUMBER = 2.00

REYNOLDS NO./10^5 =100.00

THETA IN DEGREES = 70.00

[1] DELTA = 4 DEGREES

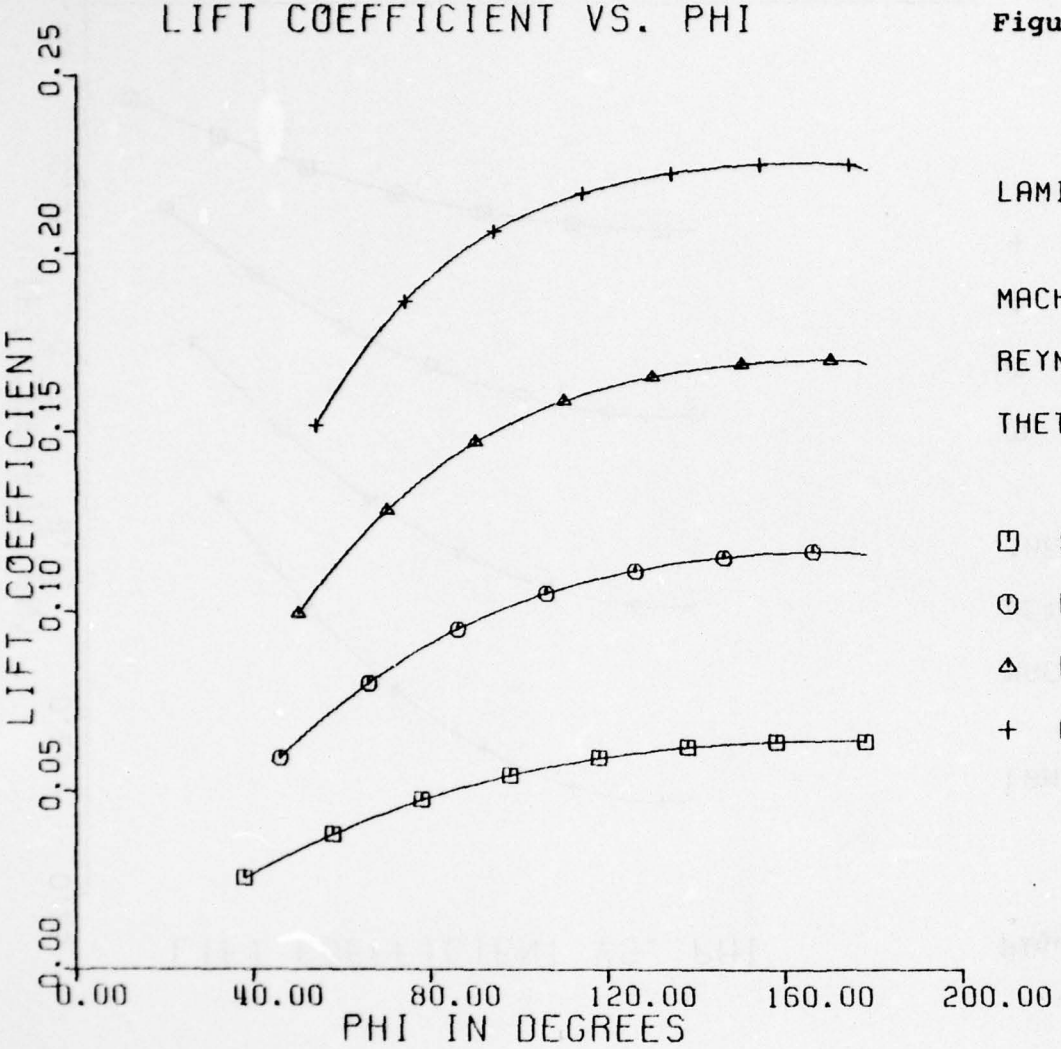

Figure 69.

LAMINAR BOUNDARY LAYER

MACH NUMBER = 3.10

REYNOLDS NO./10^5 =1.00

THETA IN DEGREES = 30.00

□ DELTA = 4 DEGREES

○ DELTA = 6 DEGREES

△ DELTA = 8 DEGREES

\+ DELTA = 10 DEGREES

AD-A053 691 MASSACHUSETTS INST OF TECH CAMBRIDGE AEROPHYSICS LAB F/G 20/4
A STUDY OF THE LIFT-TO-DRAG RATIO CAPABILITY OF CARET WING WAVE--ETC(U)
MAR 78 M D SOLOMON F44620-76-C-0049
UNCLASSIFIED TR-200 AFOSR-TR-78-0758 NL

3 OF 3
AD
A053691

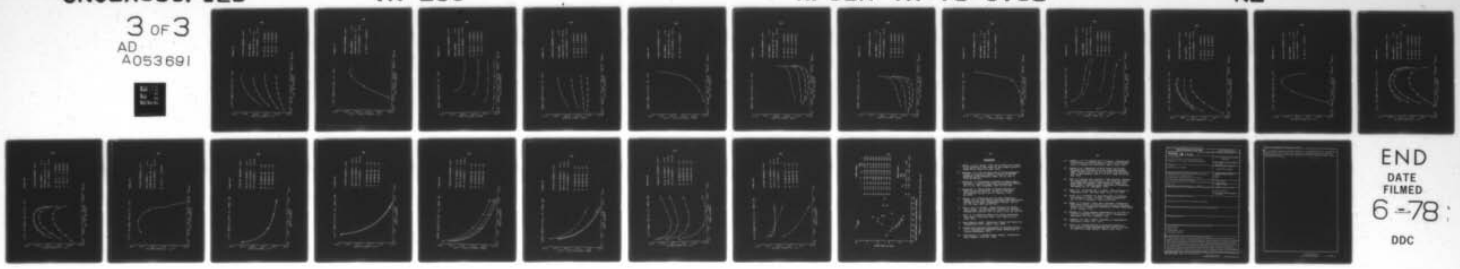

END
DATE
FILMED
6-78
DDC

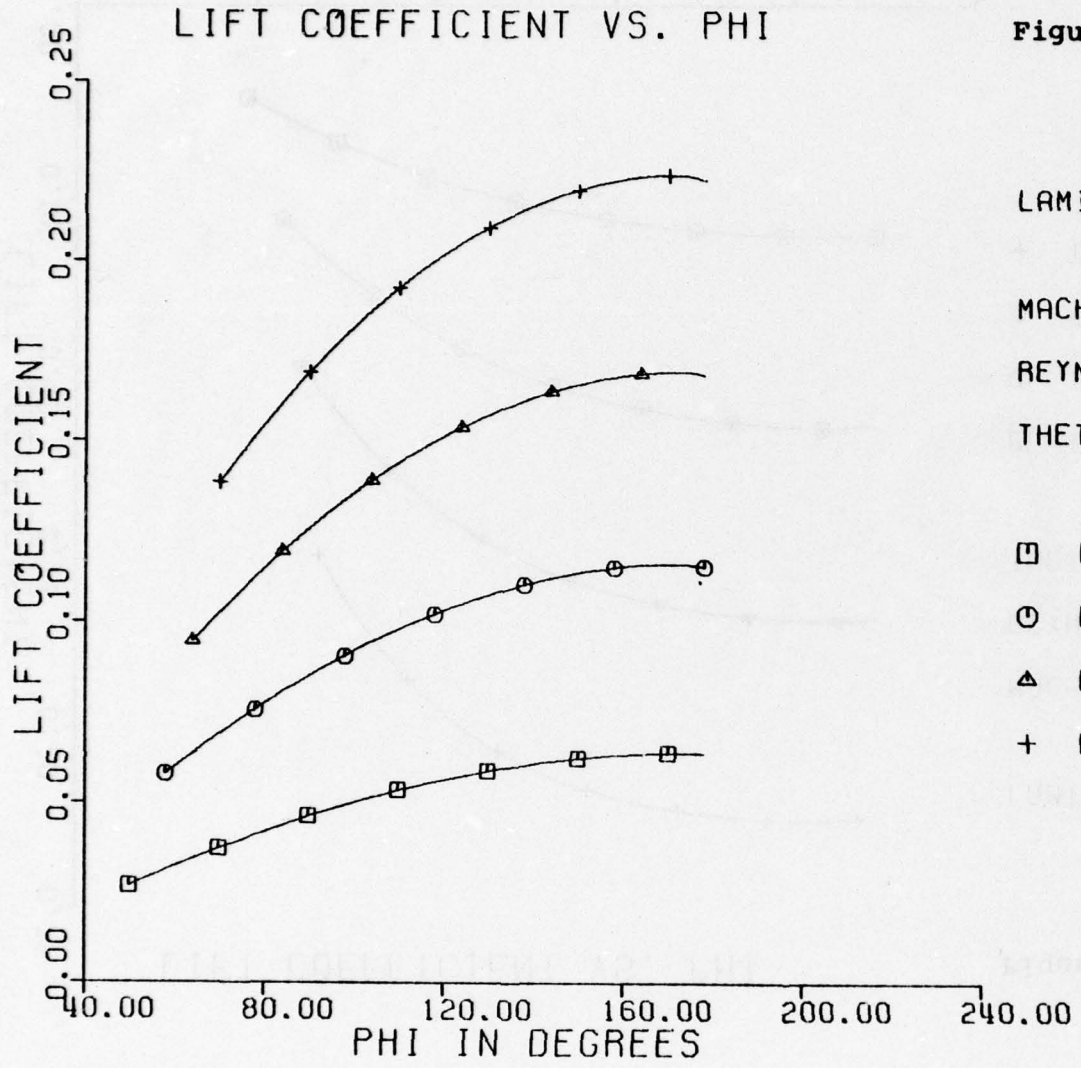

Figure 70.

LAMINAR BOUNDARY LAYER

MACH NUMBER = 3.10

REYNOLDS NO./10^5 =1.00

THETA IN DEGREES = 50.00

□ DELTA = 4 DEGREES

⊙ DELTA = 6 DEGREES

△ DELTA = 8 DEGREES

\+ DELTA = 10 DEGREES

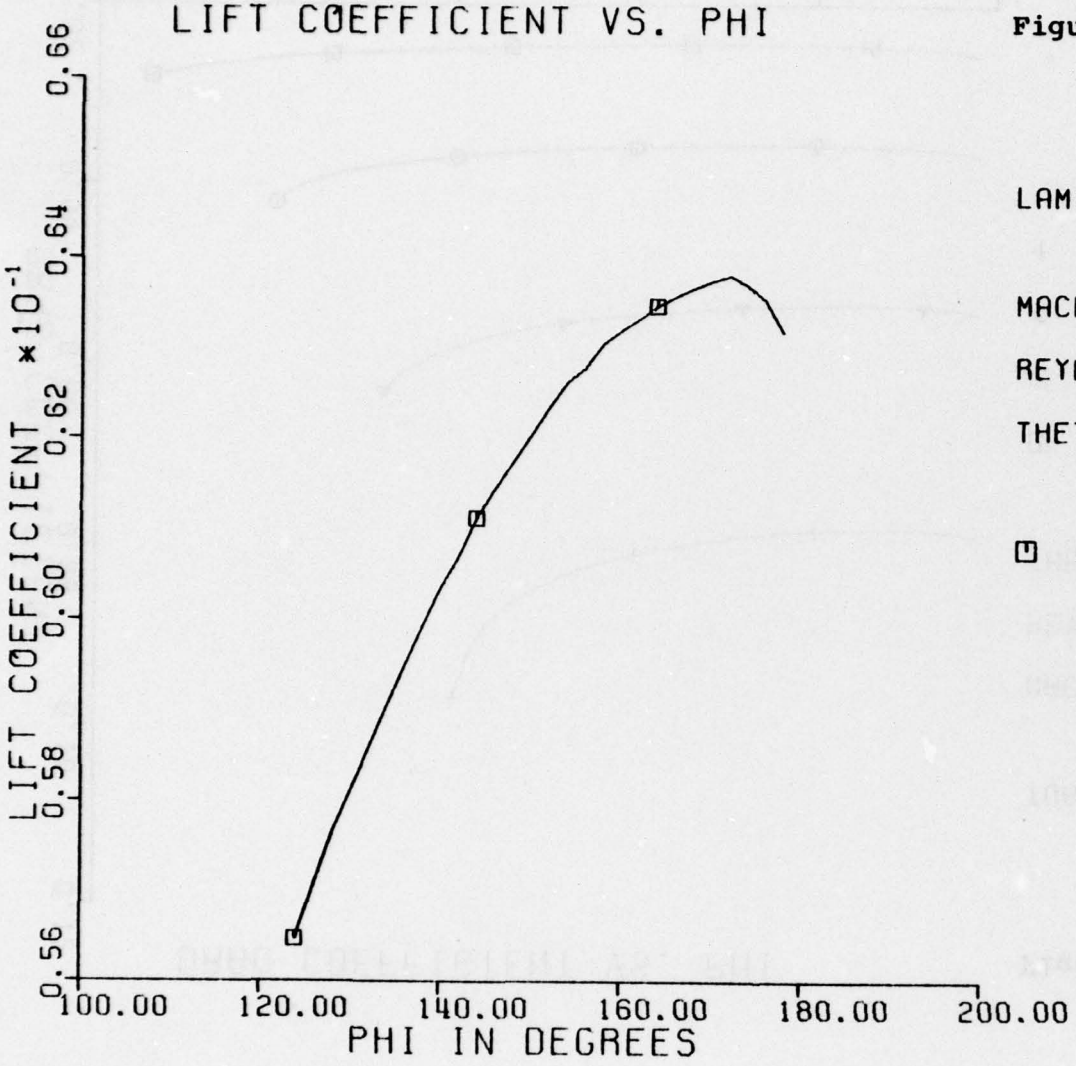

Figure 71.

LAMINAR BOUNDARY LAYER

MACH NUMBER = 3.10

REYNOLDS NO./10^5 =1.00

THETA IN DEGREES = 70.00

⊡ DELTA = 4 DEGREES

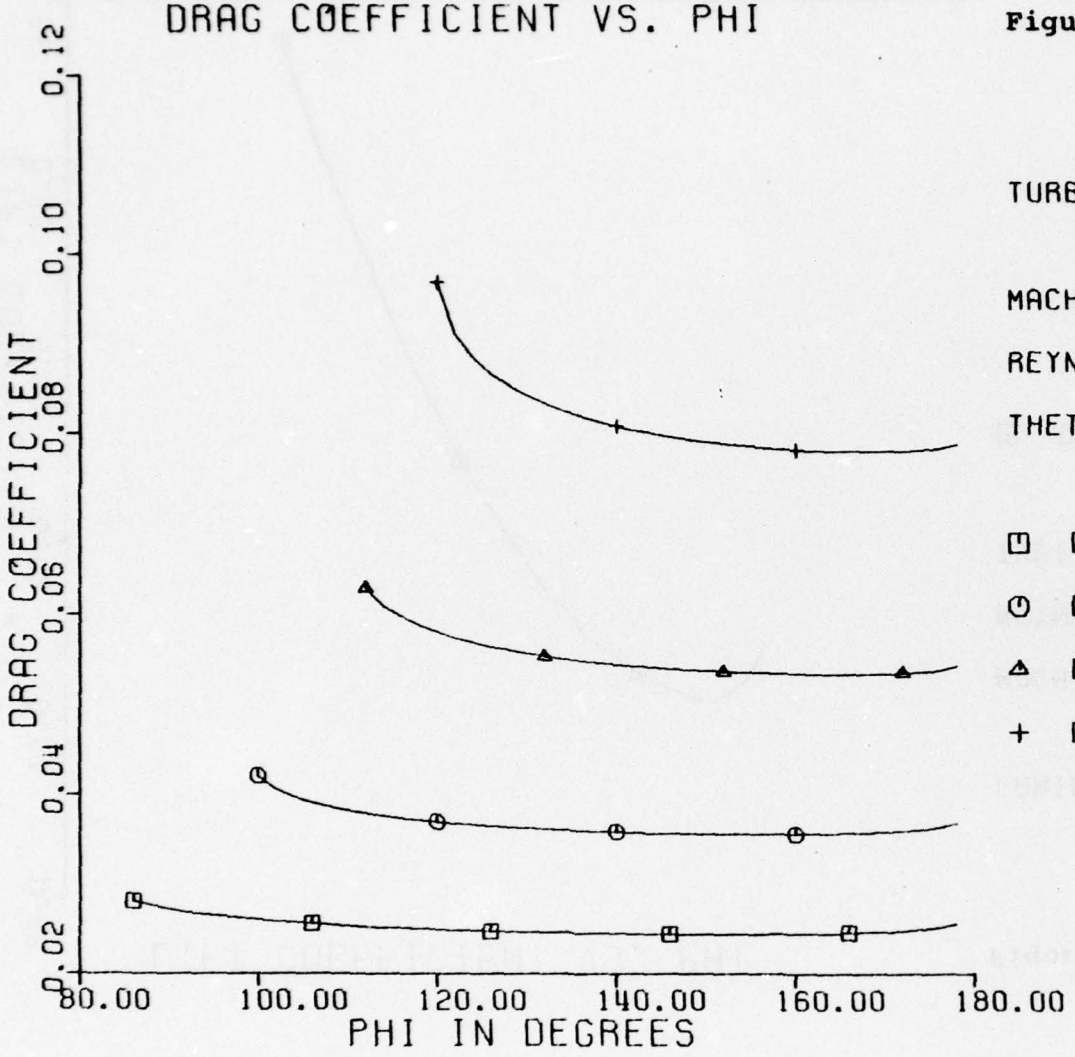
DRAG COEFFICIENT VS. PHI
DRAG COEFFICIENT
0.02
0.04
0.06
0.08
0.10
0.12
80.00
100.00
120.00
140.00
160.00
180.00
PHI IN DEGREES
TURBULENT BOUNDARY LAYER
MACH NUMBER = 2.00
REYNOLDS NO./10^5 =100.00
THETA IN DEGREES = 30.00
DELTA = 4 DEGREES
DELTA = 6 DEGREES
DELTA = 8 DEGREES
DELTA = 10 DEGREES

Figure 72.

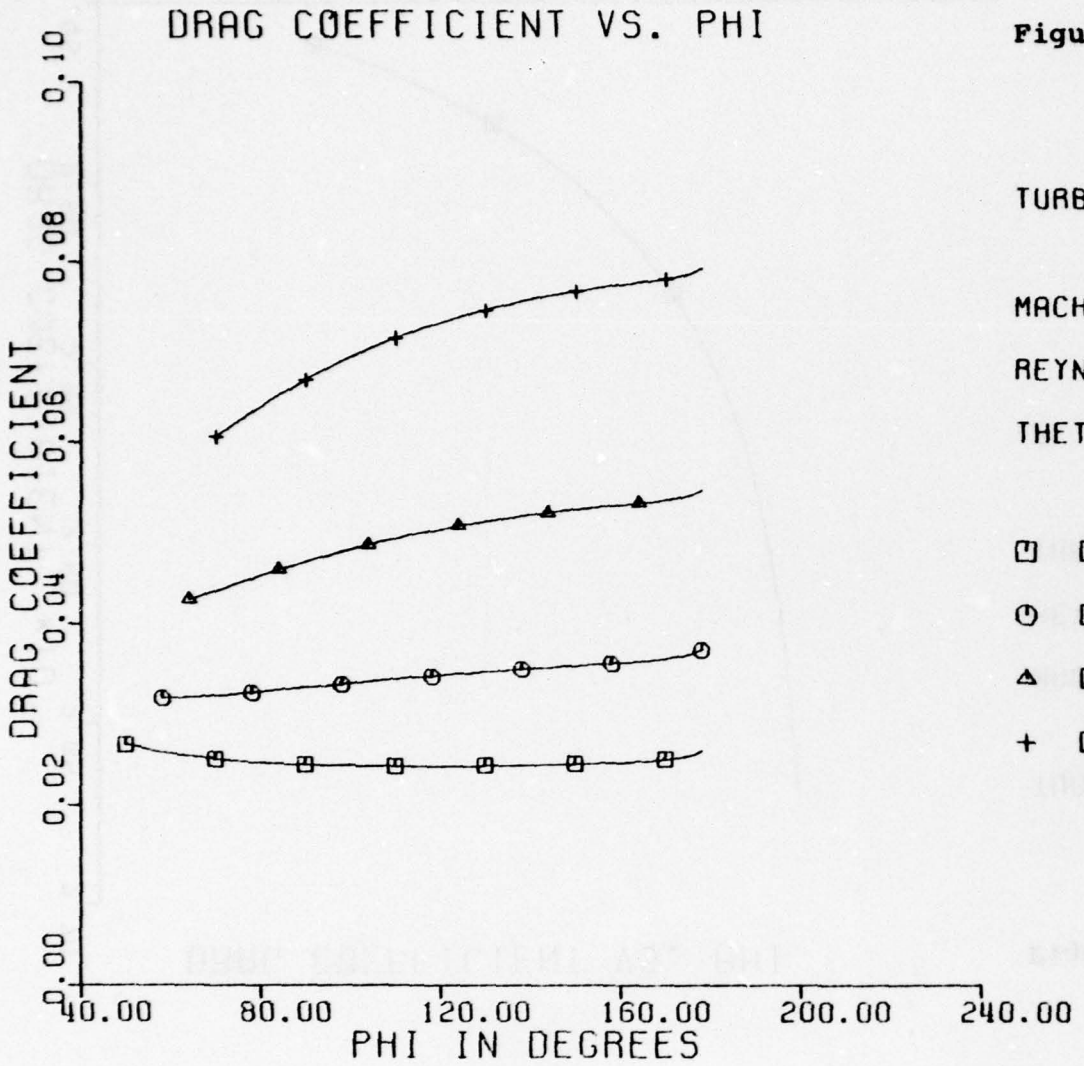

Figure 73.

TURBULENT BOUNDARY LAYER

MACH NUMBER = 2.00

REYNOLDS NO./10^5 =100.00

THETA IN DEGREES = 50.00

□ DELTA = 4 DEGREES

○ DELTA = 6 DEGREES

△ DELTA = 8 DEGREES

\+ DELTA = 10 DEGREES

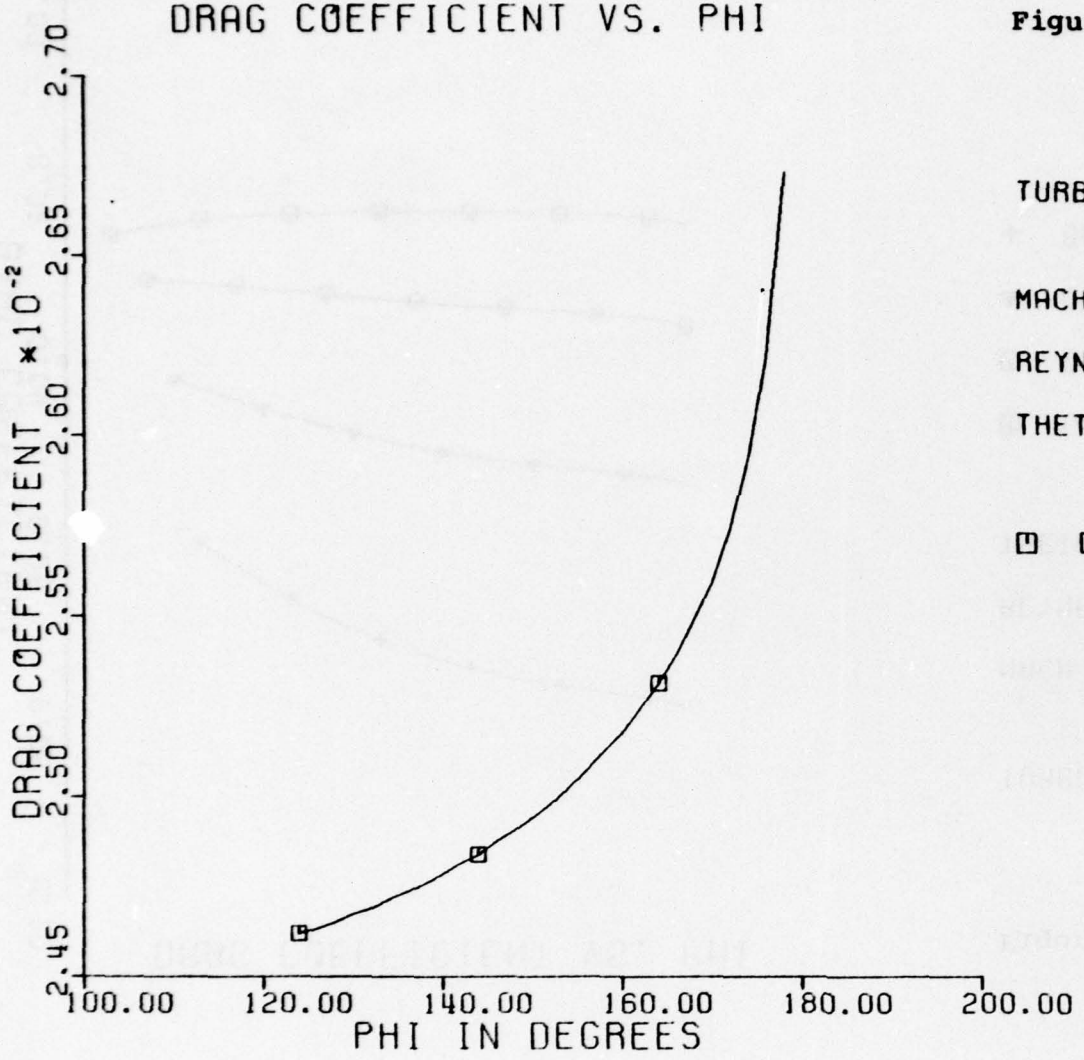

Figure 74.

TURBULENT BOUNDARY LAYER

MACH NUMBER = 2.00

REYNOLDS NO./10^5 =100.00

THETA IN DEGREES = 70.00

□ DELTA = 4 DEGREES

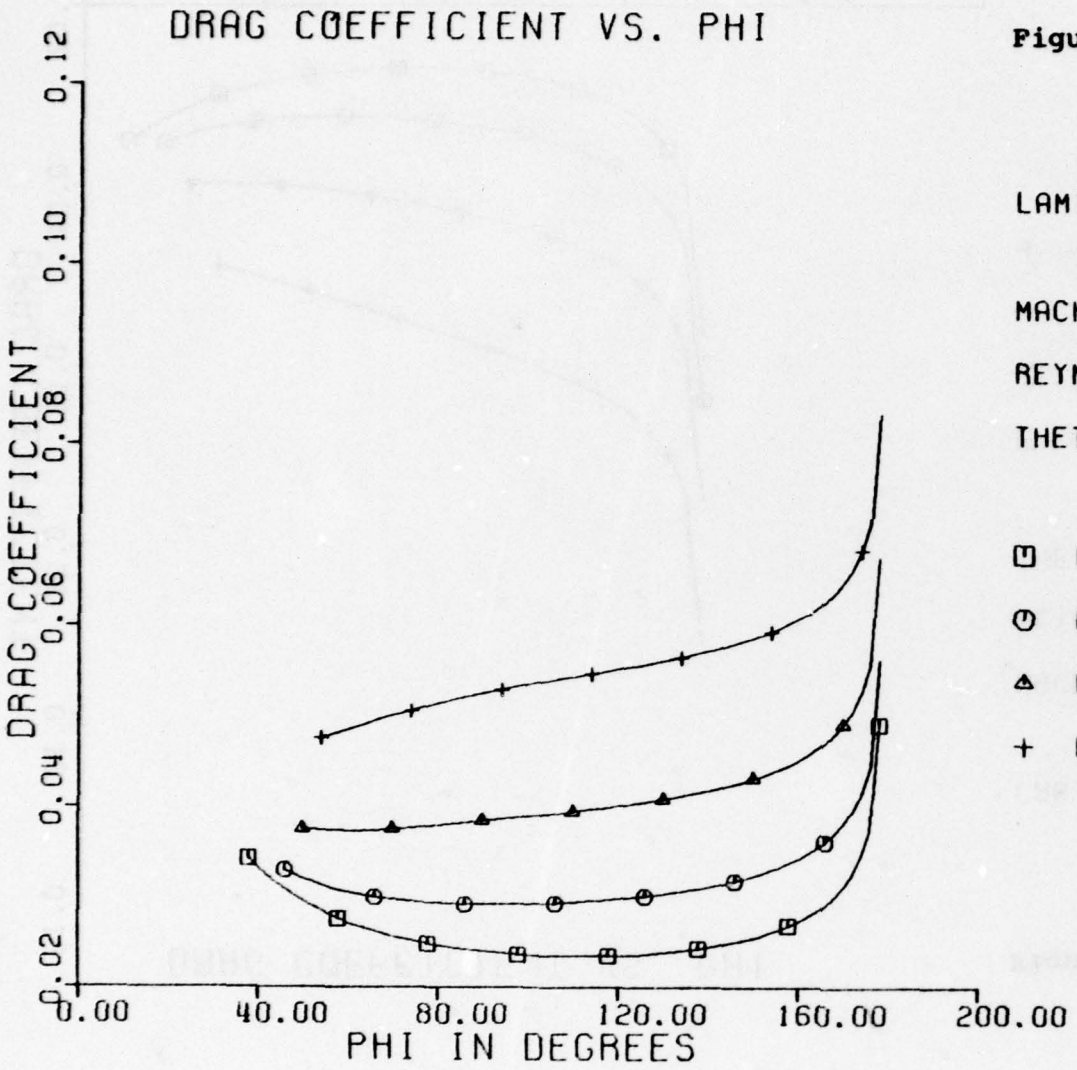

Figure 75.

LAMINAR BOUNDARY LAYER

MACH NUMBER = 3.10

REYNOLDS NO./10^5 =1.00

THETA IN DEGREES = 30.00

□ DELTA = 4 DEGREES

⊙ DELTA = 6 DEGREES

△ DELTA = 8 DEGREES

\+ DELTA = 10 DEGREES

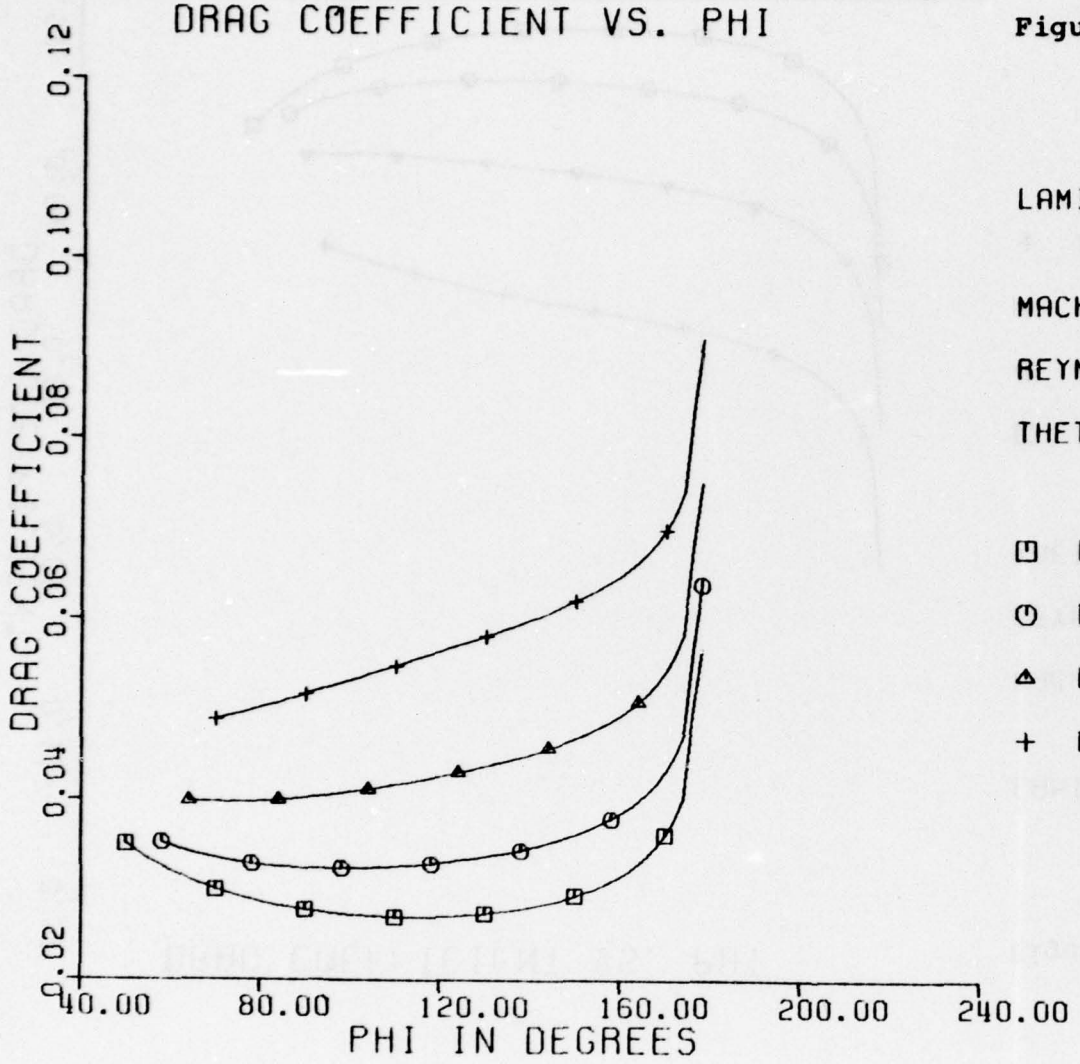

Figure 76.

LAMINAR BOUNDARY LAYER

MACH NUMBER = 3.10

REYNOLDS NO./10^5 =1.00

THETA IN DEGREES = 50.00

□ DELTA = 4 DEGREES

○ DELTA = 6 DEGREES

△ DELTA = 8 DEGREES

\+ DELTA = 10 DEGREES

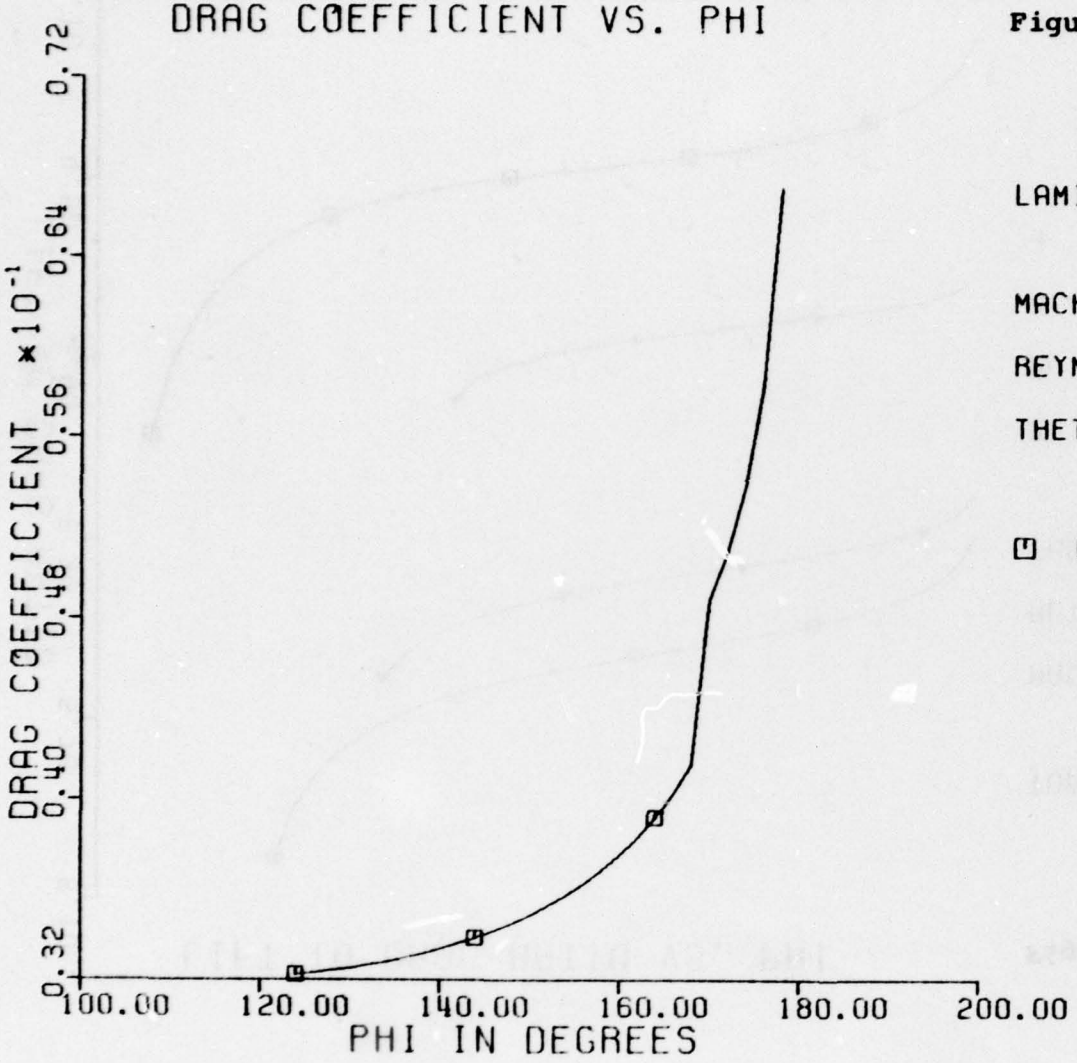

Figure 77.

LAMINAR BOUNDARY LAYER

MACH NUMBER = 3.10

REYNOLDS NO./10^5 =1.00

THETA IN DEGREES = 70.00

[1] DELTA = 4 DEGREES

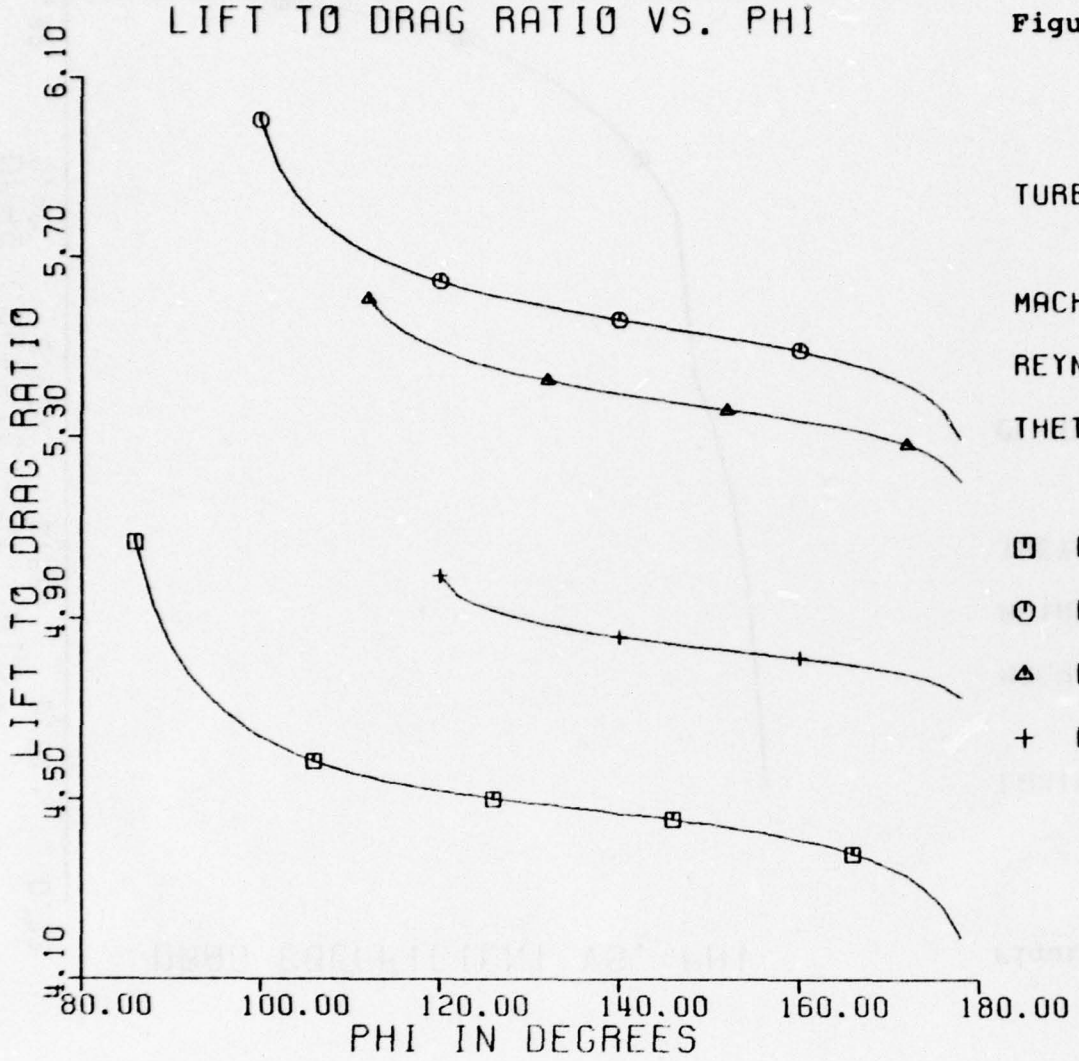

Figure 78.

TURBULENT BOUNDARY LAYER

MACH NUMBER = 2.00

REYNOLDS NO./10^5 =100.00

THETA IN DEGREES = 30.00

□ DELTA = 4 DEGREES

○ DELTA = 6 DEGREES

△ DELTA = 8 DEGREES

\+ DELTA = 10 DEGREES

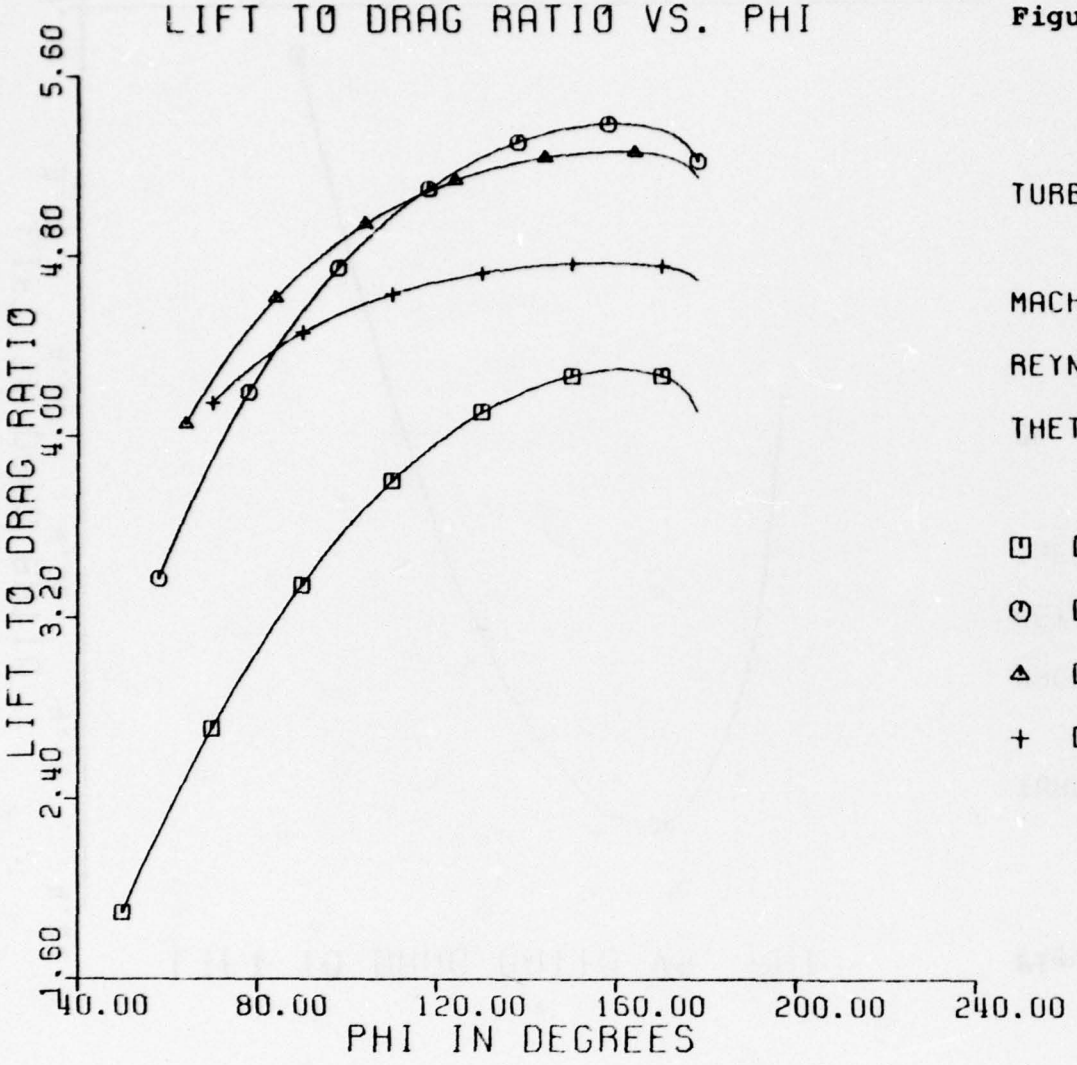

Figure 79.

TURBULENT BOUNDARY LAYER

MACH NUMBER = 2.00

REYNOLDS NO./10^5 =100.00

THETA IN DEGREES = 50.00

□ DELTA = 4 DEGREES

○ DELTA = 6 DEGREES

△ DELTA = 8 DEGREES

\+ DELTA = 10 DEGREES

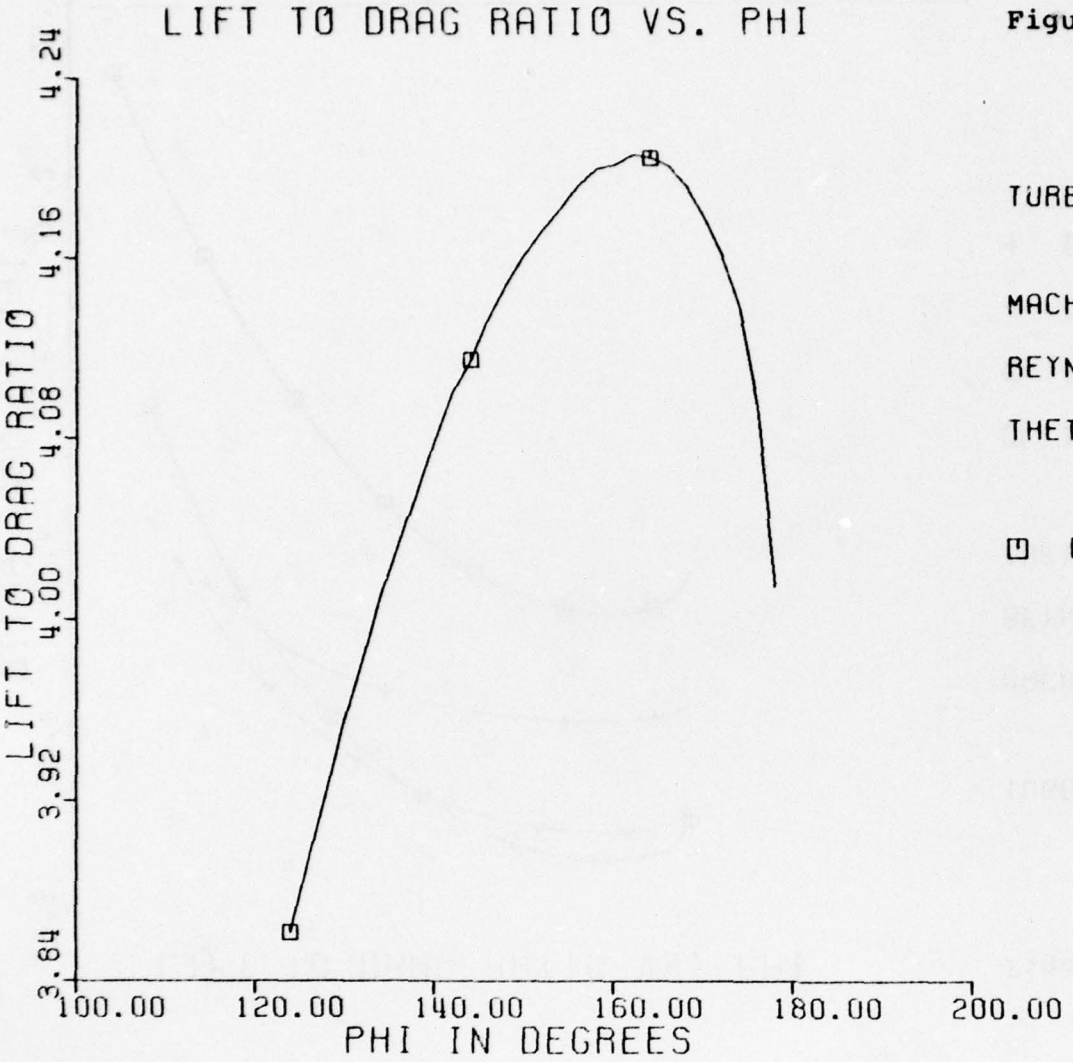

Figure 80.

TURBULENT BOUNDARY LAYER

MACH NUMBER = 2.00

REYNOLDS NO./10^5 =100.00

THETA IN DEGREES = 70.00

⊡ DELTA = 4 DEGREES

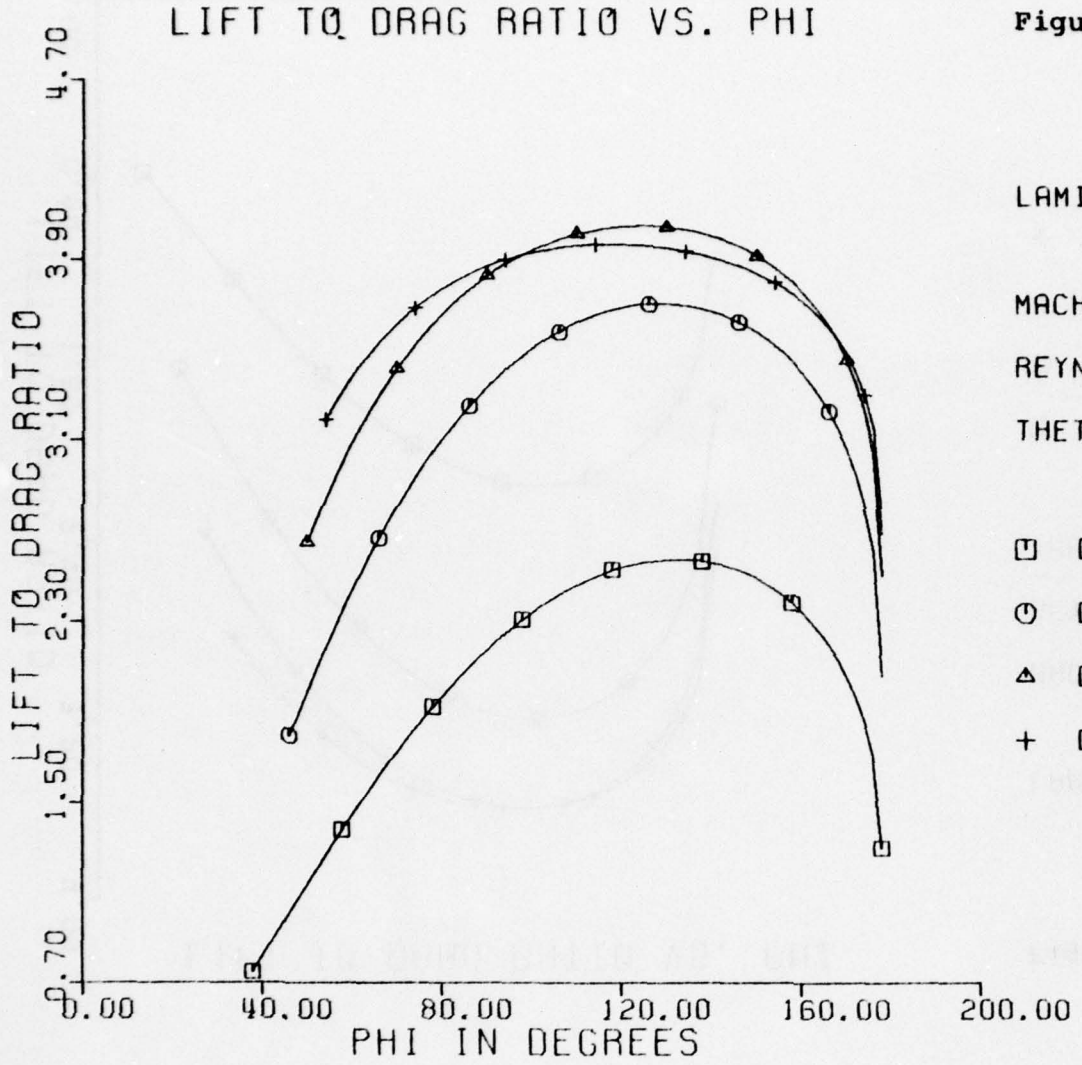

Figure 81.

LAMINAR BOUNDARY LAYER

MACH NUMBER = 3.10

REYNOLDS NO./10^5 = 1.00

THETA IN DEGREES = 30.00

□ DELTA = 4 DEGREES

○ DELTA = 6 DEGREES

△ DELTA = 8 DEGREES

\+ DELTA = 10 DEGREES

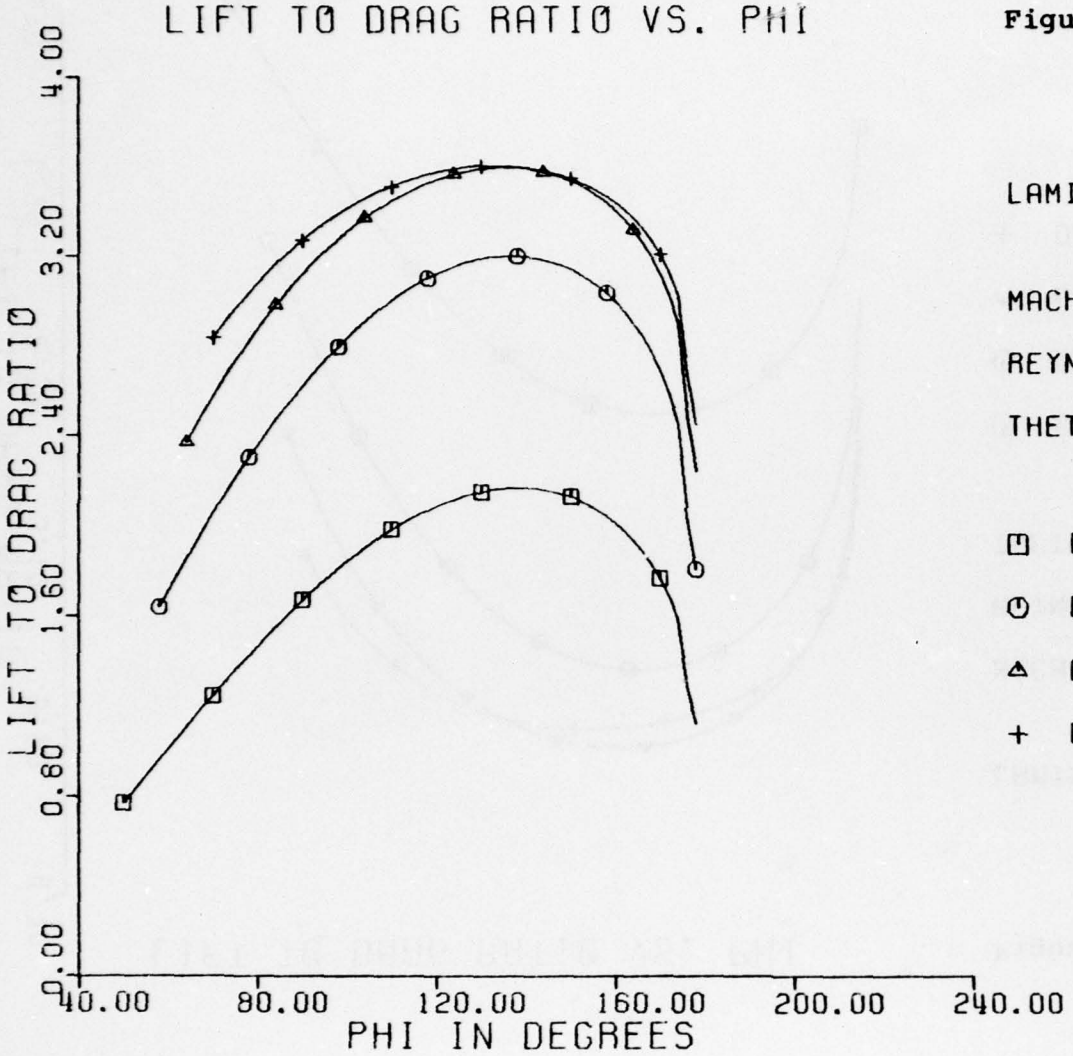

Figure 82.

LAMINAR BOUNDARY LAYER

MACH NUMBER = 3.10

REYNOLDS NO./10^5 =1.00

THETA IN DEGREES = 50.00

□ DELTA = 4 DEGREES

○ DELTA = 6 DEGREES

△ DELTA = 8 DEGREES

\+ DELTA = 10 DEGREES

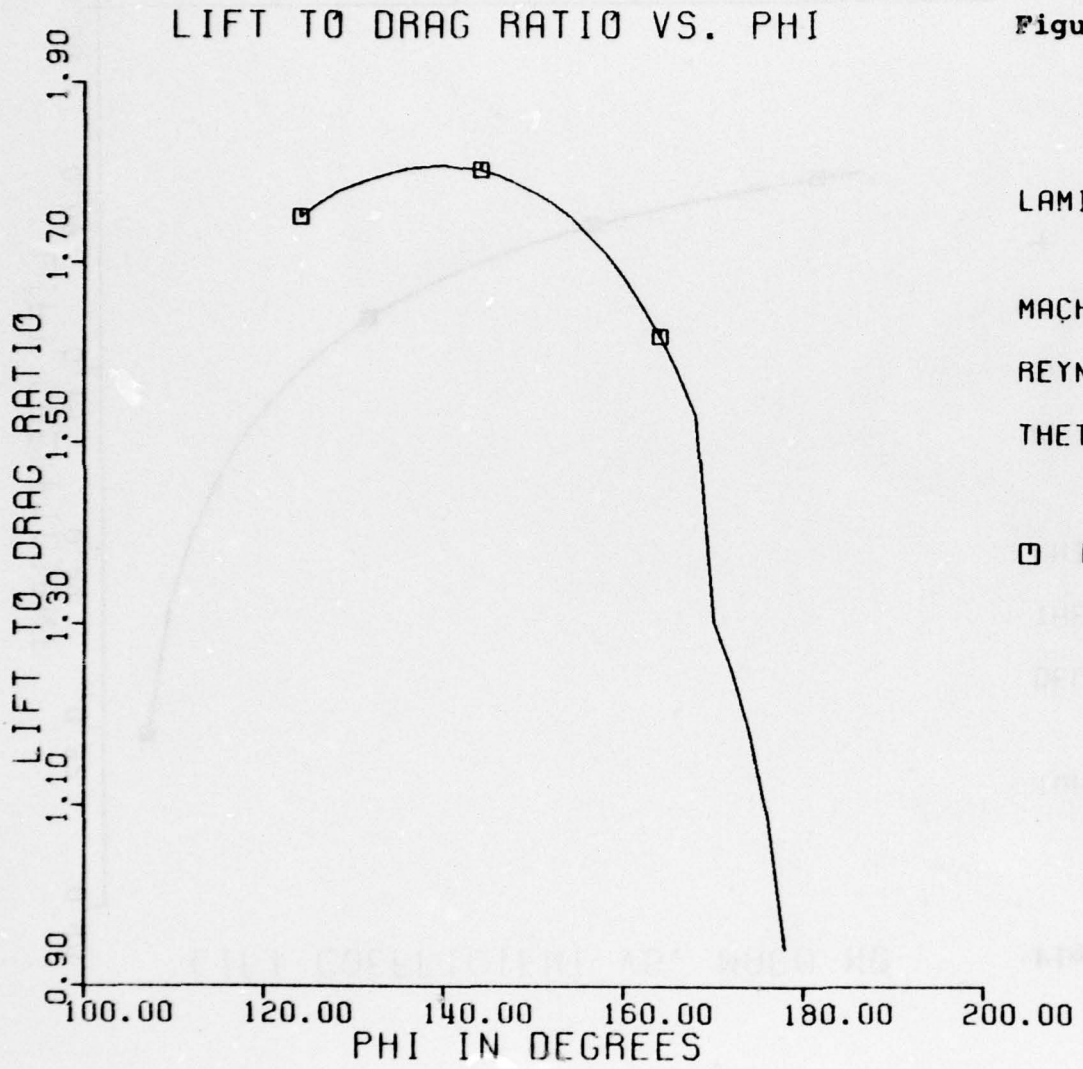

Figure 83.

LAMINAR BOUNDARY LAYER

MACH NUMBER = 3.10

REYNOLDS NO./10^5 =1.00

THETA IN DEGREES = 70.00

DELTA = 4 DEGREES

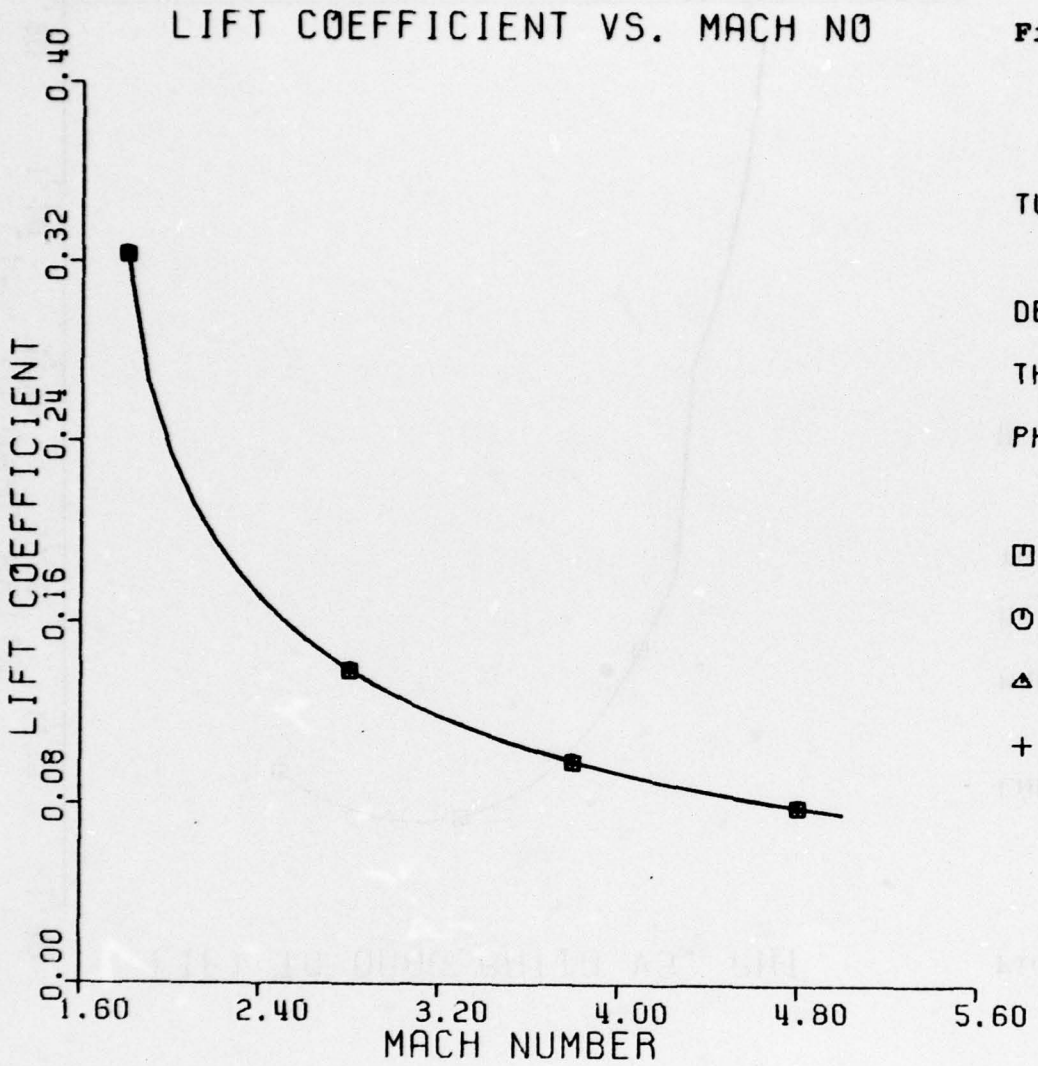

Figure 84.

TURBULENT BOUNDARY LAYER

DELTA IN DEGREES = 6.50

THETA IN DEGREES = 30.00

PHI IN DEGREES = 120.00

□ REYNOLDS NO. = 10^5

○ REYNOLDS NO. = 10^6

△ REYNOLDS NO. = 10^7

\+ REYNOLDS NO. = 10^8

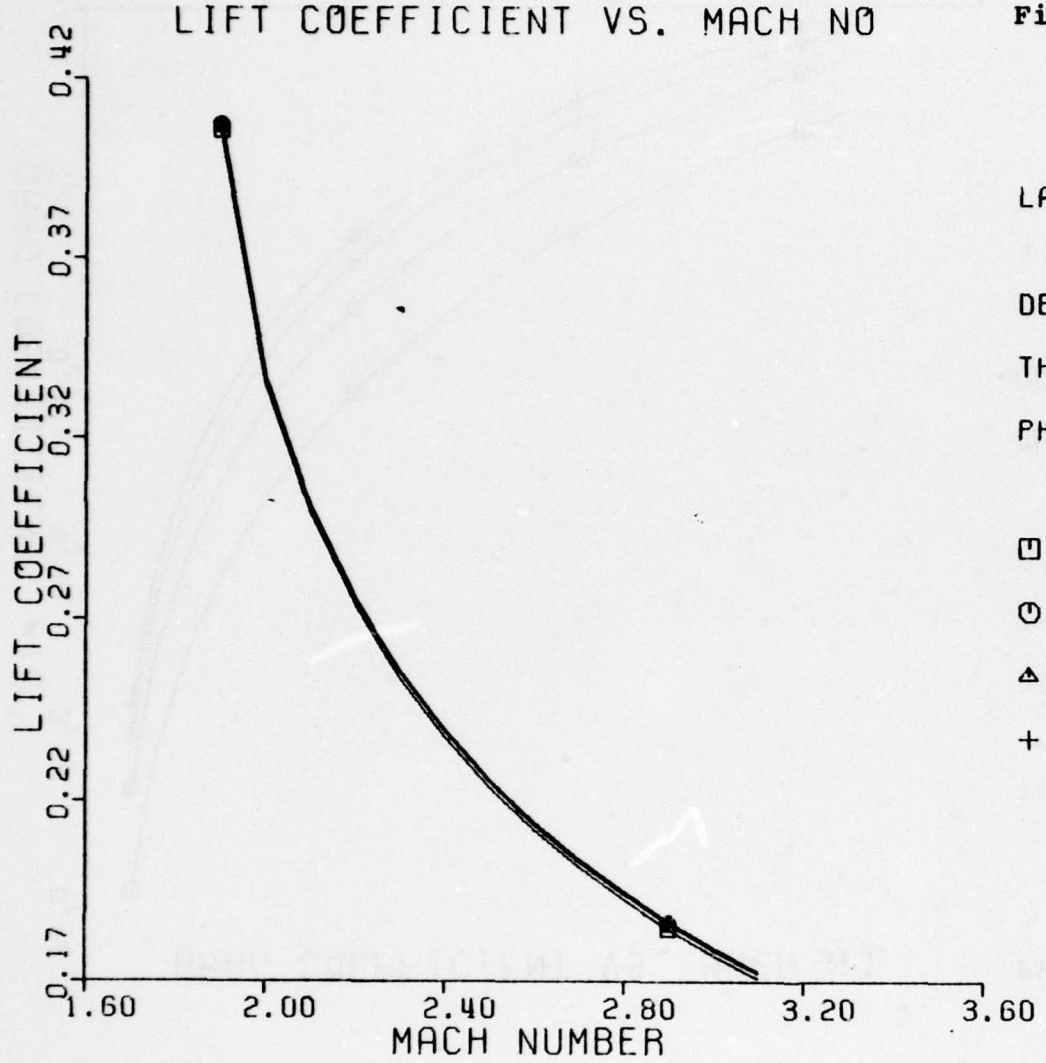

Figure 85.

LAMINAR BOUNDARY LAYER

DELTA IN DEGREES = 8.30

THETA IN DEGREES = 30.00

PHI IN DEGREES = 120.00

□ REYNOLDS NO. = 10^5

○ REYNOLDS NO. = 10^6

△ REYNOLDS NO. = 10^7

\+ REYNOLDS NO. = 10^8

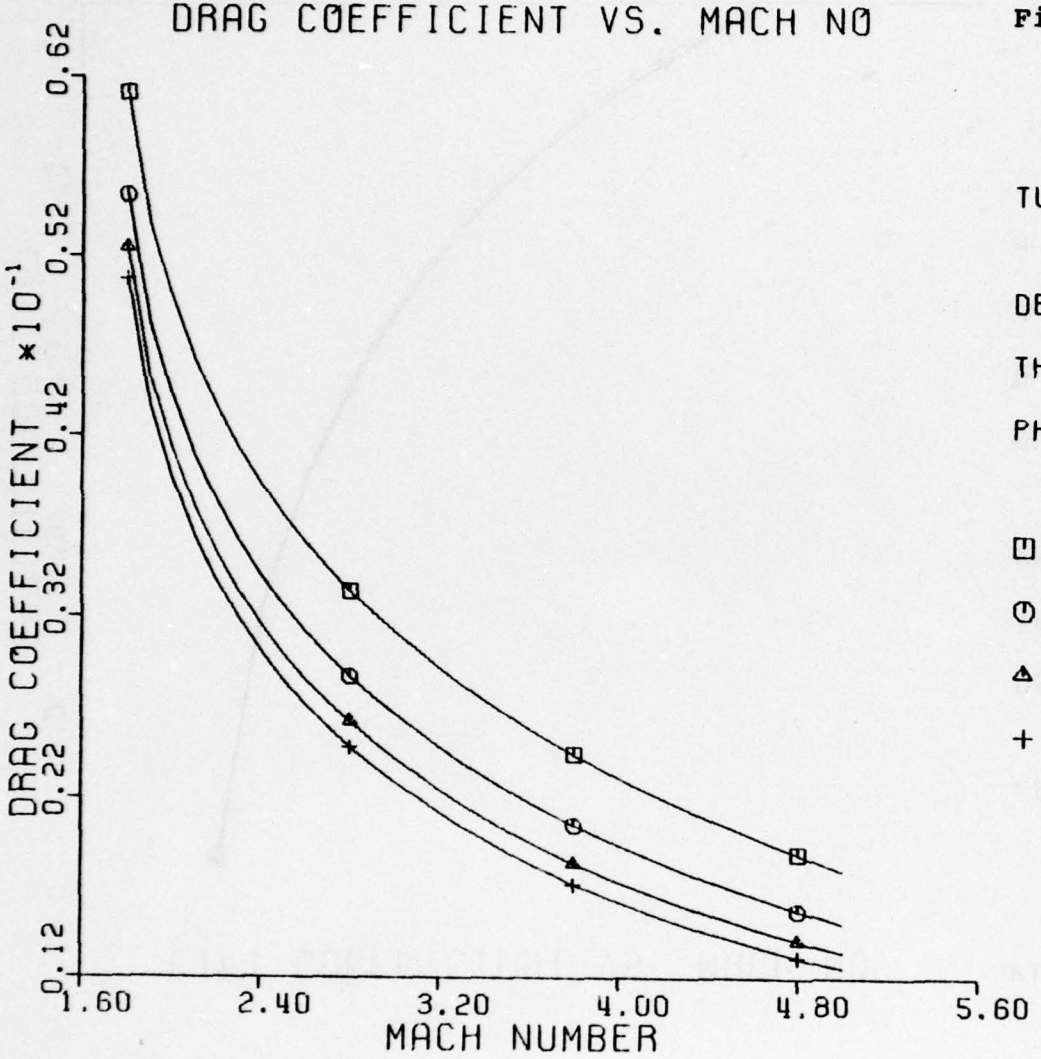

Figure 86.

TURBULENT BOUNDARY LAYER

DELTA IN DEGREES = 6.50

THETA IN DEGREES = 30.00

PHI IN DEGREES = 120.00

□ REYNOLDS NO. = 10^5

○ REYNOLDS NO. = 10^6

△ REYNOLDS NO. = 10^7

\+ REYNOLDS NO. = 10^8

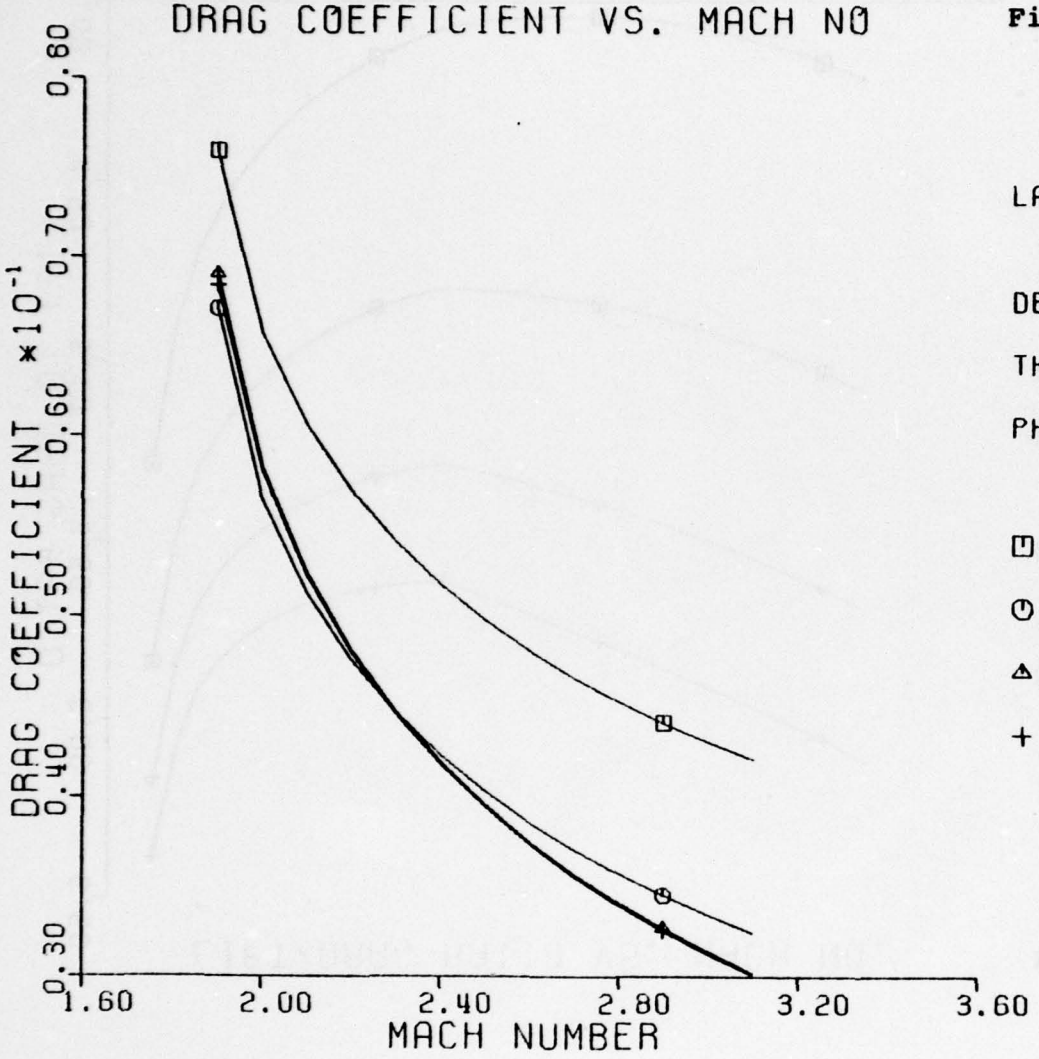

Figure 87.

LAMINAR BOUNDARY LAYER

DELTA IN DEGREES = 8.30

THETA IN DEGREES = 30.00

PHI IN DEGREES = 120.00

□ REYNOLDS NO. = 10^5

○ REYNOLDS NO. = 10^6

△ REYNOLDS NO. = 10^7

\+ REYNOLDS NO. = 10^8

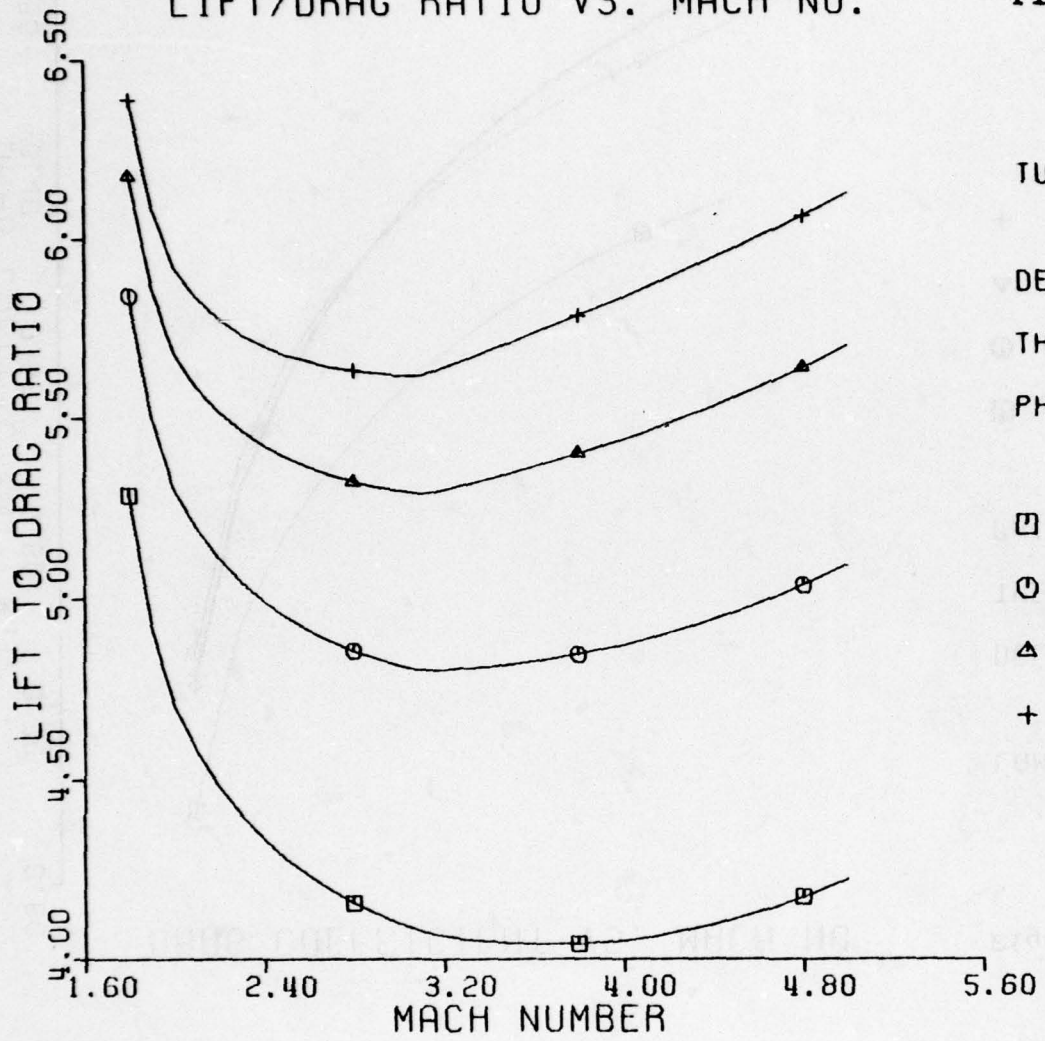

Figure 88.

TURBULENT BOUNDARY LAYER

DELTA IN DEGREES = 6.50

THETA IN DEGREES = 30.00

PHI IN DEGREES = 120.00

□ REYNOLDS NO. = 10^5

○ REYNOLDS NO. = 10^6

△ REYNOLDS NO. = 10^7

\+ REYNOLDS NO. = 10^8

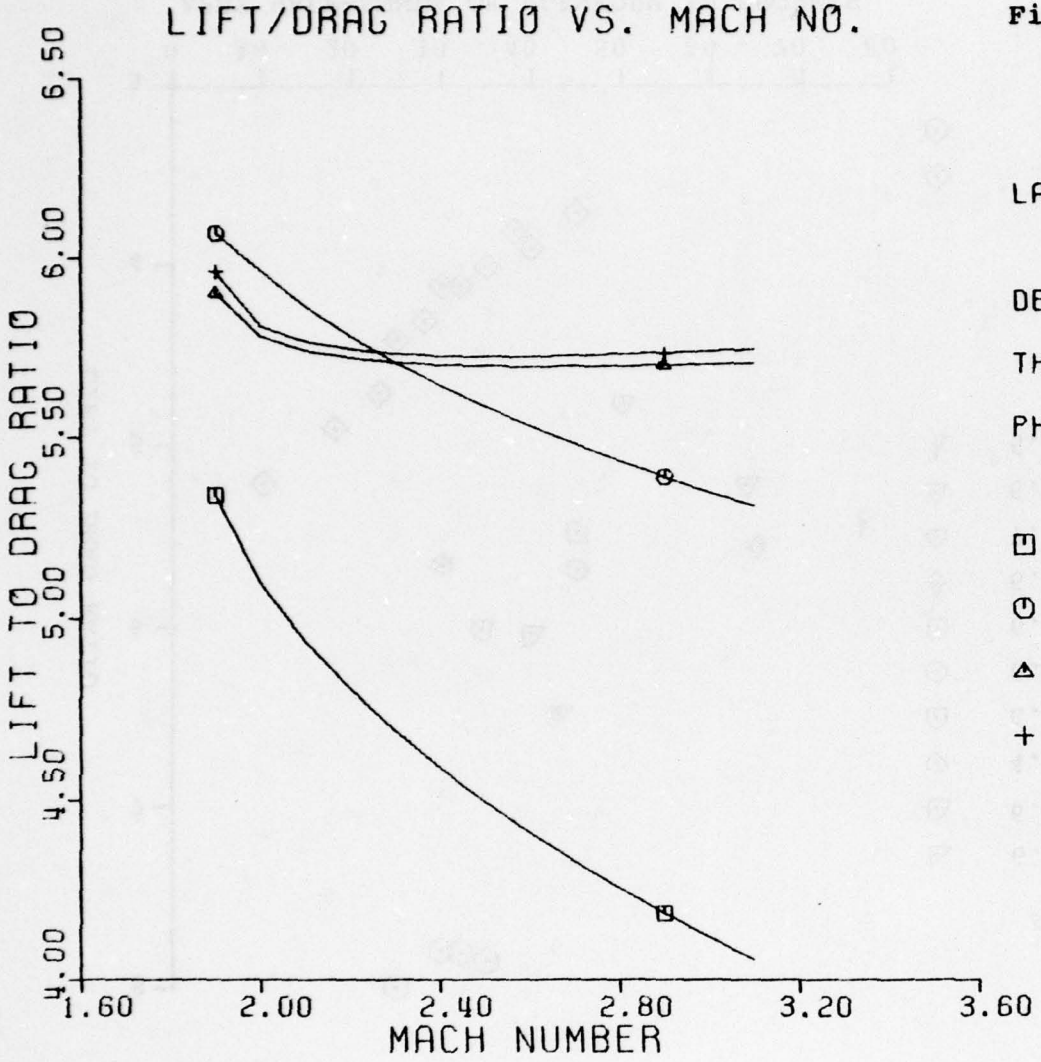

Figure 89.

LAMINAR BOUNDARY LAYER

DELTA IN DEGREES = 8.30

THETA IN DEGREES = 30.00

PHI IN DEGREES = 120.00

□ REYNOLDS NO. = 10^5

○ REYNOLDS NO. = 10^6

△ REYNOLDS NO. = 10^7

\+ REYNOLDS NO. = 10^8

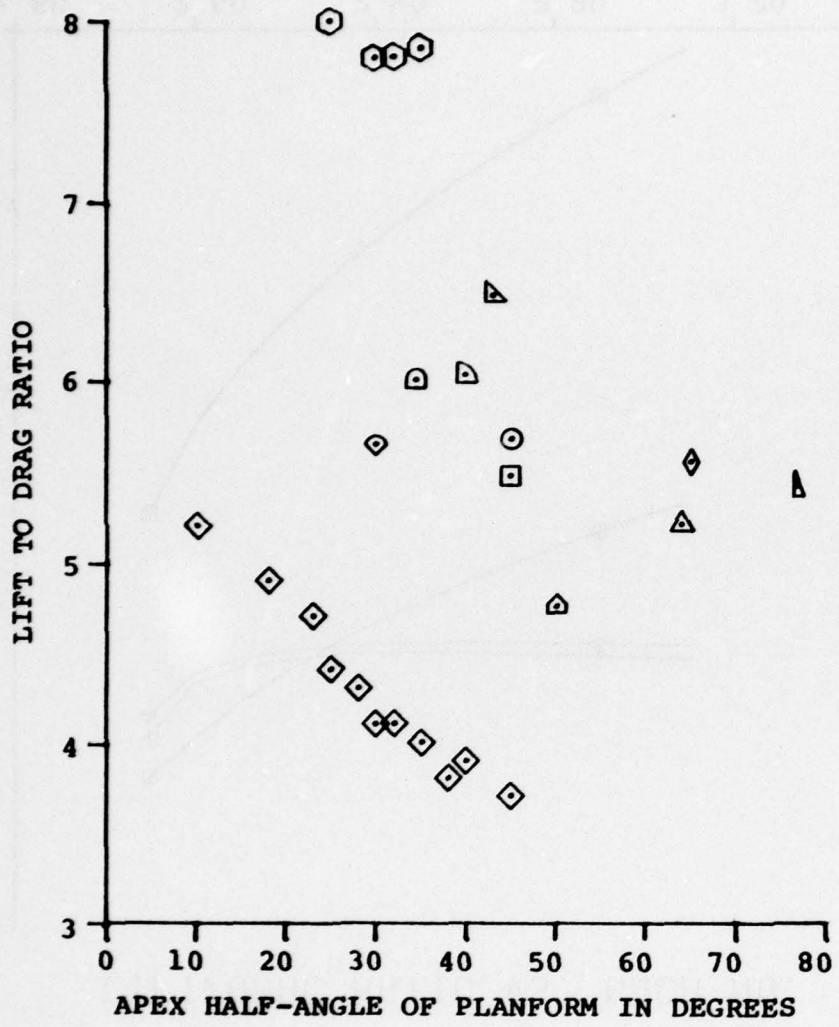

CARET WINGS

	δ	θ	Φ	M_∞	$\frac{Re_{\bar{c}}}{10^6}$	τ
◺	6.0	14	150	2.00	6.93	.052
◺	6.0	26	120	2.00	7.28	.052
◈	4.6	30	90	2.00	8.79	.052
⊙	6.0	30	100	2.00	8.06	.052
⊙	6.5	30	120	2.00	6.69	.052
⊡	6.5	30	120	1.92	1.00	.052
◈	6.4	30	150	2.00	4.56	.052
⊙	7.5	50	90	2.00	6.14	.052
△	6.8	50	120	2.00	4.66	.052
◺	6.6	50	150	2.00	3.17	.052

DELTA WINGS

	M_∞	$\frac{Re_{\bar{c}}}{10^6}$	τ
◈	1.92	0.57 - 1.25	.080
⊙	1.92	0.76 - 1.08	.013 - .018

Figure 90. Comparison of Caret Wing and Delta Wing L/D

REFERENCES

1. Seddon, J and A Spence, "The Use of Known Flow Fields as an Approach to the Design of High Speed Aircraft", AGARD CP-30, Paper #10, May, 1968.

2. Maikapar, G I, "On the Wave Drag of Non-Axisymmetric Bodies at Supersonic Speeds", Journal of Applied Mathematics and Mechanics (PMM), Vol 23, No. 2, 1959, pp 528-531.

3. Nonweiler, T, "Aerodynamic Problems of Manned Space Vehicles", Journal of the Royal Aeronautical Society, Vol 63, No. 585, September, 1959, pp 521-528.

4. Nonweiler, T, "Delta Wings of Shapes Amenable to Exact Shock-wave Theory", Journal of the Royal Aeronautical Society, Vol 67, January, 1963, pp 39-40.

5. Flower, J W, "Configurations for High Supersonic Speeds Derived from Simple Shock-waves and Expansions", Journal of the Royal Aeronautical Society, Vol 67, No. 287, May, 1963, pp 287-290.

6. Venn, J and J W Flower, "Shock Patterns for Simple Caret Wings", The Aeronautical Journal of the Royal Aeronautical Society, Vol 74, April, 1970, pp 339-348.

7. Ziph, B, "A Numerical Method for Conical Rotational Flow about a Reentrant Body", S.M. Thesis, M.I.T., June, 1976.

8. Ames Research Staff, "Equations, Tables and Charts for Compressible Flow", NACA R 1135, 1953.

9. Unpublished Schlieren Photographs of Maikapar Bodies, M.I.T. Aerophysics Laboratory under sponsorship of Lincoln Laboratory, 1972.

10. Schlichting, H, "Boundary-Layer Theory", McGraw-Hill Book Company, Sixth Ed., 1968.

11. Chapman, D R, W R Wimbrow and R H Kester, "Experimental Investigation of Base Pressure on Blunt-Trailing-Edge Wings at Supersonic Velocities", NACA R 1109, 1952.

12. Goecke, S A, "Comparison of Wind Tunnel and Flight-Measured Base Pressures from the Sharp-Leading-Edge Upper Vertical Fin of the X-15 Airplane for Turbulent Flow at Mach Numbers from 1.5 to 5.0", NASA TN D-6348, May, 1971.

13. Rom, J, Y Kronzon and A Seginer, "The Velocity, Pressure and Temperature Distributions in the Turbulent Supersonic Near Wake behind a Two-Dimensional Wedge Flat Plate Model", Technion-Israel Institute of Technology, TAE Report No. 80, September, 1968.

14. Gadd, G E, D W Holder and J D Regan, "Base Pressure in Supersonic Flow", ARC Text Rept. CP No. 271, 1955.

15. Korst, H H, "A Theory for Base Pressures in Transonic and Supersonic Flow", Journal of Applied Mechanics, Vol 23, No. 4, December, 1956, pp 593-600.

16. Adams, R, F Durgin, W Chin and P Saloomey, "Supersonic Wind Tunnel Tests of Unconventional Re-entry Configurations", M.I.T. Aerophysics Laboratory Internal Memorandum LL-13, October, 1972.

17. Solomon, M, "Pitot Pressure Measurements in the Wake of the Wire Suspended 15^{o} Pyramid", M.I.T. Aerophysics Laboratory, AR 1014, November, 1976.

18. Liepmann, H W and A Roshko, "Elements of Gasdynamics", John Wiley & Sons, Inc., 1957.

19. Love, E S, "Investigaticns at Supersonic Speeds of 22 Triangular Wings Representing Two Airfoil Sections for each of 11 Apex Angles", NACA R 1238, 1955.

SECURITY CLASSIFICATION OF THIS PAGE (When Data Entered)

REPORT DOCUMENTATION PAGE		READ INSTRUCTIONS BEFORE COMPLETING FORM
1. REPORT NUMBER AFOSR-TR- 78-0758	2. GOVT ACCESSION NO.	3. RECIPIENT'S CATALOG NUMBER
4. TITLE (and Subtitle) A STUDY OF THE LIFT-TO-DRAG RATIO CAPABILITY OF CARET WING WAVERIDERS		5. TYPE OF REPORT & PERIOD COVERED INTERIM 6. PERFORMING ORG. REPORT NUMBER MIT 200
7. AUTHOR(s) MARSHALL D SOLOMON		8. CONTRACT OR GRANT NUMBER(s) F44620-76-C-0049
9. PERFORMING ORGANIZATION NAME AND ADDRESS MASSACHUSETTS INSTITUTE OF TECHNOLOGY AEROPHYSICS LABORATORY CAMBRIDGE, MASSACHUSETTS 02139		10. PROGRAM ELEMENT, PROJECT, TASK AREA & WORK UNIT NUMBERS 2307A1 61102F
11. CONTROLLING OFFICE NAME AND ADDRESS AIR FORCE OFFICE OF SCIENTIFIC RESEARCH/NA BLDG 410 BOLLING AIR FORCE BASE, D C 20332		12. REPORT DATE March 1978 13. NUMBER OF PAGES 212
14. MONITORING AGENCY NAME & ADDRESS(if different from Controlling Office)		15. SECURITY CLASS. (of this report) UNCLASSIFIED 15a. DECLASSIFICATION/DOWNGRADING SCHEDULE

16. DISTRIBUTION STATEMENT (of this Report)

Approved for public release; distribution unlimited.

17. DISTRIBUTION STATEMENT (of the abstract entered in Block 20, if different from Report)

18. SUPPLEMENTARY NOTES

19. KEY WORDS (Continue on reverse side if necessary and identify by block number)

CARET WING
WAVERIDER
SUPERSONIC FLOW
LIFT-DRAG RATIO

20. ABSTRACT (Continue on reverse side if necessary and identify by block number)

A simple model of the off design caret wing flow field which includes the effects of an upper expansion surface, skin friction and base drag is proposed. Based on this approximate model, calculations of the lift coefficient, drag coefficient and lift-to-drag ratio as functions of body geometry, incidence, Mach number and Reynolds number are made and the dependence of the aerodynamic coefficients on these variables is identified. A test matrix covering a wide range of caret wings and flight conditions is employed in a search for wings with high lift-to-drag ratio. Caret wing performance is then compared to that of delta wings. Lift-to-drag ratios as high as 6.5 for 5 percent thick wings at

DD FORM 1 JAN 73 1473 EDITION OF 1 NOV 65 IS OBSOLETE

UNCLASSIFIED
SECURITY CLASSIFICATION OF THIS PAGE (When Data Entered)

free stream Mach number and Reynolds number of 2.0 and 10^7 were found. This performance is similar to that of delta wings. However, significantly higher caret wing lift-to-drag ratios could be achieved by replacing the blunt base with an afterbody, thereby reducing the base drag.

10,000,000